



UNIVERSITÀ DEGLI STUDI DI SALERNO



UNIVERSITÀ DEGLI STUDI DI SALERNO

Dipartimento di Farmacia

PhD Program

in **Drug Discovery and Development**

XXXIII Cycle — Academic Year 2020/2021

PhD Thesis in

***Onconutraceuticals and personalized medicine:
isolation, characterization, pharmacokinetics
and biological evaluation of antiproliferative
compounds from complex natural matrices***

Candidate

Supervisor

Emanuela Salviati

Prof. *Pietro Campiglia*

PhD Program Coordinator: Prof. Dr. *Gianluca Sbardella*

*A mio padre devo la vita,
al mio maestro una vita che vale la pena essere vissuta.*

Alessandro Magno

Index

Chapter I

Research project presentation: Onconutraceuticals and personalized medicine: isolation, characterization, pharmacokinetics and biological evaluation of antiproliferative compounds from complex natural matrices	1
1. Introduction	1
1.1. Aim of the work	2
1.2. References	4

Chapter II

Chemical profiling of bioactive constituents in hop cones and pellets extracts by online comprehensive two-dimensional liquid chromatography with tandem mass spectrometry and direct infusion Fourier transform ion cyclotron resonance mass spectrometry	7
Abstract	7
2. Introduction	8
2.1. Aim of the work	9
2.2. Results	10
<i>2.2.1. Comprehensive 2-D LC-MS/MS identification of hop cones and pellets constituents</i>	10
<i>2.2.2. Direct infusion Fourier transform ion cyclotron resonance measurements</i>	16
<i>2.2.3. System performance</i>	19
2.3. Discussion	20
2.4. Materials and methods	35
<i>2.4.1. Chemicals</i>	35

2.4.2. Sample preparation	35
2.4.3. Columns	35
2.4.4. Instrumentation	36
2.4.5. Chromatographic conditions: LC × LC-PDA-ESI-IT-TOF	37
2.4.6. Direct Infusion FT-ICR	38
2.5. Conclusions	38
2.6. References	39

Chapter III

Immunomodulatory activity of <i>Humulus lupulus</i> L. bitter acids fraction: enhancement of natural killer cells function by NKp44 activating receptor stimulation	46
Abstract	46
3. Introduction	46
3.1. Aim of the work	48
3.2. Results	49
3.2.1. Hop phytocomplex class fractionation and tentative identification by mass spectrometry	49
3.2.2. Functional and phenotypical characterization of the immunomodulatory effects of hop fraction on T and NK cell compartments	51
3.2.3. Dose response effect of hop fraction on natural killer cell receptor repertoire	55
3.2.4. Sub-fractionation of HFB fraction and its related immunostimulatory effects	56
3.3. Discussion	60
3.4. Materials and methods	62

3.4.1. Chemicals	62
3.4.2. Sample preparation	62
3.4.3. Cells	63
3.4.4. Flow Cytometry	64
3.4.5. Cytokine detection	64
3.4.6. Flow cytometric assay of NK cell cytotoxicity	65
3.4.7. Phytocomplex mass spectrometry based metabolite characterization and fractionation by semi-preparative Liquid Chromatography	66
3.4.8. Statistical analysis	66
3.5. Conclusions	67
3.6. References	67

Chapter IV

Indole-3-lactic acid, a metabolite of tryptophan, secreted by Bifidobacterium longum subspecies infantis is anti-inflammatory in the immature intestine	74
Abstract	74
4. Introduction	75
4.1. Aim of the work	76
4.2. Results	77
4.2.1. Secretory fractions of Bifidobacterium longum subsp infantis are anti-inflammatory with H4 cells	77
4.2.2. Identification of the B. infantis anti-inflammatory secretory molecule as indole-3-lactic acid	78
4.2.3. Indole-3-lactic acid (ILA) is anti-inflammatory in H4 cells	80
4.2.4. ILA is also anti-inflammatory in small intestine from a patient with NEC and other fetal enterocytes	80

<i>4.2.5. ILA causes anti-inflammation through an aryl hydrocarbon receptor (AHR) and responds to TLR-4 expression</i>	82
<i>4.2.6. ILA effect is developmentally regulated</i>	83
<i>4.2.7. Proposed mechanism for indole-3-lactic acid effect on immature enterocytes</i>	85
4.3. Discussion	87
4.4. Materials and methods	91
<i>4.4.1. Bacterial cultures and B.infantis secretory fragment separation</i>	91
<i>4.4.2. Identification of anti- inflammatory effective molecules in secretory size fractions</i>	92
<i>4.4.2.1. Chemicals</i>	92
<i>4.4.2.2. Instrumentation and ultra-high-performance liquid chromatography-tandem mass spectrometry</i>	92
<i>4.4.3. Cell cultures</i>	93
<i>4.4.4. Organoid cultures</i>	93
<i>4.4.5. Hydrocortisone treatment for H4 cells</i>	94
<i>4.4.6. Determination of the anti-inflammatory effects of B.infantis SFs and indole-3-lactic acid on H4, hydrocortisone-treated H4 (H4-HC), NEC-IEC and Caco2 cells</i>	94
<i>4.4.7. Determination of the anti-inflammatory effects of ILA on fetal and adult mouse intestinal organ culture</i>	95
<i>4.4.8. Treatment with the aryl hydrocarbon receptor (AHR) inhibitor - CH223191 in H4 cells</i>	95
<i>4.4.9. Real-time quantitative reverse transcription PCR</i>	95
<i>4.4.10. LDH Cytotoxicity Assay</i>	96
<i>4.4.11. IL-8 ELISA</i>	96
<i>4.4.12. Statistical analysis</i>	96
4.5. Conclusions	97

4.6. References	97
------------------------	----

Chapter V

Determination of phase I metabolites and glucuronide conjugates of hop bitter acids by a full scan/data dependent/targeted neutral loss UHPLC-HRMS strategy: In vitro metabolic stability and in vivo analysis after oral administration in mice	104
Abstract	104
5. Introduction	105
5.1. Aim of the work	107
5.2. Results	108
<i>5.2.1. Method validation and optimization</i>	108
<i>5.2.2. Metabolic stability</i>	110
<i>5.2.3. HRMS/MS analysis of α- and β-acids</i>	116
<i>5.2.4. Phase I and II metabolites of α- and β-acids</i>	116
<i>5.2.5. Structural characterization of α-acids phase I metabolites</i>	117
<i>5.2.6. Structural characterization of β-acids phase I metabolites</i>	118
<i>5.2.7. Structural characterization of α-acids phase II metabolites</i>	119
5.3. Discussion	122
5.4. Materials and methods	130
<i>5.4.1. Chemicals</i>	130
<i>5.4.2. Sample preparation</i>	130
<i>5.4.3. Instrumentation</i>	130
<i>5.4.4. In vitro metabolism of hop bitter acids</i>	131
<i>5.4.5. In vivo studies</i>	134
<i>5.4.5.1. Animal experiments</i>	134
<i>5.4.5.2. Plasma and urine extraction</i>	134

5.4.5.3. <i>Gastrointestinal fluid and plasma stability</i>	135
5.4.6. <i>Method validation</i>	135
5.5. Conclusions	137
5.6. References	137

Chapter VI

Matrix-assisted laser desorption/ionisation mass spectrometry imaging (MALDI-MSI) applications: Evaluation of neurotransmitter and neuropeptide analysis in heat stabilized vs fresh frozen brains and preliminary assessment of hop bitter acids distribution in liver tissues	144
6. Introduction	144
6.1. Aim of the work	145
<i>6.1.1. References</i>	145
6.2. Section I: Evaluation and optimization of neurotransmitter and neuropeptide analysis in heat stabilized vs fresh frozen brains by MALDI-MSI	146
<i>6.2.1. Abstract</i>	146
<i>6.2.2. Introduction</i>	147
<i>6.2.3. Results</i>	150
<i>6.2.3.1. Stabilization of small molecule neurotransmitters by MSI</i>	150
<i>6.2.3.2. Stabilization of neuropeptides by MSI</i>	154
<i>6.2.4. Discussion</i>	161
<i>6.2.5. Materials and methods</i>	165
<i>6.2.5.1. Chemicals</i>	165
<i>6.2.5.2. Safety and precautions</i>	165
<i>6.2.5.3. Animal experiments</i>	165
<i>6.2.5.4. Tissue sample preparation for MALDI-MSI</i>	166

<i>6.2.5.5. Chemical derivatization of catecholaminergic and serotonergic neurotransmitters</i>	166
<i>6.2.5.6. Sample preparation for MALDI-MSI analysis of neuropeptides</i>	167
<i>6.2.5.7. MALDI-MSI analysis</i>	168
<i>6.2.5.8. Neurotransmitter turnover ratio calculations in brain regions</i>	169
<i>6.2.5.9. Statistical analysis</i>	169
6.2.6. Conclusions	169
6.2.7. References	170
6.3. Section II: Preliminary Mass-Spectrometry Imaging of hop bitter acids distribution in liver tissue	177
6.3.1. Abstract	177
6.3.2. Introduction	178
6.3.3. Results and Discussion	178
6.3.4. Materials and methods	181
<i>6.3.4.1. Chemicals</i>	181
<i>6.3.4.2. Animal experiments</i>	181
<i>6.3.4.3. Detection of ICE-4 spotted on a stainless steel MALDI sample plate</i>	182
<i>6.3.4.4. Tissue sample preparation for MALDI-MSI</i>	182
<i>6.3.4.5. Sample preparation for MALDI-MSI analysis</i>	182
<i>6.3.4.6. MALDI-MSI analysis</i>	183
6.3.5. Conclusions	183
6.3.6. References	184
Chapter VII	
Supporting Informations	186
7.1. Supporting Informations for Chapter II	186
7.2. Supporting Informations for Chapter III	191
7.3. Supporting Informations for Chapter IV	197

Index

7.4. Supporting Informations for Chapter V	199
7.5. Supporting Informations for Chapter VI Section I	205
Chapter VIII	
Conclusions	216
List of Papers	220
List of additional papers	222
Participation in conferences	224

Figure captions

Chapter II

Figure 2.1. Contour plot of **hop cones** extracted at 280 nm, ¹D column: Luna[®] C18 150 × 1.0 mm, 5 μm; ²D column: Kinetex[™] C18 50 × 3.0 mm, 1.7 μm. For MS Peak identification, see Table 2.1. 14

Figure 2.2. Contour plot of **hop pellet** extracted at 280 nm, ¹D column: Luna[®] C18 150 × 1.0 mm, 5 μm; ²D column: Kinetex[™] C18 50 × 3.0 mm, 1.7 μm. For MS Peak identification, see Table 2.1. 15

Figure 2.3. MS (top) and MS/MS (bottom) spectra showing structure elucidation and fragmentation pattern of **peak 12**. 16

Figure 2.4 a-d. IT-TOF (a, b) and FT-ICR (c, d) spectra of unknown bitter acids (**peaks 66, 71**). 18

Figure 2.5. Full scan (m/z region 310–380) of DI-FT-ICR-MS showing mass accuracy and compound identification based on molecular formula. 19

Chapter III

Figure 3.1. Fractionation of hop pellets phytochemical complex in three different fractions by semi-preparative liquid chromatography (**a**) and UHPLC-UV-MS analysis of the different fractions (**b**). 50

Figure captions

Figure 3.2. a-d) Cytofluorimetric analysis of the hop fractions activity on Human Peripheral Blood Lymphocytes. Human-purified lymphocytes (PBL), negatively selected (CD14⁻) by immunomagnetic procedure from human healthy peripheral blood mononuclear cell (PBMCs), have been pre-stimulated with IL-2 at 100 IU/ml and IL-15 at 100 ng/ml for 72 h and then treated with 0.5 µg/ml of each fraction (HFA-HFB-HFC-HP) for the last 24 h. At the end of cell culture, PBL were recovered and stained using anti-CD3, anti-CD56, anti-CD69, and anti-NKG2D mAb and analyzed by flow cytometry. Representative dot plots (left) are presented (a, c). Bars graph (right) report the percentage ± SD of CD69⁺ and NKG2D⁺ of CD3⁺ gated T cells and of CD56⁺ CD3⁻ gated NK cells (D) from 3 independent experiments using different donors (b, d). Statistical analysis is indicated (ANOVA; *P < 0.05 compared with NK cells cultured in cytokines supplemented medium). **e-m)** Levels of pro- and anti-inflammatory cytokines. Human-purified lymphocytes (PBL) have been cultured in presence or absence of IL-2 at 100 IU/ml and IL-15 at 100 ng/ml for 72 h. Where indicated, PBL have been co-stimulated with 0.5 and 5 µg/ml of HFB fraction for the last 24 h of treatment. At the end of cell culture, medium from treated PBL was assayed for circulating cytokine levels by beads-based multiplex ELISA (LEGENDplex, Biolegend, USA). Results were expressed as the mean ± SD of all sample determinations conducted in duplicate. All pairwise comparisons are statistically significant (ANOVA; *P < 0.05, **P < 0.01, ***P < 0.001).

53

Figure 3.3. Cytofluorimetric analysis of hop fractions effects on CD56⁺ CD3⁻ NK cells activation. Human-purified CD56⁺ CD3⁻ NK cells cultured for 72 h in complete medium (IL-2+IL-15 supplemented), with or without 0.5 µg/ml of each fraction (HFA-HFB-HFC-HP) for the last 24 h, were stained using anti-CD3, anti-NKp44 and anti-CD56 mAb and analyzed by flow cytometry. A representative dot plot (left) is presented (a). An example for cytofluorimetric histogram profiles of treated purified NK are shown (b). Bar graphs (lower right)

Figure captions

report percentage \pm SD or alternatively the mean \pm SD of the mean fluorescence intensity (MFI) for NKp44 marker in CD56+CD3⁻ gated NK cells from three independent experiments using different donors (c). Statistical analysis is indicated (ANOVA; **P < 0.01, ***P < 0.001).

55

Figure 3.4. HFB sub-fraction effects on cytotoxic potential of CD56+CD3⁻ NK cells. Human-purified CD56+CD3⁻ NK cells cultured for 72 h in complete medium (IL-2+IL-15 supplemented), with or without increasing doses of fraction B (HFB) for the last 24 h, were stained using anti-CD3, anti-NKp44, anti-KIR3DL1, anti-CD158k and anti-CD56 mAb and analyzed by flow cytometry. Panel **a** shows the effects of titration of HFB on the surface expression of NKp44 activating receptor in CD56+CD3⁻ NK cells compartment. Panel **b** displays the effects of different concentration of HFB on the surface expression of the inhibitory receptors KIR3DL1 and CD158K by of fraction B. Panel **c** reports the effect of different B sub-fractions (HFB1-HFB2-HFB3) on NKp44 activating receptor. Panel **d** shows the percentage of lysis mediated by HFB sub-fraction. Human-purified CD56+CD3⁻ NK cells, cultured in complete medium alone (medium; circles) or treated with different HFB sub-fractions at a selected concentration of 0.5 μ g/ml. (HFB1, squares; HFB2, triangles; HFB3, diamonds) for 72 h, were then tested for cytotoxic activity against K562 cells, as described in Materials and Methods. E:T ratios are indicated. The duration of the assay was 4 h. Results were expressed as the mean \pm SD of two independent experiments conducted in triplicate. Pairwise comparisons statistically significant among treatment groups are shown (ANOVA; **P < 0.05, ***P < 0.01).

58

Figure 3.5. Extracted ion chromatogram (EIC) of hop sub-fraction 3 (HFB3) showing the main compounds detected in this fraction (top) HRMS and MS/MS spectra of bitter acids detected in sub-fraction HFB3 (bottom).

59

Chapter IV

Figure 4.1. The effects of different secretory size fractions of *B. infantis* on anti-inflammation and cytotoxicity in H4 cells. H4 cells were pretreated with or without *B. infantis* secretory size fractions (SFs) before IL-1 β stimulation (**a**) or treated with SFs alone (**b**). The secretion of IL-8 (**a, b**) and lactate dehydrogenase (LDH) (**c**) into the cell culture supernatant was determined by ELISA and cytotoxicity assay—LDH assay. Graphs represent means \pm SEM (n = 3) from three independent experiments. One-way analysis of variance (ANOVA) and Tukey's post hoc tests were used for statistical analysis (**P < 0.01, †P < 0.001, n.s., not significant).

77

Figure 4.2. Comparison of ultra-high-performance liquid chromatography-UV (UHPLC-UV) profiles of the media, < 3 and 3–10 kDa *B. infantis* SFs, and identification of indole-3-lactic acid (ILA) as the structure of the specific peaks from *B. infantis* SF by an extracted ion chromatogram (EIC). **a-c**, RP-UHPLC-UV chromatograms (280 and 254 nm) showing the comparison of *B. infantis* culture media with *B. infantis* secretion size fractions < 3 and 3–10 kDa. The circle shows the ILA peak, which is absent in culture media and present in both of the *B. infantis* SFs. To confirm ILA, was compared the ILA standard compound retention time with the *B. infantis* fractions. **d**, EIC showing the ILA [M–H][–] peak in *B. infantis* fractions (black line) overlapped with the corresponding standard (pink line). **e-h**, MS and MS/MS spectra of ILA peak in *B. infantis* fraction (**e, f**) compared with MS and MS/MS spectra of standard compound (**g, h**).

79

Figure 4.3. The effect of indole-3-lactic acid (ILA) on anti-inflammation in H4 cells, NEC enterocytes, and immature human intestinal organoids. H4 cells (**a**),

Figure captions

primary enterocytes isolated from resected intestine of a NEC patient (**b**), and immature human intestinal organoids isolated from therapeutically aborted fetuses at gestational ages 15 (**c**) and 22 weeks (**d**) were pretreated with or without ILA before IL-1 β stimulation. The secretion of IL-8 into the cell culture supernatant was determined by ELISA (N = 3). Graphs represent the mean \pm SEM from three independent experiments. One-way analysis of variance (ANOVA) and Tukey's post hoc tests were used for statistical analysis (*P < 0.05, **P < 0.01, †P < 0.001, n.s., not significant).

81

Figure 4.4. ILA anti-IL-1 β -induced IL-8 induction is mediated by aryl hydrocarbon receptor (AHR) in H4 cells and TLR-4 is required for ILA anti-inflammation in immature intestine. **a**, H4 cells were pretreated with or without different doses of AHR inhibitor—CH223191 and then treated with ILA before exposure to IL-1 β . The secretion of IL-8 into the supernatant was determined by ELISA. **b**, TLR-4-knockout immature mice (embryonic day 18.5) small intestinal organ cultures were pretreated with or without 5 μ M of ILA before IL-1 β stimulation. The secretion of microphage inflammatory protein 2 (MP2) into the supernatant was determined by ELISA. Data are represented as the mean \pm SEM, n = 3 from three independent experiments for a and n = 6 from the repeated experiments for b. One-way analysis of variance (ANOVA) and Tukey's post hoc tests were used for statistical analysis (*P < 0.05 and †P < 0.001, n.s., not significant).

83

Figure 4.5. AHR and ILA anti-inflammatory responses to IL-1 β are developmentally regulated. C57BL6 (*a*) immature (embryonic day 18.5) and (*b*) adult (8-week-old male) mice small intestinal organ cultures were pretreated with or without ILA before IL-1 β stimulation. The secretion of MP2 into the supernatant was determined by ELISA. **c**) Expression of AHR mRNA in H4 cells and hydrocortisone-treated H4 (HC-H4) cells. **d**) IL-8 reaction in HC-H4 cells'

Figure captions

exposure to ILA before an IL-1 β stimulus. **e)** AHR mRNA in H4 and Caco-2 cells. **f)** IL-8 secretions in Caco-2 cells pretreated with or without ILA before IL-1 β stimulus. Data are represented as the mean \pm SEM, n = 6 for mice and n = 3 for cells (from three independent experiments). *T* test was used for two-group and one-way analysis of variance (ANOVA), and Tukey's post hoc tests were used for multiple-group statistical analysis (*P < 0.05, **P < 0.01, †P < 0.001, n.s., not significant).

84

Figure 4.6. Cartoon of suggested mechanism of anti-inflammatory effect of ILA in *B.infantis* secretions on intestinal epithelial cells. **(1)** Degradation of lumen protein leads to the release of tryptophan (**Trp**). Under the influence of the gut microbiota, Trp is converted to indole-3-lactic acid (**ILA**) **(2)** by the indole/AHR pathways. ILA acts on the aryl hydrocarbon receptor (**AHR**) found in fetal enterocytes **(3)** thereby affecting the innate immune response in a ligand-specific fashion suppressing a pathogen-mediated inflammatory cytokine IL-1 β -induced IL-8 secretion **(4)**. TLR-4 is required for ILA anti-inflammation in immature enterocyte with the unknown mechanism **(5)**.

86

Chapter V

Figure 5.1. Metabolic stability curve of parent ICE-4 α - and β -acids expressed as Remaining of parent %.

111

Figure 5.2. Extracted ion chromatograms **(a)** and MS² spectra with the fragmentation pathways **(b-e)** of ICE-4 α -acids phase I metabolites.

118

Figure 5.3. Extracted ion chromatograms (a) and MS² spectra with the fragmentation pathways (b-e) of ICE-4 β-acids phase I metabolites. 119

Figure 5.4. Extracted ion chromatograms (a) and MS² spectra with the fragmentation pathways (b-g) of ICE-4 α-acids phase II metabolites. 122

Chapter VI Section I

Figure 6.2.1. MALDI-MS images of double derivatized dopamine (DA + [2 (FMP-10)-CH₃]) (a) and single derivatized 3-Methoxytyramine (3-MT + FMP-10) (b) in coronal rat brain sections comparing unnormalized, RMS, and IS normalized MSI data in FF and HS tissues (at bregma 2.28 mm, Paxinos and Watson, 2014). Scale bar = 2 mm. Colour scale bars are shown as percentage of maximum intensity. IS: DA-*d*₄. Lateral resolution, 150 μm. Abbreviations: RMS, root-mean square normalization; IS, Internal standard normalization; FF, fresh frozen; HS, heat stabilized. 151

Figure 6.2.2. MALDI-MS images of neurotransmitters and related metabolites acquired from FF and HS tissue sections. **a**, DA double derivatized; **b**, NE double derivatized; **c**, DOPAL double derivatized; **d**, DOPAC double derivatized; **e**, HVA single derivatized; **f**, 3-MT single derivatized; **g**, MOPAL single derivatized (coronal rat brain section at bregma 2.28 mm, Paxinos and Watson, 2014); **h**, DOPEG double derivatized; **i**, 5-HT-single derivatized; **j**, 5-HIAA single derivatized; **k**, 5-HIAL-single derivatized; **l**, GABA single derivatized; (coronal rat brain section at bregma -2.04 mm, Paxinos and Watson, 2014); **m**, **n**, Bar charts graphs reflecting normalized average intensity of precursors DA (m) NE and 5-HT (n) and their metabolites between HS and FF protocols. Error bars represent standard deviation between technical replicates (**p ≤ 0.01, *p ≤

Figure captions

0.05). Scale bar = 2 mm. Colour scale bars are shown as percentage of maximum intensity. Lateral resolution, 150 μm . Data were normalized against IS: DA- d_4 for DA, DOPAL, DOPAC, 3-MT, MOPAL, 5-HT, NE, DOPEG, 5-HIAL, 5-HIAA. HVA- d_5 for HVA; GABA- d_6 for GABA. Abbreviations: FF, fresh frozen; HS, heat stabilized.

153

Figure 6.2.3. MALDI-MS images of enkephalins in coronal rat brain sections. Imaging experiments compared the distribution of full-length peptides (**a-f, j-k, n**) and related fragments (**g-i, l-m, o**) between FF and HS tissues at bregma -2.04 mm (a-i), -5.64 mm (j-m) and -2.92 mm (n-o) (Paxinos and Watson, 2014). a, Leu-enk; b, Met-enk; c, Metorphamide; d, j, Met-enk-RF; e, Met-enk-RGL; f, k, PENK (219-229); g, l, Des-Y-Met-enk-RF; h, Met-enk-R; i, m, PENK (220-229); n, PENK (198-209); o, PENK (201-219); Scale bar = 5 mm. Colour scale bars are shown as percentage of maximum intensity. Data were normalized against RMS. Lateral resolution, 150 μm . Abbreviations: FF, fresh frozen; HS, heat stabilized.

156

Figure 6.2.4. Bar charts graphs reflecting normalized average intensity of enkephalins between HS and FF protocols. **a-c**, Full-length peptides and related fragments at bregma -2.04 mm (a), -5.64 mm (b) and -2.92 mm (c). Error bars represent standard deviation between technical replicates (**** $p \leq 0.0001$, *** $p \leq 0.001$, ** $p \leq 0.01$, * $p \leq 0.05$). Abbreviations: PIPAG, pleoiglia periaqueductal gray; SNR, reticular part of substantia nigra; HS, heat stabilized; FF, fresh frozen.

157

Figure 6.2.5. MALDI-MS images of dynorphins and tachykinins in coronal rat brain sections. Imaging experiments compared the distribution of full-length peptides (**a-d, i-l**) and related fragments (**e-h, m-n**) between FF and HS tissues at bregma -2.04 mm (a, c, e, g, i, k, m) and -5.64 mm (b, d, f, h, j, l, n) (Paxinos and Watson, 2014). a, b, Dyn A (1-8); c, d, α -Neo; e, f, Dyn A (2-8); g, h, α -Neo

Figure captions

(2-10); i, j, Neurokinin A; k, l, SP (1-11); m, n, SP (1-9); o, p, Bar charts graphs reflecting normalized average intensity of full-length peptides and related fragments at bregma -2.04 mm (o) and -5.64 mm (p) between HS and FF protocols. Error bars represent standard deviation between technical replicates ($***p \leq 0.001$, $**p \leq 0.01$, $*p \leq 0.05$). Scale bar = 5 mm. Colour scale bars are shown as percentage of maximum intensity. Data were normalized against RMS. Lateral resolution, 150 μ m. Abbreviations: PIPAG, pleoiglia periaqueductal gray; SNR, reticular part of substantia nigra; FF, fresh frozen; HS, heat stabilized.

159

Figure 6.2.6. Molecular distributions determined by MALDI-MSI in coronal rat brain sections comparing FF with HS tissues (at bregma -2.04 mm, Paxinos and Watson, 2014) of **a**, SST-28(1-12); **b**, N-EI; **c**, PEP-19 (48-62); **d**, PEP-19 (51-62) and **e**, nociception; **f**, Bar charts graphs reflecting normalized average intensity of SST-28(1-12) and N-EI between HS and FF protocols. Scale bar = 5 mm. Colour scale bars are shown as percentage of maximum intensity. Data were normalized against RMS. Lateral resolution, 150 μ m. Abbreviations: FF, fresh frozen; HS, heat stabilized.

160

Chapter VI Section II

Figure 6.3.1. MALDI-MS images of ICE-4 α - and β -acids in mouse liver sections at 1 and 2 h after oral administration. Imaging experiments compared the distribution of parent compounds and mono-oxidized metabolites. **a, f**, optical images of mouse liver sections; **b, g**, Cohumulone (m/z 347.1867, -0.28 ppm) at 1 (**b**) and 2 h (**g**); **c, h**, Mono-oxidized cohumulone (m/z 363.1813, -0.27 ppm) at 1 (**c**) and 2 h (**h**); **d, i**, Humulone (m/z 361.2019, -0.10 ppm) at 1 (**d**) and 2 h (**i**); **e, j**, Mono-oxidized Humulone (m/z 377.1970, 0.28 ppm) at 1 (**e**) and 2 h (**j**)

Figure captions

;Scale bar = 2 mm. Colour scale bars are shown as percentage of maximum intensity. Data were normalized against RMS. Lateral resolution, 100 μm .

180

Chapter VII

Figure S2.1. MS and MS/MS spectra showing structure elucidation and fragmentation pattern of **peak 31**.

186

Figure S2.2. Separation of hop cones extract, column Luna[®] HILIC 150 \times 2.1 mm, 3.0 μm , injection volume 2 μL , flow rate 0.1 mL/min, mobile phase: A) H₂O/ACN 80/20 + 0.1 % CH₃COOH; B) ACN.

187

Figure S2.3. First dimension separation of hop cones extract, column Luna[®] C18 150 \times 1.0 mm, 5.0 μm , injection volume 1 μL , flow rate 30 $\mu\text{L}/\text{min}$, mobile phase: A) 10 mM CH₃COONH₄ in H₂O, pH 9; B) ACN.

187

Figure S2.4. Shifted gradient approach employed in the ²D of LC \times LC setup.

188

Figure S5.1. UHPLC-PDA chromatograms (λ : 330 nm) (**a**, **c**) with a gradient starting from high percentage of organic modifier (50% ACN) and ESI negative - MS/MS total ion chromatograms (TIC) (**b**, **d**) of ICE-4 sample using CH₃COOH (**a**, **b**) and HCOOH (**c**, **d**) as additives of the mobile phase. **e**, UHPLC-ESI Negative - MS TIC of ICE-4 sample with optimized conditions employed for the final UHPLC-HRMS setup. Peak: 1, Cohumulone; 2, n-Humulone; 3, Adhumulone; 4, Colupulone; 5, n-Lupulone; 6, Adlupulone.

200

Figure captions

Figure S5.2. Extracted ion chromatograms (**a**) and MS² spectra with the fragmentation pathways (**b-e**) of ICE-4 α - (**b, c**) and β - (**d, e**) acids parent compounds. 201

Figure S5.3. UHPLC-HRMS base peak chromatograms (BPC) of mouse liver microsomal digested at 0, 30, 60 and 120 min (**a**), mouse plasma at 1 and 2 h (**b**) and urine at 24 and 48 h (**c**) extracts. 202

Figure S5.4. UHPLC-PDA chromatograms (λ : 330 nm) of ICE-4 sample subjected to gastric (0.1 M HCl, pH 2) (**a**), intestinal (HCOONH₄ 10 mM, adjusted to pH 8 with NaOH) (**b**) and mouse plasma (**c**) stability evaluation. **Time points:** T0, 0 min; T1, 30 min; T2, 60 min; T3, 120 min. 203

Figure S5.5. Potential prediction of glucuronide derivative of α - and iso- α -acids by FAME3 (<https://nerdd.zbh.uni-hamburg.de/fame3/>). As a result, the approach proposed as first hits the hydroxyl substituents in position C3 and C4 for α -acids and C1 and C2 for iso- α -acids as most probable SOM for UGTs catalyzed glucuronidation. 204

Figure S6.2.1. Optical images of coronal rat sections from four HS brains and four FF brains, which shows the changes to the tissue structure caused by heating. The HS tissues appear dryer, their edges are jagged and some holes can be observed (distance from bregma, 2.28 mm, Paxinos and Watson, 2014). Abbreviations: FF, fresh frozen; HS, heat stabilized. 205

Figure S6.2.2. Molecular distributions determined by MALDI-MSI in coronal rat brain sections comparing FF with HS tissues. **a**, PENK (114-133); **b**, PENK (212-229); **c**, PENK A (239-260); **d**, Dyn B (1-13); **e**, Dyn B (1-6); **f**, Dyn B (15-28) (distance from bregma, -2.04 mm, Paxinos and Watson, 2014); **g**, β -Neo; **h**,

Figure captions

C-terminal flanking peptide; **i**, neuropeptide gamma (distance from bregma, -2.92 mm, Paxinos and Watson, 2014); **j**, Bar charts graphs reflecting normalized average intensity of full-length peptides and related fragments between HS and FF protocols. Error bars represent standard deviation between technical replicates ($***p \leq 0.001$, $**p \leq 0.01$, $*p \leq 0.05$). Scale bar = 5 mm. Colour scale bars are shown as percentage of maximum intensity. Data were normalized against RMS. Lateral resolution, $150 \mu\text{m}$. Abbreviations: FF, fresh frozen; HS, heat stabilized.

206

Figure S6.2.3. Molecular distributions determined by MALDI-MSI in coronal rat brain sections comparing FF with HS tissues. **a**, cerebellin 1; **b**, cerebellin 1 (2-16); **c**, cerebellin 1 (1-15); **d**, cerebellin 1 (2-15); **e**, cerebellin 4 (66-77); **f**, PC1 (619-628); **g**, Bar charts graphs reflecting normalized average intensity of peptides between HS and FF protocols. Error bars represent standard deviation between technical replicates ($***p \leq 0.001$). Scale bar = 5 mm. Colour scale bars are shown as percentage of maximum intensity. Data were normalized against RMS. Lateral resolution, $150 \mu\text{m}$. Abbreviations: FF, fresh frozen; HS, heat stabilized.

207

Figure S6.2.4. Schematic of the experiments performed in rat brains to monitor preservation of neurotransmitters and neuropeptides from *post mortem* degradation, comparing fresh freezing and heat-stabilization as tissue fixation approaches. Eight rats were sacrificed by decapitation and the brains were quickly removed. Four brains were immediately frozen by immersion in -45 °C dry-ice-cooled isopentane and stored at -80 °C, the other four brains were heated at 95 °C within 1 min following decapitation with minimal compression and cavity vacuum, using the Stabilizer T1™ instrument. MALDI-MSI for both neurotransmitters and neuropeptide were performed on coronal rat sections at six levels, distance from bregma: 2.28 mm, 0.00 mm, -2.04 mm, -2.92 mm, -5.04

Figure captions

mm, -5.64 mm (Paxinos and Watson, 2014). Abbreviations: FF, fresh frozen;
HS, heat stabilized.

Table captions

Chapter II

Table 2.1. LC × LC-PDA-IT-TOF characterization of hop cones and pellets extracts. 25

Chapter V

Table 5.1. Parameters for analytical method validation. Values are expressed as mean of three experiments ± standard deviation. 113

Table 5.2. Parameters of ICE-4 α- and β-acids *in vitro* metabolic stability. Values are expressed as mean of three experiments ± standard deviation. 114

Table 5.3. Quantitative profile of ICE-4 α- and β-acids in mouse plasma and urine samples. Values are expressed as mean of three replicates ± standard deviation. 115

Table 5.4. Observed metabolites of ICE-4 α- and β-acids in mouse liver microsomes, in mouse plasma and urine, Abbreviation: P, parent compound; O, oxidation; OH, hydroxylation; Gluc., glucuronidation. 126

Table S2.1. DI-FT-ICR identification of hop cones and pellets extracts based on Accurate Formula and Compound Crawler Database searching. 188

Table S2.2. Peak capacity values corrected for undersampling (*) and orthogonalithy A_0 . 190

Table S2.3. Repeatability data for 2D peak areas and 2D retention times. 191

Table captions

Table S3.1. List of all compounds detected in the hop pellets fractions.	193
Table S3.2. Quantitative profile of bitter acids in hop target phytocomplex and sub-fraction B3.	197
Table S4.1. <i>B. infantis</i> culture media. The table shows the ingredients of the <i>B. infantis</i> culture media that is a modification of the combination of the intestinal epithelial cell culture media and the <i>B. infantis</i> culture media. Abbreviation: MEMNEAA- MEM non-essential amino acids, BPE-Bovine pituitary extract, BHI- Brain and heart infusion broth.	198
Table S5.1. Concentrations of α - and β -acids in ICE-4 standard solutions at each concentration level of calibration curves.	199
Table S6.2.1. Complete list of the neurotransmitters detected in heat-stabilized (HS) and fresh frozen (FF) brain tissues by MALDI MSI.	210
Table S6.2.2. Average intensity ratio between metabolite and neurotransmitter for heat stabilized (HS) and fresh frozen (FF) brain tissues.	211

CHAPTER I:

Research project presentation: Onconutraceuticals and personalized medicine: isolation, characterization, pharmacokinetics and biological evaluation of antiproliferative compounds from complex natural matrices

1. Introduction

Bioactive secondary metabolites from phytocomplexes possess a broad spectrum of healthy properties, and more often are included in formulations employed as side or complementary therapy to drugs in the treatment of chronic diseases, in the growing field of *onconutraceuticals*^[1]. This new topic is directed to the development of new nutraceuticals products, which could be useful not only for the prevention of cancer, but also a valid support to the pharmacological therapies acting in additive or synergic way and, at the same time, reduce side effects of drugs^[2]. One of the most novel and promising strategies in cancer treatment consists in using natural immunomodulators as adjuvants in chemotherapy protocols, which are characterized by lower toxicity and price compared to drugs, in order to improve the immune response and reduce the suppression effect produced by drugs^[3]. This project is focused to characterize bioactive molecules obtained from natural matrices that are able to modulate the physiological processes underlying the onset of cancer or, that possess immunomodulatory activities, directing their use towards the prevention and as support to drugs for the treatment of important cancer pathologies and chronic disease. Furthermore, the study aims to develop and apply suitable analytical techniques that can be used in pharmaceutical and biomedical

field, in particular characterize in detail their chemical diversity, to elucidate the fate of target compounds after assumption, and, finally, understand their mechanism of action by the analysis of metabolic changes occurring in biological systems following their employment in disease conditions, and highlight the potential positive modulation of key molecular pathways.

1.1. Aim of the work

The first part of the project has been focused on chemical characterization and the evaluation of the immunomodulatory potential of secondary metabolites deriving from the extract of *Humulus lupulus* L. (hop). Hop is a flowering perennial plant belonging to the family of Cannabaceae with a millennial history. A plethora of healthy properties has been attributed to hop and its compounds, such as antioxidant, anti-inflammatory, and anti-proliferative [4, 5], due to the various and complex content of bioactive secondary metabolites. In the natural products field, one of the main challenges is the complexity of crude extracts. In this regard, high resolution analytical techniques cover a pivotal role for the identification of novel compound and to avoid dereplication [6, 7]. In the present study, efficient and high-resolution analytical techniques, namely online comprehensive two dimensional Liquid Chromatography (LC × LC) coupled to Tandem Mass Spectrometry (MS/MS) and Direct Infusion Fourier Transform Ion Cyclotron Resonance Mass Spectrometry (DI-FT-ICR-MS) has been developed and optimized for a detailed metabolite profiling of the hop phytocomplex and to identify the main bioactive molecules (**Chapter II**). Subsequently, besides the entire phytocomplex, class specific fractions obtained by semi-preparative Liquid Chromatography, have been tested through flow cytometric assay for the ability to modulate the immune

response of CD3+ T cells and the innate compartment of CD3-CD56+ Natural Killer (NK) cells, with regard to their phenotype and cytotoxic activity (**Chapter III**).

The use of nutraceuticals in combination with probiotics as therapeutic agents for gastrointestinal disorders is rapidly moving into clinical usage ^[8]. For this reason, part of the research activity has been aimed to investigate the role of breastmilk probiotics as immunomodulators and anti-inflammatory for the prevention or reduction of necrotizing enterocolitis (NEC) in the very premature infant. In particular, molecular cutoff fractionation and ultra-high-performance liquid chromatography-tandem mass spectrometry analysis have been used for the identification and isolation of an anti-inflammatory tryptophan metabolite of *Bifidobacterium longum* subsp *infantis* (*B. infantis*) secretions, which has been then tested in human fetal small intestinal cell line and necrotizing colitis enterocytes in order to establish its anti-inflammatory effects in immature intestinal enterocytes and elucidate the mechanism of action (**Chapter IV**).

A critical and still poorly understood aspect is the metabolic stability of natural compounds, which has a deep influence on pharmacokinetic characteristics and thus their bioavailability ^[9]. For this purpose, in the next phase of the project, an ultra high performance liquid chromatography-high resolution mass spectrometry (UHPLC-HRMS) method has been developed and validated to assess the metabolic stability of hop α - and β -acids and the detection of their I and II phase metabolites *in vitro* and *in vivo* (**Chapter V**).

One of the most controversial and debated arguments is the ability of natural compounds, but also of synthetic drugs, to reach specific tissues and exploit their healthy effects. The most common methods to assess bioavailability of active

molecules employ biofluids, such as plasma concentration, as predictive indicator of tissue uptake. On the other hand, tissue analysis by LC-MS require homogenization and further extraction, which, while reflecting the total amount in the tissue, cannot provide geometric and spatial information on localization of molecules in target tissue, as well as the molecular changes following their distribution among the region of the tissues. Moreover, in modern, personalized medicine, there is the need of chemical characterization of tissue biopsies, or the evaluation of the drug distribution, and their effect in target organs. Mass spectrometry imaging (MSI) is a powerful, label-free, analytical tool that able to detect hundreds of molecules simultaneously in a single experiment, both endogenous and xenobiotics, with subsequent *in situ* visualization of the localization of each ion in a single tissue section^[10, 11]. In this work, Matrix-assisted laser desorption/ionisation mass spectrometry imaging (MALDI-MSI) methods has been developed to map the spatial distribution of both small molecule neurotransmitters and neuropeptides in rat brain sections, comparing two tissue stabilization protocols to reduce *post mortem* metabolic reactions. Subsequently, MALDI-MSI has been applied to visualize the distribution of *Humulus lupulus* L. secondary metabolites in liver samples (**Chapter VI**).

1.2. References

^[1] D’Incalci, M., Steward, W.P., Gescher, A.J. Use of cancer chemopreventive phytochemicals as antineoplastic agents. *Lancet Oncol.* 2005, 6, 899–904.

^[2] Surh, Y.J. Cancer chemoprevention with dietary phytochemicals. *Nat. Rev. Cancer* 2003, 3, 768–780.

[3] Mohamed, S.I.A., Jantan, I., Haque, Md. A. Naturally occurring immunomodulators with antitumor activity: An insight on their mechanisms of action. *Int. Immunopharmacol.* 2017, *50*, 291–204.

[4] Gerhauser, C., Alt, A., Heiss, H., Gamal-Eldeen, A., Klimo, K., Knauft, J., Neumann, I., Scherf, H.R., Frank, N., Bartsch, H., Becker, H. Cancer chemopreventive activity of xanthohumol, a natural product derived from hop. *Mol. Canc. Therap.* 2002, *1*, 959–969.

[5] Milligan, S.R., Kalita, J.C., Heyerick, A., Rong, H., De Cooman, L., De Keukeleire, D. Identification of a potent phytoestrogen in hops (*Humulus lupulus* L.) and beer. *J. Clin. Endocrinol. Metab.* 1999, *84*, 2249–2252.

[6] Koehn, E.F., Carter, G.T. The evolving role of natural products in drug discovery. *Nat. Rev. Drug. Discov.* 2005, *3*, 206–220.

[7] Dugo, P., Cacciola, F., Kumm, T., Dugo, G., Mondello, L. Comprehensive multidimensional liquid chromatography: theory and applications. *J. Chromatogr. A* 2008, *1184*, 353–368.

[8] Penner, R., Fedorak, R.N., Madsen, K.L. Probiotics and nutraceuticals: non-medicinal treatments of gastrointestinal diseases. *Curr. Opin. Pharmacol.* 2005, *5*, 596–603.

[9] Masimirembwa, C.M., Bredberg, U., Andersson, T.B. Metabolic stability for drug discovery and development. *Clin. Pharmacokinet.* 2003, *42*, 515–528.

[10] Norris, J.L., Caprioli, R.M. Analysis of Tissue Specimens by Matrix-Assisted Laser Desorption/Ionization Imaging Mass Spectrometry in Biological and Clinical Research. *Chem. Rev.* 2013, *113*, 2309–2342.

Chapter I: Research project presentation: Onconutraceuticals and personalized medicine: isolation, characterization, pharmacokinetics and biological evaluation of antiproliferative compounds from complex natural matrices

^[11] Caprioli, R.M., Farmer, T.B., Gile, J. Molecular imaging of biological samples: localization of peptides and proteins using MALDI–TOF MS. *Anal. Chem.* 1997, 69, 4751–4760

CHAPTER II:

Chemical profiling of bioactive constituents in hop cones and pellets extracts by online comprehensive two-dimensional liquid chromatography with tandem mass spectrometry and direct infusion Fourier transform ion cyclotron resonance mass spectrometry

Abstract

Humulus lupulus L. (hop) is highly interesting from a nutraceutical perspective. The hop phytocomplex contains a wide range of bioactive metabolites, and its characterization is challenging. To tackle such a task, in this study a combined approach consisting of online comprehensive two dimensional liquid chromatography-tandem mass spectrometry and direct infusion Fourier transform ion cyclotron mass spectrometry has been applied and compared. A reversed phase × reversed phase approach with a shifted gradient in the second dimension ensured selectivity and two dimensional space coverage. Hyphenation with an ion trap time-of-flight analyzer led to the annotation of 83 compounds in 70 min, comprising a novel quercetin derivative and six unknown bitter acids. On the other hand, the direct infusion method was able to identify 40 analytes (except isomers) with high mass accuracy (≤ 0.1 ppm) in less than 1 min analysis time. The developed approach can be used in a complementary way, combining the separation capability and high informative spectra of two dimensional liquid chromatography-tandem mass spectrometry with the ultra-high mass accuracy of direct infusion, for potential

compound discovery or the accurate profiling of bioactive compounds in different hop cultivars as well as for monitoring processing and storage of hop-based products.

2. Introduction

Humulus lupulus L., better known as hop, is a flowering perennial plant belonging to the family of Cannabaceae. Its female inflorescence, hop cones (or hops), are widely used in the brewing process, in which they play a key role in defining the aroma and bitterness of the beer, but also as a natural antibacterial agent [1]. Besides the employment in brewing industry, hops have been used for a long time as herbal medicine, especially for its antibacterial and sedative properties [2, 3]. In the last years, hop is gaining further interest in the pharmaceutical and nutraceutical sector for its antiproliferative potential [4], and phytoestrogenic activity [5], which is related to the presence of prenylated compounds such as xanthohumol and 8-prenylnaringenin. In this regard, to understand the mechanisms of different compounds and for structure activity relationship (SAR) studies, the accurate characterization of the phytocomplex is mandatory. Hop possesses a complex secondary metabolite pattern, comprising prenylated compounds, α and β bitter acids, polyphenols, and essential oils. These compounds can differ from each variety, harvesting period, processing and storage, and from fresh and dried (pellets) material [6, 7]. Different analytical methods have been employed for hops metabolite fingerprinting such as GC-MS [8], LC-MS [9], and NMR spectroscopy [10]. Many of these approaches are focused on a single class of compounds such as bitter acids or prenylflavonoids or procyanidins [11, 12] but not on the global

fingerprinting of the crude plant, which, on the other hand, can be difficult to realize with a single analytical method. Given the sample complexity, often these techniques lack enough resolution and are not sufficient to elucidate in detail the hops metabolite composition, this can lead to loss of information regarding minor or novel compounds that remain hidden behind overlapping or high abundant compounds. Comprehensive 2D-LC (LC \times LC) is one of the best strategies to obtain higher peak capacity and selectivity for the analysis of very complex samples. In this approach, the entire sample is subjected to two independent separations, the eluent from the first dimension (1D) is continuously collected and re-injected into the second dimension (2D) through an interface, that is usually a multiport switching valve, and the separated compounds can be detected with both UV and/or MS detection ^[13]. On the other hand, metabolite identification by MS detection is challenging, high mass accuracy and resolution are required to exactly calculate molecular formula that can lead to unambiguous identification through database searching. In this regard, Fourier transform ion cyclotron resonance mass spectrometry (FT-ICR-MS) is highly suitable for its intrinsic characteristics, and also allows direct injection without chromatographic separation ^[14].

2.1. Aim of the work

With the aim to provide a detailed profiling of different classes of bioactive compounds in hop, such as hydroxycinnamic acids, glycosylated flavonols, procyanindins, prenylated derivatives, and bitter acids, in this work has been applied for the first time a combined approach based on the separation capabilities of comprehensive LC \times LC coupled to photo diode array (PDA) and ion trap (IT)

TOF-MS detection together with the high mass accuracy and resolution of direct infusion FT-ICR-MS. The method is a useful tool for the simultaneous profiling of hop bioactive compounds, and, moreover, novel compounds are described here for the first time.

2.2. Results

2.2.1. Comprehensive 2-D LC-MS/MS identification of hop cones and pellets constituents

The contour plots (extracted at 280 nm) relative to the separation of the hop cones and pellets extracts are reported in **Figures 2.1** and **Figure 2.2**, respectively. A total of 83 analytes have been tentatively identified together with 18 unknown compounds (**Table 2.1**). Among them were present: hydroxycinnamic acids (10), flavonols (18), procyanidins (24), bitter acids (22), and prenylflavonoids (9). It is noteworthy that unlabeled peaks were compounds that poorly ionize in the employed MS conditions. Among hydroxycinnamic acids, chlorogenic acid isomers were detected (**peaks 1, 2, 3, 5**). Peak **1** showed a fragmentation pattern consisting of a base peak at m/z 191, resulting from the loss of the quinic acid moiety and an intense secondary fragment at m/z 179 so it was tentatively identified as 3'-caffeoylquinic acid. Peaks **2** and **3** presented both a weak secondary fragment at m/z 135, consistent with the fragmentation pattern of 5'-caffeoylquinic acid. As reported in literature ^[15], the trans isomer elutes earlier than cis, therefore they were respectively identified as trans-5'-caffeoylquinic acid and cis-5'-caffeoylquinic acid. Lastly, peak **5** presented a strong fragment at m/z 173 and a minor fragment at m/z 191, therefore it was tentatively identified as 4'-caffeoylquinic acid.

Coumaroyl and feruloylquinic acid derivatives were also present. Peaks **4**, **6**, **8**, **9** were all characterized by the same fragmentation pattern with a strong fragment at m/z 163, resulting from the neutral loss of the quinic acid moiety, and a secondary fragment at m/z 119. In particular, on the basis of the elution order, compounds **4** and **6** were tentatively assigned as *cis* and *trans*-3'-coumaroylquinic acid isomers, respectively, while **8** and **9** were identified as *cis* and *trans* 4'-coumaroylquinic acid. In fact, they presented an MS/MS fragment at m/z 173, relative to the loss of the dehydroquinic acid. Peaks **7** and **10** both showed in the MS/MS spectra a base peak at m/z 193, deriving from the loss of ferulic acid. These compounds, also referring to previously published spectra ^[16], were tentatively identified as *cis* and *trans* 3'-feruloylquinic acid. Regarding flavonol derivatives several quercetin and kaempferol glycosides were found, some of them were identified by standard retention time comparison (**14**, **15**, **21**, **37**, **38**), and by a similar MS/MS fragmentation resulting from a hexose [M-H-162]⁻ (**11**, **12**, **13**, **22**, **31**, **32**, **34**, **36**, **45**) or rutinose [M-H-308]⁻ (**14**, **37**) cleavage. LC × LC possess several advantages with respect to 1D-LC separations. As showed before, multiple compound classes can be efficiently separated in a single run. Moreover, the increased peak capacity can lead to the detection of novel compounds that remain “hidden” in LC-MS methods. In this regard, among flavonol derivatives peak **12** showed a particular fragmentation. As reported in **Figure 2.3** the MS precursor derives from in source loss of 44 Da [M-H-CO₂]⁻. MS/MS fragment at 609.1327 m/z reveals a malonyl moiety loss [M-H-86]⁻, while ion at 300.0217, belongs to the deprotonated aglycone quercetin deriving from the consecutive loss of an hexose and pentose [M-H-162-146]⁻. Finally, this compound was tentatively identified as quercetin 3-O-(malonyl-

hexoside)-O-rhamnoside, which has not been reported so far in hops by previous LC-MS methods. Peak **31** showed a similar behavior, but the fragment at m/z 285 is typical of kaempferol aglycone, thus was proposed as kaempferol 3-O-(malonyl-hexoside)-O-rhamnoside (Supporting Information Figure S2.1). Several procyanidins isomers, spanning from degree of polymerization (DP) 2 to 5, were detected. Peaks **16, 23, 27, 41, 48, 52**, all with $[M-H]^-$ at m/z 577, showed the same fragmentation pattern, with fragment at m/z 289 belong to the monomer (epi)catechin, deriving from quinone methide (QM) cleavage of the inter-flavan bond. The fragments at 425 and 407 result from a retro-Diels–Alder (RDA) mechanism $[M-H-152]^-$ and subsequent loss of water respectively, so they were identified as (epi)catechin dimers. Peaks **17, 24, 28, 42, 49, 53, 18, 25, 29, 43, 50, 54** were all characterized by the fragment at m/z 739, probably resulting from the loss of phloroglucinol unit (heterocyclic ring fission, HRF, -126 Da). These compounds were proposed as (epi)catechin trimers and tetramers, the latter detected as $[M-2H]^{2-}$ at m/z 576^[17]. Finally peaks **19, 26, 30, 44, 51, 55** were characterized by multiple losses of 289 Da, resulting from consecutive (QM) cleavages between the flavan units, and were tentatively identified as (epi)catechin pentamers^[17]. Also in this case the $[M-2H]^{2-}$ at m/z 720 was the detected form. Isomers with $DP > 2$ were detected only in cones, which can be related to degradation of higher isomers during storage or processing^[18]. The more retained compounds, in the right part of the 2D plot, were represented by bitter acids and prenylated compounds. Alpha acids (peaks: **57, 57a, 61, 67, 70, 72, 74, 76, 77, 79, 80, 87, 90, 103**) were all characterized by a similar fragmentation pattern ($-C_5H_9$; -69 Da while iso- α by $-C_6H_8O$; -96 Da), deriving from the loss of a prenyl group or side chain scission

respectively ^[19]. Whereas, β -acids (peaks: **78, 81, 82, 84, 89, 92, 93, 95**), showed the loss of 112 Da, which can be attributed to the consecutive cleavage of C₅H₉ (-69 Da) and C₃H₇ (-43 Da) groups ^[20]. Among bitter acids, compounds **66, 68, 75, 96, 102** were proposed as unknown β -acids, since they showed losses of 112 and 120 Da whereas peak **71** was proposed as unknown α -acid, showing the elimination of 96 Da. Their MS and MS/MS spectra are reported in **Figure 2.4 a, b**. Some of these compounds can be the result of oxidation reaction, which can take place during storage. Last, xanthohumol (**100**) was identified by standard retention time, while isoxanthohumol (**83**) which is characterized by same fragmentation pattern, showed a different retention time. Compounds **59** and **62** were tentatively identified as oxidized derivatives of xanthohumol [M-H+16]⁻. 8 and 6-prenylnaringenin (**94, 97**) were both characterized by the fragment at m/z 219 resulting from RDA reaction, but also in this case they were distinct by retention time difference ^[21]. It is noteworthy that resveratrol and other stilbenes were not detected in this study, probably for their low concentration, or for the MS approach used, based on data-dependent approach and not in the more sensitive selected reaction monitoring (SRM) ^[22].

Chapter II: Chemical profiling of bioactive constituents in hop cones and pellets extracts by online comprehensive two-dimensional liquid chromatography with tandem mass spectrometry and direct infusion Fourier transform ion cyclotron resonance mass spectrometry

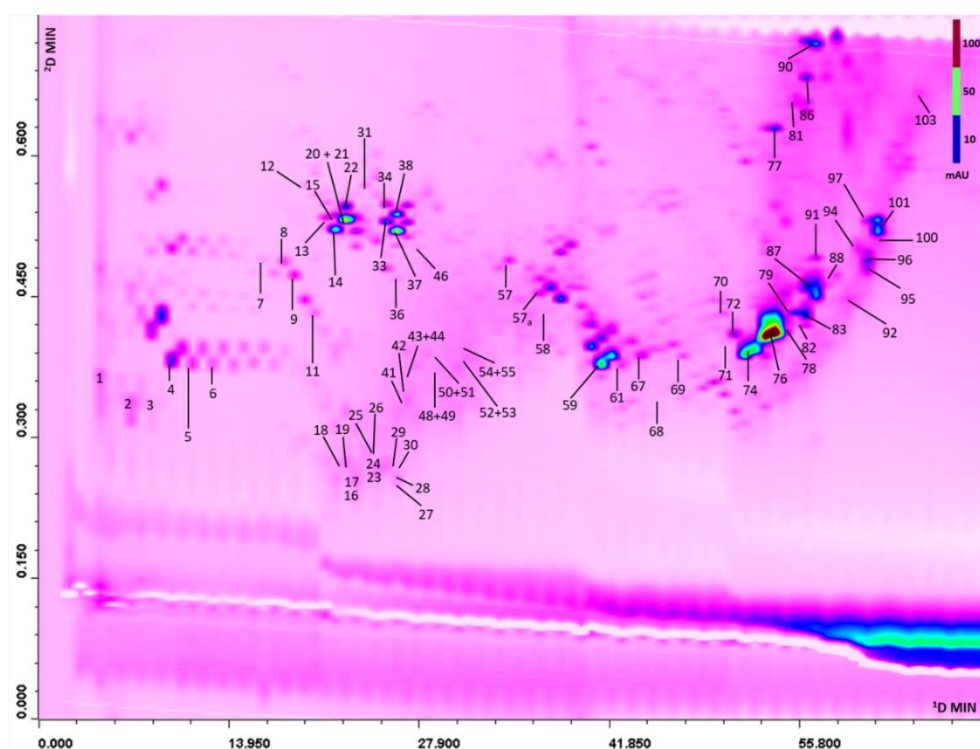


Figure 2.1. Contour plot of **hop cones** extracted at 280 nm, ¹D column: Luna[®] C18 150 × 1.0 mm, 5 μm; ²D column: Kinetex[™] C18 50 × 3.0 mm, 1.7 μm. For MS Peak identification, see Table 2.1.

Chapter II: Chemical profiling of bioactive constituents in hop cones and pellets extracts by online comprehensive two-dimensional liquid chromatography with tandem mass spectrometry and direct infusion Fourier transform ion cyclotron resonance mass spectrometry

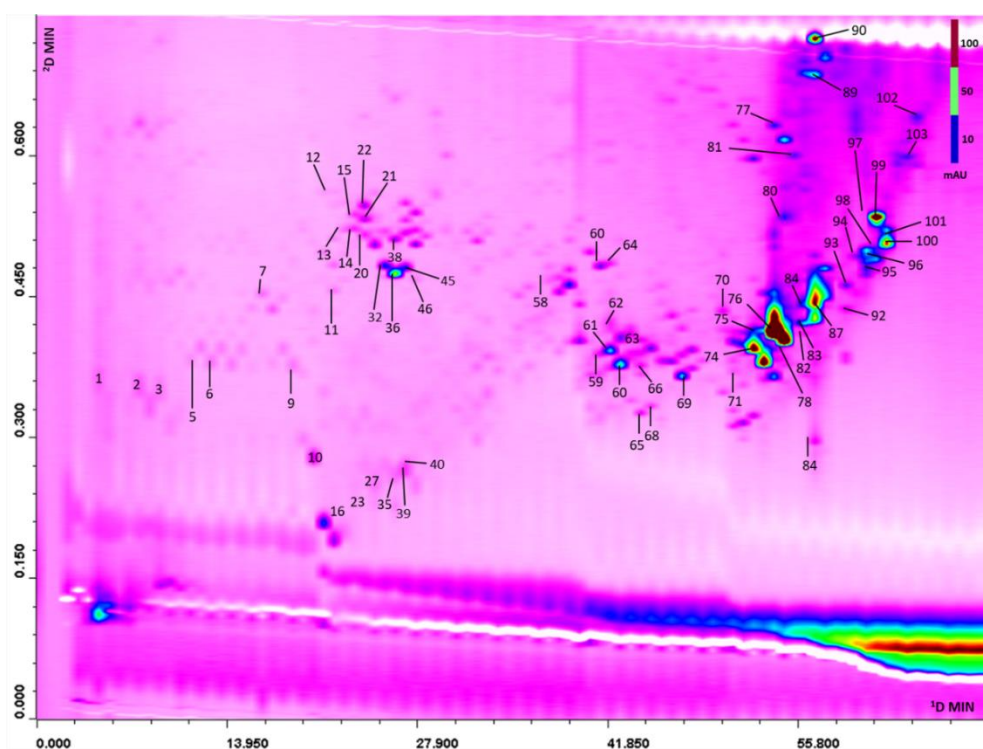


Figure 2.2. Contour plot of **hop pellet** extracted at 280 nm, ¹D column: Luna® C18 150 × 1.0 mm, 5 μm; ²D column: Kinetex™ C18 50 × 3.0 mm, 1.7 μm. For MS Peak identification, see Table 2.1.

Chapter II: Chemical profiling of bioactive constituents in hop cones and pellets extracts by online comprehensive two-dimensional liquid chromatography with tandem mass spectrometry and direct infusion Fourier transform ion cyclotron resonance mass spectrometry

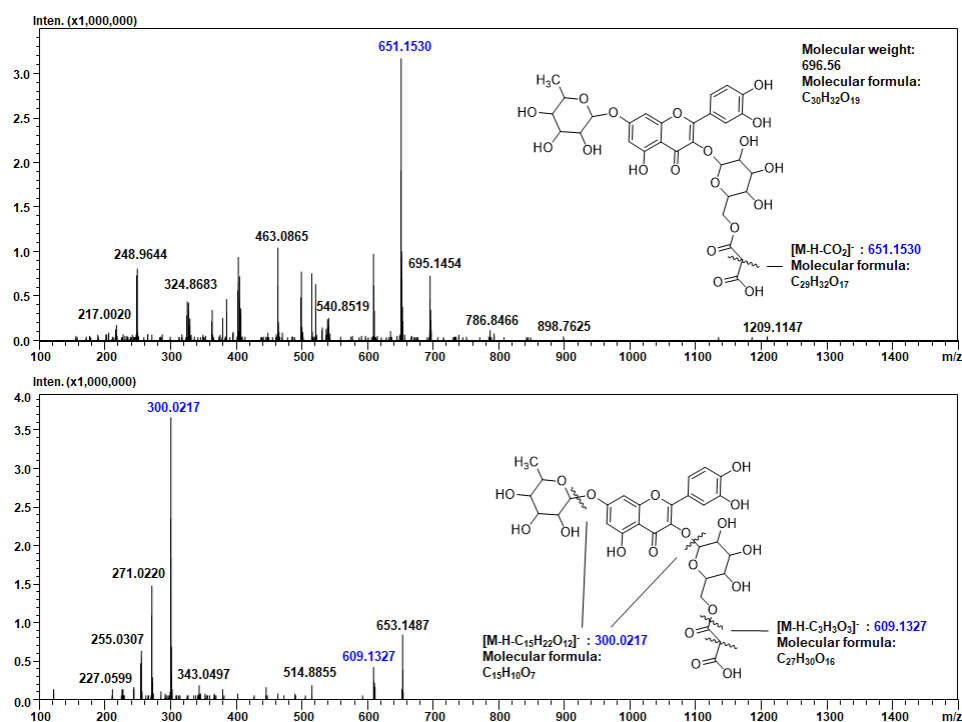


Figure 2.3. MS (top) and MS/MS (bottom) spectra showing structure elucidation and fragmentation pattern of **peak 12**.

2.2.2. Direct infusion Fourier transform ion cyclotron resonance measurements

Regarding FT-ICR MS measurements, the separation of hop compounds is achieved by high mass resolution, which in this study was roughly 150,000 at m/z 400. The obtained results can be appreciated in **Figure 2.5** showing the full scan window from 310 to 380 m/z, numerous bitter acids were simultaneously identified with minimal chance of interference from overlap of other species in the mass spectrum as highlighted in the figure expansion. The high mass accuracy allows to

unambiguous assignment of molecular formula that can be used for database searching by elemental composition, especially when combined with the high informative MS/MS spectra of IT-TOF detection. With respect to the LC × LC–IT-TOF approach, 40 compounds were identified (Supporting Information Table S2.1), in a very short analysis time (< 1 min), with a very low average mass error (0.083 ppm, **Figure 2.5**) especially for lower m/z compounds, well below the IT-TOF average value (~5 ppm). The high mass accuracy, together with isotopic fine structure, is highly beneficial for the confirmation of molecular formula of unknown compounds, such as the unknown bitter acids derivatives **66**, **68**, **71**, **96**, **102** (corresponding to **20**, **23**, **36**, **39** in Supporting Information Table S2.1). As highlighted in **Figure 2.4 c, d**, showing the isolation and fragmentation of peaks 66 and 71 by FT-ICRMS/MS, higher quality spectra were obtained for these compounds. The high mass accuracy obtained for the fragments, further confirmed their tentative identification as β (–112 Da) and α (–96 Da) acids respectively.

The RSDs of peak intensities were ≤ 20% (calculated over five consecutive infusions) for all detected peaks, which demonstrated a good stability and reproducibility of the DI-FT-ICR method.

Chapter II: Chemical profiling of bioactive constituents in hop cones and pellets extracts by online comprehensive two-dimensional liquid chromatography with tandem mass spectrometry and direct infusion Fourier transform ion cyclotron resonance mass spectrometry

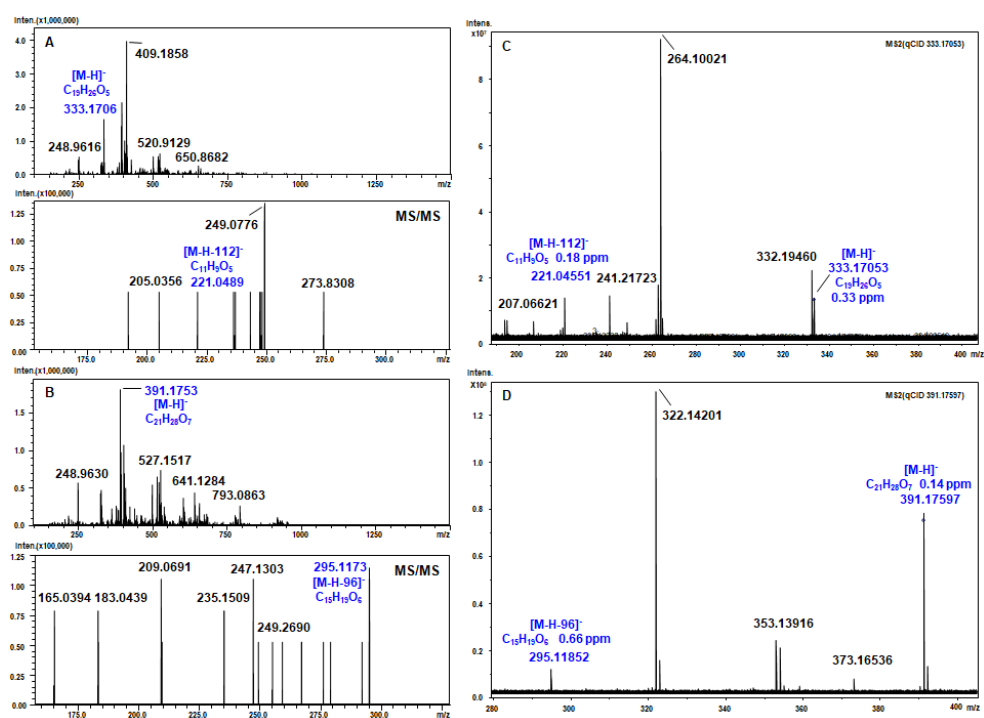


Figure 2.4 a-d. IT-TOF (a, b) and FT-ICR (c, d) spectra of unknown bitter acids (peaks 66, 71).

Chapter II: Chemical profiling of bioactive constituents in hop cones and pellets extracts by online comprehensive two-dimensional liquid chromatography with tandem mass spectrometry and direct infusion Fourier transform ion cyclotron resonance mass spectrometry

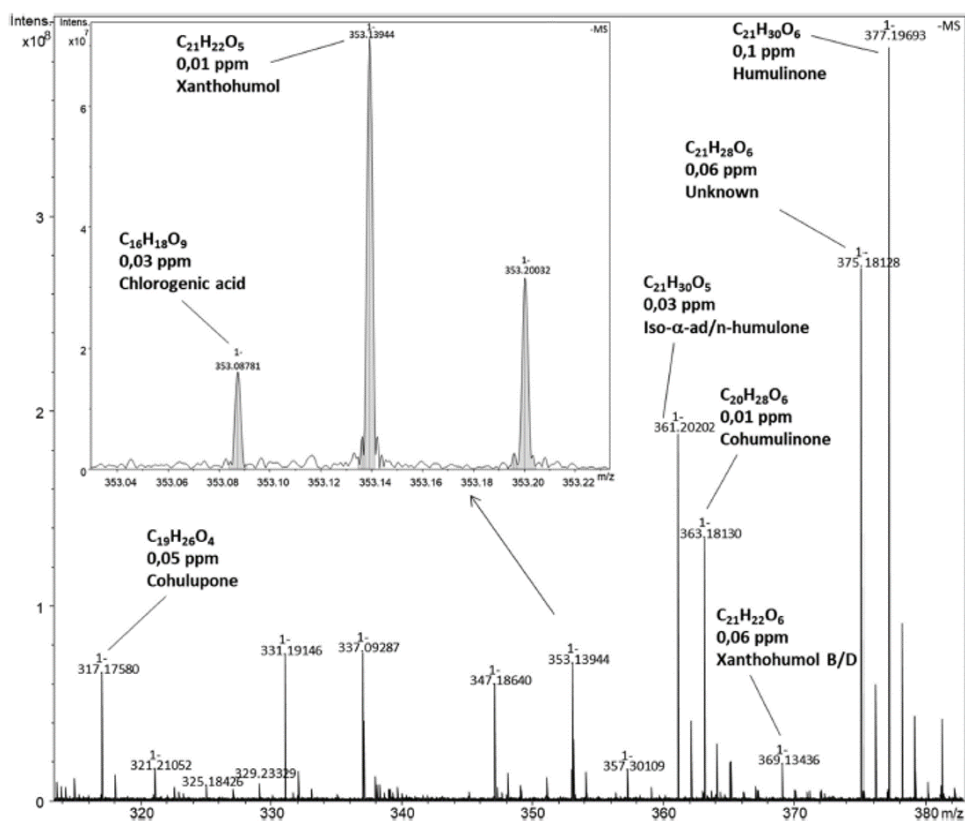


Figure 2.5. Full scan (m/z region 310–380) of DI-FT-ICR-MS showing mass accuracy and compound identification based on molecular formula.

2.2.3. System performance

System performance, in terms of peak capacity values, is reported in Supporting Information Table S2.2. The peak capacity of the LC \times LC system can be calculated by multiplying the individual peak capacities obtained for the two dimensions, resulting in a value of 2418. However, this value is only theoretical and should be

taking into account the undersampling effect ^[23] using Eq. (1), in which β is the correction factor described as:

$$\beta = \sqrt{1 + 3.35 \left(\frac{{}^2t_c}{1w} \right)^2} \quad (1)$$

Where 2t_c is 2D cycle time (which is equal to the 2D gradient time, plus the 2D re-equilibration time), and w the average 1D peak width. After this correction a peak capacity of 1478 was calculated. Moreover, the degree of dissimilarity between the two separation dimensions, or the orthogonality (A_0) of the system, must be considered ^[24, 25]. Finally, the value of 756 was obtained, which is similar to previous $RP \times RP$ approaches ^[26, 27] detailed calculation are reported in Supporting Information. To assess the repeatability, $LC \times LC$ analyses were run in triplicate, the average CV% values ≤ 0.1 and 10% for retention time and peak areas respectively (Supporting Information Table S2.3).

2.3. Discussion

The search for bioactive compounds deriving from natural or food origin is of particular interest in drug discovery, for the pharmaceutical and nutraceutical industry. In this regard, the development of advanced analytical techniques is a fundamental requirement to achieve an accurate characterization of multicomponent mixtures and link a potential effect to the presence of specific metabolites in a phytocomplex. Online comprehensive two dimensional Liquid Chromatography ($LC \times LC$), taking advantage of two different separation methods, is one of the best strategies to simplify very complex samples prior to MS analysis, expanding the potential of the MS itself in terms of sensibility and identification

capability [28]. 2D GC–MS techniques have been previously applied to the characterization of volatile fraction of hops [8, 29], whereas a stop flow 2D-LC method has been applied non-volatile metabolite characterization [30] but not in continuous comprehensive LC \times LC and without tandem MS detection. Here, LC \times LC-MS/MS platform has been applied for the detailed and multiclass accurate profiling of secondary metabolite extracted from two type of commercial hop, dried pellet and fresh cones.

In comprehensive LC \times LC, usually the two dimensions should employ different separation mechanisms to maximize the orthogonality of the system. The choice of ¹D column has a significant impact on the selectivity and peak distribution in the 2D space. Moreover, the employment of narrow or microbore columns is beneficial to inject low volumes onto the ²D column [13]. In our approach, we tested both a microbore RP column and a narrow-bore HILIC stationary phases. The coupling of HILIC with RP can provide high levels of orthogonality [26]. Despite this, an insufficient retention of most analytes was observed with the 2.0 mm i.d. HILIC column (Supporting Information Figure S2.2). In particular, the entire fraction of α - and β -acids, which are the most hydrophobic compounds, was not retained, also employing a gradient starting from lowest possible percentage of water, together with a short isocratic step at the beginning of the run (detailed conditions are given in the Supporting Information). Thus, this stationary phase was not suitable for this sample. On the other hand, with the 1.0 mm i.d. RP column, a good retention and peak distribution were obtained. To increase the differences with respect to the ²D, carried out with the same separation mode, different organic modifiers (CH₃OH and ACN) and pH conditions were tested. The best results were obtained employing a

pH of 9 and with ACN as phase B (Supporting Information Figure S2.3). The effect of gradient time and injection volume were also evaluated. An injection volume of 2 μ L was selected together with a slow gradient ramp; to sample more efficiently ¹D peaks, these conditions were used for ¹D in LC \times LC. Since the ²D was also performed in RP mode, a shifted gradient mode was considered (Supporting Information Figure S2.4), in which the percentage of organic solvent changes according to the property of the eluted fraction. This approach is highly useful in RP \times RP separations to increase the peak distribution across the 2D space ^[31]. As can be appreciated from contour plots in Figures 2.1 and Figure 2.2 peaks spread across the 2D separation space and not along a diagonal line, clearly indicating the benefits of the shifted gradient approach in the ²D of RP \times RP separations ^[32]. A slight ²D retention time shift can be noted for peaks **4** and **6**. This is due to the employment of older generation ten-port two-position switching valve, that, differently from last generation eight port valves that characterized by exactly symmetrical flow path, (denoted also as the four-port duo valves), possess still minimal differences ^[33]. Moreover, also their large ¹D peak width could contribute to this slight offset. However, this effect was not a problem in the identification of compounds, thanks to extracted ion chromatograms (EIC). Symmetrical peak shape was obtained for almost all other peaks, except for peaks **74** and **76** that were partially co-eluted in both samples, probably for their high concentration that led to peak broadening.

A sub-2 μ m RP core-shell column was selected, the performance in the ²D of LC \times LC for this column were reported previously ^[27]. The ²D was carried out at high flow rate (2.2 mL/min) and with a column temperature of 55 $^{\circ}$ C, in these conditions

an optimum compromise among backpressure values and reconditioning time was obtained, within the total D² analysis time of 45 s. These conditions were employed for the LC × LC final setup. Hyphenation with an ion trap time-of-flight analyzer led to the detection of a number of compounds higher than previous profiling analyses on hop carried out by MS or combined techniques [7, 10, 34], comprising a novel Quercetin derivative and six unknown bitter acids. Multiple compound classes were simultaneously identified and separated, without any particular extraction process or fractionation [10, 34], presenting an exhaustive snapshot of the molecules that constitute the hop phytocomplex which may be valid candidates for bioactivity studies. Furthermore, by comparing two types of matrices, it was shown that oligomeric procyanidins from dimer to pentamer were detected exclusively in fresh cones, probably due to the reduction of their content following the drying and compression processes for pellet production [6, 35], while prenylflavonoids and bitter acids profiles remained almost unchanged.

FT-ICR MS, for its high mass accuracy, resolution, and wide dynamic range, represents a useful tool for metabolomics and profiling studies [14, 36]. Differently from LC × LC–IT–TOF approach, a key advantage of the direct infusion approach relies on considerable reduction of the analysis time. This was kept below 1 min (compared to the 70 min of the LC × LC approach) per sample by introduction of the sample in infusion mode and accumulating 16 or 32 scans, with a resolution of approximately 150.000 at m/z 400. In addition, a drastic reduction of the solvent consumption is achieved. This aspect is really useful for high-throughput studies, which could be correlated to statistical analysis. Moreover, to not incur in ICR cell oversaturation, the concentration of sample used for the DI-FT-ICR was diluted

1000 times with respect to the LC \times LC method, highlighting the sensitivity of the full-scan direct injection method and the need of very low amounts of sample. Clearly, in comparison to the LC \times LC-MS/MS approach, the isomers that are resolved by chromatography can not be differentiated. Moreover, some compounds were not detected probably due to ion suppression and space charge effects in some m/z regions, due to the simultaneous arrival of multiple ions into the ESI source [37]. It should be pointed out that for all these compounds, as well as for peaks 12 and 31, other analytical techniques complementary to MS [38], such as NMR spectroscopy or isolation of pure compounds, are mandatory to confirm their identification. Nevertheless, the combination of LC-free and LC-based MS methods represent a powerful tool for deep characterization of complex, multi-analyte, natural matrices.

Chapter II: Chemical profiling of bioactive constituents in hop cones and pellets extracts by online comprehensive two-dimensional liquid chromatography with tandem mass spectrometry and direct infusion Fourier transform ion cyclotron resonance mass spectrometry

Table 2.1. LC × LC-PDA-IT-TOF characterization of hop cones and pellets extracts.

Peak	t_r	Compound	[M-H] ⁻	[MS/MS]	Error (ppm)	PDA λ_{max} (nm)	Molecular Formula	Cones	Pellets
<i>Hydroxycinnamic acid</i>									
1	4.87	3'- caffeolquinic acid (Chlorogenic acid)	353.0850	191.0625, 179.0385	0.85	320	C ₁₆ H ₁₈ O ₉	✓	✓
2	7.12	5'- caffeolquinic acid (Neo Chlorogenic acid) trans	353.0863	191.0659, 135.0522	-4.35	322	C ₁₆ H ₁₈ O ₉	✓	✓
3	8.58	5' - caffeolquinic acid (Neo chlorogenic acid) cis	353.0858	191.0588, 179.0534 135.0556	-4.28	322	C ₁₆ H ₁₈ O ₉	✓	✓
4	10.13	3'- coumaroylquinic acid cis	337.0922	163.0407, 119.0394	-2.67	304	C ₁₆ H ₁₈ O ₈	✓	×
5	11.62	4' - caffeolquinic acid	353.0891	173.0852, 191.0606	-4.25	322	C ₁₆ H ₁₈ O ₉	✓	✓
6	13.10	3'- coumaroylquinic acid trans	337.0920	163.0407, 119.0394	-2.67	308	C ₁₆ H ₁₈ O ₈	✓	✓
7	16.95	3' - feruloylquinic acid cis	367.1034	193.0575, 134.0357 149.0674	-0.27	322	C ₁₇ H ₂₀ O ₉	✓	✓
8	18.49	4' - coumaroylquinic acid cis	337.0909	173.0470, 163.0871	-5.93	226, 310	C ₁₆ H ₁₈ O ₈	✓	×
9	19.20	4' - coumaroylquinic acid trans	337.0944	173.0470, 163.0871	4.45	226, 310	C ₁₆ H ₁₈ O ₈	✓	✓
10	20.52	3' - feruloylquinic acid trans	367.1040	193.0516, 134.0216	1.36	322	C ₁₇ H ₂₀ O ₉	×	✓

Chapter II: Chemical profiling of bioactive constituents in hop cones and pellets extracts by online comprehensive two-dimensional liquid chromatography with tandem mass spectrometry and direct infusion Fourier transform ion cyclotron resonance mass spectrometry

Flavonols									
11	20.68	Quercetin 3-O-(2-rhamnosyl)-hexoside	755.2036	301.0333, 255.0535 271.0211	-0.53	256, 299	C ₃₃ H ₄₀ O ₂₀	✓	✓
12	20.82	Quercetin 3-O-(malonyl-hexoside)-O-rhamnoside	651.1530	300.0261, 271.0220 255.0307	0.61	311	C ₂₉ H ₃₂ O ₁₇	✓	✓
13	21.52	Quercetin 3-O-rhamnosyl-hexoside	609.1412	301.0250, 271.0241 255.0287	-1.81	255, 352	C ₂₇ H ₃₀ O ₁₆	✓	✓
14	22.27	Rutin [#]	609.1445	301.0362, 255.0306 271.0269	-3.45	255, 352	C ₂₇ H ₃₀ O ₁₆	✓	✓
15	22.29	Quercetin 3-O-galactoside [#]	463.0855	301.0346, 271.0255 255.0290	-3.89	255	C ₂₁ H ₂₀ O ₁₂	✓	✓
20	23.01	Quercetin 3-O-di-hexoside	609.1445	301.0362, 255.0306 271.0269	-4.43	353	C ₂₇ H ₃₀ O ₁₆	✓	✓
21	23.02	Quercetin 3-O-glucoside [#]	463.0855	301.0346, 271.0255 255.0290	-4.53	255	C ₂₁ H ₂₀ O ₁₂	✓	✓
22	23.03	Quercetin 3-O-(acetyl)-hexoside	505.0972	301.0381, 271.0204 255.0288	-3.17	311	C ₂₃ H ₂₂ O ₁₃	✓	✓
31	24.57	Kaempferol 3-O-(malonyl-hexoside)-O-rhamnoside	635.1601	285.0384, 593.1373 255.0300 227.0416	0.63	262, 345	C ₂₉ H ₃₂ O ₁₆	✓	×
32	25.98	Kaempferol 3-O-β-(O-malonyl)-hexoside	533.1861	251.0940, 255.8909	-2.81	262, 345	C ₂₃ H ₃₄ O ₁₄	×	✓
33	26.02	Kaempferol 3-O-di-hexoside	593.1413	285.0393, 255.0279 227.0656	-2.42	265, 344	C ₂₇ H ₃₀ O ₁₅	✓	×

Chapter II: Chemical profiling of bioactive constituents in hop cones and pellets extracts by online comprehensive two-dimensional liquid chromatography with tandem mass spectrometry and direct infusion Fourier transform ion cyclotron resonance mass spectrometry

34	26.06	Kaempferol 3-O-hexoside	447.0949	285.0433, 255.0302 227.0741	4.03	264, 345	C ₂₁ H ₂₀ O ₁₁	✓	×
36	26.72	Kaempferol 3-O-β-(6-O-malonyl)-hexoside	533.1861	251.0940, 255.8909	-2.81	262, 345	C ₂₃ H ₃₄ O ₁₄	✓	✓
37	26.77	Kaempferol 3-O-di-hexoside	593.1413	285.0393, 255.0279 227.0656	-2.22	265, 344	C ₂₇ H ₃₀ O ₁₅	✓	×
38	26.79	Kaempferol 3-O-hexoside	447.0949	285.0433, 255.0302 227.0741	-1.57	264, 345	C ₂₁ H ₂₀ O ₁₁	✓	✓
45	27.48	Kaempferol 3-O-glucoside [#]	447.0940	255.0279, 285.0377	1.57	264, 345	C ₂₁ H ₂₀ O ₁₂	×	✓
<i>Flavan-3-ols</i>									
35	26.50	Catechin [#]	289.0719	245.0784	-3.81	278	C ₁₅ H ₁₄ O ₆	×	✓
39	27.26	Epicatechin [#]	289.0711	245.1008	-2.42	278	C ₁₅ H ₁₄ O ₆	×	✓
<i>Procyanidins</i>									
16	22.70	Epicatechin dimer	577.1247	407.0662, 289.0448	-4.97	279	C ₃₀ H ₂₆ O ₁₂	✓	✓
17	22.71	Epicatechin trimer (EC-3)	865.1918	407.0696, 289.0663 449.0774, 577.1076	-4.51	283	C ₄₅ H ₃₈ O ₁₈	✓	×
18	22.72	Epicatechin tetramer (EC-4)	576.1180*	407.0828, 289.0769 425.0817	1.29	278	C ₆₀ H ₅₀ O ₂₄	✓	×
19	22.72		720.1428*	289.0673, 287.0524	-2.70	278	C ₇₅ H ₆₂ O ₃₀	✓	×

Chapter II: Chemical profiling of bioactive constituents in hop cones and pellets extracts by online comprehensive two-dimensional liquid chromatography with tandem mass spectrometry and direct infusion Fourier transform ion cyclotron resonance mass spectrometry

		Epicatechin pentamer (EC-5)		449.1207						
23	23.50	Epicatechin dimer isomer I	577.1247	407.0662, 289.0448	-5.97	279	C ₃₀ H ₂₆ O ₁₂	✓	✓	
24	23.51	Epicatechin trimer (EC-3) isomer I	865.1918	407.0696, 289.0663 449.0774, 577.1076	-4.51	283	C ₄₅ H ₃₈ O ₁₈	✓	×	
25	23.52	Epicatechin tetramer (EC-4) isomer I	576.1180*	407.0828, 289.0769 425.0817	4.02	278	C ₆₀ H ₅₀ O ₂₄	✓	×	
26	23.52	Epicatechin pentamer (EC-5) isomer I	720.1428*	289.0673, 287.0524 449.1207	5.10	278	C ₇₅ H ₆₂ O ₃₀	✓	×	
27	24.27	Epicatechin dimer isomer II	577.1288	407.0729, 289.0619	1.73	279	C ₃₀ H ₂₆ O ₁₂	✓	✓	
28	24.28	Epicatechin trimer (EC-3) isomer II	865.1864	407.0795, 289.0705	-4.51	283	C ₄₅ H ₃₈ O ₁₈	✓	×	
29	24.29	Epicatechin tetramer (EC-4) isomer II	576.1180*	407.0828, 289.0769 425.0817	1.54	278	C ₆₀ H ₅₀ O ₂₄	✓	×	
30	24.29	Epicatechin pentamer (EC-5) isomer II	720.1428*	289.0673, 287.0524 449.1207	1.20	278	C ₇₅ H ₆₂ O ₃₀	✓	×	
41	27.34	Epicatechin dimer isomer III	577.1288	289.0619, 407.0729 425.0919	1.73	279	C ₃₀ H ₂₆ O ₁₂	✓	×	
42	27.35	Epicatechin trimer (EC-3) isomer III	865.1864	289.0705, 407.0795 577.1189, 739.1430	-4.51	283	C ₄₅ H ₃₈ O ₁₈	✓	×	
43	27.36	Epicatechin tetramer (EC-4) isomer III	576.1180*	407.0828, 289.0769 425.0817	-3.52	278	C ₆₀ H ₅₀ O ₂₄	✓	×	
44	27.36	Epicatechin pentamer (EC-5) isomer III	720.1428*	289.0673, 287.0524 449.1207	-4.22	278	C ₇₅ H ₆₂ O ₃₀	✓	×	

Chapter II: Chemical profiling of bioactive constituents in hop cones and pellets extracts by online comprehensive two-dimensional liquid chromatography with tandem mass spectrometry and direct infusion Fourier transform ion cyclotron resonance mass spectrometry

48	30.34	Epicatechin dimer isomer IV	577.1288	289.0619, 407.0729 425.0905	1.73	279	C ₃₀ H ₂₆ O ₁₂	✓	×
49	30.35	Epicatechin trimer (EC-3) isomer IV	865.1864	289.0705, 407.0795 577.1302, 739.1650	-4.51	283	C ₄₅ H ₃₈ O ₁₈	✓	×
50	30.36	Epicatechin tetramer (EC-4) isomer IV	576.1180*	407.0828, 289.0769 425.0817	-2.51	278	C ₆₀ H ₅₀ O ₂₄	✓	×
51	30.37	Epicatechin pentamer (EC-5) isomer IV	720.1428*	289.0673, 287.0524 449.1207	1.51	278	C ₇₅ H ₆₂ O ₃₀	✓	×
52	31.10	Epicatechin dimer isomer V	577.1288	289.0619, 407.0729 425.1684	1.73	279	C ₃₀ H ₂₆ O ₁₂	✓	×
53	31.11	Epicatechin trimer (EC-3) isomer V	865.1864	407.0795, 289.0705	-4.51	283	C ₄₅ H ₃₈ O ₁₈	✓	×
54	31.12	Epicatechin tetramer (EC-4) isomer V	576.1180*	407.0828, 289.0769 425.0817	5.51	278	C ₆₀ H ₅₀ O ₂₄	✓	×
55	31.12	Epicatechin pentamer (EC-5) isomer V	720.1428*	289.0673, 287.0524 449.1207	3.15	278	C ₇₅ H ₆₂ O ₃₀	✓	×
<i>α-acids and derivatives</i>									
57	34.98	Cohumulone	363.1807	249.1125 275.1418 233.1746	-1.38	275, 310	C ₂₀ H ₂₈ O ₆	✓	×
57 _a	37.21	Cohumulone isomer	363.1807	249.1125, 275.1418 233.1746	-1.38	275, 310	C ₂₀ H ₂₈ O ₆	✓	×
61	42.40	Oxy-humulone	393.1912	349.2050, 263.1292 395.1898	-4.42	255, 323	C ₂₁ H ₃₀ O ₇	✓	✓

Chapter II: Chemical profiling of bioactive constituents in hop cones and pellets extracts by online comprehensive two-dimensional liquid chromatography with tandem mass spectrometry and direct infusion Fourier transform ion cyclotron resonance mass spectrometry

67	44.63	Oxy-adhumulinone	409.1879	263.1285, 295.1130 333.1577	0.98	285, 323	C ₂₁ H ₃₀ O ₈	✓	×
70	50.68	Humulinone	377.1928	263.1259, 221.0969	-5.04	285, 323	C ₂₁ H ₃₀ O ₆	✓	✓
72	51.41	Cohumulinone	363.1806	249.1106, 275.1332 233.1217	-1.65	275, 310	C ₂₀ H ₂₈ O ₆	✓	×
74	52.89	Cohumulinone isomer	363.1807	249.1125, 275.1418 233.1746	-1.38	275, 310	C ₂₀ H ₂₈ O ₆	✓	✓
76	54.41	Adhumulinone	377.1956	263.1285, 359.1793 223.1381	-2.38	285, 323	C ₂₁ H ₃₀ O ₆	✓	✓
77	54.63	Iso- α -ad/n-humulone	361.1998	363.1861, 265.1468	2.21	285, 323	C ₂₁ H ₃₀ O ₅	✓	✓
79	55.19	Deoxycohumulone	331.1920	262.1292, 194.0621	1.51	290, 335	C ₂₀ H ₂₈ O ₄	✓	×
80	55.28	Iso- α -ad/n-humulone	361.2015	265.1428, 363.1836	2.21	285, 323	C ₂₁ H ₃₀ O ₅	×	✓
87	57.44	Prehumulone	375.1818	306.1319	2.40	285, 325	C ₂₂ H ₃₂ O ₅	✓	✓
90	57.70	Cohumulone	347.1862	235.0624, 278.1176 223.0747	-0.58	285, 323	C ₂₀ H ₂₈ O ₅	✓	✓
103	65.14	Deoxyhumulone/deoxyadlupulone	345.2064	346.2135, 301.2297 221.0866	-2.03	290, 335	C ₂₁ H ₃₀ O ₄	✓	✓

Chapter II: Chemical profiling of bioactive constituents in hop cones and pellets extracts by online comprehensive two-dimensional liquid chromatography with tandem mass spectrometry and direct infusion Fourier transform ion cyclotron resonance mass spectrometry

<i>β-acids and derivatives</i>									
78	55.15	Cohulupone	317.1765	248.0959, 180.0271 152.2327	2.21	280, 335	C ₁₉ H ₂₆ O ₄	✓	✓
81	56.10	Lupulone E	415.2489	259.1037, 303.1277	-0.24	235, 360	C ₂₅ H ₃₆ O ₅	✓	✓
82	56.65	Postlupulone	385.1228	273.0903, 248.9524	-3.63	280, 335	C ₂₄ H ₃₄ O ₄	✓	✓
84	56.69	Lupulone E isomer I	415.2502	259.0984, 303.1511	3.61	235, 360	C ₂₅ H ₃₆ O ₅	×	✓
89	57.68	Lupulone E isomer II	415.2487	259.1036, 192.0597 371.2276	-0.72	235, 360	C ₂₅ H ₃₆ O ₅	×	✓
92	59.68	Colupulone	399.2541	287.1253, 219.0712	-0.25	280, 335	C ₂₅ H ₃₆ O ₄	✓	✓
93	59.71	Adlupulone	413.2709	301.1456, 276.1469	2.90	280, 335	C ₂₆ H ₃₈ O ₄	×	✓
95	61.23	Adlupulone isomer	413.2701	301.1448, 276.3570	4.36	280, 335	C ₂₆ H ₃₈ O ₄	✓	✓
103	65.14	Deoxyhumulone/deoxyadlupulone	345.2064	346.2135, 301.2297 221.0866	-2.03	290, 335	C ₂₁ H ₃₀ O ₄	✓	✓
<i>Prenylflavonoids</i>									
59	41.64	Ox-Xanthohumol derivative 1	369.1336	191.0420, 247.0340	-5.40	255, 307	C ₂₁ H ₂₂ O ₆	✓	✓

Chapter II: Chemical profiling of bioactive constituents in hop cones and pellets extracts by online comprehensive two-dimensional liquid chromatography with tandem mass spectrometry and direct infusion Fourier transform ion cyclotron resonance mass spectrometry

62	42.42	Ox-Xanthohumol derivative 2	369.1356	191.0396, 247.0338	3.25	255, 307	C ₂₁ H ₂₂ O ₆	×	✓
83	56.67	Iso-Xanthohumol	353.1392	233.0821, 189.0277 165.0467	-0.85	290, 325	C ₂₁ H ₂₂ O ₅	✓	✓
94	60.50	8-Prenyl-naringenin	339.1229	219.0672, 245.0805	-1.75	294, 337	C ₂₀ H ₂₀ O ₅	✓	✓
97	61.28	6-Prenyl-naringenin	339.1225	219.0623, 245.5915	-1.3	292, 337	C ₂₀ H ₂₀ O ₅	✓	✓
98	61.98	Desmethylxanthohumol	339.1252	150.0011, 175.0792 220.6890	4.13	370	C ₂₀ H ₂₀ O ₅	×	✓
99	62.73	Desmethylxanthohumol isomer	339.1268	150.0884, 175.0759	5.14	370	C ₂₀ H ₂₀ O ₅	✓	✓
100	62.76	Xanthohumol [#]	353.1405	233.0921, 189.0277 175.0147	-0.85	370	C ₂₁ H ₂₂ O ₅	✓	✓
101	62.79	Diprenyl naringenin	407.1885	287.1307, 243.1390	2.70	292, 337	C ₂₅ H ₂₈ O ₅	✓	✓
Unknown									
40	27.28	Unknown	557.1866	289.1074, 301.0985	2.50	273	C ₃₂ H ₂₉ O ₉	×	✓
46	28.22	Unknown	489.1038	353.9013	-5.93	266	C ₂₁ H ₃₀ O ₁₃	✓	✓
58	37.94	Unknown	237.1116	193.4907	8.77	269	C ₁₃ H ₁₈ O ₄	✓	✓
60	41.73	Unknown	195.0684	151.0749	6.77	278, 291	C ₁₀ H ₁₂ O ₄	×	✓

Chapter II: Chemical profiling of bioactive constituents in hop cones and pellets extracts by online comprehensive two-dimensional liquid chromatography with tandem mass spectrometry and direct infusion Fourier transform ion cyclotron resonance mass spectrometry

63	42.43	Unknown	251.1293	253.1937, 123.0991	1.59	268	C ₁₄ H ₂₀ O ₄	×	✓
64	42.49	Unknown	195.0684	151.0749	8.71	278, 291	C ₁₀ H ₁₂ O ₄	×	✓
65	44.58	Unknown	411.1489	233.0867, 151.0689 347.1238	0.90	273, 316	C ₁₆ H ₂₈ O ₁₂	×	✓
66	44.61	Unknown β-acid	333.1701	249.0842, 221.0769	-0.30	275	C ₁₉ H ₂₆ O ₅	×	✓
68	45.33	Unknown β-acid	333.1706	249.0766, 221.0489	-1.80	275	C ₁₉ H ₂₆ O ₅	✓	✓
69	47.61	Unknown	411.1516	233.0882, 251.0987 347.1524	0.90	275, 310	C ₁₆ H ₂₈ O ₁₂	×	✓
71	51.38	Unknown α-acid	391.1756	235.0494, 295.1238	-1.53	278	C ₂₁ H ₂₈ O ₇	✓	✓
75	53.66	Unknown β-acid	447.2495	335.1234, 262.1461 282.1230, 378.1776	-5.50	293	C ₂₉ H ₃₆ O ₄	×	✓
85	57.29	Unknown	349.1285	251.1265, 331.1070 351.1390	-2.29	270	C ₁₈ H ₂₂ O ₇	×	✓
86	56.93	Unknown	447.2382	415.2041, 233.07897 349.1997	-1.34	299	C ₂₅ H ₃₆ O ₇	✓	×
88	57.49	Unknown	375.1811	273.0805, 357.1682 251.1160	-1.84	268, 330	C ₂₁ H ₂₈ O ₆	✓	×
91	58.23	Unknown	375.1811	273.0805, 357.1682 251.1160	-1.84	268, 330	C ₂₁ H ₂₈ O ₆	✓	×
96	61.25	Unknown β-acid	305.1415	193.0946, 123.8334	-0.33	268, 330	C ₁₇ H ₂₂ O ₅	✓	✓

Chapter II: Chemical profiling of bioactive constituents in hop cones and pellets extracts by online comprehensive two-dimensional liquid chromatography with tandem mass spectrometry and direct infusion Fourier transform ion cyclotron resonance mass spectrometry

102	64.33	Unknown β -acid	351.1271	353.1918, 231.0691 188.8398	4.10	278	C ₂₁ H ₂₀ O ₅	×	✓
-----	-------	-----------------------	----------	--------------------------------	------	-----	--	---	---

* Detected as [M-2H]²⁻

Identified according to the standard retention time

2.4. Materials and methods

2.4.1. Chemicals

Ultra pure water (H₂O) was obtained by a Direct-8 Milli-Q system (Millipore, Milan, Italy), LC-MS grade acetonitrile (ACN), methanol (CH₃OH), LC-MS additives acetic acid (CH₃COOH), ammonium formate (CH₃COONH₄) were all purchased from Sigma–Aldrich (St. Louis, Mo, USA). Standards of: quercetin-3-*O*-glucoside, quercetin-3-*O*-galactoside, rutin, xanthohumol and kaempferol-3-*O*-glucoside were purchased from ExtraSynthese (Lione, France). Standards of (+)-catechin and (-)-epicatechin were purchased from Sigma Aldrich.

2.4.2. Sample preparation

Hop cones (originary of Calabria region) and pellets (variety Hallertauer Magnum and Target T90) were kindly donated by AEFEE craft brewery company (Castel San Giorgio, Salerno, Italy). Cones and pellets were grounded in a porcelain mortar, 1 g of sample was extracted with 12.5 mL of CH₃OH and kept under stirring for 15 minutes in the dark at room temperature. The operation was repeated three times. The supernatants were pooled, dried under reduced pressure and lyophilized. The sample was injected in a concentration of 20 mg/mL in the LC × LC setup whereas 10 µg/mL were infused in DI-FT-ICR-MS.

2.4.3. Columns

For LC × LC analyses a Luna[®] C18 was employed as ¹D with geometry (L × I.D): 150 mm × 1.0 mm, 5.0 µm (200 Å) from Phenomenex[®] (Castel Maggiore, Bologna, Italy), whereas a Kinetex[™] C18 50 mm × 3.0 mm, 1.7 µm (80 Å) from

Phenomenex[®] was used in the ²D. Moreover, a Luna[®] HILIC 150 mm × 2.0 mm, 3.0 μm (200 Å) from Phenomenex[®] was used for comparison purpose as first dimension column.

2.4.4. Instrumentation

Mono-dimensional LC and LC × LC analyses were performed on a Shimadzu Nexera (Shimadzu, Milan, Italy), consisting of a CBM-20A controller, four LC-30AD dual-plunger parallel-flow pumps, a DGU-20 A5 degasser, an SPD-M20A PDA detector (equipped with 2.5 μL detector flow cell volume), a CTO-20AC column oven, a SIL-30AC autosampler. The two dimensions were connected by an ultra-high pressure 10 port-two position switching valve with micro-electric actuator (model FCV-12 AH, 1.034 bar; Shimadzu, Kyoto, Japan), placed inside the column oven and equipped with two 22.5 μL stainless steel sampling loops. A 35 cm × 0.130 mm I.D. viper capillary was used to connect the autosampler to ¹D column (4.6 μL), while a 10 cm × 0.130 mm I.D viper capillary was used to connect the 10 port switching valve with ²D column (1.32 μL). All other connections were 0.130 mm I.D. and kept of the shortest length possible. A total extra-column volume of 28.6 μL was determined injecting toluene by using a zero dead volume union in place of the column. Both dimensions and the switching valve were controlled by the LCMS solution[®] software (Version 5.54, Shimadzu). The instrument was coupled online with a LCMS-IT-TOF (Shimadzu, Kyoto, Japan) equipped with an electrospray source (ESI) operated in negative mode. The LC × LC data were visualized and elaborated into two and three dimensions using Chromsquare[®] ver. 1.5.01 software (Chromaleont, Messina, Italy). Direct infusion high resolution mass

spectra were obtained on a Bruker Solarix XR FT-ICR 7-Tesla (Bruker Daltonics, Bremen, Germany) equipped with an Apollo II ESI source operating in negative-ion mode.

2.4.5. Chromatographic conditions: LC × LC-PDA-ESI-IT-TOF

¹D separation was carried out employing as mobile phases: A) 10 mM CH₃COONH₄ in H₂O adjusted to pH 9 with NH₄OH; B) ACN, with the following gradient: 0-40 min 5-30% B, 40-50 min, 35-70% B, 50-52 min, 70-98% B, 52-70 min hold 98% B. The flow rate was set to 30 μL/min. Column oven was set to 25 °C, 2 μL of extract were injected. For ²D separation mobile phases were: A) 0.1 % CH₃COOH in H₂O, B) ACN plus 0.1 % CH₃COOH v/v. The ²D separation was performed with a continuous shifted gradient approach (detailed conditions are reported in Supporting Information). Flow rate was set to 2.2 mL/min. Column oven was set to 55 °C. The modulation time was 45 s, corresponding to an injected volume of 22.5 μL. PDA detection parameters were: sampling rate 100 Hz, time constant 0.025 s, wavelength 254–500 nm. The flow from the LC was split by a tee union (Valco[®], Houston TX, U.S.A) so that 0.5 mL/min entered in the ESI source. Interface and curved desolvation line (CDL) temperature: 250 °C, nebulizing and drying gas (N₂): 1.5 and 10 L/min. Probe voltage -3.5 kV. MS Scan: 150-1600 m/z, MS/MS: Data dependent mode. Scan speed was 10 spectra/s. For the prediction of molecular formula the “Formula Predictor” software (Shimadzu) was used with the following settings: maximum deviation from mass accuracy: 10 ppm, fragment ion information, and nitrogen rule. The identification of compounds was based on accurate MS and MS/MS spectra, retention time of available standards, and

comparison with literature. Moreover the following free on-line databases were consulted: Mass bank of North America (<https://mona.fiehnlab.ucdavis.edu/>), Phenol-Explorer (www.phenol-explorer.eu) and Sirius (<https://bio.informatik.uni-jena.de/software/sirius/>) for in silico MS/MS spectra matching.

2.4.6. Direct infusion FT-ICR

For HRMS measurements, the instrument was tuned with a standard solution of sodium trifluoroacetate (NaTFA). Spectra were recorded in the range 150-1600 m/z, with an ion accumulation of 0.010 ms with 16 scan of time-domain transient signals in 2 mega-point time-domain data sets (1M). Source parameters: Dry gas temperature 200 °C, nebulizer (N₂) and drying gas (Air) 1.0 and 4.0 L/min., capillary voltage +4.0 kV. Samples were infused by a Hamilton syringe at 240 µL/h. The instrument was controlled by Bruker FTMS Control, MS spectra were elaborated with Compass Data Analysis version 4.2 (Bruker), identification of compounds based on accurate MS measurements was performed by Compound Crawler ver. 3.0 (Bruker).

2.5. Conclusions

The characterization of hop phytochemicals is a challenging task. In this approach, we investigated the composition of hop cones and pellets extracts by the combination of two different analytical methods, namely LC × LC-MS/MS and Direct Infusion FT-ICR-MS. Without any particular extraction process, the developed platform was able to detect 101 compounds, comprising a novel quercetin derivative and several unknown bitter acids. The LC × LC-IT-TOF approach was able to resolve with satisfactory selectivity multiple compound

classes, as well isomeric compounds, thanks to the coupling of different separation dimensions, and is very suitable for accurate profiling or novel compound discovery. On the other hand, the Direct Infusion FT-ICR method led to a fast and accurate profiling in a very short analysis time (< 1 min). The ultra-high mass accuracy provided can be very useful for the assignment of molecular formula, leading to more confident identification results. The combination of these two approaches can be used for the detailed profiling of bioactive compounds present in different hop varieties as well as to monitor the composition during storage or processing of hop-based formulations.

2.6. References

- ^[1] Moir, M.J. Hops A Millennium Review. *Am. Soc. Brew. Chem.* 2000, 58, 131–146.
- ^[2] Zanolli, L., Zavatti, M. Pharmacognostic and pharmacological profile of *Humulus lupulus*. *J. Ethnopharmacol.* 2008, 116, 383–396.
- ^[3] Sarris, J., Panossian, A., Schweitzer, I., Stough, C., Scholey, A. Herbal medicine for depression, anxiety and insomnia: A review of psychopharmacology and clinical evidence. *Eur. Neuropsychopharmacol.* 2011, 21, 841–860.
- ^[4] Gerhauser, C., Alt, A., Heiss, E., Gamal-Eldeen, A., Klimo, K., Knauft, J., Neumann, I., Scherf, H.R., Frank, N., Bartsch, H., Becker, H. Cancer chemopreventive activity of xanthohumol, a natural product derived from hop. *Mol. Canc. Therap.* 2002, 1, 959–969.

[5] Milligan, S.R., Kalita, J.C., Heyerick, A., Rong, H., De Cooman, L., De Keukeleire, D. Identification of a potent phytoestrogen in hops (*Humulus lupulus* L.) and beer. *J. Clin. Endocrinol. Metab.* 1999, 84, 2249–2252.

[6] Canbaş, A., Erten, H., Özşahin, F. The effects of storage temperature on the chemical composition of hop pellets. *Process Biochem.* 2001, 36, 1053–1058.

[7] Kavalier, A.R., Litt, A., Ma, C., Pitra, N.J., Coles, M.C., Kennelly, E.J., Matthews, P.D., Phytochemical and Morphological Characterization of Hop (*Humulus lupulus* L.). Cones over Five Developmental Stages Using High Performance Liquid Chromatography Coupled to Time-of-Flight Mass Spectrometry, Ultrahigh Performance Liquid Chromatography Photodiode Array Detection, and Light Microscopy Techniques. *J. Agric. Food Chem.* 2011, 59, 4783–4793.

[8] Eyres, G.T., Marriott, P.J., Dufour, J.P. Comparison of odor-active compounds in the spicy fraction of hop (*Humulus lupulus* L.) essential oil from four different varieties. *J. Agric. Food Chem.* 2007, 55, 6252–6261.

[9] Stevens, J.F., Taylor, A.W., Deinzer, M.L. Quantitative analysis of xanthohumol and related prenylflavonoids in hops and beer by liquid chromatography–tandem mass spectrometry. *J. Chromatogr. A* 1999, 832, 97–107.

[10] Farag, M.A., Porzel, A., Schmidt, J., Wessjohann, L.A. Metabolite profiling and fingerprinting of commercial cultivars of *Humulus lupulus* L. (hop): a comparison of MS and NMR methods in metabolomics. *Metabolomics* 2012, 8, 492–507.

[11] Ceslova, L., Holcapek, M., Fidler, M., Drstickova, J., Lisa, M. Characterization of prenylflavonoids and hop bitter acids in various classes of

Czech beers and hop extracts using high-performance liquid chromatography–mass spectrometry. *J. Chromatogr. A* 2009, *1216*, 7249–7257.

^[12] Olšovská, J., Kameník, Z., Čejka, P., Jurková, M., Mikyškam, A. Ultra-high-performance liquid chromatography profiling method for chemical screening of proanthocyanidins in Czech hops. *Talanta* 2013, *116*, 919–926.

^[13] Dugo, P., Cacciola, F., Kumm, T., Dugo, G., Mondello, L. Comprehensive multidimensional liquid chromatography: theory and applications. *J. Chromatogr. A* 2008, *1184*, 353–368.

^[14] Brown, S.C, Kruppa, G., Dasseux, J.L. Metabolomics applications of FT–ICR mass spectrometry. *Mass Spectrom. Rev.* 2005, *24*, 223–231.

^[15] Clifford, M.N., Kirkpatrick, J., Kuhnert, N., Roozendaal, H., Rodrigues Salgado, P. LC–MSn analysis of the cis isomers of chlorogenic acids. *Food Chem.* 2008, *106*, 379–385.

^[16] Nand, A., Abrankó, L. Profiling of hydroxycinnamoylquinic acids in plant extracts using in–source CID fragmentation. *J. Mass Spectrom.* 2016, *51*, 1130–1145.

^[17] Sommella, E., Pepe, G., Pagano, F., Ostacolo, C., Tenore, G.C., Russo, M.T., Novellino, E., Manfra, M., Campiglia, P. Detailed polyphenolic profiling of Annurca apple (*M. pumila* Miller cv Annurca) by a combination of RP–UHPLC and HILIC, both hyphenated to IT–TOF mass spectrometry. *Food Res. Int.* 2015, *76*, 466–477.

^[18] Outtrup, H., in: Hemingway, R.W, Laks, P.E, (Eds.). Proanthocyanidins, The Brewing Process, and the Quality of Beer. Plant Polyphenols, Basic Life Sciences. Springer 1992, 849–858.

[19] Quifer-Rada, P., Vallverdú-Queralt, P.A., Martínez-Huélamo, M., Chiva-Blanch G., Jáuregui, O., Estruch, R., Lamuela-Raventós, R. A comprehensive characterisation of beer polyphenols by high resolution mass spectrometry (LC-ESI-LTQ-Orbitrap-MS). *Food Chem.* 2015, *169*, 336–343.

[20] Hofte, A.J.P., van der Hoeven, R.A.M., Fung, S.Y., Verpoorte, R., Tjaden, U.R., van der Greef, J. Characterization of hop acids by liquid chromatography with negative electrospray ionization mass spectrometry. *J. Am. Soc. Brew. Chem.* 1998, *56*, 118–123.

[21] Prencipe, F.P., Brighenti, V., Rodolfi, M., Mongelli, A., dall'Asta, C., Ganino, T., Bruni, T.R., Pellati, F. Development of a new high-performance liquid chromatography method with diode array and electrospray ionization-mass spectrometry detection for the metabolite fingerprinting of bioactive compounds in *Humulus lupulus* L. *J. Chromatogr. A* 2014, *1349*, 50–59.

[22] Chiva-Blanch, G., Urpi-Sarda, M., Rotchés-Ribalta, M., Zamora-Ros, R., Llorach, R., Lamuela-Raventós, R.M., Estruch, R., Andrés-Lacueva, C. Determination of resveratrol and piceid in beer matrices by solid-phase extraction and liquid chromatography-tandem mass spectrometry. *J. Chromatogr. A* 2011, *1218*, 698–705.

[23] Filgueira, M.R., Huang, Y., Witt, K., Castells, C., Carr, P.W. Improving peak capacity in fast on-line comprehensive two dimensional liquid chromatography with post first dimension flow-splitting. *Anal. Chem.* 2011, *83*, 9531–9539.

[24] Camenzuli, M., Schoenmakers, P.J. A new measure of orthogonality for multi-dimensional chromatography. *Anal. Chim. Acta* 2014, *838*, 93–101.

[25] Pirok, B.W.J., Gargano, A.F.G., Schoenmakers, P. J. Optimizing separations in online comprehensive two-dimensional liquid chromatography. *J. Sep. Sci.* 2017, 1–31.

[26] Sommella, E., Ismail, O.H., Pagano, F., Pepe, G., Ostacolo, C., Mazzocanti, G., Russo, M., Novellino, E., Gasparrini, F., Campiglia, P. Development of an improved online comprehensive hydrophilic interaction chromatography × reversed-phase ultra-high-pressure liquid chromatography platform for complex multiclass polyphenolic sample analysis. *J. Sep. Sci.* 2017, 40, 2188–2197.

[27] Sommella, E., Pepe, G., Ventre, G., Pagano, F., Manfra, M., Pierri, G., Ismail, O., Ciogli, A., Campiglia, P. Evaluation of two sub-2 µm stationary phases, core-shell and totally porous monodisperse, in the second dimension of on-line comprehensive two dimensional liquid chromatography, a case study: separation of milk peptides after expiration date. *J Chromatogr A.* 2015, 1375, 54–61.

[28] Donato, P., Cacciola, F., Mondello, L., Dugo, P. Comprehensive chromatographic separations in proteomics, *J. Chromatogr. A.* 2011, 1218, 8777–8790.

[29] Van Opstaele, F., Praet, T., Aerts, G., De Cooman, L. Characterization of novel single-variety oxygenated sesquiterpenoid hop oil fractions via headspace solid-phase microextraction and gas chromatography-mass spectrometry/olfactometry. *J. Agric. Food Chem.* 2013, 61, 10555–10564.

[30] Blahova, E., Jandera, P., Cacciola, F., Mondello, L. Two-dimensional and serial column reversed-phase separation of phenolic antioxidants on octadecyl-, polyethyleneglycol-, and pentafluorophenylpropylsilica columns. *J. Sep. Sci.* 2006, 29, 555–566.

[31] Donato, P., Rigano, F., Cacciola, F., Schure, M., Farnetti, S., Russo, M., Dugo, P., Mondello, L. Comprehensive two–dimensional liquid chromatography–tandem mass spectrometry for the simultaneous determination of wine polyphenols and target contaminants. *J. Chromatogr. A* 2016, *1458*, 54–62.

[32] Leme, G.M., Cacciola, F., Donato, P., Cavalheiro, A.J., Dugo, P., Mondello, L. Continuous vs. segmented second–dimension system gradients for comprehensive two–dimensional liquid chromatography of sugarcane (*Saccharum* spp.). *Anal. Bioanal. Chem.* 2014, *406*, 4315–4324.

[33] Česla, P., Křenková, J. Fraction transfer process in on–line comprehensive two–dimensional liquid–phase separations. *J. Sep. Sci.* 2017, *40*, 109–123.

[34] Kavalier, A.R., Ma, C., Figueroa, M., Kincaid, D., Matthews, P.D., Kennelly, E.J. Targeted analysis of polyphenol metabolism during development of hop (*Humulus lupulus* L.) cones following treatment with prohexadione-calcium. *Food Chem.* 2014, *145*, 254–263.

[35] Di Mattia, C., Martuscelli, M., Sacchetti, G., Scheirlinck, I., Beheydt, B., Mastrocola, D., Pittia, P. Effect of fermentation and drying on procyanidins, antiradical activity and reducing properties of cocoa beans. *Food Bioprocess. Technol.* 2013, *6*, 3420–3432.

[36] Forcisi, S., Moritz, F., Kanawati, B., Tziotis, D., Lehmann, R., Schmitt-Kopplin, P. Liquid chromatography-mass spectrometry in metabolomics research: Mass analyzers in ultra high pressure liquid chromatography coupling. *J. Chromatogr. A* 2013, *1292*, 51–65.

[37] Han, F., Li, Y., Zhang, X., Song, A., Zhang, J., Yin, R. Comparative study of direct injection analysis and liquid chromatography mass spectrometry for

Chapter II: Chemical profiling of bioactive constituents in hop cones and pellets extracts by online comprehensive two-dimensional liquid chromatography with tandem mass spectrometry and direct infusion Fourier transform ion cyclotron resonance mass spectrometry

identification of chemical constituents in Kudiezi injection by FT-ICR MS. *Int. J. Mass Spectrom.* 2016, 405, 32–38.

^[38] Přichystal, J., Schug, K.A., Lemr, K., Novák, J., Havlíček, V. Structural Analysis of Natural Products. *Anal.Chem.* 2016, 88, 10338–10346.

CHAPTER III:

Immunomodulatory activity of *Humulus lupulus* L. bitter acids fraction: enhancement of natural killer cells function by NKp44 activating receptor stimulation

Abstract

Hop contains numerous metabolites with anticancer potential. Despite this, their immunomodulatory activity, and in particular of bitter acids, is unknown. In this study, we demonstrated that a hop pellet extract fraction containing bitter acids possesses immunomodulatory activity by enhancing Natural Killer (NK) cells function. After fractionation by semi-preparative Liquid Chromatography, three different fractions were obtained. The phytocomplex and the fractions were tested to verify the ability to modulate the NK compartment. Cytofluorimetric analysis revealed that a fraction containing bitter acids was able to up-regulate of NKG2D and NKp44 activating receptors. A further simplification yield a fraction mainly composed by Humulinones and Cohulupone derivatives that at the concentration of 0.1 µg/mL induced selective activation of Nkp44 receptor and enhanced the cytolytic activity of NK cells against leukemia cell line K562. Those results point out the possible use of hop bitter acids as natural immunomodulator and adjuvants in chemotherapy protocols.

3. Introduction

Numerous epidemiological data correlate the influence of dietary habits with the onset of oncologic diseases ^[1]. In this regard, the interest towards foods that,

Chapter III: Immunomodulatory activity of Humulus lupulus L. bitter acids fraction: enhancement of natural killer cells function by NKp44 activating receptor stimulation

consumed regularly, can provide benefits to the human health in reducing the onset of cancer ^[2], is continuously growing in current therapeutic protocols, and paves the way to the employment of novel nutraceuticals formulations based on phytochemical extracts with potential anticancer activity. This approach is useful not only for the prevention of cancer, but could be also a valid support to the pharmacological therapies. In fact, nutraceuticals can be used in a combined way with drugs, counteracting their side effects and lowering their dosages ^[3]. The most recent antitumor strategies involve the use of natural immunomodulators, characterized by low toxicity and lower price compared to drugs. These substances can be employed during chemotherapy, with the aim to improve the immune response against the tumors, that overcome the immune surveillance, and to reduce the suppression effect produced by the chemotherapeutic drugs ^[4]. Cytotoxic immune cells, including natural killer (NK) cells and CD8+ T cells, are important in tumor surveillance. CD8+ T cells are key players in adaptive immune responses, and have been shown to be crucial for protective responses against a wide range of tumors through cytokine expression and cytolytic activity ^[5]. Contrariwise, natural killer (NK) cells are innate immune lymphocytes involved in the early fight against viral infections, local tumor growth and even metastases, without prior immunization or activation ^[6, 7]. NK cells express various receptors, and their functions tightly depend on the balance between activating and inhibitory signals ^[8]. Normally, NK cells inhibitory receptors recognize self-MHC class I molecule in healthy cells, being so responsible of the self-tolerance ^[9]. Instead, the cancer cells loss or downregulate one or several MHC class I molecules, while overexpress ligands for activating receptors, therefore NK cells can recognize and destroy them

[10]. Unfortunately, several cancer diseases are characterized by a dysregulation of NK cell activity both in peripheral blood and tumor site and present defective expression of activating receptors and overexpression of inhibitory receptors [11]. Several phytochemicals, extracted from natural matrices, have shown to be able to enhance the cytolytic activity of NK cells by direct modulation or making target cells more susceptible [12]. In this regard, many studies have demonstrated that the flavonol quercetin and the flavanone naringenin, two polyphenols present in fruit and vegetable in a wide concentration range, induce the expression of the activating receptor [13, 14]. Moreover, resveratrol directly modulates the activity of NK cells together with the sensitization of malignant cells to NK cytotoxicity [15, 16]. *Humulus lupulus* L., better known as hop, is a flowering perennial plant belonging to the family of Cannabaceae. Its female inflorescence, hop cones, are mainly used in the brewing process, defining the aroma and bitterness of the beer, but also as natural antibacterial agent [17]. The hop phytocomplex contains numerous secondary metabolites, such as glycosylated and prenylated flavonoids, procyanidins, α and β -bitter acids and essential oils [18]. Their concentration and presence can differ from each cultivar, harvesting period, processing, and between fresh and dried (pellets) material. Hop metabolites, in particular prenylated derivatives and bitter acids, demonstrated beneficial health properties, also in the treatment of cancer [19-23].

3.1. Aim of the work

Several scientific evidences have been collected about the cancer preventive potential of hop compounds related to its antioxidant, anti-angiogenic [24] and anti-inflammatory activities [25]. Nevertheless, the immunomodulatory potential of the hop bioactive compounds, namely the ability to modulate the cytotoxic potential of

lymphocytes and in particular of innate compartment of NK cells, has been scarcely investigated. For this purpose, in the present study the ability of hop secondary metabolites to induce the finely tune of the NK immune responses has been investigated. Indeed, besides the entire phytocomplex and class specific fractions obtained through an analytical workflow were tested for the ability to target NK cell functions with regard to their phenotype and cytotoxic activity.

3.2. Results

3.2.1. Hop phytocomplex class fractionation and tentative identification by mass spectrometry

With the aim to test the immunomodulatory activity of different hop metabolites, the entire phytocomplex was fractionated in class of metabolites by Reversed Phase semi-preparative Liquid Chromatography. As can be appreciated from **Figure 3.1 a**, three main fractions were collected on the basis of the retention time, and thus hydrophobicity. Fraction A contained hydroxycinnamic acids, glycosylated flavonols and oligomeric procyanidins, fraction B was composed by α and β and iso- α bitter acids, while fractions C prenylated flavonoids (**Figure 3.1 b**). The identity of metabolites in the three fractions was assessed by further UHPLC-MS/MS analysis and supported by comparison with the MS/MS data deriving from the previously developed method (Chapter II). The list of tentatively annotated compounds is reported in Supporting Information Table S3.1.

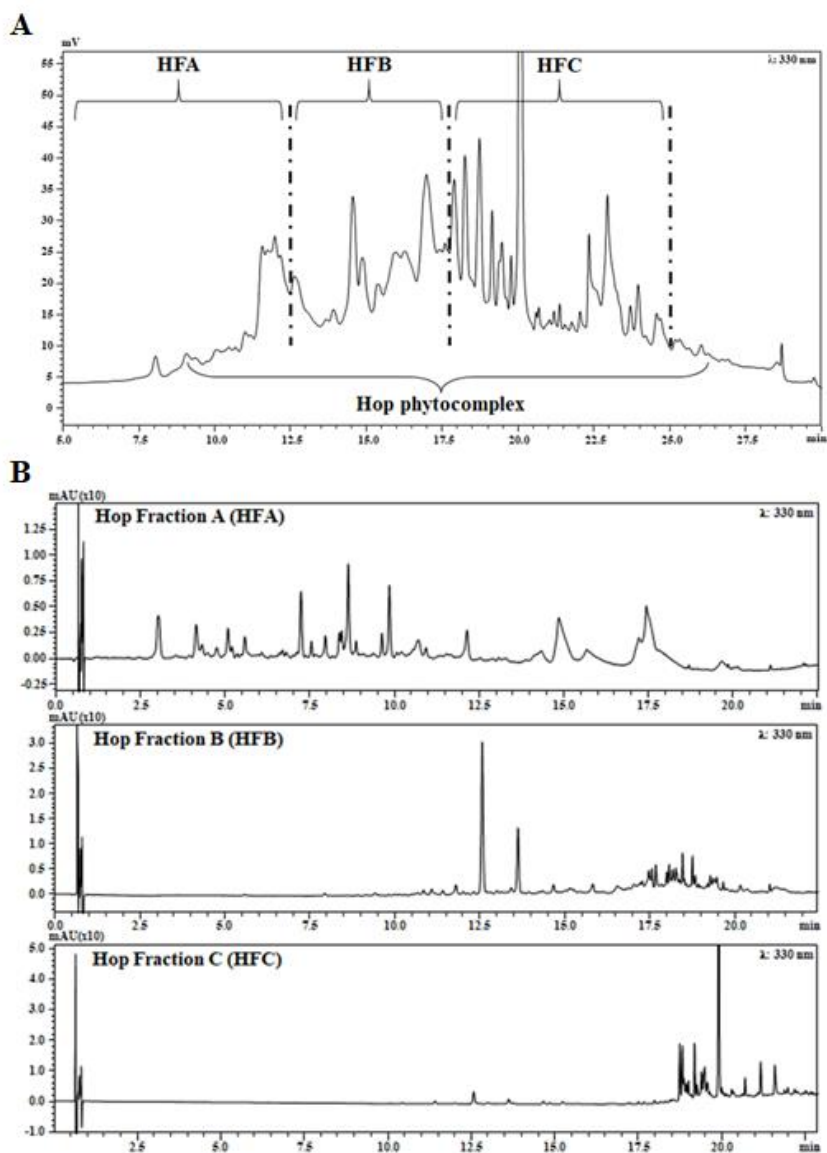


Figure 3.1. Fractionation of hop pellets phytocomplex in three different fractions by semi-preparative liquid chromatography (a) and UHPLC-UV-MS analysis of the different fractions (b).

3.2.2. Functional and phenotypical characterization of the immunomodulatory effects of hop fraction on T and NK cell compartments

Next, the ability of the three different fractions to affect lymphocyte cell population with particular attention to CD3⁺ T cells and CD3⁻CD56⁺ Natural Killer (NK) cells has been evaluated. Specifically, the effects of a selected concentration (0.5 µg/ml) of the entire phytocomplex and main fractions on human-purified Peripheral Blood Lymphocytes (PBL), stimulated with IL-2 and IL-15 cytokines for 72 h, which led to the generation of Lymphokine-activated killer LAK cells, has been analyzed. Interestingly, cytofluorimetric analysis revealed that in the presence of Fraction B (HFB), NK but not T cells displayed a sharp and significant up-regulation of NKG2D-activating receptors, whereas surface expression of CD69 early activation marker on two cell subsets was not affected (**Figure 3.2 a-d**). Furthermore, the analysis of cyto-chemokine secretory profile of resting and cytokines primed-PBL (e.g. LAK) co-stimulated with HFB revealed a peculiar dual action; while HFB had a dose-response (0.5 µg -5 µg/ml) immunosuppressive effect on resting (non-stimulated) PBL by inhibiting TNF-alpha, IFN-gamma, IL-6, MCP-1, IL-8 secretion, it didn't interfere with the activity of IL-2+IL-15 primed-PBL, with the exclusion of IL-10 secretion, cytokine critical to inhibit the immune responses (**Figure 3.2 e-m**).

This first evidence prompted us to deeply dissect hop co-stimulatory actions on NK cell compartment, upon proper cytokine priming. For this purpose, the effects of entire phytocomplex (HP) and its main fractions (HFA, HFB, HFC) on human-purified NK cells in the presence of cytokine support (IL-2 and IL-15) have been evaluated. Consistent with previous data, the costimulatory action of HFB induced

Chapter III: Immunomodulatory activity of Humulus lupulus L. bitter acids fraction: enhancement of natural killer cells function by NKp44 activating receptor stimulation

a significant up-regulation of the natural cytotoxicity receptor (NCR) NKp44 in cytokines-primed NK cells, in terms both of percentage of positive cells (**Figure 3.3 a**) and mean fluorescence intensity (**Figure 3.3 b, c**). On the contrary, HFA and HFC showed an inhibitory effect on the NKp44 expression profile in the same experimental conditions (**Figure 3.3 c**).

Chapter III: Immunomodulatory activity of *Humulus lupulus L.* bitter acids fraction: enhancement of natural killer cells function by NKp44 activating receptor stimulation

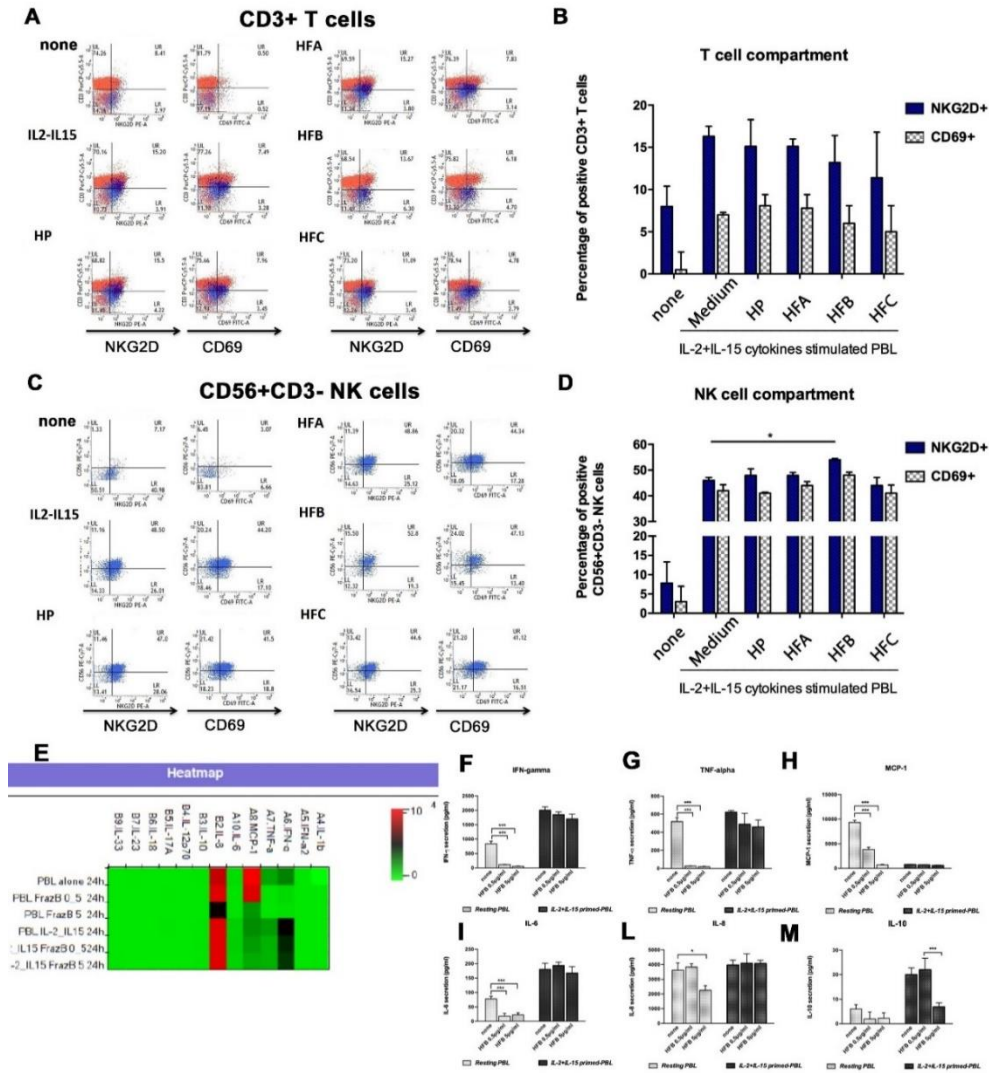


Figure 3.2. a-d) Cytofluorimetric analysis of the hop fractions activity on Human Peripheral Blood Lymphocytes. Human-purified lymphocytes (PBL), negatively selected (CD14⁻) by immunomagnetic procedure from human healthy peripheral blood mononuclear cell (PBMCs), have been pre-stimulated with IL-2 at 100 IU/ml and IL-15 at

Chapter III: Immunomodulatory activity of Humulus lupulus L. bitter acids fraction: enhancement of natural killer cells function by NKp44 activating receptor stimulation

100 ng/ml for 72 h and then treated with 0.5 µg/ml of each fraction (HFA-HFB-HFC-HP) for the last 24 h. At the end of cell culture, PBL were recovered and stained using anti-CD3, anti-CD56, anti-CD69, and anti-NKG2D mAb and analyzed by flow cytometry. Representative dot plots (left) are presented (a, c). Bars graph (right) report the percentage ± SD of CD69⁺ and NKG2D⁺ of CD3⁺ gated T cells and of CD56⁺ CD3⁻ gated NK cells (D) from 3 independent experiments using different donors (b, d). Statistical analysis is indicated (ANOVA; *P < 0.05 compared with NK cells cultured in cytokines supplemented medium). **e-m**) Levels of pro- and anti-inflammatory cytokines. Human-purified lymphocytes (PBL) have been cultured in presence or absence of IL-2 at 100 IU/ml and IL-15 at 100 ng/ml for 72 h. Where indicated, PBL have been co-stimulated with 0.5 and 5 µg/ml of HFB fraction for the last 24 h of treatment. At the end of cell culture, medium from treated PBL was assayed for circulating cytokine levels by beads-based multiplex ELISA (LEGENDplex, Biolegend, USA). Results were expressed as the mean ± SD of all sample determinations conducted in duplicate. All pairwise comparisons are statistically significant (ANOVA; *P < 0.05, **P < 0.01, ***P < 0.001).

Chapter III: Immunomodulatory activity of *Humulus lupulus L.* bitter acids fraction: enhancement of natural killer cells function by NKp44 activating receptor stimulation

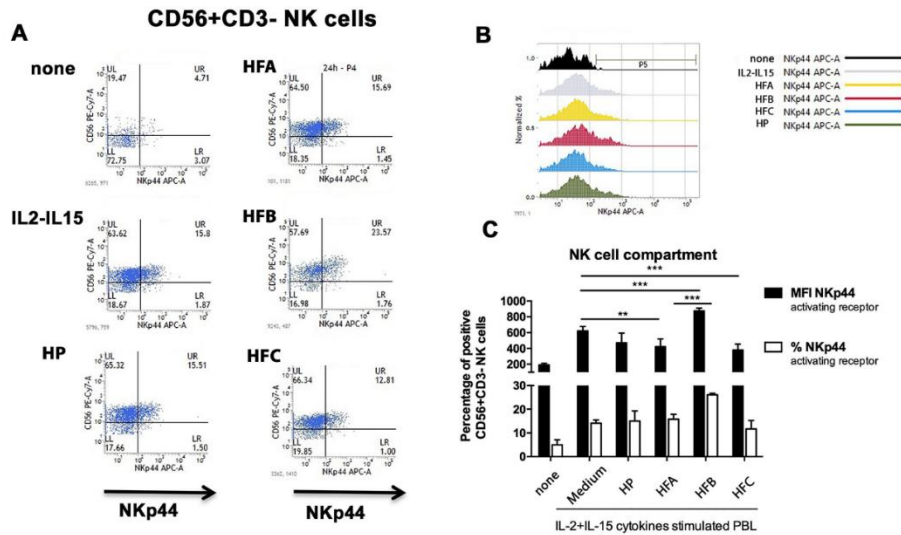


Figure 3.3. Cytofluorimetric analysis of hop fractions effects on CD56+ CD3–NK cells activation. Human-purified CD56+CD3–NK cells cultured for 72 h in complete medium (IL-2+IL-15 supplemented), with or without 0.5 µg/ml of each fraction (HFA-HFB-HFC-HP) for the last 24 h, were stained using anti-CD3, anti-NKp44 and anti-CD56 mAb and analyzed by flow cytometry. A representative dot plot (left) is presented (a). An example for cytofluorimetric histogram profiles of treated purified NK are shown (b). Bar graphs (lower right) report percentage ± SD or alternatively the mean ± SD of the mean fluorescence intensity (MFI) for NKp44 marker in CD56+CD3– gated NK cells from three independent experiments using different donors (c). Statistical analysis is indicated (ANOVA; **P < 0.01, ***P < 0.001).

3.2.3. Dose response effect of hop fraction on natural killer cell receptor repertoire

To corroborate these findings, next the effects of HFB active fraction in dose response from 0.1 µg/ml to 1 µg/ml have been investigated. Therefore, NK cells

from healthy donors were maintained in culture medium, supplemented with IL-2 and IL-15 cytokines, in the presence or absence of increasing doses of HFB. Interestingly, the stimulation of NK cells with 0.1 µg/ml and 0.5 µg/ml HFB induced a sharp up-regulation of NKp44 on cytokines-primed NK cells. Worth of note the entire phytocomplex (HP) at the concentration of 10 µg/ml showed the same stimulatory effect. On the contrary the treatment with the highest dose of HFB (1µg/ml) significantly decreased the NKp44 expression (**Figure 3.4 a**). This phenomenon might be partly explained by the desensitization of NKp44 activating receptor and its rapid internalization [26].

As the activity of NK cells is finely controlled by the relative balance of inhibitory and activating receptors on their surface, we also tested the influence of HFB fraction on KIR3DL1 and CD158k inhibitory receptors on the surface of cytokines-primed NK cells (**Figure 3.4 b**). Interestingly, HFB co-treatment at the highest dose of 1 µg/ml resulted in a significant up-regulation of both inhibitory receptors analyzed while their surface expression was not affected neither by the stimulation with 0.1 µg/ml and 0.5 µg/ml HFB, or by the entire phytocomplex HP, raising the intriguing possibility that dosage-related dual activity of HFB can diversify the human NK cell response.

3.2.4. Sub-fractionation of HFB fraction and its related immunostimulatory effects

Given the interest in the B fraction, this was further simplified (by semi-prep liquid chromatography) into three sub-fraction HFB1, HFB2, HFB3. Interestingly, flow cytometric analysis of NKp44 surface expression on stimulated NK cells, showed HFB3 0.1 µg/ml as the most active sub-fraction in inducing the activating

receptor (**Figure 3.4 c**). The main compounds in this sub-fraction are the four α -acids namely humulinone, adhumulinone, oxy-adhumulinone, cohumulinone and the β -acid cohulupone, their structures as well as tandem mass spectra are reported in **Figure 3.5**. Since no pure individual corresponding standards are available, and their chemical synthesis would be time consuming and highly expensive, these compounds were quantified using a mixture of few α - and β -acids as surrogate standards that however are slightly different from the compounds in the fraction of interest ^[27]. The quantitative analysis of HFB3, reported in Supporting Information 3.2 and Table S3.2, showed that the most abundant compounds were humulinone and cohulupone.

As it is associated with the NK cytotoxic function, it seemed interesting to determine whether the HFB sub-fractions treatment of cytokines-primed NK cells may enhance their cytolytic activity against the NK-susceptible target cell line K562 at different E:T ratios. Data on **Figure 3.4 d** clearly show that cytokines-primed NK cells displayed intermediate levels of cytotoxicity with respect to the higher efficiency of killing by IL-2-primed NK cells co-treated with HFB3. No cytotoxic improvement was detected after HFB1 and HFB2 co-treatment.

Chapter III: Immunomodulatory activity of *Humulus lupulus L.* bitter acids fraction: enhancement of natural killer cells function by NKp44 activating receptor stimulation

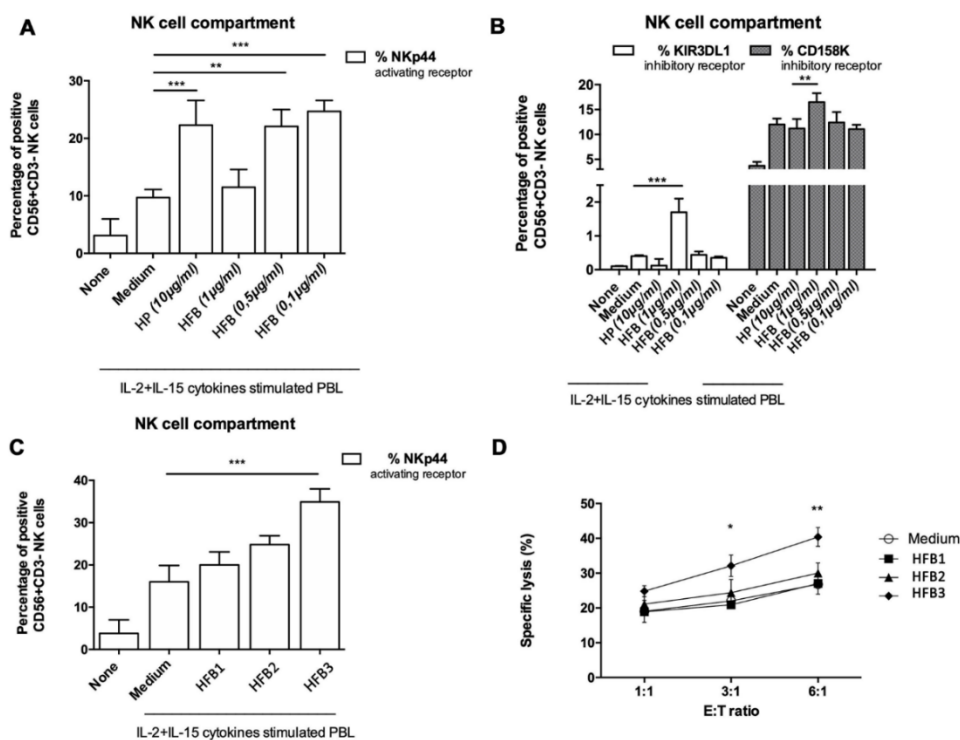


Figure 3.4. HFB sub-fraction effects on cytotoxic potential of CD56+CD3⁻ NK cells. Human-purified CD56+CD3⁻ NK cells cultured for 72 h in complete medium (IL-2+IL-15 supplemented), with or without increasing doses of fraction B (HFB) for the last 24 h, were stained using anti-CD3, anti-NKp44, anti-KIR3DL1, anti-CD158k and anti-CD56 mAb and analyzed by flow cytometry. Panel **a** shows the effects of titration of HFB on the surface expression of NKp44 activating receptor in CD56+CD3⁻NK cells compartment. Panel **b** displays the effects of different concentration of HFB on the surface expression of the inhibitory receptors KIR3DL1 and CD158K by of fraction B. Panel **c** reports the effect of different B sub-fractions (HFB1-HFB2-HFB3) on NKp44 activating receptor. Panel **d** shows the percentage of lysis mediated by HFB sub-fraction. Human-purified CD56+CD3⁻ NK cells, cultured in complete medium alone (medium; circles) or treated

Chapter III: Immunomodulatory activity of Humulus lupulus L. bitter acids fraction: enhancement of natural killer cells function by NKp44 activating receptor stimulation

with different HFB sub-fractions at a selected concentration of 0.5 µg/ml. (HFB1, squares; HFB2, triangles; HFB3, diamonds) for 72 h, were then tested for cytotoxic activity against K562 cells, as described in Materials and Methods. E:T ratios are indicated. The duration of the assay was 4 h. Results were expressed as the mean ± SD of two independent experiments conducted in triplicate. Pairwise comparisons statistically significant among treatment groups are shown (ANOVA; **P < 0.05, ***P < 0.01).

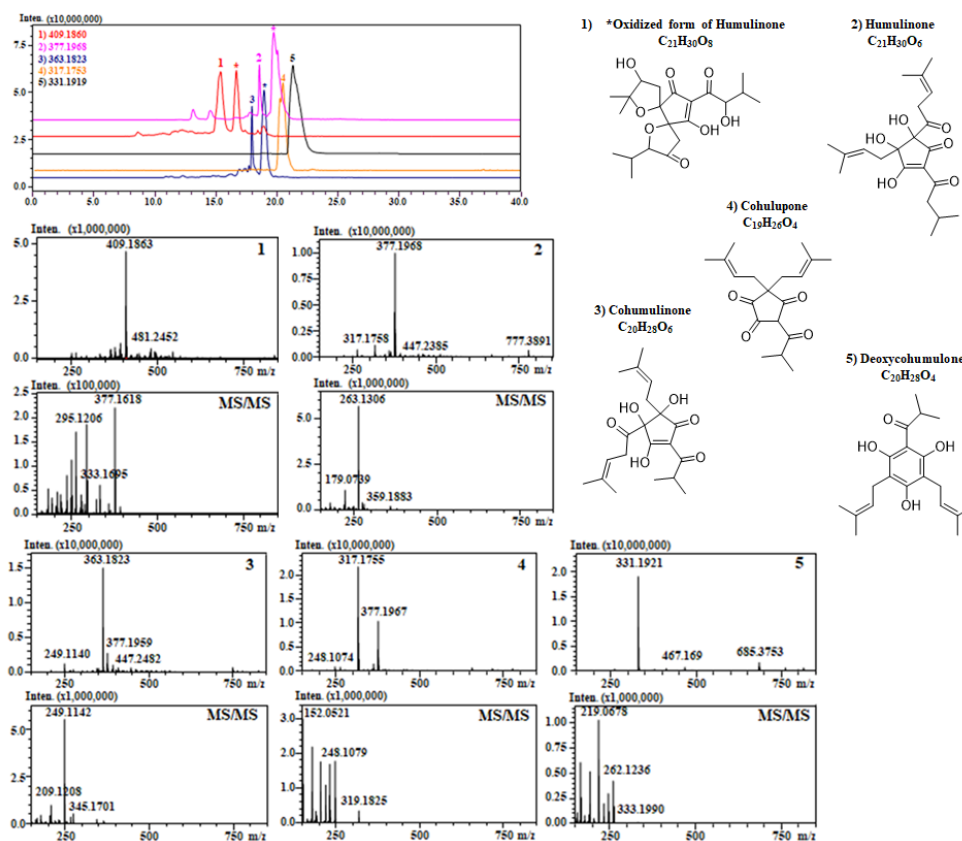


Figure 3.5. Extracted ion chromatogram (EIC) of hop sub-fraction 3 (HFB3) showing the main compounds detected in this fraction (top) HRMS and MS/MS spectra of bitter acids detected in sub-fraction HFB3 (bottom).

3.3. Discussion

There is a growing interest to use phytochemical compounds in therapeutic protocols to modulate the complex immune system in the prevention of chronic diseases, and are ideal candidates as immunostimulatory in chemotherapy without displaying side effects [28]. Several phytochemicals have been reported to be NK cell stimulators, such as Curcumin [29] and Ginsenosides [30]. Among *Humulus lupulus* compounds only Xanthohumol has been reported to affect cytotoxic activity of splenic T cells [31]. Taking advantage from an *in vitro* human experimental cell model, here we proceeded to evaluate both the entire phytocomplex and class specific fractions for their ability to finely modulate NK cells functions in both resting and in cytokines primed-conditions. While according to Gao et al. [31], the most active fraction (HFB) has been shown to inhibit the secretion of IFN-gamma and TNF-alpha by human resting PBL, no significant effect was reported under activating conditions.

Notably, HFB is comprised of bitter acids; these compounds, which are prenylated phloroglucinol derivatives, are divided into α (or humulones) and β (or lupulones), and are responsible for the beer bitterness and are highly abundant in hop cones [32]. Alpha acids are isomerized into the more water soluble iso- α acids during the wort boiling conditions of the brewing process, which are the main responsible of the bitter taste. Bitter acids, in particular β -acids, are extremely sensitive to oxidation, this is why hops are rapidly dried and pelleted [33]. Hop bitter acids have been reported as promising compounds in cancer chemoprevention [34]. Hop extracts consisting of 49.39% α -acids and 24.94% β -acids have been reported to activate the mitochondrial apoptotic pathway [35]. Both humulone and lupulone

have been reported to inhibit the proliferation of human leukemia U937 cells and colon cancer cells SW620 respectively [36,37]. Besides a direct cytotoxic action, here we uncover new complementary anti-tumor activity of this class of compounds.

Indeed, in this study selected concentrations of class specific fractions was tested on human peripheral blood mononuclear cells cultured in the presence or absence of cytokines cocktail (IL-2/IL-15), that play a major role in NK cell survival and activation (e.g. LAK cells) [38]. The results here shown demonstrated that a bitter acid fraction (HFB) potently synergizes with IL-2 and IL-15 and up-regulates NKp44 activating receptor on NK cell surface. The activity of NK cells is regulated by a fine balance of activating and inhibitory signals, mediated by different surface receptors [39]. Further, the effect achieved by test compounds was also linked to the concentration used, which is in accordance with similar studies carried out by Zhang et al. with Genistein, who reported an increased activity of NK cells using a concentration range of 0.1-0.5 mmol/L and an opposite effect at increasing concentrations [40]. Accordingly, the granule exocytosis and cytotoxicity against tumor target cells are enhanced, suggesting that this hop bitter acids fraction may serve as a novel costimulatory ligand in NK cells. In the search for the molecular mechanism subtending the specific biological activity of HBF, many evidences indicated that isoprenylated compounds, both natural and synthetic ones, can exert immunostimulatory activity by stimulating the innate immune artillery. Isopentenyl diphosphate (IPP) accumulation in myeloid cells when PBMC are treated with aminobisphosphonates potently stimulate V γ 9V δ 2 T cells in the peripheral blood [41]. At the same way, it was previously reported that the isoprenoid compound N6-Isopentenyladenosine (i6A) and its N6-benzyl adenosine derivative are endowed

with a potent ability to boost innate cytotoxic compartment of NK cells at low doses [42], while inhibiting them to the highest doses in a murine model of croton oil-induced dermatitis *in vivo* [43]. Here, the proved immune regulatory role of Hop bitter acids can represent new promising tool for immune intervention to boost immune surveillance, that will be interesting to explore in more detail in different physiopathological contexts *in vivo*. Indeed, by enhancing NK-mediated tumor elimination while mediating direct tumor cytotoxicity, it may give support in modern regimen of immunotherapy combined with chemotherapy. Moreover, these findings pave the way to drug discovery campaigns aimed at the identification of chemically accessible small molecules with immune modulatory properties.

3.4. Materials and methods

3.4.1. Chemicals

Ultrapure water (H₂O) was obtained by a Direct-8 Milli-Q system (Millipore, Milan, Italy), LC-MS-grade acetonitrile (ACN), methanol (CH₃OH), LC-MS additives acetic acid (CH₃COOH), were all purchased from Sigma-Aldrich (St. Louis, MO, USA). Standards of quercetin-3-*O*-glucoside, quercetin-3-*O*-galactoside, rutin, procyanidin B2, kaempferol-3-*O*-glucoside and xanthohumol were purchased from ExtraSynthese (Lione, France).

3.4.2. Sample preparation

Hop pellet is produced by pressing hop powders, which are subsequently packaged under vacuum and stored at -2 to +4°C [44] and this material was used in this work. Hop pellets (Target T90) were kindly donated by a local brewery company (AEFFE, Castel San Giorgio, Salerno, Italy). The whole phytocomplex

was extracted from hop pellets as reported in Chapter II. In detail, 1 g of sample was extracted with 12.5 mL of CH₃OH and kept under stirring for 15 minutes in the dark at room temperature. The operation was repeated three times. The supernatants were pooled, dried under reduced pressure and lyophilized. Sample was solubilized in methanol, filtered on a 0.45 µm nylon membrane prior injection in the LC system.

3.4.3. Cells

All donors gave written, informed consent in accordance with the Declaration of Helsinki to the use of their residual buffy coats for research purposes, under approval of the University Hospital of Salerno Review Board. Peripheral Blood Mononuclear Cells (PBMCs) from healthy donors were isolated over Ficoll-Hypaque gradients (lymphocyte separation medium; MP Biomedicals, Aurora, OH, USA). Peripheral Blood Lymphocytes (CD14-) have been negatively selected by immunomagnetic procedure (CD14 MicroBeads, Miltenyi Biotec, Bergisch Gladbach, Germany) from PBMCs and resuspended at 4×10^6 /ml in RPMI-1640 culture medium (Gibco) supplemented with 10% fetal bovine serum, penicillin/streptomycin (1%) (Lonza), L-glutamine (1%), sodium pyruvate (1%) (Lonza) and NEAA (1%) (Lonza). Cells have been pre-activated with IL-2 at 100 IU/ml (Roche GmbH) and IL-15 at 100 ng/ml (Invivogen) for 72 h and then co-stimulated with 0.5 µg/ml of each compound (HFA-HFB-HFC-HP), or 1.0 µg/ml, 0.5 µg/ml, 0.1 µg/ml of HFB, or finally with 0.1 µg/ml of each sub fraction (HFB1-HFB2-HFB3) for the last 24 h. Then, human NK cells were negatively selected from PBMCs by an immunomagnetic procedure (NK cell isolation kit; Miltenyi Biotec, Calderara di Reno, Italy). According to cytometry, typical purified NK cells

were 98% pure. NK cells were plated in 96-well round-bottom plates (Falcon, Becton Dickinson, Franklin Lakes, NJ, USA) at the concentration of 4×10^5 cells/well and treated as described above. The cell line K562 (ATCC) was maintained in RPMI complete medium. All cell cultures were maintained at 37°C in humidified 5% CO₂ atmosphere.

3.4.4. Flow Cytometry

Before the flow cytometry acquisition and analysis, the cells have been washed with PBS and resuspended in staining buffer (PBS 2%FBS). For each analysis about 1×10^6 cells have been collected. Conjugated monoclonal antibodies against CD3, CD56, CD69, NKG2D, CD107a have been purchased from BD Biosciences, CD158K and KIR3DL1 from R&D Systems, NKp44 from Miltenyi Biotec. After 20 min incubation at 4°C in the dark, cells were washed and resuspended in PBS for the FACS acquisition. For each test, cells were analyzed using FACS Verse Flow Cytometer (BD Biosciences).

3.4.5. Cytokine detection

For cytokines measurement on conditioned medium collected from stimulated PBL, a beads-based multiplex ELISA (LEGENDplex, Biolegend, USA) was used. Diluted cell culture supernatants were incubated for 2 hours with the beads and detection antibodies, followed by 30 min incubation with SA-PE as reported elsewhere ^[45]. After washing, beads were resuspended in washing buffer and acquired using a FACS VERSE flow cytometer (BD Biosciences). Data were analyzed with the LEGENDplex Data Analysis Software; concentration values

were exported to Excel and then subjected to statistical analysis by using GraphPad prism 6.0 software for Windows (GraphPad software).

3.4.6. Flow cytometric assay of NK cell cytotoxicity

Purified NK cells of healthy donors were stimulated with IL-2 and IL-15 in the presence or absence of each indicated test substance following the experimental procedure described above. Then they were used as effectors against the K562 human cell line using the fluorescent CFDA NK cytotoxicity assay. Briefly, the K562 target cells were labeled with CFDA (Molecular Probes, Eugene, OR, USA). Target cells were mixed with effector cells at different E:T ratios and incubated at 37°C for 4 h in 96-well round-bottom plates (Falcon, Becton Dickinson) in a final volume of 200 µl RPMI 1640 complete medium/well in a humidified 5% CO₂. In parallel, target cells were incubated alone to measure spontaneous cell death. At the end of the incubation time, the total contents of the U-bottom plate were transferred to Falcon tubes, put in ice, and incubated with PI, 30 µg/ml for 10 min, followed by flow cytometric analysis within 1 h. During data acquisition, a “live gate” was set on a CFDA-stained target cell population using a FL1 histogram, and 5000 target events were collected. For data analysis, target cells (R1) were analyzed further in a F1/F3 dot plot, where dead target cells (CFDA+PI+) were visualized on the upper-right quadrant. The percentage of target cell death (cytotoxicity) was calculated as follows: (% of experimental dead target cells in the sample - % of spontaneously dead target cells)/(% of maximal cytotoxicity - % of spontaneously dead target cells) × 100.

3.4.7. Phytocomplex mass spectrometry based metabolite characterization and fractionation by semi-preparative Liquid Chromatography

The whole phytocomplex was characterized as reported in Chapter II. Phytocomplex fractionation was performed on a semi-prep HPLC system LC20AP system (Shimadzu, Milan, Italy). A Luna[®] C18 column 250 mm × 10 mm, 5 μm was employed at a flow rate of 6 mL/min, mobile phase was: A) 0.1% CH₃COOH in H₂O, B) 0.1% CH₃COOH in ACN. Analysis was performed in gradient as follows: 0 min, 5%B, 10 min, 5-40%B, 15 min, 40-75%B, 17 min, 75-100%B, 22 min 100%B. Detection was performed by photo diode array (PDA) and chromatograms were extracted at 280 and 330 nm. Three fractions were collected based on the retention time. In order to assess the correct fractionation process, the obtained crude fractions were further screened on a UHPLC Nexera coupled to an IT-TOF mass spectrometer (Shimadzu, Milan, Italy). The confirmation of metabolite identity was assessed High resolution MS and MS/MS spectra, retention time of available standards, and comparison with online database (Mass bank of north America (MoNA) and PubChem) and previous MS/MS data obtained on the same MS device [Chapter II]. Detailed UHPLC-MS/MS parameters are reported in Supporting Information 3.1.

3.4.8. Statistical analysis

Statistical analysis have been performed in all the experiments shown by using the GraphPad prism 6.0 software for Windows (GraphPad software). For each type of assay or phenotypic analysis, data obtained from multiple experiments are calculated as mean ± SD and analyzed for statistical significance using the two-

tailed Student's t-test, for independent groups, or ANOVA. p values <0.05 have been considered significant (*p<0.05, **p<0.01 and ***p<0.001).

3.5. Conclusions

The employment of phytochemical based nutraceuticals as immunostimulators is growing. In this regard, *Humulus lupulus* L. contains an interesting class of compounds, known as bitter acids. The present study demonstrated for the first time that a bitter acids fraction is able to modulate the NK cell compartment increasing their cytolytic activity. In particular, a sub-fraction containing the alpha and beta acids induces activation of Nkp44 receptor and enhances cytolytic activity of NK cells against myelogenous leukemia cell line K562. These data highlights the potential of hop bitter acids as natural immunostimulants and their possible role as adjuvants in chemotherapy protocols.

3.6. References

- [1] Doll, R., Peto, R. The causes of cancer: quantitative estimates of avoidable risks of cancer in the United States today. *J. Nat. Cancer Instit.* 1981, *66*, 1191–1308.
- [2] Gupta, S.C., Kim, J.H., Prasad, S., Aggarwal, B.B. Regulation of survival, proliferation, invasion, angiogenesis, and metastasis of tumor cells through modulation of inflammatory pathways by nutraceuticals. *Cancer Metastasis Rev.* 2010, *29*, 405–434.
- [3] Shukla, Y., George, J. Combinatorial strategies employing nutraceuticals for cancer development. *Ann. N.Y. Acad. Sci.* 2011, *1229*, 162–175.

Chapter III: Immunomodulatory activity of Humulus lupulus L. bitter acids fraction: enhancement of natural killer cells function by NKp44 activating receptor stimulation

^[4] Sprengers, D., Janssen, H.L. Immunomodulatory therapy for chronic hepatitis B virus infection in children. *Fund. Clin. Pharmacol.* 2005, 19, 17–26.

^[5] Shankaran, V., Ikeda, H., Bruce, A.T., White, J. M., Swanson, P. E., Old, L. J., Schreiber, R. D. IFN and lymphocytes prevent primary tumour development and shape tumour immunogenicity. *Nature* 2001, 410, 1107–1111.

^[6] Vivier, E., Tomasello, E., Baratin, M., Walzer, T., Ugolini, S. Functions of natural killer cells. *Nat.Immunol.* 2008, 9, 503–510.

^[7] Wu, J., Lanier, L.L. Natural killer cells and cancer. *Adv. Cancer Res.* 2003, 90, 127–156.

^[8] Raulet, D.H. Interplay of natural killer cells and their receptors with the adaptive immune response. *Nat. Immunol.* 2004, 5, 996–1002.

^[9] Dondero, A., Mantovani, A., Moretta, A., Bottino, C. Human NK cells and NK receptors. *Immun. Lett.* 2014, 161, 168–173.

^[10] Mandal, A., Viswanathan, C. Natural killer cells: In health and disease. *Hematol. Oncol. Stem Cell Ther.* 2015, 8, 47–55.

^[11] Levy, E.M., Roberti, M.P., Mordoh, J. Natural killer cells in human cancer: from biological functions to clinical applications. *J. Biomed. Biotechnol.* 2011, 676198.

^[12] Burkard, M., Leischner, C., Lauer, U.M., Busch, C., Venturelli, S., Frank, J. Dietary flavonoids and modulation of natural killer cells: implications in malignant and viral diseases. *J. Nutr. Biochem.* 2017, 46, 1–12.

^[13] Bae, J.H., Kim, J.Y., Kim, M.J, Chang, S.H., Park, Y.S., Son, C.H., Park, S.J., Chung, J.S., Lee, E.Y., Kim, S.H., Kang, C.D.B. Quercetin enhances

Chapter III: Immunomodulatory activity of Humulus lupulus L. bitter acids fraction: enhancement of natural killer cells function by NKp44 activating receptor stimulation

susceptibility to NK cell-mediated lysis of tumor cells through induction of NKG2D ligands and suppression of HSP70. *J. Immunother.* 2010, 33, 391–401.

[14] Kim, J.H, Lee, J.K. Naringenin enhances NK cell lysis activity by increasing the expression of NKG2D ligands on Burkitt's lymphoma cells. *Arch. Pharm. Res.* 2015, 38, 2042–2048.

[15] Li, Q., Huyan, T., Ye, L.J., Li, J., Shi, J.L, Huang, Q.S. Concentration-dependent biphasic effects of resveratrol on human natural killer cells in vitro. *J. Agric. Food Chem.* 2014, 62, 10928–10935.

[16] Lu, C.C., Chen, J.K. Resveratrol enhances perforin expression and NK cell cytotoxicity through NKG2D-dependent pathways. *J. Cell. Physiol.* 2010, 223, 343–351.

[17] Moir, M. Hops—A Millennium Review. *J. Am. Soc. Brew. Chem.* 2000, 58, 131–146.

[18] Sommella, E., Pagano, F., Salviati, E., Chieppa, M., Bertamino, A., Manfra, M., Sala, M., Novellino, E., Campiglia, P. Chemical profiling of bioactive constituents in hop cones and pellets extracts by online comprehensive two-dimensional liquid chromatography with tandem mass spectrometry and direct infusion Fourier transform ion cyclotron resonance mass spectrometry. *J. Sep. Sci.* 2018, 41, 1548–1557.

[19] Sbardella, M., Perina, D.P., Andrade, C., Santos, C.B., Cairo, P.L.G., Marques, E.L.S., Rezende, R.P., Costa, L.B., Miyada, V.S. Effects of dietary hop β -acids or colistin on the performance, nutrient digestibility, and intestinal health of weanling pigs. *Anim. Feed Sci. Tech.* 2016, 217, 67–75.

Chapter III: Immunomodulatory activity of Humulus lupulus L. bitter acids fraction: enhancement of natural killer cells function by NKp44 activating receptor stimulation

^[20] Machado, J.C., Faria, A., Melo, A. Ferreira, M.P.L.V.O.I. Antiproliferative effect of beer and hop compounds against human colorectal adenocarcinoma Caco-2 cells. *J. Funct. Foods*. 2017, *36*, 255–261.

^[21] Gerhauser, C., Alt, A., Heiss, E., Gamal-Eldeen, A., Klimo, K., Knauff, J., Neumann, I., Scherf, H.R., Frank, N., Bartsch, H., Becker, H. Cancer chemopreventive activity of xanthohumol, a natural product derived from hop. *Mol. Cancer Ther.* 2002, *1*, 959–969.

^[22] Dorn, C., Weiss, T.S., Heilmann, J., Hellerbrand, C. Xanthohumol, a prenylated chalcone derived from hops, inhibits proliferation, migration and interleukin-8 expression of hepatocellular carcinoma cells. *Int. J. Oncol.* 2010, *36*, 435–441.

^[23] Venturelli, S., Burkard, M., Biendl, M., Lauer, U.M., Frank, J., Busch, C. Prenylated chalcones and flavonoids for the prevention and treatment of cancer. *Nutrition* 2016, *32*, 1171–1178.

^[24] Negrão, R., Costa, R., Duarte, D., Taveira, Gomes, T., Mendanha, M., Moura, L., Vasques, L., Azevedo, I., Soares, R. Angiogenesis and inflammation signaling are targets of beer polyphenols on vascular cells. *J. Cell. Biochem.* 2010, *111*, 1270–1279.

^[25] Yadav, V.R., Prasad, S., Sung, B., Aggarwal, B.B. The role of chalcones in suppression of NF- κ B-mediated inflammation and cancer. *Int. Immunopharmacol.* 2011, *11*, 295–309.

^[26] Jaeger, B.N, Vivier, E. When NK cells overcome their lack of education. *J. Clin. Invest.* 2012, *122*, 3053–3056.

Chapter III: Immunomodulatory activity of Humulus lupulus L. bitter acids fraction: enhancement of natural killer cells function by NKp44 activating receptor stimulation

^[27] Česlová, L., Holčapek, M., Fidler, M., Drštičková, J., Lísa, M. Characterization of prenylflavonoids and hop bitter acids in various classes of Czech beers and hop extracts using high-performance liquid chromatography-mass spectrometry. *J. Chromatogr. A* 2009, 1216, 7249–7257.

^[28] Mojzer, B. E., Hrnčíř, K.M., Škerget, M., Knez, Z., Bren, U. Polyphenols: Extraction Methods, Antioxidative Action, Bioavailability and Anticarcinogenic Effect. *Molecules* 2016, 21, 901.

^[29] Bhaumik, S., Jyothi, M. D., Khar, A. Differential modulation of nitric oxide production by curcumin in host macrophages and NK cells. *FEBS Letters* 2000, 483, 78–82.

^[30] Chen, F., Sun, Y., Zheng, S.L., Qin, Y., McClements, D.J., Hu, J.N., Deng, Z.Y. Antitumor and immunomodulatory effects of ginsenoside Rh2 and its octyl ester derivative in H22 tumor-bearing mice. *J. Funct. Foods* 2017, 32, 382–390.

^[31] Gao, X., Deeb, D., Liu, Y., Dulchavsky, S.A., Gautam, S.C. Immunomodulatory activity of xanthohumol: inhibition of T cell proliferation, cell-mediated cytotoxicity and Th1 cytokine production through suppression of NF-κB. *Immunopharmacol. Immunotoxicol.* 2009, 31, 477–484.

^[32] De Keukeleire, J., Ooms, G., Heyerick, A., Roldan-Ruiz, I., Van Bockstaele, E., De Keukeleire, D.J. Formation and accumulation of alpha-acids, beta-acids, desmethylxanthohumol, and xanthohumol during flowering of hops (*Humulus lupulus* L.). *J. Agric. Food Chem.* 2003, 51, 4436–4441.

^[33] Van Cleemput, M., Cattoor, K., De Bosscher, K., Haegeman, G., De Keukeleire, D., Heyerick, A. Hop (*Humulus lupulus*)-derived bitter acids as multipotent bioactive compounds. *J. Nat. Prod.* 2009, 72, 1220–1230.

Chapter III: Immunomodulatory activity of Humulus lupulus L. bitter acids fraction: enhancement of natural killer cells function by NKp44 activating receptor stimulation

[34] Knez Hrnčič, M., Španinger, E., Košir, I.J., Knez, Z., Bren, U. Hop Compounds: Extraction Techniques, Chemical Analyses, Antioxidative, Antimicrobial, and Anticarcinogenic Effects. *Nutrients* 2019, *11*, 257.

[35] Chen, W.J., Lin, J.K. Mechanisms of cancer chemoprevention by hop bitter acids (beer aroma) through induction of apoptosis mediated by Fas and caspase cascades. *J. Agric. Food Chem.* 2004, *52*, 55–64.

[36] Honma, Y., Tobe, H., Makishima, M., Yokoyama, A., Okabe–Kado, J. Induction of differentiation of myelogenous leukemia cells by humulone, a bitter in the hop. *Leuk. Res.* 1998, *22*, 605–610.

[37] Lamy, V., Roussi, S., Chaabi, M., Gossé, F., Schall, N., Lobstein, A., Raul, F. Chemopreventive effects of lupulone, a hop beta–acid, on human colon cancer–derived metastatic SW620 cells and in a rat model of colon carcinogenesis. *Carcinogenesis* 2007, *28*, 1575–1581.

[38] Leong, J.W., Chase, J.M., Romee, R., Schneider, S.E., Sullivan, R.P., Cooper, M.A., Fehniger, T.A. Preactivation with IL–12, IL–15, and IL–18 induces CD25 and a functional high–affinity IL–2 receptor on human cytokine–induced memory–like natural killer cells. *Biol. Blood Marrow Transplant.* 2014, *20*, 463–473.

[39] Koch, J., Steinle, A., Watzl, C., Mandelboim, O. Activating natural cytotoxicity receptors of natural killer cells in cancer and infection. *Trends Immunol.* 2013, *34*, 182–191.

[40] Zhang, Y., Song, T. T., Cunnick, J. E., Murphy, P.A., Hendrich, S. Daidzein and genistein glucuronides in vitro are weakly estrogenic and activate human

Chapter III: Immunomodulatory activity of Humulus lupulus L. bitter acids fraction: enhancement of natural killer cells function by NKp44 activating receptor stimulation

natural killer cells at nutritionally relevant concentrations. *J. Nutr.* 1999, *129*, 399–405.

[41] Lo Presti, E., Pizzolato, G., Corsale, A. M., Caccamo, N., Sireci, G., Dieli, F., Meraviglia, S. $\gamma\delta$ T Cells and Tumor Microenvironment: From Immunosurveillance to Tumor Evasion. *Front. Immunol.* 2018, *9*, 1935.

[42] Ciaglia, E., Pisanti, S., Picardi, P., Laezza, C., Malfitano, A.M., D'Alessandro, A., Gazzero, P., Vitale, M., Carbone, E., Bifulco, M. N6-isopentenyladenosine, an endogenous isoprenoid end product, directly affects cytotoxic and regulatory functions of human NK cells through FDPS modulation. *J. Leukoc. Biol.* 2013, *94*, 1207–1219.

[43] Ciaglia, E., Pisanti, S., Picardi, P., Laezza, C., Sosa, S., Tubaro, A., Vitale, M., Gazzero, P., Malfitano, A.M., Bifulco, M. N6-isopentenyladenosine affects cytotoxic activity and cytokines production by IL-2 activated NK cells and exerts topical anti-inflammatory activity in mice. *Pharmacol. Res.* 2014, *89*, 1–10.

[44] Canbas, A., Erten, H., Özşahin, F. The effects of storage temperature on the chemical composition of hop pellets. *Proc. Biochem.* 2001, *36*, 1053–1058.

[45] Ciaglia, E., Montella, F., Maciag, A., Scala, P., Ferrario, A., Banco, C., Carrizzo, A., Spinelli, C.C., Cattaneo, M., De Candia, P., Vecchione, C., Villa, F., Puca, A.A. Longevity-Associated Variant of BPIFB4 Mitigates Monocyte-Mediated Acquired Immune Response. *J. Gerontol. A Biol. Sci. Med. Sci.* 2019, *20*, 1–7.

CHAPTER IV:

Indole-3-lactic acid, a metabolite of tryptophan, secreted by *Bifidobacterium longum subspecies infantis* is anti-inflammatory in the immature intestine

Abstract

Necrotizing enterocolitis (NEC), a necrotic inflammation of the intestine, represents a major health problem in the very premature infant. Although prevention is difficult, the ingestion of maternal-expressed breastmilk in conjunction with a probiotic provides an interesting option for prevention. In this study, the mechanism for breastmilk/probiotic protection has been investigated. Ultra-high-performance liquid chromatography-tandem mass spectrometry was used to identify indole-3-lactic acid (ILA), a metabolite of breastmilk tryptophan, as the anti-inflammatory molecule of *B. infantis* secretions. ILA was tested on human fetal small intestinal cell line, necrotizing colitis enterocytes and also fetal human organoids, providing to be able to reduce the inflammatory cytokine IL-8 response after IL-1 β stimulus through the interaction with the factor aryl hydrocarbon receptor (AHR), preventing the transcription of IL-8. However, ILA was developmentally functional in immature but not mature intestinal enterocytes. Therefore, *B. infantis probiotics* and ingested breastmilk act in a complementary manner to produce a molecule that could become useful in the treatment of all at risk premature infants for necrotizing enterocolitis if safety and clinical studies are performed.

4. Introduction

Neonatal necrotizing enterocolitis (NEC) is an extensive intestinal inflammatory disease that affects very low birth weight premature infants generally with postmenstrual ages of 28-31 weeks ^[1]. This condition results in an inflammatory necrosis principally of the distal small intestine and the colon, leading, to considerable morbidity, mortality and medical expense ^[2].

The rapid progress of the symptoms, often within hours, requires a frequent radiological surveillance of neonates to guide management and the treatment of the disease ^[1]. In this regard, in addition to the consequences of advanced NEC in survived infant as stricture formation and short bowel syndrome ^[1, 3], it is important to not underestimate the effects that the constant radiation exposure can have on cognition, reproduction and increase the onset of chronic disease and cancer mortality risks in children ^[4]. The treatments with laparotomy and primary peritoneal drainage can also be invasive and often the result of surgery can be poor, which is why it is increasingly mandatory to invest in an effective strategy for the disease prevention.

The research group of Dr. W. Allan Walker, Director of the Division of Nutrition (DON) at Harvard Medical School (HMS), with whose collaboration this study was conducted, proved that the combination of maternal-expressed breastmilk with probiotics provides an interesting option for protection from NEC ^[5, 6]. This result is based on their previous studies. In particular, they hypothesized that NEC is in part caused by an aberrant reaction of the immature intestine to colonizing bacteria ^[7-9], when the immature intestine of the newborn interact with the enormous numbers of colonizing bacteria of the extrauterine environment ^[10,11]. In this

condition, the immature human intestinal cells favor inflammation over immune homeostasis with microbial-epithelial interaction ^[12]. Inflammation can be evoked by commensal as well as pathogenic organisms impart ^[7] because of a developmentally regulated innate immune response and an increased surface expression of TLR-4 receptors ^[13] as well as overexpressed signaling molecules (NFK β and IL-8) and under expressed regulatory molecules (SIGIRR, IRAK-M, A-20, etc.) ^[8]. However, paradoxically it has been shown that feeding mother's-expressed breastmilk or probiotics to the premature can either prevent or reduce the severity of NEC ^[14, 15]. Although expressed breastmilk contains many passively protective factors and microorganisms ^[16], has been reported that breastmilk ingestion can stimulate the proliferation of a so-called "pioneer" bacteria over formula-fed infants that are uniquely suited for activation of protective immune responses and anti-inflammation ^[17, 18].

A common "pioneer" bacterium associated with ingested breastmilk is *Bifidobacterium longum* subsp *infantis* (*B. infantis*) ^[18]. *B. infantis* secretions can protect against an IL-1 β (a common inflammatory cytokine in NEC-induced inflammation ^[19-21] and require a TLR-4 receptor to be effective ^[5, 20].

4.1. Aim of the work

As stated above, based on the previous consideration, has been recently demonstrated that feeding expressed breastmilk with *B. infantis* is clinically the best way to prevent NEC ^[5, 6]. The aim of this study was to identify the anti-inflammatory molecules of *B. infantis* secretions, provide evidence for the isolation and identification of the bioactive molecule/s and begin to determine its anti-inflammatory mechanism in the immature human and mouse small intestine.

4.2. Results

4.2.1. Secretory fractions of *Bifidobacterium longum* subsp *infantis* are anti-inflammatory with H4 cells

Bacterial secretions from *Bifidobacterium longum* subsp *infantis* were specifically separated into different sized fractions (> 3 kDa, 3-10 kDa, >10 kDa) and exposed to H4 cells before adding the inflammatory stimulus IL-1 β , which is regularly found in the intestinal secretions of prematures developing NEC [22]. A highly significant reduction in IL-8 secretion was seen with all fractions (**Figure 4.1 a**) and when the fractions were exposed to H4 cells in the absence of IL-1 β , they had no effect on inflammation (**Figure 4.1 b**) and the bacterial secretion fractions were not cytotoxic (**Figure 4.1 c**).

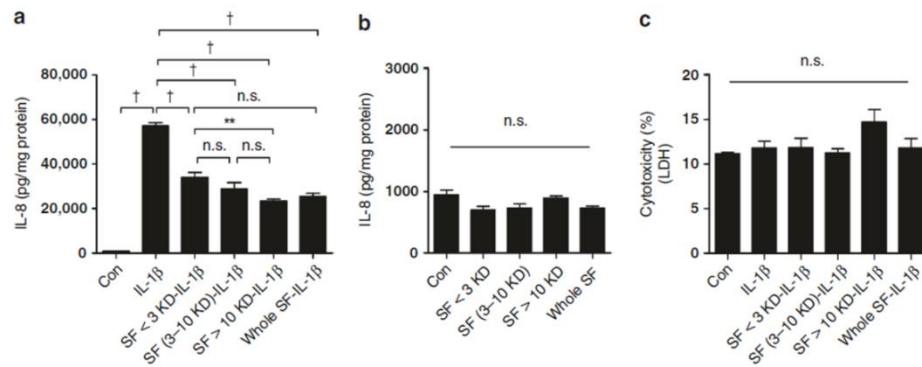


Figure 4.1. The effects of different secretory size fractions of *B. infantis* on anti-inflammation and cytotoxicity in H4 cells. H4 cells were pretreated with or without *B. infantis* secretory size fractions (SFs) before IL-1 β stimulation (**a**) or treated with SFs alone (**b**). The secretion of IL-8 (**a**, **b**) and lactate dehydrogenase (LDH) (**c**) into the cell culture supernatant was determined by ELISA and cytotoxicity assay—LDH assay. Graphs represent means \pm SEM ($n = 3$) from three independent experiments. One-way analysis of

variance (ANOVA) and Tukey's post hoc tests were used for statistical analysis (**P < 0.01, †P < 0.001, n.s., not significant).

4.2.2. Identification of the *B. infantis* anti-inflammatory secretory molecule as indole-3-lactic acid

To identify the metabolites in the different molecular weight fractions of *B. infantis* secretions, Ultra high-performance liquid chromatography (UHPLC) coupled to high resolution Mass Spectrometry (HRMS) was employed in a typical untargeted workflow [23, 24]. Reversed phase (RP) chromatography ensured a good separation of both polar and non-polar analytes. The metabolite profile of secretions revealed the presence of multiple analytes such as amino acids, sugars, dipeptides, nucleosides, glycolipids and fatty acids. By comparison of UV-MS traces relative to the separation of cell media alone and < 3 kDa, 3-10 kDa and < 10 kDa (not shown) *B. Infantis* size fractions, an intense peak possessing absorbance at 280 nm was revealed, notably, this peak was absent in the media (**Figure 4.2 a-c**). The high resolution MS spectrum showed an ion with m/z 204.0659 [M-H]⁻ in negative ESI, with a molecular formula of C₁₁H₁₁NO₃. This was identified as indole-3-lactic acid (ILA). The MS/MS fragmentation pattern and retention time were consistent with those reported in on-line spectral libraries. The identity was confirmed with MSI level 1 identification through further comparison with the standard (**Figure 4.2 d-h**). The amount of ILA in the different sized fractions was comprised between 22.17 to 33.12 µg/mL. The differences in ILA content among the fractions is probably due to different mechanical properties of the molecular cut-off centrifugal filters employed for the fractionation.

Chapter IV: Indole-3-lactic acid, a metabolite of tryptophan, secreted by *Bifidobacterium longum* subspecies *infantis* is anti-inflammatory in the immature intestine

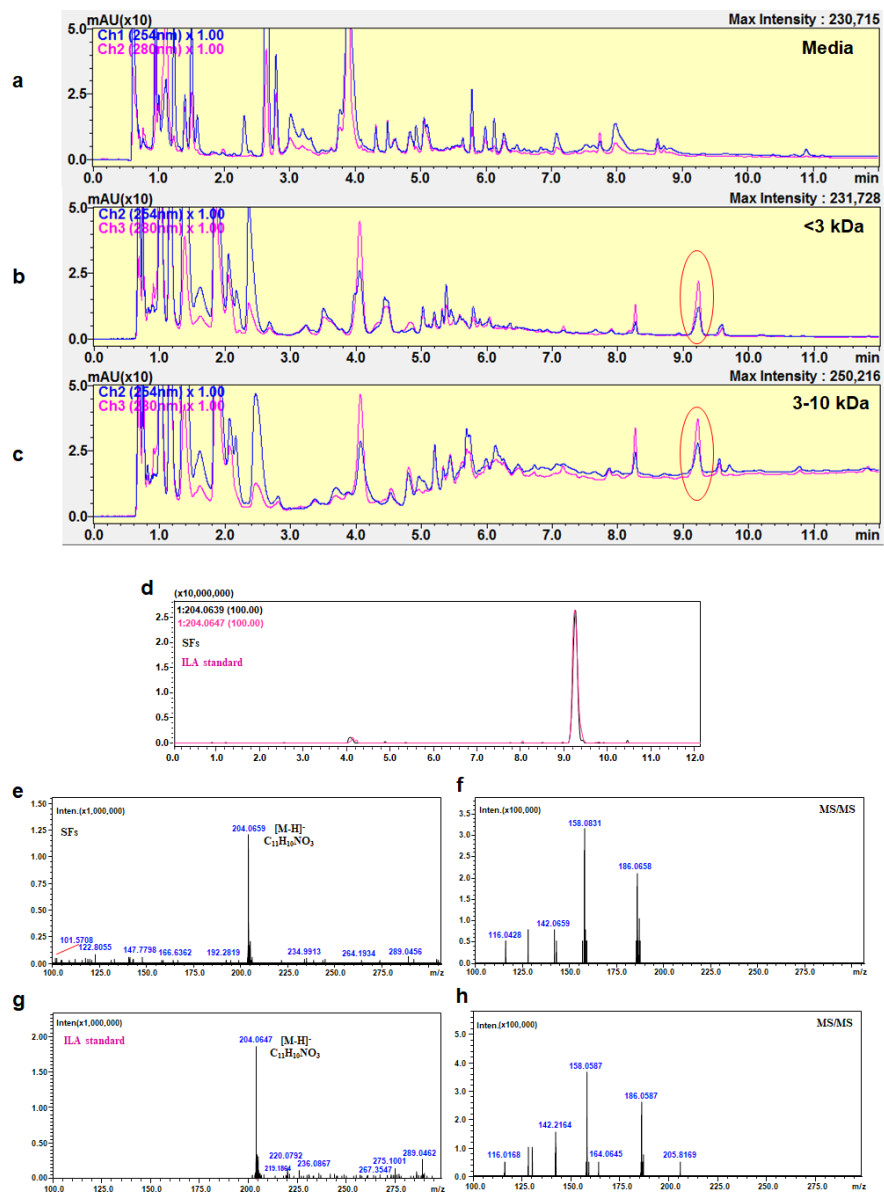


Figure 4.2. Comparison of ultra-high-performance liquid chromatography-UV (UHPLC-UV) profiles of the media, < 3 and 3–10 kDa *B. infantis* SFs, and identification of indole-

3-lactic acid (ILA) as the structure of the specific peaks from *B. infantis* SFs by an extracted ion chromatogram (EIC). **a-c**, RP-UHPLC-UV chromatograms (280 and 254 nm) showing the comparison of *B. infantis* culture media with *B. infantis* secretion size fractions < 3 and 3–10 kDa. The circle shows the ILA peak, which is absent in culture media and present in both of the *B. infantis* SFs. To confirm ILA, was compared the ILA standard compound retention time with the *B. infantis* fractions. **d**, EIC showing the ILA [M–H][–] peak in *B. infantis* fractions (black line) overlapped with the corresponding standard (pink line). **e-h**, MS and MS/MS spectra of ILA peak in *B. infantis* fraction (e, f) compared with MS and MS/MS spectra of standard compound (g, h).

4.2.3. Indole-3-lactic acid (ILA) is anti-inflammatory in H4 cells

Having identified the peak in sized fractions of *B. infantis* secretions as ILA, it was tested for its anti-inflammatory activity in H4 cells. Accordingly, H4 cells were treated with ILA before exposing them to IL-1 β and then measuring IL-8 as a representative inflammatory cytokine by ELISA assay. At levels of 1 μ M, 5 μ M and 20 μ M, ILA was significantly anti-inflammatory following IL-1 β stimulus (**Figure 4.3 a**). However, at the same doses of ILA alone, without any inflammatory stimuli, no inflammation was noted and the various doses were not cytotoxic (data not shown).

4.2.4. ILA is also anti-inflammatory in small intestine from a patient with NEC and other fetal enterocytes

To confirm that ILA was generally anti-inflammatory in immature intestine, a primary cell line isolated from resected small intestine from a NEC patient (**Figure 4.3 b**) and organoids from the therapeutically aborted human fetuses at 15 (**Figure 4.3 c**) and 22 (**Figure 4.3 d**) weeks gestation were exposed to ILA before adding

IL-1 β . The various concentrations of ILA resulted in a significant anti-inflammatory effect.

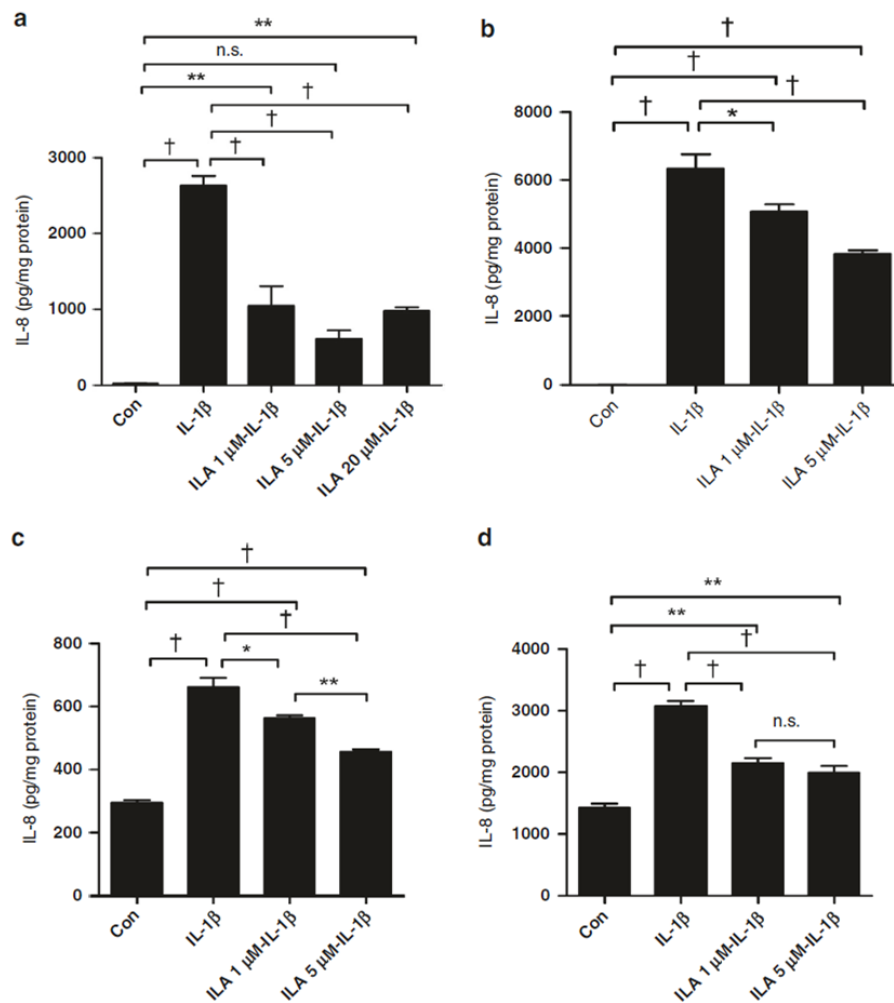


Figure 4.3. The effect of indole-3-lactic acid (ILA) on anti-inflammation in H4 cells, NEC enterocytes, and immature human intestinal organoids. H4 cells (**a**), primary enterocytes isolated from resected intestine of a NEC patient (**b**), and immature human intestinal

organoids isolated from therapeutically aborted fetuses at gestational ages 15 (c) and 22 weeks (d) were pretreated with or without ILA before IL-1 β stimulation. The secretion of IL-8 into the cell culture supernatant was determined by ELISA (N = 3). Graphs represent the mean \pm SEM from three independent experiments. One-way analysis of variance (ANOVA) and Tukey's post hoc tests were used for statistical analysis (*P < 0.05, **P < 0.01, †P < 0.001, n.s., not significant).

4.2.5. ILA causes anti-inflammation through an aryl hydrocarbon receptor (AHR) and responds to TLR-4 expression

It has been reported that ILA interacts with an AHR in intestinal epithelial cells [25, 26]. To determine if this receptor/transcription factor is involved in the anti-inflammatory effect of H4 cells, we determined the expression of AHR and the effect of the AHR inhibitor CH223191 (24) on ILA anti-inflammation after IL-1 β stimulation. **Figure 4.4 a** shows that inhibition of AHR abrogates the anti-inflammatory effects of ILA in H4 cells. However, in TLR-4 knockout fetal mice, the anti-inflammation was lost without a TLR-4 receptor (**Figure 4.4 b**).

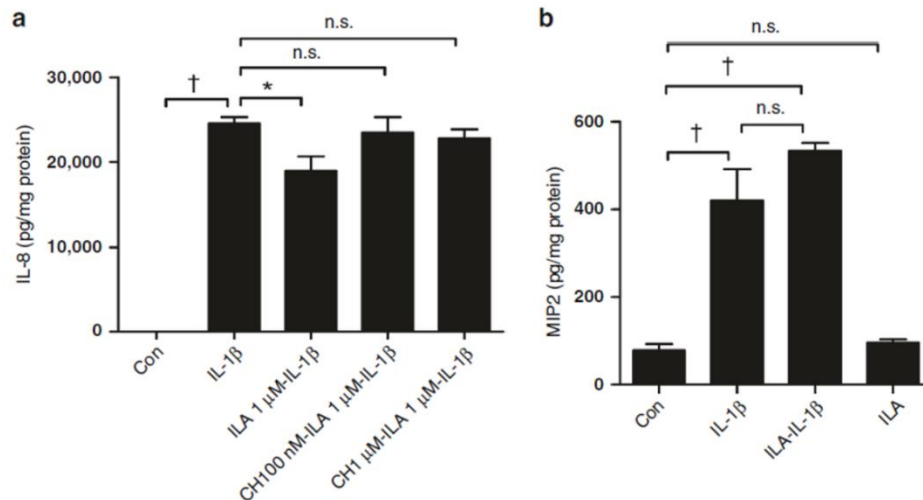


Figure 4.4. ILA anti-IL-1 β -induced IL-8 induction is mediated by aryl hydrocarbon receptor (AHR) in H4 cells and TLR-4 is required for ILA anti-inflammation in immature intestine. **a**, H4 cells were pretreated with or without different doses of AHR inhibitor—CH223191 and then treated with ILA before exposure to IL-1 β . The secretion of IL-8 into the supernatant was determined by ELISA. **b**, TLR-4-knockout immature mice (embryonic day 18.5) small intestinal organ cultures were pretreated with or without 5 μ M of ILA before IL-1 β stimulation. The secretion of microphage inflammatory protein 2 (MIP2) into the supernatant was determined by ELISA. Data are represented as the mean \pm SEM, $n = 3$ from three independent experiments for **a** and $n = 6$, from the repeated experiments for **b**. One-way analysis of variance (ANOVA) and Tukey's post hoc tests were used for statistical analysis (* $P < 0.05$ and † $P < 0.001$, n.s., not significant).

4.2.6. ILA effect is developmentally regulated

To determine if ILA was anti-inflammatory *in vivo* in both fetal and adult intestine, C57BL/6J fetal and adult mouse small intestinal organ cultures were exposed to ILA before stimulating with IL-1 β . A significant reduction in IL-1 β

inflammation was observed in fetal mouse (**Figure 4.5 a**) but not adult (**Figure 4.5 b**) small intestine. Therefore, it was assumed that ILA anti-inflammatory effect was developmentally regulated in human intestines. In fact, when ILA was tested on both H4 cells and H4 cells treated with hydrocortisone (a trophic agent shown to induce maturation of fetal enterocytes) [27] and on Caco2 cells before an IL-1 β stimulus, AHR mRNA expression was reduced in hydrocortisone-treated H4 cells (Figure 4.5 c) and anti-inflammation of ILA was lost (**Figure 4.5 d**). Moreover, AHR in Caco2 cells was reduced (**Figure 4.5 e**) and ILA had no effect on IL8 secretions (**Figure 4.5 f**).

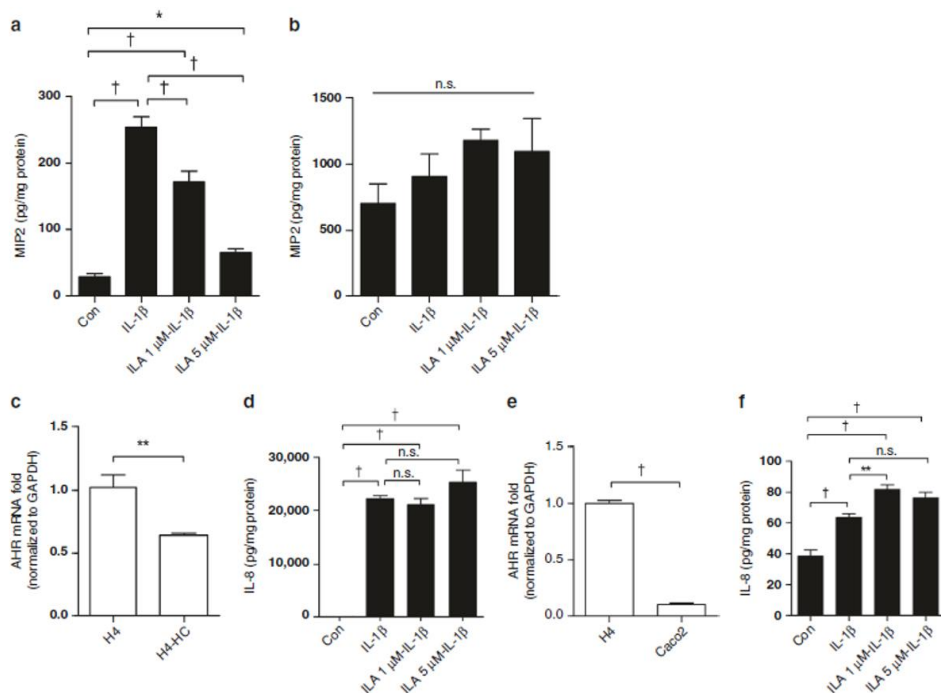


Figure 4.5. AHR and ILA anti-inflammatory responses to IL-1 β are developmentally regulated. C57BL6 (a) immature (embryonic day 18.5) and (b) adult (8-week-old male)

mice small intestinal organ cultures were pretreated with or without ILA before IL-1 β stimulation. The secretion of MP2 into the supernatant was determined by ELISA. **c)** Expression of AHR mRNA in H4 cells and hydrocortisone-treated H4 (HC-H4) cells. **d)** IL-8 reaction in HC-H4 cells' exposure to ILA before an IL-1 β stimulus. **e)** AHR mRNA in H4 and Caco-2 cells. **f)** IL-8 secretions in Caco-2 cells pretreated with or without ILA before IL-1 β stimulus. Data are represented as the mean \pm SEM, n = 6 for mice and n = 3 for cells (from three independent experiments). *T* test was used for two-group and one-way analysis of variance (ANOVA), and Tukey's post hoc tests were used for multiple-group statistical analysis (*P < 0.05, **P < 0.01, †P < 0.001, n.s., not significant).

4.2.7. Proposed mechanism for indole-3-lactic acid effect on immature enterocytes

Figure 4.6 is a cartoon that depicts the proposed mechanism of anti-inflammation activity of indole-3-lactic acid in fetal enterocytes. Based on the results presented above, has been assumed that *Bifidobacterium longum* subsp *infantis*, present in the intestine of premature infants fed mothers expressed breastmilk, metabolize breastmilk tryptophan to produce indole-3-lactic acid, which acts to inhibit the transcription factor's (AHR) stimulation of IL-8 only in the immature intestine that express TLR-4 on their surface and thus protect against the excessive intestinal inflammation seen in the premature that thought to be a contributing factor in necrotizing enterocolitis.

Chapter IV: Indole-3-lactic acid, a metabolite of tryptophan, secreted by *Bifidobacterium longum* subspecies *infantis* is anti-inflammatory in the immature intestine

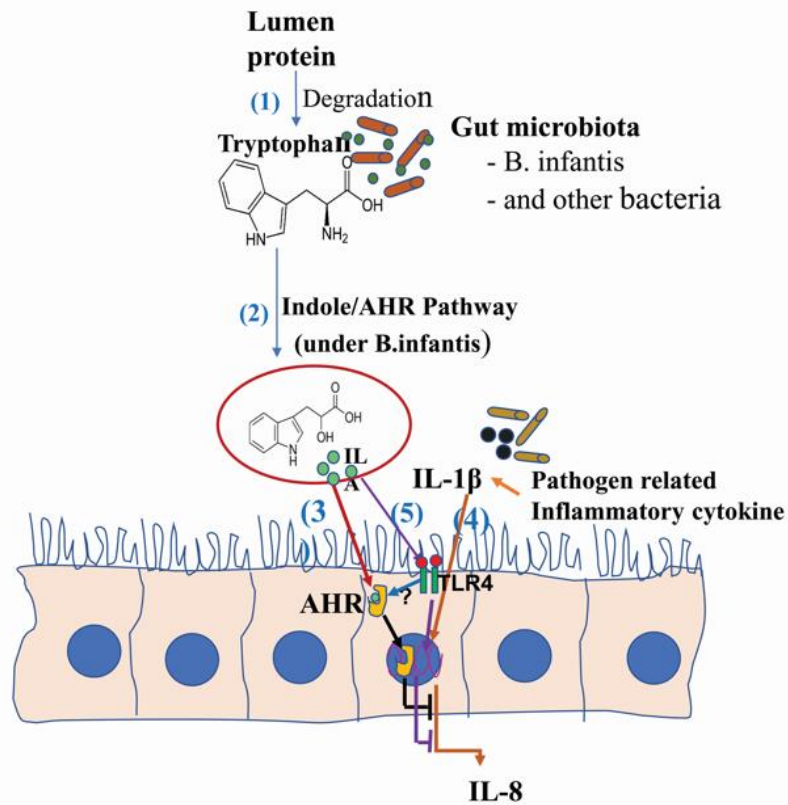


Figure 4.6. Cartoon of suggested mechanism of anti-inflammatory effect of ILA in *B. infantis* secretions on intestinal epithelial cells. (1) Degradation of lumen protein leads to the release of tryptophan (**Trp**). Under the influence of the gut microbiota, Trp is converted to indole-3-lactic acid (**ILA**) (2) by the indole/AHR pathways. ILA acts on the aryl hydrocarbon receptor (**AHR**) found in fetal enterocytes (3) thereby affecting the innate immune response in a ligand-specific fashion suppressing a pathogen-mediated inflammatory cytokine IL-1 β -induced IL-8 secretion (4). TLR-4 is required for ILA anti-inflammation in immature enterocyte with the unknown mechanism (5).

4.3. Discussion

Recent scientific investigation have demonstrated that *B. infantis* and its secretions were anti-inflammatory in *ex-vivo* experiments using a human fetal primary small intestinal cell line (H4 cells) and *in vivo* in fetal mouse small intestine [5, 20, 21], suggesting that this “pioneer” bacterium, known to exist as part of the initial colonizing microbiota of breastfed newborns and breastmilk itself, potentially act in concert to impart protection against the severe intestinal inflammatory necrosis leading to NEC [28, 29]. Ganguli K. et al reported that size fractions of *B. infantis* secretions (5-10 kDa) protected against an LPS-stimulated inflammatory response in a primary human small intestinal cell line [20] and subsequently has been demonstrated that anti-inflammatory secretions from *B. infantis* requires an increased enterocyte surface level expression of TLR-4 receptors [13, 30] and affects the developmentally expressed transcription factor, AP-1, to interfere with IL-8 stimulated inflammation [19]. More recently, using transcription profiles of RNA isolated from H4 cells exposed to *B. infantis* secretions has been reported that the transcription of tight junction genes (occludin and claudin) increase following IL-1 β inflammatory stimulus and intercellular transport is reduced [31].

In this study, these scientific evidences were extended to determine the structure of the molecules in *B. infantis* secretions that mediates enterocyte anti-inflammation. The metabolite profiles of cell media were compared with the > 3kDa, 3-10 kDa and >10 kDa fractions after UHPLC-MS/MS analysis. From the comparison of the UHPLC-MS profiles and peak alignment revealed a consistently different peak between the media alone and the > 3 kDa, 3-10 kDa and >10 kDa (data not shown) fractions possessing strong absorbance in the UV range (λ :

280nm), which suggested an aromatic moiety, eluting at roughly 9 minutes in a reversed phase gradient. The accurate mass spectrometry measurement provided the molecular formula: $C_{11}H_{11}NO_3$ and by tandem mass spectrometry fragmentation, assisted by spectral library matching, it was finally identified as indole-3-lactic acid (ILA). Since all other compounds (amino acids, sugars, small peptides and fatty acids) were also present in the media itself, ILA was recognized as the principal difference and its abundance was consistent with the metabolism of tryptophan from *B. infantis*. It is important to recognize that all strains of *Bifidobacteria* studied are capable of producing indole-3-lactic acid (ILA) from tryptophan [32-33]. However, ILA is only anti-inflammatory in fetal intestine and breastmilk contains tryptophan capable of producing ILA [35]. This suggests that *B. infantis* in combination with expressed breastmilk may be the best way to prevent NEC. ILA is an indole metabolite of tryptophan [33]. In fact, tryptophan is a substrate for intestinal bacteria, leading to important metabolites. It has previously been reported that a number of colonizing intestinal bacteria, particularly gram negative organisms, can metabolize the amino acid tryptophan to produce metabolic pathways that improve health and provides immunologic protection [32, 33]. This is particularly true in the early life when *Bifidobacteria* are abundant in breastfed babies and in experimental animals have been shown to influence development of immunologic defense [34]. Mainly lactic acid bacteria convert amino acids to secondary metabolites. The process starts with a deamination step, which in the case of aromatic amino acids is operated by the enzyme aromatic aminotransferase that converts amino acids into alpha-ketoacids. These compounds are further converted by dehydrogenases to hydroxy acids. The presence of ILA has also been

Chapter IV: Indole-3-lactic acid, a metabolite of tryptophan, secreted by Bifidobacterium longum subspecies infantis is anti-inflammatory in the immature intestine

reported in *Lactobacillus casei* and *Helveticus* [32, 35] and this molecule has shown anti-inflammatory activity in keratinocytes against ultraviolet-B induced damages [32]. Increased amounts of these tryptophan metabolites were found in other bacterial species such as *Megamonas hypermegale*, *Roseburia intestinalis*, *Ruminococcus obeum*, *E. rectale* and *F. prausnitzii* [35].

Of particular importance are the indole metabolites, such as indole-3-lactic acid (ILA) and indole-3-pyruvic acid (IPA), that use the aryl hydro-carbon receptor (AHR) in enterocytes and immunocytes, a ligand-activated transcription factor stimulated by dietary and microbial metabolites, to activate the immune system and other intestinal functions for purposes of homeostasis [32, 33, 36, 37]. Low tryptophan levels and a decrease in AHR have been reported in active patients with inflammatory bowel disease [38], while indole metabolites of tryptophan have been used in animal models to treat colitis [35]. In like manner, the role of tryptophan metabolite deficiency has been associated with irritable bowel syndrome and metabolic syndrome. Furthermore, decreased levels of AHR receptors have been found in patients with multiple sclerosis [39].

In the present study, ILA was incubated with H4 cells at the concentration found in secretions and at higher concentrations before a stimulus with IL-1 β , the molecule was anti-inflammatory *ex vivo* in H4 cells, in a primary cell line from resected small intestine of patient with necrotizing enterocolitis and, additionally, in fetal organoids, suggesting that ILA is generalized effective in fetal enterocytes. Following AHR inhibition in fetal enterocytes, the anti-inflammatory effect was lost, supposing that ILA is a potential ligand for AHR and the interaction with the receptor is involved in the pathway for anti-inflammation in fetal enterocytes.

Moreover, the anti-inflammatory effect of ILA following IL-1 β action was lost in fetal mice with the TLR-4 receptor knocked out, proving that TLR-4, present in abundance on the surface of fetal enterocytes, regulate the anti-inflammatory process.

However, ILA was effective only in fetal intestine, in both mouse models and human enterocytes, but when ILA and IL-1 β were used on the cortisone-treated cells and Caco2 cells, they lacked an anti-inflammatory response, strongly suggesting that ILA is only anti-inflammatory in fetal but not adult intestine. In this regard, the measurement of the AHR gene in fetal enterocytes treated with hydrocortisone and Caco2 cells, demonstrated that the receptor genetic level was high in fetal enterocytes and lower in cortisone-treated fetal enterocytes and Caco2 cells.

Therefore, indole-3-lactic acid, a breakdown product of the amino acid tryptophan, present in large amounts in breastmilk, is produced by *B. infantis* metabolism and mediates the mechanism of anti-inflammatory in immature intestine. ILA requires the interaction with TLR-4 and the inhibition of AHR receptor to interfere with the transcription of the inflammatory cytokine IL-8 that causes excessive inflammation in the premature intestine, resulting in NEC. Breastmilk, particularly colostrum, has high levels of the essential amino acid tryptophan ^[15, 16] and ingestion of maternal-expressed breastmilk in prematures is protective against NEC ^[15, 16, 18]. It has also been reported that breastmilk-induced bacteria (*B. infantis*, *Lactobacillus acidophilus* and *Bacteroides fragilis*), known as “pioneer” bacteria ^[18], are specifically stimulated with initial colonization with

ingested breastmilk in premature infants ^[17], therefore they can function as probiotics to protect against the expression of NEC in prematures ^[6, 17].

ILA produced by *B. infantis* interaction with ingested breastmilk functions in a complementary manner and could become useful in the treatment of all at risk premature infants for necrotizing enterocolitis if safety and clinical studies are performed.

4.4. Materials and methods

4.4.1. Bacterial cultures and B.infantis secretory fragment separation

Bifidobacterium longum subsp *infantis* (*B. infantis*), obtained from ATCC (Manassas, VA) (ATCC No. 15697), was cultured anaerobically in a media modified from the combination of Mann-Rogosa-Sharpe (MRS) broth (DIFCO; BD Bio- science, Franklin Lakes, NJ) and H4 cell culture media (Supporting Information Table S4.1) ^[12, 20]. *B. infantis* conditioned media at the stationary growth phase was prepared by centrifugation of probiotic cultures at 3700 rpm (equal 2936 g) (Sorvall legend RT+ centrifuge, ThermoFisher Scientific, MA) for 10 min at 4°C and then by use of 0.22-µm filtration to eliminate residual bacteria. The tested filtrate was used for *B.infantis* secretory fractions (**SFs**) separation by high speed centrifugation (3220g, 30 min at 4°C) (Eppendorf centrifuge 5810R, Eppendorf North America, NY) with different sizes of the Amicon Ultra centrifugal filters (MilliporeSigma, MA). The secretory fractions (< 3 kDA, 3-10 kDA and < 10 kDA) were used to test anti-inflammatory effects in H4 cells before subjecting them to the characteristic identification.

4.4.2. Identification of anti-inflammatory effective molecules in secretory size fractions

4.4.2.1. Chemicals

Liquid chromatography–mass spectrometry (LC-MS) grade water, acetonitrile and acetic acid were purchased from VWR (Milan, Italy).

4.4.2.2. Instrumentation and ultra-high-performance liquid chromatography-tandem mass spectrometry

B.infantis secretory fractions (**SFs**) were filtered on a 0.45 µm nylon filter (Phenomenex[®], Bologna, Italy) and directly injected into an ultra-high-performance liquid chromatography-tandem mass spectrometry (UHPLC-MS/MS). Analyses were performed on a Nexera UHPLC system coupled to a hybrid Ion trap-Time of flight (IT-TOF) mass spectrometer (Shimadzu, Kyoto, Japan). For the separation of < 3KDA, 3-10KDA and < 10KDA *B. Infantis* fractions a KinetexTM EVO C18 column with geometry 150 mm × 2.1 mm, 2.6 µm (Phenomenex[®]) was used, at a flow rate was 0.5 mL/min, with the following gradient: 0-18 min, 1-30%B, 18-19 min, 30-98%B, hold for 1.50 min, returning to 1%B in 0.1 min. Column oven was set to 45° C, photodiode array detection (PDA) was set to 254 and 280 nm. MS detection was performed in both positive and negative electrospray ionization (ESI) mode, interface temperature was set to 250°C, curve desolvation line: 250°C, nebulizer and drying gas 1.5 and 10L/min. MS1 range 100-1500, MS/MS: data dependent acquisition (DDA), precursors were searched in the range 100-1500 with execution trigger 10⁵, collision energy 35%, dynamic exclusion 30s. The molecular formulas were obtained through Formula Predictor (Shimadzu). MS file was

converted in mzXML format and analyzed by MZmine2. Data were deconvoluted, deisotoped and aligned. Spectral annotation was performed against HMDB and MassBank of North America (MoNA) database, with max mass accuracy tolerance of 10 ppm. For quantitative analysis, an external calibration method was employed, a calibration curve with five levels were built, triplicate analysis of each point was run. The UHPLC-MS/MS conditions were the same as described above. Extracted ion chromatogram (EIC) of ILA MS/MS transition 204-158 were employed.

4.4.3. Cell cultures

H4 cells, a human fetal non-transformed primary small intestinal epithelial cell line characterized by Dr. W. Allan Walker laboratory, were cultured as previous described ^[40]. NEC-IEC were isolated and cultured from the viable margins of resected ileal NEC tissues from a NEC neonate at 25-week gestation and were cultured as previous described ^[13]. The use of two human cell lines had the permission of Partners IRB #2011P003833 at Massachusetts General Hospital. Caco-2 cells were obtained from the American Type Culture Collection (ATCC, Manassas, VA) and cultured as previous described ^[41].

4.4.4. Organoid cultures

Human sample procedures were approved by institutional review board protocols IRB 1999P003833 (Brigham and Women's Hospital, Boston, MA) and IRB 2016P000949 (Massachusetts General Hospital, Boston, MA) for the derivation of fetal enterospheres (FEnS). The human fetal intestinal organoids were derived as described previously ^[41]. In this experiment the FEnS used was from gestational age 15 and 22 weeks therapeutically aborted fetuses. When the culture

reached confluence, it was apically treated with 5 mmol/L N-[(3,5-Difluorophenyl) acetyl]-L-alanyl-2-phenyl] glycine-1, 1-dimethylethyl ester (DAPT) in DMEM/F12 for 48 hours to promote cell differentiation. The monolayers were treated with 20 μ M of ILA for 24 hours before being stimulated with human IL-1 β (1ng/ml for 24 hours) basolaterally. The supernatants from the basolateral side were collected for an IL-8 protein assay by an enzyme-linked immune sorbent assay (ELISA).

4.4.5. Hydrocortisone treatment for H4 cells

H4 cells cultured in 12-well tissue culture plates to 40% confluence were treated with or without hydrocortisone (HC) (Sigma, St. Louis, MO) at 1 μ M for five days (23). The cells were collected for total RNA isolation and the aryl hydrocarbon receptor (AHR) mRNA was determined by real time quantitative reverse transcription PCR (qRT-PCR) as described later.

4.4.6. Determination of the anti-inflammatory effects of B.infantis SFs and indole-3-lactic acid on H4, hydrocortisone-treated H4 (H4-HC), NEC-IEC and Caco2 cells

H4 cells were pretreated with or without *B.infantis* SFs at the concentration of 10% or indole-3-lactic acid (ILA) (1 μ M, 5 μ M and 20 μ M) for 24 h and then stimulated with 1ng/ml of recombinant mouse IL-1 β (R&D Systems, Minneapolis, MN) for 24 h, or treated with *B. infantis* SFs or different doses of ILA alone. The IL8 secretion into the cell culture supernatants was determined by **ELISA**. The effects of ILA on IL-1 β -induced IL8 secretion was also determined in H4-HC, NEC-IEC and Caco2 cells with the dose range (1 μ M and 5 μ M of ILA).

4.4.7. Determination of the anti-inflammatory effects of ILA on fetal and adult mouse intestinal organ culture

C57BL/6J and TLR-4 knockout mice (Jackson Laboratory) were bred and housed in a specific pathogen free facility. Animals were given water and standard laboratory chow *ad libitum*. Timed pregnant mice (embryonic day 18.5) were established as previous described [5]. Fetal mice from two mouse strains and C57BL/6J (8-week old male) adult mice small intestinal tissues were collected and cut into 3-mm pieces and maintained in organ culture media [5]. After 1-2 h at 37°C, tissues were pretreated with and without ILA (1 μM and 5 μM) for 24 h and then stimulated with 1ng/ml of recombinant mouse IL-1β (R&D Systems, Minneapolis, MN) for 24 h. Supernatants were collected and stored at -20°C for ELISA analysis. Animal procedures had been previously approved by the Massachusetts General Hospital Subcommittee on Research Animal Care and Use committee (2018N000070).

4.4.8. Treatment with the aryl hydrocarbon receptor (AHR) inhibitor - CH223191 in H4 cells

H4 cells were pretreated with or without various doses of AHR inhibitor-CH223191(Sigma, St. Louis, MO) for 30 minutes [42] and then treated as described with ILA (1 μM) for 24 h before exposure to IL-1β (1 ng/ml) for 24 h. IL8 secretion into the cell culture supernatants was determined by ELISA.

4.4.9. Real-time quantitative reverse transcription PCR

The total RNA of the cells was isolated by Trizol combination with Neasy RNA isolation kit (ThermoFisch Scientific, Grand Island, NY). RNA was reverse

transcribed with random hexamers using an Advantage RT-for -PCR kit (Clontech, Mountain View, CA). The cDNA was amplified using iQ SYBR Green Supermix (Bio-Rad, Philadelphia, PA). Glyceraldehyde 3-phosphate dehydrogenase (GAPDH) primers were amplified in all samples to represent the housekeeper gene. The change in the normalized transcript level was expressed relative to the control sample with a change of n in CT representing a 2^{-n} . Primer sequences used in this study were as follows:

Human *GAPDH*, forward, 5'- ATGGGGAAGGTGAAGGTCG-3',
and reverse, 5'- GGGGTCATTGATGGCAACAATA-3'
Human *AHR*, forward, 5'- CTTAGGCTCAGCGTCAGTTAC-3',
and reverse, 5'- CGTTTCTTTCAGTAGGGGAGGAT- 3'

4.4.10. LDH Cytotoxicity Assay

For each experiment with *B. infantis* size fragments (SF) or ILA, lactate dehydrogenase (LDH) cytotoxic assay was performed by using a LDH Assay Kit (Roche Applied Science, Branford, CT) .

4.4.11. IL-8 ELISA

Secreted human IL-8 and mouse IL-8 homologue protein - Macrophage-inflammatory protein 2 (MIP-2) were measured by ELISA using human IL-8 and mouse MIP2 detection kits (R&D Systems, Minneapolis, MN).

4.4.12. Statistical Analysis

All data are presented as the mean \pm standard error of the mean (SEM). The unpaired Student's t-test was used to compare the mean of two groups. One-way

ANOVA and Turkey post-hoc test were used to compare the mean of multiple groups. Differences of $p < 0.05$ were considered significant (* $p < 0.05$, ** $p < 0.01$, † $p < 0.001$) (GraphPad Prism 6).

4.5. Conclusions

The results presented in this work provide a mechanistic explanation to support the additive effect of breastmilk and probiotics in the prevention of NEC. Additional *in vivo* studies in animals are required and safety studies in humans before a large scale, single protocol clinical trial can be done to determine efficacy. This approach could potentially become a routine management of all premature infants.

4.6. References

[1] Neu, J., Walker, W.A. Necrotizing enterocolitis. *N. Engl. J. Med.* 2011, 364, 255–264.

[2] Holman, R.C., Stoll, J.B., Curns, A.T., Yorita, K.L., Steiner, C.A., Schonberger, L.B. Necrotising enterocolitis hospitalisations among neonates in the United States. *Paediatr. Perinat. Epidemiol.* 2006, 20, 498–506.

[3] Hall N.J., Pierro A. Surgical Treatment in Newborns of Necrotizing Enterocolitis. *Neonatology* 2018, 1395–1401.

[4] Baird, R., Tessier, R., Guilbault, M.P., Puligandla, P., Saint–Martin, C. Imaging, radiation exposure, and attributable cancer risk for neonates with necrotizing enterocolitis. *J. Pediatr. Surg.* 2013, 48, 1000–1005.

[5] Meng, D., Zhu, W., Shi, H.N., Lu, L., Wijendran, V., Xu, W., Walker, W.A. Toll–like receptor–4 in human and mouse colonic epithelium is developmentally

Chapter IV: Indole-3-lactic acid, a metabolite of tryptophan, secreted by Bifidobacterium longum subspecies infantis is anti-inflammatory in the immature intestine

regulated: a possible role in necrotizing enterocolitis. *Pediatr. Res.* 2015, 77, 416–424.

^[6] Repa, A., Thanhaeuser, M., Endress, D., Weber, M., Kreissl, A., Binder, C., Berger, A., Haiden, N. Probiotics (*Lactobacillus acidophilus* and *Bifidobacterium infantis*) prevent NEC in VLBW infants fed breast milk but not formula. *Pediatr. Res.* 2015, 77, 381–388.

^[7] Claud, E.C., Lu, L., Anton, P.M., Savidge, T., Walker, W.A., Cherayi, B.J. Developmentally-regulated I κ B expression in intestinal epithelium and susceptibility to flagellin-induced inflammation. *Proc. Natl. Acad. Sci. U.S.A.* 2004, 101, 7404–7408.

^[8] Nanthakumar, N., Meng, D., Goldstein, A.M., Zhu, W., Lu, L., Uauy, R., Llanos, A., Claud, E.C., Walker, W.A. The mechanism of excessive intestinal inflammation in necrotizing enterocolitis: an immature innate immune response. *PLoS One* 2011, 6, e17776–17785.

^[9] Weng, M., Walker, W.A. The role of gut microbiota in programming the immune phenotype. *J. Dev. Orig. Health Dis.* 2013, 4, 203–214.

^[10] Groer, M.W., Gregory, K.E., Louis-Jacques, A., Thibeau, S., Walker, W.A. The very low birth weight infant microbiome and childhood health. *Birth Defects Res. (Part C) Embryo Today* 2015, 105, 252–264.

^[11] Palmer, C., Bik, E.M., Di Giulio, D.B., Relman, D.A., Brown, P.O. Development of the human infant intestinal microbiota. *PLoS Biol.* 2007, 5, e177–185.

Chapter IV: Indole-3-lactic acid, a metabolite of tryptophan, secreted by Bifidobacterium longum subspecies infantis is anti-inflammatory in the immature intestine

[12] Nanthakumar, N., Fusunyan, R.D., Sanderson, I.R., Walker, W.A. Inflammation in the developing human intestine: A possible pathophysiologic basis for necrotizing enterocolitis. *Proc. Natl. Acad. Sci. U.S.A.* 2000, 97, 6043–6048.

[13] Meng, D., Zhu, W., Ganguli, K., Shi, H., Walker, W.A. Anti-inflammatory effects of Bifidobacterium longum subsp infantis secretion on fetal human enterocytes are mediated by TLR4 receptors. *Am. J. Physiol. Gastrointest. Liver Physiol.* 2016, 311, G744–G753.

[14] Gareau, M.G., Sherman, P.M., Walker, W.A. Probiotics and the gut microbiota in intestinal health and disease. *Nature Rev. Gastroenterol. & Hepatol.* 2010, 7, 503–514.

[15] O'Rourke, L., Clarke, G., Nolan, A., Watkins, C., Dinan, T.G., Stanton, C., Ross, R.P., Ryan, C.A. Tryptophan metabolic profile in term and preterm breast milk: implications for health. *J. Nutr. Sci.* 2018, 7, e13.

[16] Donnet–Hughes, A., Schriffin, E., Walker, W.A. Protective properties of human milk and bacterial colonization of the neonatal gut. In: Duggan, C., Koletzko, B., Watkins, J., Walker, W.A. *Nutrition In Pediatrics Basic Science and Clinical Aspects. 5th ed.* Chinese Publications Inc., New Haven, CT. Eds. 2017, 250–260.

[17] Gregory, K.E., Samuel, B.S., Houghteling, P., Shan, G., Ausubel, F.M., Sadreyev, R.I., Allan Walker, A.W. Influence of maternal breast milk ingestion on acquisition of the intestinal microbiome in preterm infants. *Microbiome.* 2016, 4, 68.

Chapter IV: Indole-3-lactic acid, a metabolite of tryptophan, secreted by Bifidobacterium longum subspecies infantis is anti-inflammatory in the immature intestine

^[18] Jost, T., Lacroix, C., Braegger, C.P., Chassard, C. New insights in gut microbiota establishment in healthy breast fed neonates. *Plos One* 2012, 7, e44595–44803.

^[19] Cahill, C., Zhu, W., Oziolor, E., Yang, Y-J., Tam, B., Rajanala, S., Rogers, J.T., Walker, W.A. Differential expression of the activator protein 1 transcription factor regulates interleukin-1 beta induction of interleukin 6 in the developing enterocyte. *Plos One* 2016, 11, e0145184–0145195.

^[20] Ganguli, K., Meng, D., Rautava, S., Lu, L., Walker, W.A., Nanthakumar, N. Probiotics prevent necrotizing enterocolitis by modulating enterocyte genes that regulate innate immune-mediated inflammation. *Am. J. Physiol. Gastrointest. Liver. Physiol.* 2013, 304, G132–G141. ^[21] Guo, S., Gillingham, T., Guo, Y., Meng, D., Zhu, W., Walker, W.A., Ganguli, K. Secretions of Bifidobacterium infantis and Lactobacillus acidophilus protect intestinal epithelial barrier function. *J. Pediatr. Gastroenterol. Nutr.* 2017, 64, 404–412.

^[22] Henry, M.C.W., Moss, R.L. Necrotizing enterocolitis. *Annu. Rev. Med.* 2009, 60, 111–124.

^[23] Theodoridis, G.A., Gika, H.G., Want, E.J., Wilson, I.D. Liquid chromatography–mass spectrometry based global metabolite profiling: A review. *Anal. Chim. Acta* 2012, 711, 7–16.

^[24] Cajka, T., Fiehn, O. Toward merging untargeted and targeted methods in mass spectrometry–based metabolomics and lipidomics. *Anal. Chem.* 2016, 88, 524–545.

^[25] Metidji, A., Omenetti, S., Crotta, S., Li, Y., Nye, E., Ross, E., Li, V., Maradana, M.R., Schiering, C., Stockinger, B. The environmental sensor AHR

Chapter IV: Indole-3-lactic acid, a metabolite of tryptophan, secreted by Bifidobacterium longum subspecies infantis is anti-inflammatory in the immature intestine

protects from inflammatory damage by maintaining intestinal stem cell homeostasis and barrier integrity. *Immunity* 2018, 49, 353–362.

[26] Hubbard, T.D., Murray, I.A., Perdew, G.H. Indole and tryptophan metabolism: endogenous and dietary routes to Ah receptor activation. *Drug Metab. Dispos.* 2015, 43, 1522–1535.

[27] Lu, L., Li, T., William, G., Petit, E., Walker, W.A. Hydrocortisone induces changes in gene expression and differentiation in immature human enterocytes. *Am. J. Physiol. Gastrointest. Liver Physiol.* 2011, 300, G425–G432.

[28] Ganguli, K., Walker, W.A. Treatment of necrotizing enterocolitis with probiotics. *Gastroenterol. Clin. North Am.* 2012, 41, 733–746.

[29] Olsen, R., Greisen, G., Schröder, M., Brok, J. Prophylactic probiotics for preterm infants: a systematic review and meta-analysis of observational studies. *Neonatology* 2016, 109, 105–112.

[30] Good, M., Sodhi, C.P., Egan, C.E., Afrazi, A., Jia, H., Yamaguchi, Y., Lu, P., Branca, M.F., Ma, C., Prindle, T. Jr, Mielo, S., Pompa, A., Hodzic, Z., Ozolek, J.A., Hackam, D.J. Breast milk protects against the development of necrotizing enterocolitis through inhibition of Toll-like receptor 4 in the intestinal epithelium via activation of the epidermal growth factor receptor. *Mucosal Immunol.* 2015, 8, 1166–1179.

[31] Guo, S., Guo, Y., Ergun, A., Lu, L., Walker, W.A., Ganguli, K. Secreted metabolites of *Bifidobacterium infantis* and *Lactobacillus acidophilus* protect immature human enterocytes from IL-1 β -induced inflammation: A transcription profiling analysis. *Plos One* 2015, 10, e0124549–0124557.

Chapter IV: Indole-3-lactic acid, a metabolite of tryptophan, secreted by Bifidobacterium longum subspecies infantis is anti-inflammatory in the immature intestine

^[32] Roager, H.M., Licht, T.R. Microbial tryptophan catabolites in health and disease. *Nat. Commun.* 2018, 9, 3294–3300.

^[33] Vogel, C.F., Sciallo, E., Li, W., Wong, P., Lazennec, G., Matsumura, F. RelB, a new partner of aryl hydrocarbon receptor–mediated transcription. *Mol. Endocrinol.* 2007, 21, 2941–2955.

^[34] Laursen, M., Bahl, M., Michaelsen, K., Licht, T. First foods and gut microbes. *Front. Microbiol.* 2017, 8, 356.

^[35] Aoki, R., Aoki–Yoshida, A., Suzuki, C., Takayama, Y. Indole–3–pyruvic acid, an aryl hydrocarbon receptor activator, suppresses experimental colitis in mice. *J. Immunol.* 2018, 201, 3683–3693.

^[36] Ehrlich, A.M., Henrick, B., Pacheco, A., Taft, D., Xu, G., Huda, N., Lozada-Contreras, M., Goodson, M., Slupsky, C., Mills, D. and Raybould, H. Bifidobacterium grown on human milk oligosaccharides produce tryptophan metabolite Indole-3-lactic acid that significantly decreases inflammation in intestinal cells in vitro. *FASEB J.* 2018, 32, Ib359.

^[37] Aragazzini, F., Ferrari, A., Pacini, N., Gualandris, R. Indole–3–lactic acid as a tryptophan metabolite produced by Bifidobacterium spp. *Appl. Environ. Microbiol.* 1979, 38, 544–546.

^[38] Nikolaus, S. Schulte, B., Al–Massad, N., Thieme, F., Schulte, D.M., Bethge, J., Rehman, A., Tran, F., Aden, K., Häsler, R., Moll, N., Schütze, G., Schwarz, M.J., Waetzig, G.H., Rosenstiel, P., Krawczak, M., Szymczak, S., Schreiber, S. Increased tryptophan metabolism is associated with activity of inflammatory bowel diseases. *Gastroenterology* 2017, 153, 1504–1516.

Chapter IV: Indole-3-lactic acid, a metabolite of tryptophan, secreted by Bifidobacterium longum subspecies infantis is anti-inflammatory in the immature intestine

[39] Rothhammer, V., Mascanfroni, I.D., Bunse, L., Takenaka, M.C., Kenison, J.E., Mayo, L., Chao, C.C., Patel, B., Yan, R., Blain, M., Alvarez, J.I., Kébir, H., Anandasabapathy, N., Izquierdo, G., Jung, S., Obholzer, N., Pochet, N., Clish, C.B., Prinz, M., Prat, A., Antel, J., Quintana, FJ. Type I interferons and microbial metabolites of tryptophan modulate astrocyte activity and central nervous system inflammation via the aryl hydrocarbon receptor. *Nat. Med.* 2016, 22, 586–597.

[40] Sanderson, I. R., Ezzell, R. M., Kedinger, M., Erlanger, M., Xu, Z. X., Pringault, E., Leon–Robine, S., Louvard, D., Walker, W. A. Human fetal enterocytes in vitro: modulation of the phenotype by extracellular matrix. *Proc. Natl. Acad. Sci. U.S.A.* 1996, 93, 7717–7722.

[41] Senger, S., Ingano, L., Freire, R., Anselmo, A., Zhu, W., Sadreyev, R., Walker, W.A., Fasano, A. Human fetal–derived enterospheres provide insights on intestinal development and a novel model to study Necrotizing Enterocolitis (NEC). *Cell. Mol. Gastroenterol. Hepatol.* 2018, 5, 549–568.

[42] Zhao, B., Degroot, D.E., Hayashi, A., He, G., Denison, M.S. CH223191 is a ligand–selective antagonist of the Ah (Dioxin) receptor. *Toxicol Sci.* 2010, 117, 393–403.

Chapter V: Determination of phase I metabolites and glucuronide conjugates of hop bitter acids metabolites by a full scan/data dependent/targeted neutral loss acquisition UHPLC-HRMS strategy: In vitro microsomal stability and in vivo analysis after oral administration in mice

CHAPTER V

Determination of phase I metabolites and glucuronide conjugates of hop bitter acids by a full scan/data dependent/targeted neutral loss UHPLC-HRMS strategy: In vitro metabolic stability and in vivo analysis after oral administration in mice

Abstract

Bitter acids are a class of prenylated phloroglucinol derivatives present in *Humulus lupulus* L., known for their multiple healthy-beneficial properties, nevertheless, research regarding their metabolism and stability is lacking. For this purpose, the aim of this study was the development and validation of an ultra high performance liquid chromatography-high resolution mass spectrometry (UHPLC-HRMS) method to assess the metabolic stability of hop α - and β -acids and the detection of their metabolites *in vitro* and *in vivo*. Mice liver microsomes were used to assess metabolic stability, *in vitro* $t_{1/2}$ and clearance values calculated, showing a slow and moderate metabolism for α -acids ($avg t_{1/2}$: 120.01min, $avg CL_{int}$ 11.96 $\mu\text{L}/\text{min}/\text{mg}$), while β -acids were metabolized faster ($avg t_{1/2}$: 103.01min, $avg CL_{int}$: 13.83 $\mu\text{L}/\text{min}/\text{mg}$). Furthermore, phase I metabolites and phase II glucuronide were characterized both in *in vitro*, and *in vivo*, in mouse plasma and urine after oral administration, by a combined full scan/data dependent/targeted neutral loss (FS/DDA/tNL) strategy. As a result, 12 phase I metabolites, including 2 novel

potential di-oxygenated metabolites (M6, M7) of humulones were detected. In addition, the tNL was able to detect for the first time 10 glucuronide conjugates of α -acids, comprising 7 glucuronide derivatives of oxidized phase I metabolites (M16-M22). The proposed method extends the current knowledge regarding metabolization of hop α - and β -acids and could be applied for the comprehension of the metabolic fate of this class of compounds in different species, as well as for *in vivo* pharmacokinetic studies.

5. Introduction

Hop (*Humulus lupulus* L.) is a flowering perennial plant belonging to the family of Cannabaceae with a millennial history. While the 95% of Hop production is mainly directed to the brewing industry as flavoring, foaming and preserving agent ^[1] its remaining employment are numerous, such as in phytomedicine, dietary supplement and nutraceuticals fields. This is related to the various and complex content of bioactive secondary metabolites, such as phenolic acids, catechins, procyanidins, glycosylated and prenylated flavonoids, essential oils and bitter acids, which, furthermore, make its characterization challenging ^[2] [Chapter II]. A plethora of healthy properties has been attributed to hop and its compounds, such as antioxidant, anti-inflammatory, and antiproliferative ^[3], in particular in cancer prevention. In this regard, xanthohumol and its derivatives have been extensively investigated ^[4-5]. While the chemopreventive activity of different natural compounds has been largely reported both *in vitro* and *in vivo*, the number of biotransformation of these compounds that occur *in vivo* is huge, and still represents a dark matter, resulting in an open debate on their effective activity in relationship

Chapter V: Determination of phase I metabolites and glucuronide conjugates of hop bitter acids metabolites by a full scan/data dependent/targeted neutral loss acquisition UHPLC-HRMS strategy: In vitro microsomal stability and in vivo analysis after oral administration in mice

with their metabolic stability and bioavailability ^[6]. Regarding hop compounds metabolism, particular attention has been focused on prenylflavonoids, such as xanthohumol and 8-prenylnaringen. Several studies showed the metabolic conversion of xanthohumol and isoxanthohumol into the estrogenic 8-prenylnaringenin ^[7-8], besides, its bioavailability and metabolism has been studied *in vitro* and *in vivo* ^[9-11]. Among hop compounds, bitter acids are a particular class of prenylated phloroglucinol derivatives, which are divided into two series: α and β -acids, these compounds have been defined “multipotent compounds” for the wide number of healthy properties that have been linked to these molecules, such as antiproliferative, pro-apoptotic, anti-angiogenic ^[12] and, recently, immunomodulatory ^[13] [Chapter III]. In comparison to hop prenylated flavonoids, the metabolism of bitter acids has been less investigated, in particular α and β -acids *in vitro* phase I metabolism has been reported using rabbit liver microsomes ^[14], while bioavailability of α and β -acids and their reduced derivatives (Iso- α , IAA) has been studied by Caco-2 cell models ^[15]. IAA have been monitored also *in vivo*, following oral and intravenous administration in rabbits as well as in humans, after beer consumption ^[16, 17]. These studies were mainly focused on the precursors, and beer oxidation products, while the possible formation of phase II metabolites have not been demonstrated ^[14]. Phase II metabolism is in fact one of the main routes of metabolism for numerous plant secondary metabolites, and glucuronide conjugation by uridine 5'-diphospho (UDP)-glucuronosyltransferases (UGTs) has been reported to possess a preminent role for hop prenylated flavonoids ^[18]. The impact of conjugation is fundamental for understanding the bioavailability of

natural compounds, since glucuronidation is an important mechanism for the clearance of many xenobiotics ^[19], and it is also a key aspect to take into account into the drug discovery and development process. The detection of glucuronide metabolites of α and β -acids has not been reported so far both *in vitro* and *in vivo*, this is due mainly to the employment of deconjugation enzymes ^[16] as well as for the exclusive employment of targeted MS methods focused on known analytes m/z, through selected ion monitoring (SIM) or selected reaction monitoring (SRM) strategies. SRM is limited by the selection of specific transitions to monitor, and from the lack of reference standards for this class of compounds, which limits the potential of this techniques, and as result, precursors outside the SRM transition(s) will not be detected. Therefore, high resolution mass spectrometry (HRMS) is essential for the detection of unknown metabolites and accurate molecular formula assignment in both MS and MS/MS stages ^[20], to provide structural information regarding these metabolites.

5.1. Aim of the work

The objective of this work is the application of ultra high performance liquid chromatography (UHPLC) coupled to HRMS for the analysis of the *in vitro* metabolic stability of a bitter acids mixture and investigate the formation of I and II phase metabolites, after incubation with mice liver microsomes. Furthermore, the method has been extended to the determination of *in vivo* metabolites, after oral administration in mice model. Taking advantage of multiple scan options of the Q-Exactive platform, the analysis was performed with a full scan (FS) and data dependent acquisition (DDA), and, in addition, a targeted neutral loss scan (tNL),

resulting in a combined approach (FS/DDA/tNL). The obtained results will show the formation of numerous metabolites, including novel oxidated and, for the first time, glucuronide derivatives, resulting into an extended knowledge of bitter acids biotransformation, which could be further applied for pharmacokinetic studies both *in vitro* and *in vivo*.

5.2. Results

5.2.1. Method validation and optimization

The analytical method has been validated for linearity, linear range, limits of detections (LODs), limits of quantitation (LOQs), accuracy, precision, recovery, and matrix effect. The results are reported in Table 5.1. Satisfactory linearity was achieved for each compound with a correlation coefficient (R^2) ≥ 0.998 . The LODs and LOQs were calculated for each bitter acid present in the standard ICE-4 mixture. LOD were ≤ 3.5 and 0.36 ng/mL in plasma and urine, respectively, while LOQ were ≤ 11.8 and 0.96 ng/mL in plasma and urine, respectively. These results highlight the high sensitivity that can be achieved through the HRMS selectivity, obtaining LOD and LOQ values close or even lower than previous Triple Quadrupole MS methods for the quantitative analysis of hop prenylflavonoids [21, 22]. Moreover, method accuracy was calculated as percentage relative errors at low, medium and high concentration level of the calibration curves with acceptable values between 0.14 and 14.08 %. Precision has been evaluated considering intra-day and inter-day repeatability, showing good retention time and concentration repeatability in the same day with average CV% values = 0.037 ± 0.01 and 1.130 ± 1.40 , respectively, and also within two consecutive days with average CV% values

Chapter V: Determination of phase I metabolites and glucuronide conjugates of hop bitter acids metabolites by a full scan/data dependent/targeted neutral loss acquisition UHPLC-HRMS strategy: In vitro microsomal stability and in vivo analysis after oral administration in mice

= 0.010 ± 0.01 for retention time and 1.579 ± 0.55 for concentration. Plasma and urine extraction showed optimal recovery values in the range of 104 ± 0.039 for plasma and $100.01 \% \pm 17.66$ for urine. Matrix effect evaluation has demonstrated that while for plasma and microsomes a subtle ion enhancement occurred, for urine there was a little ion suppression, despite SPE extraction. This could be due to the removal of salts through SPE but not of other polar compounds which could be responsible for ionization competition and subsequent ion suppression effects. Mobile phases additive and gradient were investigated to achieve satisfactory sensitivity and resolution of α and β -acids present in ICE-4 standard mixture using a core-shell C18 stationary phase.

Employing a gradient starting from high percentage of organic modifier (50% ACN), together with a slow gradient ramp, at flow rate of 0.4 mL/min with a column temperature of 45 °C, the separation of all six analytes of standard was obtained in less than 20 minutes, the separation between the critical pair of isomers n+adhumulone and n+adlupulone was satisfactory, especially for α -acids, although complete baseline separation was not possible (Supporting Information Figure S5.1 a, c). The contribute to selectivity and resolution of the two different additive of the mobile phase, acetic acid (CH₃COOH) and formic acid (HCOOH) was similar, however HCOOH provided the better ionization efficiency, resulting in highest sensitivity in particular of β -acids (Supporting Information Figure S5.1 b, d). Nevertheless, even if this gradient was satisfactory for ICE-4 standard separation, it was not suitable for the more polar analytes resulting from *in vitro* and *in vivo* metabolism, because the more hydrophilic compounds would not be retained at this

percentage. Hence, a different gradient ramp, starting from lower percentage of acetonitrile (2%) was tested which resulted in a similar resolution, but in higher analysis time (Supporting Information Figure S5.1 e).

5.2.2. Metabolic stability

The metabolic stability of α - and β -acids was investigated by plotting the remaining percentage of parent compounds after 120 min, compared with that at 0 min, against the incubation time. **Figure 5.1** shows the metabolic stability curve and the bar charts graph reflecting the fold reduction of parent compounds, respectively.

After 2 h, average RP % for α -acids was 43.42 ± 5.16 , while for β -acids was 38.95 ± 3.49 , indicating that α -acids presented a higher metabolic stability than β -acids. These results are in accordance with *in vitro* metabolic stability obtained on rabbit microsomes ^[14], although different percentage have been found in the present investigation. These discrepancies can be related to the use of microsomes from different organisms. Among α -acids, cohumulone was the most stable with RP % value = 52.32 ± 2.99 , differently from the isomers n+adhumulone, whose RP % values at 120 min were 43.67 ± 2.49 and 47.74 ± 3.96 , respectively. In particular, *in vitro* $t_{1/2}$ (106.59 ± 8.27) showed that humulone, despite a moderate clearance (*in vitro* $CL_{int} = 13.20 \pm 0.26$; Hepatic $CL_{int} = 1.01 \pm 0.10$) was the most rapidly metabolized α -acid.

Regarding β acids, more than 58% of colupulone was metabolized after 2 h and its *in vitro* $t_{1/2}$ was 106.32 ± 4.32 . Significant differences were observed among the isomers n-lupulone and adlupulone. The calculated *in vitro* $t_{1/2}$ values ($117.52 \pm$

2.82 and 85.21 ± 5.17 , respectively) suggested that adlupulone is metabolized faster than its isomer, but also of all bitter acids present in the sample. This result is further supported by *in vitro* CL_{int} value = 16.30 ± 0.99 and Hepatic CL_{int} = 1.25 ± 0.08 , indicating that adlupulone displayed a higher clearance than α and other β -acids considered in this study. All the parameters of α and β -acids *in vitro* metabolic stability are reported in **Table 5.2**.

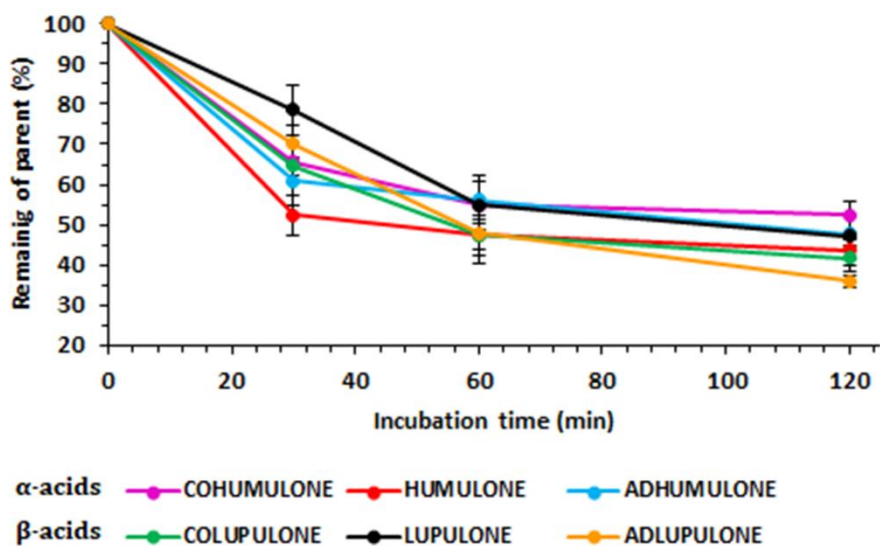


Figure 5.1. Metabolic stability curve of parent ICE-4 α - and β -acids expressed as Remaining of parent %.

Following *in vivo* administration of ICE-4 sample, both parent compounds and related metabolites of α - and β -acids were detected in plasma at 1 and 2 h and in urine at 24 h and 48 h. Since the response factor of the metabolites can be altered by several inevitable parameters as the changes in the metabolite structures, the semi-quantitative analysis using the calibration curve of parent molecules could not

Chapter V: Determination of phase I metabolites and glucuronide conjugates of hop bitter acids metabolites by a full scan/data dependent/targeted neutral loss acquisition UHPLC-HRMS strategy: In vitro microsomal stability and in vivo analysis after oral administration in mice

provide an accurate determination of the metabolite concentrations, therefore only parent compounds were quantified in plasma and urine. Quantitative data, reported in **Table 5.3**, reflect the metabolic trend and highlight how the quantitative profile of α - and β -acids decrease in plasma over 120 min, while the amount excreted in the urine increase after 48 h.

Chapter V: Determination of phase I metabolites and glucuronide conjugates of hop bitter acids metabolites by a full scan/data dependent/targeted neutral loss acquisition UHPLC-HRMS strategy: In vitro microsomal stability and in vivo analysis after oral administration in mice

Table 5.1. Parameters for analytical method validation. Values are expressed as mean of three experiments \pm standard deviation.

Compound	Recovery %	Matrix effect	LOD	LOQ	Recovery %	Matrix effect	LOD (ng/mL)	LOQ
		(%)	(ng/mL)	(ng/mL)	(%)	(%)	(ng/mL)	(ng/mL)
Plasma				Urine				
Cohumulone	104 \pm 4.31	4 \pm 0.04	1.52	4.96	68 \pm 1.91	19 \pm 0.05	0.21	0.71
α-acids Humulone	108 \pm 5.15	8 \pm 0.05	2.51	8.53	103 \pm 4.44	-3 \pm 0.01	0.25	0.84
Adhumulone	107 \pm 5.35	7 \pm 0.05	2.93	9.51	113 \pm 2.90	-13 \pm 0.08	0.36	1.20
Colupulone	101 \pm 4.74	-1 \pm 0.04	3.55	11.80	108 \pm 0.88	-8 \pm 0.02	0.29	0.96
β-acids Lupulone	103 \pm 4.62	-3 \pm 0.03	3.23	11.65	115 \pm 0.66	-16 \pm 0.01	0.24	0.80
Adlupulone	101 \pm 3.13	-1 \pm 0.01	0.47	1.42	93 \pm 1.73	7 \pm 0.01	0.17	0.58

Chapter V: Determination of phase I metabolites and glucuronide conjugates of hop bitter acids metabolites by a full scan/data dependent/targeted neutral loss acquisition UHPLC-HRMS strategy: *In vitro* microsomal stability and *in vivo* analysis after oral administration in mice

Table 5.2. Parameters of ICE-4 α - and β -acids *in vitro* metabolic stability. Values are expressed as mean of three experiments \pm standard deviation.

Compound	RP% 30 min	RP% 60 min	RP% 120 min	k (min ⁻¹)	<i>in vitro</i> t _{1/2} (min)	<i>in vitro</i> CL _{int} (μ L/min/mg)	Hepatic CL _{int} (mL/min)	ER
Cohumulone	65.65 \pm 0.64	54.91 \pm 3.59	52.32 \pm 2.99	0.006 \pm 0.01	135.63 \pm 6.76	10.30 \pm 0.27	0.79 \pm 0.09	0.70 \pm 0.03
α-acids								
Humulone	52.51 \pm 0.15	47.49 \pm 3.20	43.67 \pm 2.49	0.007 \pm 0.01	106.59 \pm 8.27	13.20 \pm 0.26	1.01 \pm 0.10	0.64 \pm 0.04
Adhumulone	60.90 \pm 1.10	56.14 \pm 2.68	47.74 \pm 3.96	0.008 \pm 0.01	117.81 \pm 7.62	12.40 \pm 0.96	0.95 \pm 0.30	0.66 \pm 0.07
β-acids								
Colupulone	64.67 \pm 2.30	47.57 \pm 1.09	41.55 \pm 5.53	0.008 \pm 0.01	106.32 \pm 4.32	13.40 \pm 0.11	1.03 \pm 0.24	0.64 \pm 0.05
Lupulone	78.48 \pm 0.93	55.00 \pm 0.89	47.22 \pm 0.83	0.006 \pm 0.01	117.52 \pm 2.83	11.80 \pm 0.28	0.90 \pm 0.02	0.67 \pm 0.01
Adlupulone	70.21 \pm 1.81	47.93 \pm 0.46	35.89 \pm 1.48	0.009 \pm 0.01	85.21 \pm 5.18	16.30 \pm 0.99	1.25 \pm 0.08	0.59 \pm 0.01
Average RP%: α-acids = 43.42 \pm 5.16; β-acids = 38.95 \pm 3.49								

Abbreviation: RP%, reduction of parent %; k, elimination rate constant; *in vitro* t_{1/2}, *in vitro* half-life; *in vitro* CL_{int}, *in vitro* intrinsic clearance; Hepatic CL_{int}, Hepatic intrinsic clearance; ER, extraction ratio.

Chapter V: Determination of phase I metabolites and glucuronide conjugates of hop bitter acids metabolites by a full scan/data dependent/targeted neutral loss acquisition UHPLC-HRMS strategy: In vitro microsomal stability and in vivo analysis after oral administration in mice

Table 5.3. Quantitative profile of ICE-4 α - and β -acids in mouse plasma and urine samples. Values are expressed as mean of three replicates \pm standard deviation.

Compound		Plasma		Urine	
Time point		60 min ($\mu\text{g/mL}$)	120 min ($\mu\text{g/mL}$)	24 h (ng/mL)	48 h (ng/mL)
α -acids	Cohumulone	13.35 \pm 0.01	5.286 \pm 0.03	36.41 \pm 0.67	58.86 \pm 4.35
	Humulone	18.30 \pm 0.32	6.413 \pm 0.16	29.14 \pm 4.06	115.20 \pm 2.13
	Adhumulone	11.03 \pm 0.08	4.342 \pm 0.14	36.23 \pm 5.12	79.83 \pm 0.04
β -acids	Colupulone	1.26 \pm 0.01	1.141 \pm 0.03	6.21 \pm 0.02	9.30 \pm 0.47
	Lupulone	1.67 \pm 0.02	1.410 \pm 0.03	4.54 \pm 0.01	8.24 \pm 0.14
	Adlupulone	0.27 \pm 0.02	0.268 \pm 0.01	1.78 \pm 0.01	2.55 \pm 0.13

5.2.3. HRMS/MS analysis of α - and β -acids

The HRMS/MS spectra of parent α - and β -acids provided enough specific fragmentation pattern which could be used to confirm the identification of proposed metabolites. Alpha acids were all characterized by a specific fragmentation pattern constituted by a major fragment ion derived from the removal of prenyl group (C_5H_9 , -69 Da) and a minor fragment ion derived from the loss of 112 Da, produced by the consecutive loss of C_5H_9 (-69 Da) and C_3H_7 units (-43 Da), which subsequently undergoes to the loss of CO (-28 Da) ^[2]. Moreover, the fragment derived from loss of H_2O (-18 Da) is also present.

Differently from α -acids, the major fragment ion of β -acids derived from the loss of 112 Da, generated by the consecutive loss of C_5H_9 (-69 Da) and C_3H_7 (-43 Da) groups, while two minor fragments ions result from the removal of prenyl group (C_5H_9 , -69 Da) and of the group C_3H_8 (-44 Da), respectively ^[2]. Other characteristic fragments indicated the multi-prenyl substituted structure of β -acids. Indeed, they derived from the sequential loss of two prenyl groups ($2 \times C_5H_9$ with rearrangement -137 Da) and from the additional loss of C_3H_7 (-43 Da) (Supporting Information Figure S5.2).

5.2.4. Phase I and II metabolites of α - and β -acids

The metabolites present in mouse liver microsomes, plasma and urine were tentatively characterized by their accurate mass, fragmentation pattern and retention times; they were summarized in **Table 5.4**. The high mass accuracy (average mass error < 3 ppm) ensures a high confidence for the assignment of molecular formula

of proposed metabolites. Phase I metabolites included mono-oxidized metabolites and di-oxidized metabolites, resulting to isomerization and/or hydroxylation reaction. Phase II metabolites included glucuronide conjugates. Figure S5.3 in Supporting Information shows the base peak chromatograms of mouse liver microsomal digest, plasma and urine extracts.

5.2.5. Structural characterization of α -acids phase I metabolites

M1-M3 were detected in both *in vitro* and *in vivo* experiments. **M1** eluted at t_r of 13.84 with precursor ion at m/z 363.1813, 15.999 Da higher than cohumulone, **M2** and **M3** (t_r : 14.64 and 14.77, respectively) presented the same precursor ion at m/z 377.1968, and the same mass difference respect to n+adhumulone, suggesting that they were all mono-oxidized metabolites of the related parent compounds. Their fragment ions at m/z 278.1158 ($C_{15}H_{18}O_5$) and 292.1315 ($C_{16}H_{20}O_5$), reproduce the same characteristic fragments of the parents, derived from the consecutive loss of C_5H_9 and OH groups, confirming that, as previously ^[14] reported, they correspond to oxidation products from α -acids, well-known as humulinones (**Figure 5.2 b, c**).

Other α -acids phase I metabolites, resulting from both *in vitro* and *in vivo* metabolic studies, were here detected. **M4** and **M5** (t_r : 10.97 and 11.01, respectively) with $[M-H]^-$ at m/z 393.1918 ($C_{22}H_{29}O_7$) have been proposed as di-oxidized metabolites of n+adhumulone ^[14]. In particular, the fragment ion at m/z 308.1266 ($C_{16}H_{19}O_5$), deriving from the removal of C_5H_9O (-85 Da) suggested that one hydroxylation could occur at prenyl moiety. Interestingly, *in vivo* study revealed two novel potential di-oxidized metabolites of n+adhumulone, here namely **M6** and

Chapter V: Determination of phase I metabolites and glucuronide conjugates of hop bitter acids metabolites by a full scan/data dependent/targeted neutral loss acquisition UHPLC-HRMS strategy: In vitro microsomal stability and in vivo analysis after oral administration in mice

and **M12** (t_r of 17.38, 18.12 and 18.16 respectively) showed all a 16 Da mass difference, indicating a single oxidation. The fragment ions at m/z 287.1287 ($C_{17}H_{19}O_4$) and 301.1446 ($C_{18}H_{21}O_4$), possess the same fragment ions of parent compounds, derived from the loss of 112 Da and OH group, confirming that they correspond to the well-known oxidation metabolites of β -acids, resulting in the cyclization to hulupone derivatives [14] (**Figure 5.3 a-e**).

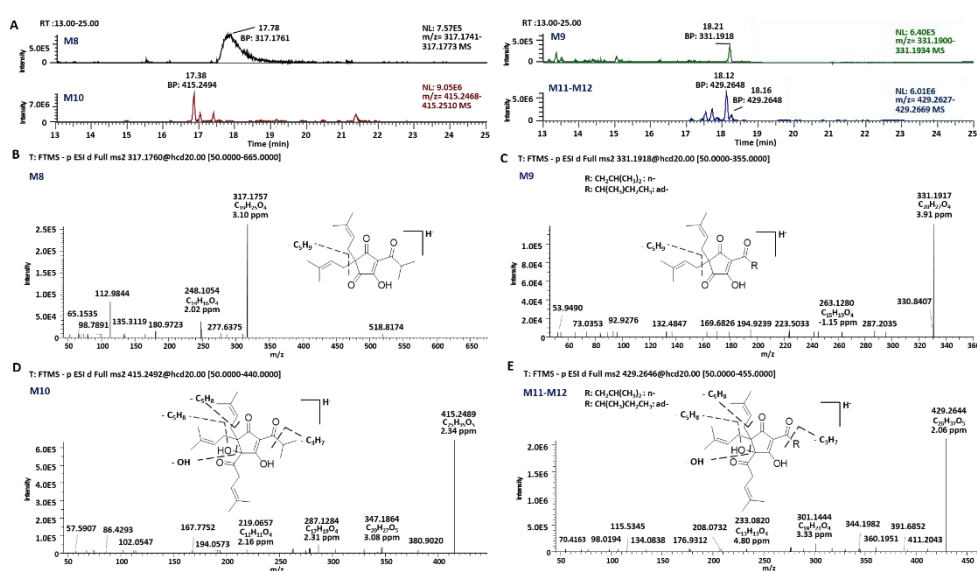


Figure 5.3. Extracted ion chromatograms (a) and MS² spectra with the fragmentation pathways (b-e) of ICE-4 β -acids phase I metabolites.

5.2.7. Structural characterization of α -acids phase II metabolites

α - and β -acids phase I metabolites have been characterized by DDA acquisition. For many years, one of the most valid strategies to detect phase II metabolites has

been the neutral loss (NL) scan on triple quadrupole instruments [23, 24]. Despite the sensitivity, these approaches suffer from the lack of selectivity due to low resolution. On the contrary, high mass accuracy in both MS and MS/MS stages, high resolution and stepped HCD fragmentation provides informative MS/MS spectra, resulting in more confident metabolite characterization. Here a targeted NL strategy was performed by implementing an inclusion list which takes into account the accurate masses of α and β -acids and their oxidized metabolites plus the potential loss of glucuronide moiety ($C_6H_8O_6$, 176.0320 Da). This resulted in the detection of several glucuronide conjugated not only after microsomal metabolism but also in plasma and urine samples.

Metabolites **M13**, **M14** and **M15** were detected after *in vitro* and *in vivo* experiments and were tentatively identified as cohumulone and n+adhumulone glucuronide (**Figure 5.4 b, c**) In fact, they were all characterized by the same fragmentation pattern, consisting of a main fragment ion, corresponding to their precursor ion after the cleavage of $C_6H_8O_6$, and the characteristic fragments of α -acids, such as the loss of C_5H_9 group. Moreover, glucuronide derivatives of oxidized I phase metabolites were detected *in vivo* both in plasma and urine. In particular, **M16** eluted at at r_t of 10.61 with precursor ion at m/z 539.2138 ($C_{26}H_{35}O_{12}$), showed the fragment ion at m/z 363.1810 ($C_{20}H_{27}O_6$) and 278.1158 ($C_{15}H_{18}O_5$), suggesting that it corresponds to **M1**-glucuronide. **M17** and **M18** (r_t : 11.33 and 11.41) presented the same parent ion at m/z 553.2287 ($C_{27}H_{37}O_{12}$). Considering the fragments at m/z 377.1968 ($-C_6H_8O_6$, 176 Da) and 292.1315 (-

Chapter V: Determination of phase I metabolites and glucuronide conjugates of hop bitter acids metabolites by a full scan/data dependent/targeted neutral loss acquisition UHPLC-HRMS strategy: In vitro microsomal stability and in vivo analysis after oral administration in mice

C₅H₉O, 85 Da), they were tentatively identified as **M2** and **M3** glucuronides (**Figure 5.4 d, e**)

M19 and **M20** showed m/z at 569.2245 (C₂₇H₃₇O₁₃) and main fragment ions at 393.1918 (C₂₂H₂₉O₇) and 308.1266, again deriving from the cleavage of oxidized prenyl side chain, so they were proposed as **M4** and **M5**-glucuronide. Lastly, **M21** and **M22** both with [M-H]⁻ at m/z 567.2087 (C₂₇H₃₅O₁₃) (r_t: 12.72 and 12.90, respectively) were characterized by the same fragmentation pattern, consisting of a main fragment ion at m/z 291.1240 (C₁₆H₁₉O₅) and another fragment at 391.1761 (C₂₂H₂₇O₇), therefore they were tentatively identified as **M6** and **M7** glucuronides (**Figure 5.4 f, g**).

Chapter V: Determination of phase I metabolites and glucuronide conjugates of hop bitter acids metabolites by a full scan/data dependent/targeted neutral loss acquisition UHPLC-HRMS strategy: *In vitro* microsomal stability and *in vivo* analysis after oral administration in mice

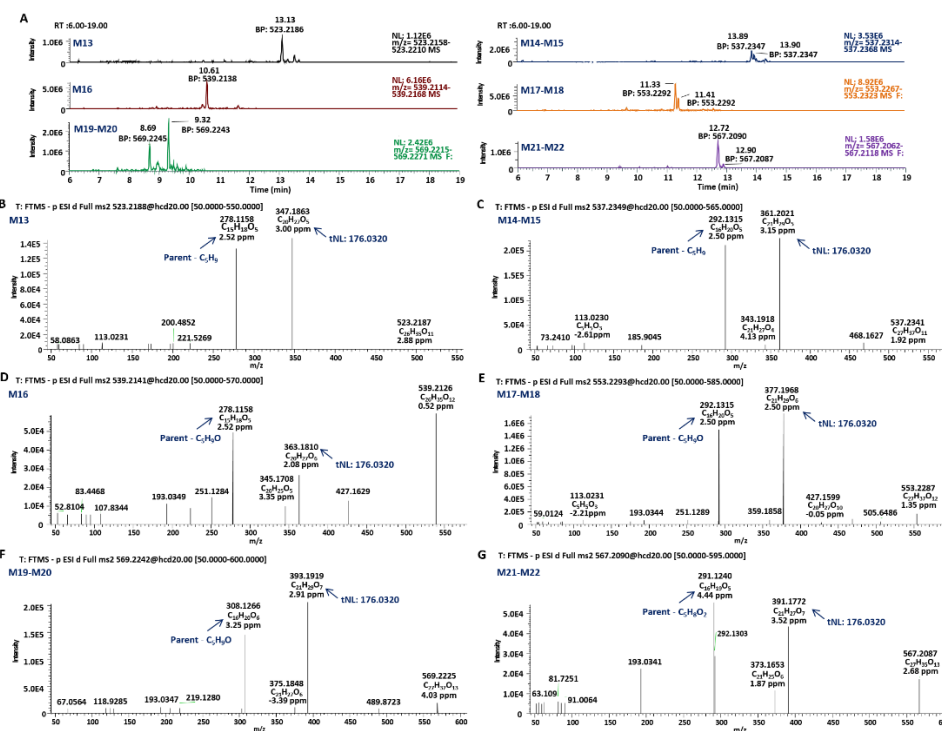


Figure 5.4. Extracted ion chromatograms (a) and MS² spectra with the fragmentation pathways (b-g) of ICE-4 α -acids phase II metabolites.

5.3. Discussion

In the present study, the metabolic stability of hop bitter acids has been evaluated, showing that α -acids are more stable than β -acids. Noteworthy *in vitro* clearance and *in vitro* $t_{1/2}$ for α - and β -acids are here reported for the first time. These parameters can provide an estimate of the *in vivo* metabolic stability of the molecules and information for further bioavailability evaluation [25]. From the result here presented, hop α - and β -acids can be considered molecules with relative low

Chapter V: Determination of phase I metabolites and glucuronide conjugates of hop bitter acids metabolites by a full scan/data dependent/targeted neutral loss acquisition UHPLC-HRMS strategy: In vitro microsomal stability and in vivo analysis after oral administration in mice

extraction ratio. Liver microsomes are the most frequently used tool for profiling and identification of drug metabolites, since they contain most of the enzymes that metabolize drugs, in particular CYP450^[26]. In this work, mouse model microsomes were chosen as the most used for preliminary metabolic screening^[27, 28]. However, drug metabolism is species dependent, and humans can show different results from animals in drug metabolism^[29]. For this reason, comparison between liver microsomes of different species is needed, in order to have an accurate prediction of *in vivo* metabolism.

When subjected to *in vitro* gastro-intestinal digestion, both α - and β -acids remained stable, in fact, no significant changes were noted in peak areas and no transformation products were detected (Supporting Information Figure S5.4), suggesting that the molecules maintain their chemical properties during digestion. In addition, all bitter acids showed a higher plasma stability, which plays an important role in pharmacokinetics evaluation, since unstable compounds tend to have rapid clearance and short half-life, resulting in poor *in vivo* performance^[6, 30]. Therefore, these results are in accordance with the long *in vitro* $t_{1/2}$ and the low to moderate *in vitro* clearance discussed above.

The multiple acquisition option and high mass accuracy of Q-Exactive platform was highly suitable to follow the metabolic fate of target compounds and for the detection and characterization of their metabolites both *in vitro* and *in vivo*. In particular, the combined approach FS/DDA/tNL was mandatory to demonstrate that for α -acids glucuronide conjugate metabolism should be taken into account. Clearly, without isolation and NMR characterization, the exact location of

glucuronidation site is merely putative, even if the isolation of pure compounds in sufficient amount could be economically prohibitive. Despite this a useful approach is represented from *in silico* prediction of potential sites of metabolism (SOM), in this regard QSAR based approaches have been used with success ^[31], and implemented in several free online tools based on structural formula of chemicals or descriptors. For this purpose, we have investigated the potential prediction of glucuronide derivatives of α - and iso- α -acids the open source FAME3 (<https://nerdd.zbh.uni-hamburg.de/fame3/>) ^[32], as a result, the approach proposed as first hits the hydroxyl substituents in position C3 and C4 for α -acids and C1 and C2 for iso- α -acids as most probable SOM for UGTs catalyzed glucuronidation, results from *in silico* prediction are reported in Supporting Information Figure S5.5.

The formation of α and β -acid conjugates has not been demonstrated so far, this because previous studies mainly employed SIM or SRM approaches ^[14, 33], or enzymatic deconjugation ^[15]. A significant phase II metabolism has been proposed for dihydro iso- α -acids (DHIAA), but no derivative has been described so far ^[16]. Here we showed a significant glucuronidation of α -acids, suggesting also a possible conjugation of IAA and DHIAA. Notably, regarding β -acids, no glucuronide conjugates were detected neither *in vitro* nor *in vivo*. The discrepancy could be attributed to the additional prenyl side chain resulting in steric hindrance to glucuronide conjugation, besides, it has been reported that extra prenylation influences the intestinal absorption of β -acids ^[3, 15]. However, it is not excluded that other conjugations, such as sulphate conjugation, may occur, and this is currently

Chapter V: Determination of phase I metabolites and glucuronide conjugates of hop bitter acids metabolites by a full scan/data dependent/targeted neutral loss acquisition UHPLC-HRMS strategy: In vitro microsomal stability and in vivo analysis after oral administration in mice

under evaluation, together with the possible isolation of derivatives for detailed NMR characterization.

Chapter V: Determination of phase I metabolites and glucuronide conjugates of hop bitter acids metabolites by a full scan/data dependent/targeted neutral loss acquisition UHPLC-HRMS strategy: In vitro microsomal stability and in vivo analysis after oral administration in mice

Table 5.4. Observed metabolites of ICE-4 α - and β -acids in mouse liver microsomes, in mouse plasma and urine, Abbreviation: P, parent compound; O, oxidation; OH, hydroxylation; Gluc., glucuronidation.

Compound	r_t (min)	[M-H] ⁻	Fragment ions	Error (ppm)	Molecular Formula	Metabolization	In vitro	In vivo
<i>Parent α- and β-acids</i>								
Cohumulone	17.48	347.1863	278.1158; 235.0606; 207.0656	2.82	C ₂₀ H ₂₇ O ₅	P	✓	✓
n-humulone	18.30	361.2020	292.1315; 249.0766; 207.0657	2.98	C ₂₁ H ₂₉ O ₅	P	✓	✓
Adhumulone	18.48	361.2020	292.1315; 249.0766; 207.0657	2.98	C ₂₁ H ₂₉ O ₅	P	✓	✓
Colupulone	21.01	399.2540	287.1287; 330.1287; 219.0658	2.61	C ₂₅ H ₃₅ O ₄	P	✓	✓
n-Lupulone	21.80	413.2698	301.1446; 344.1991; 233.0808	2.83	C ₂₆ H ₃₇ O ₄	P	✓	✓
Adlupulone	21.95	413.2698	301.1446; 344.1991; 233.0808	2.83	C ₂₆ H ₃₇ O ₄	P	✓	✓
<i>α-acids phase I metabolites</i>								

Chapter V: Determination of phase I metabolites and glucuronide conjugates of hop bitter acids metabolites by a full scan/data dependent/targeted neutral loss acquisition UHPLC-HRMS strategy: In vitro microsomal stability and in vivo analysis after oral administration in mice

M1	13.84	363.1814	278.1158; 235.0603; 207.0642	3.25	C ₂₀ H ₂₇ O ₆	P + O	✓	✓
M2	14.64	377.1968	292.1315; 249.0765;	2.42	C ₂₁ H ₂₉ O ₆	P + O	✓	✓
M3	14.77	377.1968	292.1315; 249.0765;	2.42	C ₂₁ H ₂₉ O ₆	P + O	✓	✓
M4	10.97	393.1917	308.1263; 375.1819; 291.1231; 249.0760	2.45	C ₂₁ H ₂₉ O ₇	P + O + OH	✓	✓
M5	11.01	393.1917	308.1263; 375.1819; 291.1231; 249.0760	2.45	C ₂₁ H ₂₉ O ₇	P + O + OH	✓	✓
M6	14.35	391.1761	291.1237; 221.1179	2.52	C ₂₁ H ₂₇ O ₇	P + O + O	×	✓
M7	14.57	391.1761	291.1237; 221.1179	2.52	C ₂₁ H ₂₇ O ₇	P + O + O	×	✓
<i>β-acids phase I metabolites</i>								
M8	17.78	317.1757	248.1054; 135.3119;	3.10	C ₁₉ H ₂₅ O ₄	P + O	✓	✓
M9	18.21	331.1917	263.1280; 287.2035	3.91	C ₂₀ H ₂₇ O ₄	P + O	✓	✓
M10	17.38	415.2489	347.1864; 287.1284; 219.2657	2.34	C ₂₅ H ₃₅ O ₅	P + O	✓	✓

Chapter V: Determination of phase I metabolites and glucuronide conjugates of hop bitter acids metabolites by a full scan/data dependent/targeted neutral loss acquisition UHPLC-HRMS strategy: In vitro microsomal stability and in vivo analysis after oral administration in mice

M11	18.12	429.2644	301.1444; 233.0820	2.06	C ₂₆ H ₃₇ O ₅	P + O	✓	✓
M12	18.16	429.2644	301.1444; 233.0820	2.06	C ₂₆ H ₃₇ O ₅	P + O	✓	✓
<i>α-acids phase II glucuronide</i>								
M13	13.13	523.2187	347.1863; 278.1158;	2.88	C ₂₆ H ₃₅ O ₁₁	P + Gluc.	✓	✓
M14	13.89	537.2351	361.2021; 292.1315; 343.1918	1.92	C ₂₇ H ₃₇ O ₁₁	P + Gluc.	✓	✓
M14	13.90	537.2351	361.2021; 292.1315; 343.1918	1.92	C ₂₇ H ₃₇ O ₁₁	P + Gluc.	✓	✓
M16	10.61	539.2126	363.1810; 278.1152; 345.1708	0.52	C ₂₆ H ₃₅ O ₁₂	P + O + Gluc.	×	✓
M17	11.33	553.2287	377.1968; 292.1315	1.35	C ₂₇ H ₃₇ O ₁₂	P + O + Gluc.	×	✓
M18	11.41	553.2287	377.1968; 292.1315	1.35	C ₂₇ H ₃₇ O ₁₂	P + O + Gluc.	×	✓
M19	8.69	569.2225	393.1919; 308.1966; 375.1848	4.03	C ₂₇ H ₃₇ O ₁₃	P + O + OH + Gluc.	×	✓
M20	9.32	569.225	393.1919; 308.1966; 375.1848	4.03	C ₂₇ H ₃₇ O ₁₃	P + O + OH + Gluc..	×	✓

Chapter V: Determination of phase I metabolites and glucuronide conjugates of hop bitter acids metabolites by a full scan/data dependent/targeted neutral loss acquisition UHPLC-HRMS strategy: In vitro microsomal stability and in vivo analysis after oral administration in mice

M21	12.72	567.2087	391.1772; 291.1240: 373.1643	2.68	C ₂₇ H ₃₅ O ₁₃	P + O + O + Gluc.	×	✓
M22	12.90	567.2087	391.1772; 291.1240: 373.1643	2.68	C ₂₇ H ₃₅ O ₁₃	P + O + O + Gluc.	×	✓

5.4. Materials and methods

5.4.1. Chemicals

LC-MS-grade Water (H₂O) acetonitrile (ACN), methanol (CH₃OH), additives formic acid (HCOOH), were all purchased from Sigma-Aldrich (St. Louis, MO, USA). International calibration standard ICE-4 bitter acids mixture was purchased by LaborVeritas (Zurich, Switzerland). Microsomes from liver, pooled from CD-1 male mouse, Uridine 5'-diphosphoglucuronic acid (UDPGA) trisodium salt, Nicotinamide adenine dinucleotide phosphate (NADPH), Alamethicin from *trichoderma viride* were purchased by Merck (Milan, Italy). Unless stated otherwise other reagent were all purchased by Merck.

5.4.2. Sample preparation

International Calibration Extract 4 (ICE-4) for α - and β -acids was reported to contain 10.88% cohumulone; 31.60% n+adhumulone; 13.02% colupulone; 13.52% n+adlupulone. Stock solution (10 mg/mL) of ICE-4 standard was prepared weighing 150 mg in a 15-mL volumetric flask. 8 mL of CH₃OH were added to the flask, which was sonicated for 10 min and filled to volume with CH₃OH. The ICE-4 stock solution was filtered through a 0.45 μ m nylon filter and was diluted with CH₃OH to concentration of working solutions.

5.4.3. Instrumentation

UHPLC-HRMS/MS analysis were performed on a Thermo Ultimate RS 3000 coupled online to a Q-Exactive hybrid quadrupole Orbitrap mass spectrometer

(Thermo Fisher Scientific, Bremen, Germany) equipped with a heated electrospray ionization probe (HESI II). The separation was carried on a Kinetex[®] EVO[™] C18 (100 × 2.1 mm; 2.6 μm, 100Å) protected with a SecurityGuard[™] precolumn (5 × 2.1 mm) (Phenomenex, Bologna, Italy). The column temperature was set at 45 °C, a flow-rate of 0.4 mL/min was used, mobile phase consisted of (A): H₂O with 0.1% HCOOH (v/v) and (B): ACN with 0.1% HCOOH (v/v). The following gradient has been used: 0 min, 2%B, 15 min, 60%B, 25 min, 90%B, 26 min, 100 %B, hold for 5 min, returning to 2% in 0.1 min. 5 μL were injected. HRMS analysis was performed with Full MS (*m/z* 100-850) and data-dependent acquisition (DDA) at a resolution of 35,000 and 15,000 FWHM at *m/z* 200 respectively, a targeted neutral loss scan (tNL) was set with an inclusion list of possible metabolites based on their accurate mass; stepped normalized collision energy (NCE) with values of 15, 25 and 30 was used. Negative ESI was employed. Source parameters were: Sheath gas pressure, 50 arbitrary units; auxiliary gas flow, 13 arbitrary units; spray voltage, -2.50 kV; capillary temperature, 260 °C; auxiliary gas heater temperature, 300 °C, S-lens RF value: 30 arbitrary units. Three replicates of each sample were performed, QC were randomly inserted in the batch to monitor system stability over time.

5.4.4. In vitro metabolism of hop bitter acids

2 μL of ICE-4 (5 mg/mL, which corresponded to Cohumulone 1.6 mM; n-Humulone 3.3 mM; Adhumulone 1.05 mM; Colupulone 1.7 mM; n-Lupulone 1.3 mM; Adlupulone 0.4 mM) were incubated with 163 μL of 100 mM phosphate buffer (pH 7.4), 5 μL of 20 mg/mL of mouse microsomes (obtaining a final concentration of microsomes protein content of 0.5 mg/mL) and 20 μL of UGT

Chapter V: Determination of phase I metabolites and glucuronide conjugates of hop bitter acids metabolites by a full scan/data dependent/targeted neutral loss acquisition UHPLC-HRMS strategy: In vitro microsomal stability and in vivo analysis after oral administration in mice

solution consisting of 5 mM UDPGA, 25 µg Alamethicin/mg microsomal proteins and 1 mM MgCl in reaction mixture. After pre-incubation at 37 °C for 10 min, the mixture was incubated with 10 µL of the 20 mM NADPH at 37 °C in a Thermomixer comfort (Eppendorf, Hamburg, Germany) for 0, 30 min, 60 min and 120 min. The reactions were quenched adding 200 µL of the ice-cold CH₃OH/ACN (90:10 v/v), then the samples were centrifuged at 14,680 rpm, for 5 min at 25 °C. (Eppendorf® microcentrifuge 5424, Hamburg, Germany). The supernatants were dried under nitrogen and were reconstituted in 100 µL of CH₃OH/H₂O (70:30) + 0.1% HCOOH (v/v) prior LC-HRMS/MS analysis. Each experiment was conducted in triplicate.

The control at 0 min was obtained by addition of the organic solvent immediately after incubation with microsomes. Xanthohumol (1 mM) was used as positive control and incubated in parallel, while the negative control was prepared by incubation up to 120 min without NADPH to ensure that metabolite formation was dependent on the presence of NADPH.

5.4.4.1. Calculation of in vitro metabolic stability parameters

The extent of metabolism is expressed as remaining percentage of parent compound using the following equation:

$$\text{Remaining of parent \% (RP\%)} = \left(\frac{\text{parent compound concentration after microsomal digestion}}{\text{parent compound concentration in control at 0 min}} \right) \times 100 \quad (1)$$

Chapter V: Determination of phase I metabolites and glucuronide conjugates of hop bitter acids metabolites by a full scan/data dependent/targeted neutral loss acquisition UHPLC-HRMS strategy: In vitro microsomal stability and in vivo analysis after oral administration in mice

The metabolic stability curves were created by plotting the remaining of parent compounds % (RP %) (y- axis) against the incubation time (x- axis). The elimination rate constant (k , min^{-1}) was the slope of the linear range creating by plotting the natural logarithm (Ln) of RP% at 0 and 120 min against the incubation time ^[34]. *In vitro* $t_{1/2}$, *in vitro* intrinsic clearance (*in vitro* CL_{int}), Hepatic intrinsic clearance (Hepatic CL_{int}) and extraction ratio (ER) were calculated using the following equations ^[34, 35] :

$$\text{In vitro } t_{1/2} (\text{min}) = \text{Ln}(2)/k \quad (2)$$

$$\text{In vitro } \text{CL}_{\text{int}} (\mu\text{L}/\text{min}/\text{mg}) = k \times \left(\frac{\mu\text{L incubation}}{\text{mg microsomes protein content}} \right) \quad (3)$$

$$\text{Hepatic } \text{CL}_{\text{int}} (\text{mL}/\text{min}) = \text{In vitro } \text{CL}_{\text{int}} (\text{mL}/\text{min}/\text{mg}) \times \text{MPPGL} (\text{mg}/\text{g}) \times \text{WL} (\text{g}) \quad (4)$$

$$\text{ER} = \frac{Q \times f_u}{Q + (f_u \times \text{Hepatic } \text{CL}_{\text{int}})} \quad (5)$$

Where **MPPGL** is 45 mg microsomes protein per g liver ^[36]; **WL** is the liver weight (1.7 g for mouse); **Q** is the hepatic blood flow (1.8 mL/min for mouse) ^[37]; f_u is the free fraction in blood, assumed as 1.

5.4.5. In vivo studies

5.4.5.1. Animal experiments

All experiments involving animals were conform to the guidelines for the Care and Use of Laboratory Animals published from Directive 2010/63/EU of the European Parliament.

Male C57BL/6 mice (25 ± 0.7 g body weight) were housed in groups (2-4 mice per cage) in a specific pathogen-free controlled environment (inverted 12 h light cycle; lights off at 10:00 hours). All mice had free access to standard mice chow and water.

ICE-4 sample was dissolved in 70% CH₃CH₂OH and was administered by a single gavage (dosage 400 µg/Kg) in a total volume of 200 µL.

For plasma sample collection, after treatment mice were sacrificed at 1 hour (1 h) and at 2 hours (1 h) from administration. Control mice were treated with vehicle alone. At these time points blood was collected from the heart through cardiac puncture of isofluorane-anesthetized mice in heparinized tube, and rapidly centrifuged at 2200 rpm for 15 minutes to obtain plasma samples.

In some mice housed in a metabolic cage, urine samples were collected after 24 and 48 hours.

5.4.5.2. Plasma and urine extraction

For α - and β -acids and related metabolites extraction, 25 µL of plasma were thawed on ice and 100 µL of ice-cold CH₃OH/ACN (90:10 v/v) were added. Samples were vortexed for 30 s and finally centrifuged at 14,680 rpm, for 5 min at 4°C. 80 µL of supernatant were dried under nitrogen.

Chapter V: Determination of phase I metabolites and glucuronide conjugates of hop bitter acids metabolites by a full scan/data dependent/targeted neutral loss acquisition UHPLC-HRMS strategy: In vitro microsomal stability and in vivo analysis after oral administration in mice

Urine extraction was performed as follows: 0.5 mL of urine samples were thawed on ice and diluted with 0.5 mL of H₂O. Samples were vortexed for 30s and were subjected to solid phase extraction (SPE). Samples were loaded on Strata-X 33 μ Polymeric Reversed Phase 100 mg/3 mL cartridge (Phenomenex, Bologna, Italy), previously conditioned with 2 mL of CH₃OH and equilibrated with 2 mL of H₂O. 3 mL of H₂O were used for washing phase and finally the samples were eluted with 3 mL of CH₃OH/ACN (90:10 v/v) and eluates were dried under nitrogen.

The dried samples were reconstituted in 100 μ L of MeOH/H₂O (70:30) + 0.1% HCOOH (v/v) and injected in LC-HRMS/MS.

5.4.5.3. Gastrointestinal fluid and plasma stability

For *in vitro* gastrointestinal and plasma stability assessment, 25 μ L of ICE-4 solution (3 mg/mL) was added to 150 μ L of 0.1 N HCl solution (pH 2), 10 mM HCOONH₄ solution (pH adjusted to 7.4 with NH₄OH, and plasma control sample. The mixtures were kept under gentle stirring at 37°C. During incubation, aliquots were withdrawn at 0, 60, 120 and 180 min, extracted and analyzed as described previously.

5.4.6. Method validation

ICE-4 mixture was selected as external standards for the quantification of parent α - and β acids in both *in vitro* and *in vivo* stability studies. Matrix matched calibration curves were obtained as follow: 10 μ L of ICE-4 1000 μ g/mL solution in CH₃OH were added to 90 μ L of matrix to obtain a 100 μ g/mL of ICE-4 stock solutions.

Chapter V: Determination of phase I metabolites and glucuronide conjugates of hop bitter acids metabolites by a full scan/data dependent/targeted neutral loss acquisition UHPLC-HRMS strategy: In vitro microsomal stability and in vivo analysis after oral administration in mice

Calibration curve in the range of 0.5–100 µg/mL (total ICE-4 concentration) with six concentration levels, were used to generate calibration curve from regression analysis ($R^2 \geq 0.999$) and apply to quantitation of α - and β -acids in plasma. Calibration curve for urine was constructed in the range of 0.5 – 25 µg/mL ($R^2 \geq 0.998$). Identical standard solutions were also prepared in methanol and used for the assessment of matrix effects.

Note that each standard concentration level contained different amounts of the individual analytes, reflected in the concentrations shown in Table S5.1.

Repeatability was established by triplicate injections of samples and solutions at low, medium, and high concentration levels of the calibration curve with the same chromatographic conditions and analyst at the same day and within two consecutive days and results were expressed as CV % for concentration and retention time.

Limits of detection (LODs) and quantification (LOQs) were calculated by the ratio between the standard deviation (SD) and analytical curve slope multiplied by 3 and 10, respectively.

Recovery was assessed by spiking a known amount of ICE-4 standard solution in methanol at low, medium and high concentration range in control samples, which were subsequently extracted as described in section 5.4.5.2.

Quality control (QC) were prepared by serially diluting the 100 µg/mL spiked blank serum sample to obtain plasma sample containing 20 µg/mL of ICE-4 solution.

5.5. Conclusions

In this study, a UHPLC-HRMS method was developed and validated to investigate the metabolic stability of hop bitter acids. After *in vitro* incubation with mice liver microsomes, both α - and β -acids showed relative slow metabolism and excretion rates with long *in vitro* $t_{1/2}$ and moderate hepatic CL_{int} . Furthermore, I and II phase metabolites were profiled and initially characterized *in vitro* by microsomal digestion and *in vivo*, in mouse plasma and urine following oral administration, beside the quantification of the parent compounds in the biological samples.

The FS-DDA approach showed the formation of 7 phase I metabolites of α -acids, comprising novel n+adhumulone metabolites deriving from oxidative metabolic pathways. Moreover, 5 mono-oxidized metabolites of β -acids were confirmed. On the other hand, the tNL approach allowed to detect for the first time α -acids glucuronide conjugates, and, exclusively *in vivo*, glucuronide derivatives of oxidized phase I metabolites. These data extended the knowledge of metabolic profile of hop bitter acids and could provide a concrete help in predicting their pharmacokinetic profiles.

5.6. References

[1] Moir, M. Hops—A millennium review. *J. Am. Soc. of Brew. Chem.* 2000, 58, 131–146.

[2] Sommella, E., Pagano, F., Salviati, E., Chieppa, M., Bertamino, A., Manfra, M., Sala, M., Novellino, E., Campiglia, P. Chemical profiling of bioactive constituents in hop cones and pellets extracts by online comprehensive two-dimensional liquid chromatography with tandem mass spectrometry and direct

Chapter V: Determination of phase I metabolites and glucuronide conjugates of hop bitter acids metabolites by a full scan/data dependent/targeted neutral loss acquisition UHPLC-HRMS strategy: In vitro microsomal stability and in vivo analysis after oral administration in mice

infusion Fourier transform ion cyclotron resonance mass spectrometry, *J. Sep.Sci.* 2018, *41*, 1548–1557.

[3] Karabin, M., Hudcova, T., Jelinek, L., Dostalek, P. Biotransformations and biological activities of hop flavonoids. *Biotechn. Adv.* 2015, *33*, 1063–1090.

[4] Gerhauser, C., Alt, A., Heiss, E., Gamal-Eldeen, A., Klimo, K., Knauft, J., Neumann, I., Scherf, H.-R., Frank, N., Bartsch, H., Becker, H. Cancer chemopreventive activity of xanthohumol, a natural product derived from hop. *Mol. Cancer Ther.* 2002, *1*, 959–969.

[5] Dietz, B.M., Kang, Y.-H., Liu, G., Egger, A.L., Yao, P., Chadwick, L.R., Pauli, G.F., Farnsworth, N.R., Mesecar, A.D., Van Breemen, R.B., Bolton, J.L. Xanthohumol isolated from *Humulus lupulus* inhibits menadione-induced DNA damage through induction of quinone reductase, *Chem. Res. Toxicol.* 2005, *18*, 1296–1305.

[6] Gao, S., Hu, M. Bioavailability Challenges Associated with Development of Anti-Cancer Phenolics, *Song Mini Rev. Med. Chem.* 2010, *10*, 550–567.

[7] Possemiers, S., Bolca, S., Grootaert, C., Heyerick, A., Decroos, K., Dhooge, W., De Keukeleire, D., Rabot, S., Verstraete, W., Van de Wiele, T. The prenylflavonoid isoxanthohumol from hops (*Humulus lupulus* L.) is activated into the potent phytoestrogen 8-prenylnaringenin in vitro and in the human intestine. *J. Nutr.* 2006, *136*, 1862–1867.

[8] Possemiers, S., Heyerick, A., Robbens, V., De Keukeleire, D., Verstraete, W. Activation of proestrogens from hops (*Humulus lupulus* L.) by intestinal

Chapter V: Determination of phase I metabolites and glucuronide conjugates of hop bitter acids metabolites by a full scan/data dependent/targeted neutral loss acquisition UHPLC-HRMS strategy: In vitro microsomal stability and in vivo analysis after oral administration in mice

microbiota; Conversion of isoxanthohumol into 8-prenylnaringenin. *J. Agric. Food Chem.* 2005, 53, 6281–6288.

^[9] Nikolic, D., Li, Y., Chadwick, L.R., Pauli, G.F., van Breemen, R.B. Metabolism of xanthohumol and isoxanthohumol, prenylated flavonoids from hops (*Humulus lupulus* L.), by human liver microsomes. *J. Mass Spectrom.* 2005, 40, 289–299.

^[10] Legette, L., Karnpracha, C., Reed, R.L., Choi, J., Bobe, G., Christensen, J.M., Rodriguez-Proteau, R., Purnell, J.Q., Stevens, J.F. Human pharmacokinetics of xanthohumol, an antihyperglycemic flavonoid from hops. *Mol. Nutr. Food Res.* 2014, 58, 248–255.

^[11] Jirásko, R., Holčapek, M., Vrublová, E., Ulrichová, J., Šimánek, V. Identification of new phase II metabolites of xanthohumol in rat in vivo biotransformation of hop extracts using high-performance liquid chromatography electrospray ionization tandem mass spectrometry. *J. Chromatogr. A* 2010, 1217, 4100–4108.

^[12] Van Cleemput, M., Cattoor, K., De Bosscher, K., Haegeman, G., De Keukeleire, D., Heyerick, A. Hop (*Humulus lupulus*)–Derived Bitter Acids as Multipotent Bioactive Compounds. *J. Nat. Prod.* 2009, 72, 1220–1230.

^[13] Salviati, E., Ciaglia, E., Sommella, E., Montella, F., Bertamino, A., Ostacolo, C., Parrino, B., Rubino, R., Vecchione, C., Puca, A., Novellino, E., Campiglia, P. Immunomodulatory activity of *Humulus lupulus* bitter acids fraction: Enhancement of natural killer cells function by NKp44 activating receptor stimulation. *J. Funct. Foods* 2019, 61, 103469.

Chapter V: Determination of phase I metabolites and glucuronide conjugates of hop bitter acids metabolites by a full scan/data dependent/targeted neutral loss acquisition UHPLC-HRMS strategy: In vitro microsomal stability and in vivo analysis after oral administration in mice

^[14] Cattoor, K., Dresel, M., De Bock, L., Boussery, K., Van Bocxlaer, J., Remon, J.P., De Keukeleire, D., Deforce, D., Hofmann, T., Heyerick, A. Metabolism of hop-derived bitter acids. *J. Agric. Food Chem.* 2013, *61*, 7916–7924.

^[15] Cattoor, K., Bracke, M., Deforce, D., De Keukeleire, D., Heyerick, A. Transport of hop bitter acids across intestinal Caco-2 cell monolayers. *J. Agric. Food Chem.* 2010, *58*, 4132–4140.

^[16] Cattoor, K., Remon, J.P., Boussery, K., Van Bocxlaer, J., Bracke, M., De Keukeleire, D., Deforce, D. Heyerick, A. Bioavailability of hop-derived iso- α -acids and reduced derivatives. *Food Funct.* 2011, *2*, 412–422.

^[17] Rodda, L.N., Gerostamoulos, D., Drummer, O.H. The rapid identification and quantification of iso- α -acids and reduced iso- α -acids in blood using UHPLC-MS/MS: validation of a novel marker for beer consumption. *Anal. Bioanal. Chem.* 2013, *405*, 9755–9767.

^[18] Ruefer, C.E., Gerhauser, C., Frank, N., Becker, H., Kulling, S.E. In vitro phase II metabolism of xanthohumol by human UDP-glucuronosyltransferases and sulfotransferases. *Mol. Nutr. Food Res.* 2005, *49*, 851–856.

^[19] Ge, S., Tu, Y., Hu, M. Challenges and opportunities with predicting in vivo phase II metabolism via glucuronidation from in vitro data. *Curr. Pharmacol. Rep.* 2016, *2*, 326–338.

^[20] Meyer, M.R., Maurer, H.H. Current applications of high-resolution mass spectrometry in drug metabolism studies. *Anal. Bioanal. Chem.* 2012, *403*, 1221–1231.

Chapter V: Determination of phase I metabolites and glucuronide conjugates of hop bitter acids metabolites by a full scan/data dependent/targeted neutral loss acquisition UHPLC-HRMS strategy: In vitro microsomal stability and in vivo analysis after oral administration in mice

[21] Method development and validation for Ultra-high-pressure LC/MS/MS determination of hop prenylflavonoids in human serum. Yuan, Y., Qiu, X., Nikolic, D., Dahl, J.H., van Breemen, R.B. *J. AOAC Int.* 2012, 95, 1744–1749.

[22] Overk, C. R., Guo, J., Chadwick, L. R., Lantvit, D. D., Minassi, A., Appendino, G., Chen, S. N., Lankin, D. C., Farnsworth, N. R., Pauli, G. F., van Breemen, R. B., & Bolton, J. L. In vivo estrogenic comparisons of *Trifolium pratense* (red clover) *Humulus lupulus* (hops), and the pure compounds isoxanthohumol and 8-prenylnaringenin. *Chem. Biol. Interact.* 2008, 176, 30–39.

[23] Hopfgartner, G., Husser, C., Zell, M. Rapid screening and characterization of drug metabolites using a new quadrupole-linear ion trap mass spectrometer. *J. Mass Spectrom.* 2003, 38, 138–150.

[24] Lutz, U., Lutz, R.W., Lutz, W.K. Metabolic profiling of glucuronides in human urine by LC-MS/MS and Partial Least-Squares, discriminant analysis for classification and prediction of gender. *Anal. Chem.* 2006, 78, 4564–4571.

[25] Obach, R.S., Baxter, J.G., Liston, T.E., Silber, B.M., Jones, B.C., MacIntyre, F., Rance, D.J., Wastall, P. The prediction of human pharmacokinetic parameters from preclinical and in vitro metabolism data. *J. Pharmacol. Exp. Ther.* 1997, 283, 46–58.

[26] Zanger, U.M., Schwab, M. Cytochrome P450 enzymes in drug metabolism: regulation of gene expression, enzyme activities, and impact of genetic variation *Pharmacol. Ther.* 2013, 138, 103–141.

[27] Hill, J.R. In vitro drug metabolism using liver microsomes. *Curr. Protoc. Pharmacol.* 2004, 23, 8.1–7.8.11.

Chapter V: Determination of phase I metabolites and glucuronide conjugates of hop bitter acids metabolites by a full scan/data dependent/targeted neutral loss acquisition UHPLC-HRMS strategy: In vitro microsomal stability and in vivo analysis after oral administration in mice

^[28] Renn, A. Su, B–H., Liu, H., Sun, J., Tseng, Y.J. Advances in the prediction of mouse liver microsomal studies: From machine learning to deep learning. *WIREs Comput. Mol. Sci.* 2021, 11, e1479.

^[29] Martignoni, M., Groothuis, G.M., de Kanter, R. Species differences between mouse, rat, dog, monkey 18 and human CYP–mediated drug metabolism, inhibition and induction. *Expert Opin. Drug Metab. Toxicol.* 2006, 2, 875–894.

^[30] Kerns, E.H. Drug–like properties: concepts, structure design and methods from ADME to Toxicity Optimization. Burlington, MA, USA, 2008, 169.

^[31] Wu, B., Wang, X., Zhang, S., Hu, M. Accurate prediction of glucuronidation of structurally diverse phenolics by human UGT1A9 using combined experimental and in silico approaches. *Pharm. Res.* 2012, 29, 1544–1561.

^[32] Šicho, M., Stork, C., Mazzolari, A., de Bruyn Kops, C., Pedretti, A., Testa, B., Vistoli, G., Svozil, D., Kirchmair, J. FAME 3: Predicting the Sites of Metabolism in Synthetic Compounds, and Natural Products for Phase 1 and Phase 2 Metabolic Enzymes. *J. Chem. Inf. Model.* 2019, 59, 3400–3412.

^[33] Rodda, L.N., Gerostamoulos, D., Drummer, O.H. Pharmacokinetics of iso– α –acids in volunteers following the consumption of beer. *J. Anal. Toxicol.* 2014, 38, 354–359.

^[34] AlRabiah, H., Kadi, A.A., Attwa, M.W., Mostafaa, G.A.E. Development and validation of an HPLC–MS/MS method for the determination of filgotinib, a selective Janus kinase 1 inhibitor: Application to a metabolic stability study. *J. Chromatogr. B* 2020, 1154, 122195.

Chapter V: Determination of phase I metabolites and glucuronide conjugates of hop bitter acids metabolites by a full scan/data dependent/targeted neutral loss acquisition UHPLC-HRMS strategy: In vitro microsomal stability and in vivo analysis after oral administration in mice

^[35] Gao, Y., Liu, R., Gautam, N., Ma, B., Xie, Z., Sun, B., Zheng, H., Liu, D., Lou, H. Determination of the in vitro metabolic stability and metabolites of the anticancer derivative riccardin D–N in human and mouse hepatic S9 fractions using HPLC–Q–LIT–MS. *J. Pharm. Biomed. Anal.* 2019, 174, 734–743.

^[36] Barter, Z.E., Bayliss, M.K., Beaune, P.H., Boobis, A.R., Carlile, D.J., Edwards, R.J., Houston, J.B., Lake, B.G., Lipscomb, J.C., Pelkonen, O.R., Tucker, G.T., Rostami–Hodjegan, A. Scaling factors for the extrapolation of in vivo metabolic drug clearance from in vitro data: reaching a consensus on values of human microsomal protein and hepatocellularity per gram of liver. *Curr. Drug Metab.* 2007, 8, 33–45.

^[37] Davies, B., Morris, T. Physiological parameters in laboratory animals and humans. *Pharm. Res.* 1993, 10, 1093–1095.

Chapter VI

Matrix-assisted laser desorption/ionisation mass spectrometry imaging (MALDI-MSI) applications: Evaluation of neurotransmitter and neuropeptide analysis in heat stabilized vs fresh frozen brains and preliminary assessment of hop bitter acids distribution in liver tissues

6. Introduction

In natural compounds field, as in drug discovery and development, detailed understanding of pharmacological activity, metabolism, toxicological effects and distribution in the body is required. For an active compound to exert its desired effects it must reach biological receptors at the target site, but also undesired accumulation of compound or metabolites in tissues could occur which can lead to strong toxicological effects ^[1, 2]. Mass spectrometry (MS) coupled to different separation techniques is the gold standard for the analysis of biofluids, as a predictive indicator of tissue uptake. However, compound or metabolite levels measured in plasma often do not accurately represent the levels present within organs or organ subcompartments and therefore cannot be relied upon for understanding of efficacy or toxicology of bioactive molecules within the body ^[3]. On the other hand, the analysis of metabolites in tissues requires their homogenization and further extraction, which causes the loss of “spatial information”. These data can be crucial to understand in detail the distribution in a given district, and evaluate the molecular alterations that occur after the exposure of a given bioactive compound.

Imaging techniques allow the spatial localization of molecules have revolutionized medicine, helping in diagnosis and understanding the pathologies. Techniques such as magnetic resonance imaging (MRI), positron emission tomography (PET), fluorescence microscopy and radiolabeling can visualize localization of target molecules but these techniques can only monitor few molecules at time and require the use of molecular tags or labels and a priori knowledge of target compounds.

Matrix-assisted laser desorption/ionisation mass spectrometry imaging (MALDI-MSI) is a powerful label-free analytical tool that allows mapping of the spatial distributions and the abundance of a wide variety of biomolecules in tissue samples ^[4]. The technique is capable of detecting hundreds of molecules simultaneously in a single experiment, with subsequent *in situ* visualization of their localization in a tissue section ^[5, 6].

6.1. Aim of the work

MALDI-MSI methods has been developed to map the spatial distribution of both small molecule neurotransmitters and neuropeptides in rat brain sections, comparing two tissue stabilization protocols to reduce *post mortem* metabolic reactions (**Section I**).

Subsequently, MALDI-MSI has been applied to visualize the distribution of *Humulus lupulus* L. secondary metabolites in mouse liver samples (**Section II**).

6.1.1. References

^[1] Nilsson, A., Goodwin, R.J., Shariatgorji, M., Vallianatou, T., Webborn, P.J., Andrén, P.E. Mass spectrometry imaging in drug development. *Anal. Chem.* 2015, 87, 1437-1455.

^[2] Prideaux, B, Stoeckli, M. Mass spectrometry imaging for drug distribution studies. *J Proteomics*, 2012, 75, 4999-5013.

^[3] Soars, M.G., Webborn, P.J. H., Riley, R.J. Impact of hepatic uptake transporters on pharmacokinetics and drug-drug interactions: use of assays and models for decision making in the pharmaceutical industry. *Molecular Pharmaceutics*, 2009, 6, 1662-1677.

^[4] Norris, J.L., Caprioli, R.M. Analysis of Tissue Specimens by Matrix-Assisted Laser Desorption/Ionization Imaging Mass Spectrometry in Biological and Clinical Research. *Chem. Rev.* 2013, 113, 2309–2342.

^[5] Caprioli, R.M., Farmer, T.B., Gile, J. Molecular imaging of biological samples: localization of peptides and proteins using MALDI–TOF MS. *Anal. Chem.* 1997, 69, 4751–4760.

^[6] Shariatgorji, M.; Strittmatter, N.; Nilsson, A.; Källback, P.; Alvarsson, A.; Zhang, X.; Vallianatou, T., Svenningsson, P., Goodwin, J.A.R., Andrén, P.E. . Simultaneous imaging of multiple neurotransmitters and neuroactive substances in the brain by desorption electrospray ionization mass spectrometry. *Neuroimage* 2016, 136, 129–138.

6.2. Section I: Evaluation and optimization of neurotransmitter and neuropeptide analysis in heat stabilized vs fresh frozen brains by MALDI-MSI

6.2.1. Abstract

One of the main challenges analysing chemical messengers in the brain is the optimization of tissue sampling and preparation protocols. Limiting *post mortem*

time and enzyme activity is critical to identify low-abundance neurotransmitters and neuropeptides. In this study, a rapid and uniform conductive heat transfer method was compared with a conventional fresh freezing protocol. Together with a selective chemical derivatization method and an optimized normalization approach using internal standards, was employed to simultaneously image neurotransmitters and their related metabolites by MALDI mass spectrometry imaging (MSI). Although the heat stabilization did not showed differences in the levels of precursors dopamine, norepinephrine, and serotonin, their related metabolites (DOPAL, DOPAC, HVA, MOPAL, DOPEG and 5-HIAA) were all significantly lower, revealing a reduced neurotransmitter turnover ratios in heat stabilized brains compared to fresh frozen. *In situ* markers associated with the stabilization of enkephalin, dynorphin, and tachykinin derived neuropeptides were also imaged, showing that, without heat stabilization, degradation fragments of full-length peptides occur in fresh frozen tissues. Heat stabilization enabled the detection of very low-abundant neuropeptides such as the C-terminal flanking peptide, neuropeptide gamma, and nociceptin, which remained intact and could be exclusively imaged in heat stabilized brains. Our data provide evidence for the potential use of the heat stabilization prior to MALDI-MSI analyses to improve the examination of the *in vivo* state of neuronal chemical messengers in brain tissues.

6.2.2. Introduction

Changes in concentration of neurotransmitters and neuropeptides are involved in several neurological diseases such as in Parkinson's disease, Alzheimer's disease, depression, and drug addiction ^[1-7]. In addition to measure their concentrations in brain tissues, the knowledge of the spatial distribution of these

signalling messengers in the brain is of great importance, not only to better understand their involvement in pathological conditions, but also to develop more focused and effective treatments [8, 9]. One of the main challenges of studying signalling molecules in the brain by MALDI-MSI is the sample preparation. Immediately after euthanasia and dissection of the tissues, rapid molecular degradation may occur [10]. Snap-freezing of tissues is a widely employed method used to reduce *post mortem* enzymatic activities. However, dissection and freezing of the brain may take some time and some enzymes may also be reactivated during thawing [11]. To circumvent these drawbacks, several strategies have been adopted to stabilize tissue samples and limit the degradation of biomolecules. Among *in vivo* fixation techniques, focused microwave irradiation (FMW) to the brain, by which the tissues are rapidly heated to 85-95 °C, was developed to irreversibly deactivate enzymes, preventing *post mortem* metabolism of neurotransmitters and neuropeptides [12-15]. Also, *in situ* freezing (ISF) is a powerful method to minimize *post mortem* changes in contents of cerebral labile neurotransmitters and metabolites [16, 17], as well as the use of enzyme inhibitors, such as 3-mercaptopropionic acid, a glutamic acid decarboxylase (GAD) inhibitor, which prevent the *post mortem* increase in GABA levels [18-20]. However, these stabilization techniques may display some limitations, such as toxicity, ethical restrictions, time-consumption, and high costs. Furthermore, overheating with consequent destruction of the sample area or uneven heating throughout the tissue during FMW, may result in reversible enzymatic activity [21]. An alternative tissue stabilizing technique, which use a combination of heat and pressure under vacuum, for the fixation of target brain samples has been proposed prior to peptidomic analysis by nano-LC-ESI-MS/MS platforms. Heat stabilization (HS) was

performed using an instrument that enable rapid and efficient heat transfer through a lower and upper conductive heat block during vacuum application, ensuring homogenous heating at 95 °C in any part of the sample. The developed method has proved to be very useful for reducing the degradation processes of proteins and peptides, as well as, to preserve their post-translational modifications (PTMs) [22-24].

Nevertheless, the visualization of the distribution of the neuronal messengers and their related metabolites across the heat stabilized (HS) brain tissues has been scarcely investigated. For this purpose, in this work we performed MALDI-MSI analysis to highlight the *post mortem* degradation differences among heat stabilized and fresh frozen (FF) brain tissues for key neurotransmitters, metabolites and neuropeptides. Furthermore, a recently developed reactive matrix 4-(anthracen-9-yl)-2-fluoro-1-methylpyridin-1-ium iodide salt (FMP-10), which enables selective *in situ* chemical derivatization of the neurotransmitters, was employed to simultaneously image the catecholaminergic and serotonergic signalling systems, including precursors and metabolites [25]. MALDI-MSI showed that the heat treatment does not affect the spatial information and effectively limits *post mortem* metabolic degradation of neurotransmitters and neuropeptides, resulting in informative molecular profiles, which can be used for the understanding of molecular changes in both healthy and diseases conditions, as well as their modulation following drugs treatment.

6.2.3. Results

6.2.3.1. Stabilization of small molecule neurotransmitters by MSI

Tissue morphology is affected by HS. The main challenge was represented by the changes to the tissue morphology caused by heating. The HS tissues appeared dryer, the tissue edges were jagged due to the difficulties in the cutting, and some holes could be observed (Supporting Information Figure S6.2.1). The alteration in tissue structure caused by the heat treatment influenced the reactive matrix deposition so that the consecutive analyte extraction, desorption and ionization worsened the quality of the MS images, in terms of number of effective pixels and image contrast compared to fresh frozen section .

Internal standards improve pixel-to-pixel variation. We evaluated the chemical derivatization method with FMP-10 and confirmed that the derivatization of the target molecules occurred in the HS tissues (Supporting Information Table S6.2.1). In FF tissue sections, normalized by RMS, Dopamine (DA), 3-Methoxytyramine (3-MT) and homovanillic acid (HVA) presented high intensity across the striatal regions, while in the HS samples RMS normalization was not able to effectively reduce ion suppression artefacts and appeared almost similar to the unnormalized image (**Figure 6.2.1**). For this reason, we optimized a mixture of internal standards suitable for the normalization of the ion intensity of the neurotransmitters detected in the HS tissue. The catecholaminergic and serotonergic neurotransmitters, and its downstream metabolism products, were normalized against the internal standard DA-*d*₄, except for the homovanillic acid, which was normalized against the labelled compound HVA-*d*₅. The transmitter γ -aminobutyric acid (GABA) was normalized against the labelled compound GABA-

*d*₆. We observed that for the normalization of each endogenous neurotransmitter, its IS must be selected in the form with the same number of derivatized functional groups and the same type of structural rearrangements. The IS normalization provided a more uniform signal intensity across the brain regions, both in FF and HS. However, while in FF samples IS normalized image appears similar in effectiveness to RMS normalization, in HS tissues it has proven to be crucial to reduce the effects of the ion suppression arising from the HS tissues inhomogeneity and to improve the level of pixel-to-pixel variation, to provide a higher definition of the brain structure and to reach a uniform distribution of the signals (**Figure 6.2.1**).

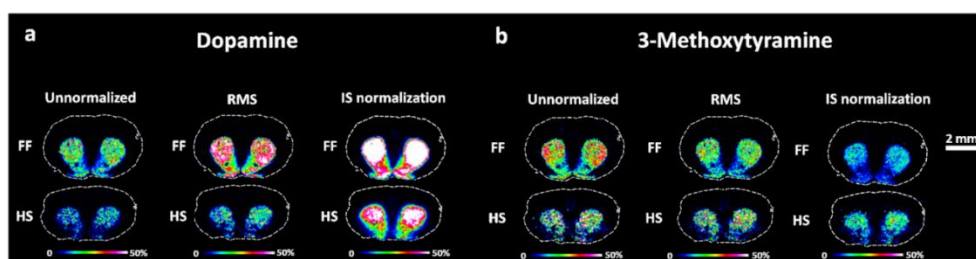


Figure 6.2.1. MALDI-MS images of double derivatized dopamine (DA + [2 (FMP-10)-CH₃]) (**a**) and single derivatized 3-Methoxytyramine (3-MT + FMP-10]) (**b**) in coronal rat brain sections comparing unnormalized, RMS, and IS normalized MSI data in FF and HS tissues (at bregma 2.28 mm, Paxinos and Watson, 2014). Scale bar = 2 mm. Colour scale bars are shown as percentage of maximum intensity. IS: DA-*d*₄. Lateral resolution, 150 μ m. Abbreviations: RMS, root-mean square normalization; IS, Internal standard normalization; FF, fresh frozen; HS, heat stabilized.

HS effect on neurotransmitter metabolites. Next, we studied the effect of HS on the catecholamine and serotonin systems. MALDI-MSI was applied to map the lateral distribution of neurotransmitters and their related metabolites (Supporting

Information Table S6.2.1). We observed no significant differences in the detection of DA (**Figure 6.2.2 a**) and norepinephrine (NE, **Figure 6.2.2 b**) between HS and FF in the striatum. Instead, the different stabilization processes affected the related metabolites. We found that the main metabolites of DA, 3,4-dihydroxyphenylacetaldehyde (DOPAL, **Figure 6.2.2 c**), 3,4-dihydroxyphenylacetic acid (DOPAC, **Figure 6.2.2 d**), and HVA (**Figure 6.2.2 e**), were respectively 1.5, 1.4 and 2.3 fold higher in the striatum of FF brains compared to HS tissues, as can be observed in bar chart graph depicted in **Figure 6.2.2 m**. We observed no significant changes in the levels of 3-MT (**Figure 6.2.2 f**) in FF tissues, while the metabolite 3-methoxy-4-hydroxyphenylacetaldehyde (MOPAL, **Figure 6.2.2 g**) was 2.3 fold higher in FF brains (**Figure 6.2.2 m**). Moreover, we found that the metabolite of NE, dihydroxyphenylethylene glycol (DOPEG, **Figure 6.2.2 h**), was clearly detected in FF brains but not detected in HS tissues.

We further evaluated the effect of HS on the serotonin (5-HT) pathway, with no significant differences in the detection of 5-HT (**Figure 6.2.2 i**) between HS and FF tissues. On the contrary, the metabolite 5-hydroxyindoleacetic acid (5-HIAA, **Figure 6.2.2 j**) was 2.3 times higher in FF brains (**Figure 6.2.2 n**), while the metabolite 5-hydroxyindolealdehyde (5-HIAL) (**Figure 6.2.2 k**) was clearly detected in FF tissues but was not detected in HS sections. Lastly, we found that GABA (**Figure 6.2.2 l**) levels were significantly lower (1.2 fold, **Figure 6.2.2 n**) in all brain regions of HS tissues. Those results were further supported by a reduced metabolite/neurotransmitter ratio in HS brain regions (Supporting Information Table S6.2.2).

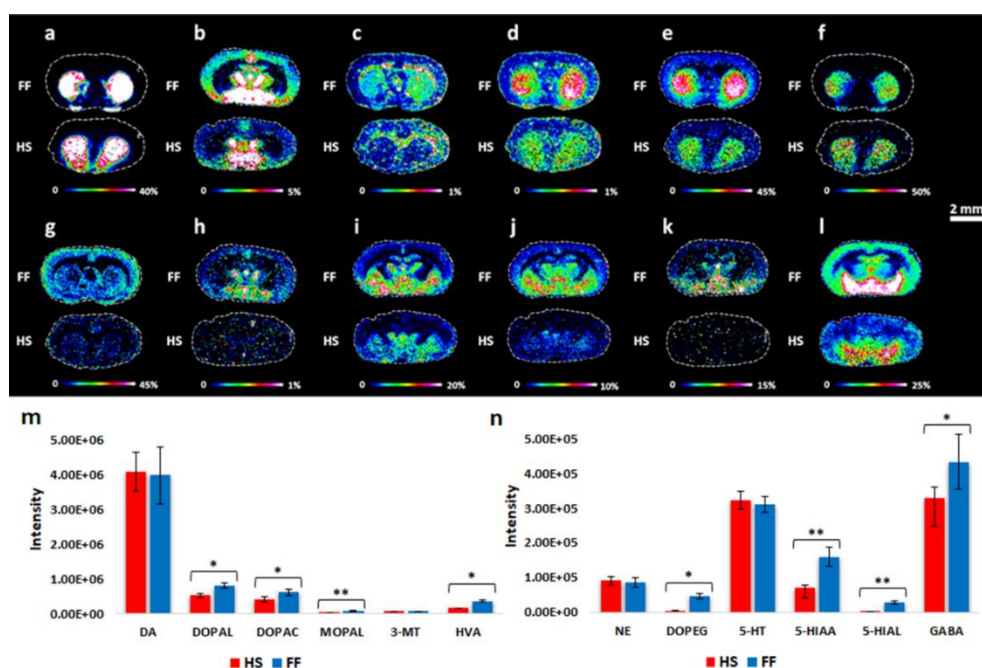


Figure 6.2.2. MALDI-MS images of neurotransmitters and related metabolites acquired from FF and HS tissue sections. **a**, DA double derivatized; **b**, NE double derivatized; **c**, DOPAL double derivatized; **d**, DOPAC double derivatized; **e**, HVA single derivatized; **f**, 3-MT single derivatized; **g**, MOPAL single derivatized (coronal rat brain section at bregma 2.28 mm, Paxinos and Watson, 2014); **h**, DOPEG double derivatized; **i**, 5-HT-single derivatized; **j**, 5-HIAA single derivatized; **k**, 5-HIAL-single derivatized; **l**, GABA single derivatized; (coronal rat brain section at bregma -2.04 mm, Paxinos and Watson, 2014); **m**, **n**, Bar charts graphs reflecting normalized average intensity of precursors DA (**m**) NE and 5-HT (**n**) and their metabolites between HS and FF protocols. Error bars represent standard deviation between technical replicates (** $p \leq 0.01$, * $p \leq 0.05$). Scale bar = 2 mm. Colour scale bars are shown as percentage of maximum intensity. Lateral resolution, 150 μm . Data were normalized against IS: DA- d_4 for DA, DOPAL, DOPAC, 3-MT, MOPAL, 5-HT, NE, DOPEG, 5-HIAL, 5-HIAA. HVA- d_5 for HVA; GABA- d_6 for GABA. Abbreviations: FF, fresh frozen; HS, heat stabilized.

6.2.3.2. Stabilization of neuropeptides by MSI

Increased detection of peptides by HS. We investigated the effects of the HS by mapping neuropeptides in rat brains. A high number of peptides (in total 44) were mapped across both HS and FF brain tissues, including peptides derived from, e.g., proenkephalin (PENK) and prodynorphin (PDYN) precursors. Moreover, tachykinin neuropeptides, peptides derived from the cerebellin 1 precursor, neuropeptide-EI, neurotensin, and nociceptin peptides were detected (Supporting Information Table S6.2.3). Twenty six neuropeptides have been previously reported by us ^[6]. The remaining 18 peptides were detected for the first time by MALDI-MSI. The tentative identification of the neuropeptides was based on the ultra-high mass accuracy provided by MALDI-FTICR-MS and subsequently confirmed by LC-MS/MS analyses.

PENK neuropeptides. Leu-enk (**Figure 6.2.3 a**), Met-enk (**Figure 6.2.3 b**) and metorphamide (**Figure 6.2.3 c**) were respectively 2.8, 2.9 and 2.5 fold higher in the globus pallidus (GP) of HS tissues than FF. (Figure 4a). Moreover, Met-enk-RF (**Figure 6.2.3 d**), Met-enk-RGL (**Figure 6.2.3 e**) and PENK (219-229) (**Figure 6.2.3 f**) were highly abundant in GP of HS (2.1, 1.2 and 3.9 fold, respectively) (**Figure 6.2.4 a**), they were also present at low abundance in the caudate putamen (CPu). Instead, in FF tissues, the same PENK neuropeptides were clearly detected in GP (**Figure 6.2.4 a**), but almost undetectable in the other brain structures. The discrepancies may be due to the rapid enzymatic degradation of PENK neuropeptides, whose levels decreased over *post mortem* time and were only detected in the structure in which they were particularly abundant. In fact, the opposite was observed for the related shorter peptides, considered possible

degradation products: PENK Des-Y-Met-enk-RF, Met-enk-R and PENK (220-229) (**Figure 6.2.3 g -i**, respectively) whose levels were 9.8, 1.9 and 4.3 fold greater in the GP of FF tissues than HS (**Figure 6.2.4 a**). A similar trend was assessed at level -5.64 mm from bregma, at which the full-length peptides Met-enk-RF (**Figure 6.2.3 j**) and PENK (219-229) (**Figure 6.2.3 k**) were respectively 2 and 6 times higher in the pleoiglia periaqueductal gray (PIPAG) and the reticular part of substantia nigra (SNR) of HS tissues (**Figure 6.2.4 b**), while the peptide fragments were present in higher levels in the same structures of FF tissues (**Figure 6.2.3 l, m**) (7 and 4 fold, respectively, **Figure 6.2.4 b**).

Furthermore, we observed that full length PENK (198-209) (**Figure 3n**) was twice higher in HS brains compared to FF tissues (**Figure 6.2.4 c**). On the contrary, the degradation product PENK (201-209) (**Figure 6.2.3 o**), was clearly detected in FF tissues and not detected in HS tissues coronal rat brain section at bregma -2.92 mm)

There were no significant differences on the detection of PENK (114-133), PENK (212-229) and PENK A (239-260) between FF and HS tissues (Supporting Information Figure S6.2.2).

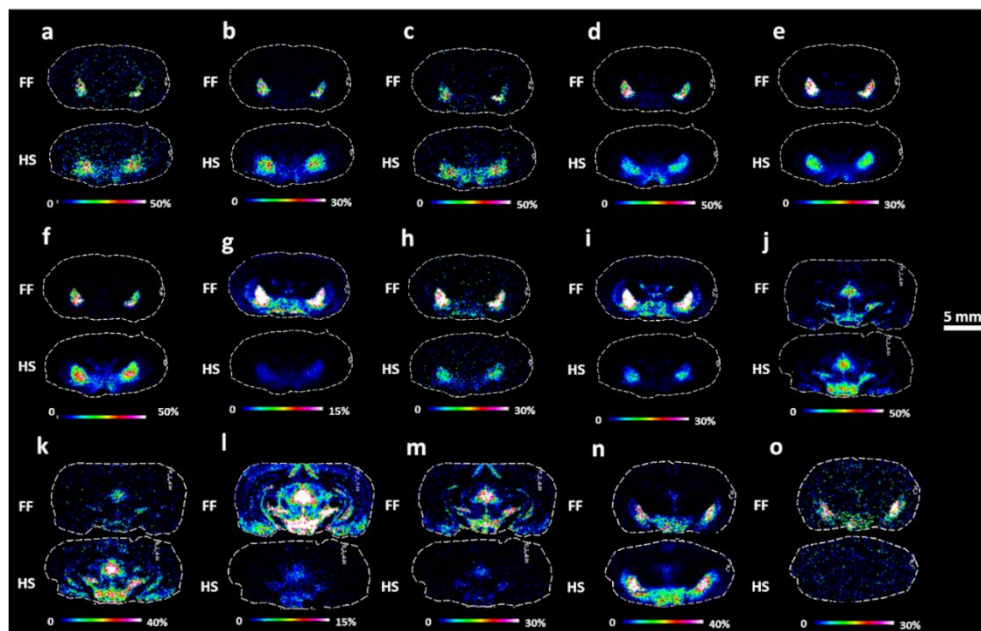


Figure 6.2.3. MALDI-MS images of enkephalins in coronal rat brain sections. Imaging experiments compared the distribution of full-length peptides (**a-f, j-k, n**) and related fragments (**g-i, l-m, o**) between FF and HS tissues at bregma -2.04 mm (**a-i**), -5.64 mm (**j-m**) and -2.92 mm (**n-o**) (Paxinos and Watson, 2014). **a**, Leu-enk; **b**, Met-enk; **c**, Metorphamide; **d, j**, Met-enk-RF; **e**, Met-enk-RGL; **f, k**, PENK (219-229); **g, l**, Des-Y-Met-enk-RF; **h**, Met-enk-R; **i, m**, PENK (220-229); **n**, PENK (198-209); **o**, PENK (201-219); Scale bar = 5 mm. Colour scale bars are shown as percentage of maximum intensity. Data were normalized against RMS. Lateral resolution, 150 μ m. Abbreviations: FF, fresh frozen; HS, heat stabilized.

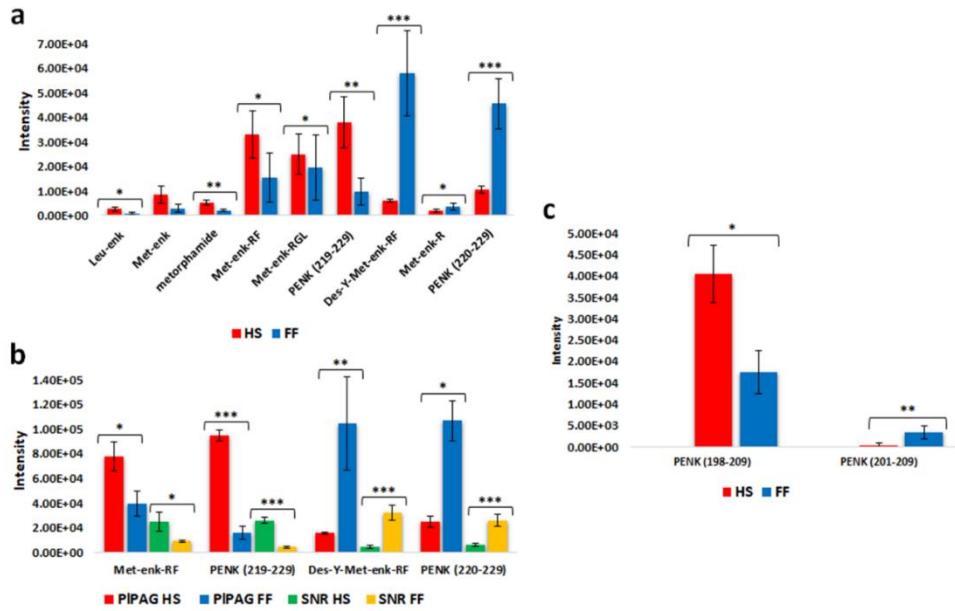


Figure 6.2.4. Bar charts graphs reflecting normalized average intensity of enkephalins between HS and FF protocols. **a-c**, Full-length peptides and related fragments at bregma -2.04 mm (**a**), -5.64 mm (**b**) and -2.92 mm (**c**). Error bars represent standard deviation between technical replicates ($****p \leq 0.0001$, $***p \leq 0.001$, $**p \leq 0.01$, $*p \leq 0.05$). Abbreviations: PIPAG, pleiglial periaqueductal gray; SNR, reticular part of substantia nigra; HS, heat stabilized; FF, fresh frozen.

PDYN and tachykinin neuropeptides. When investigating PDYN and tachykinin neuropeptides we found that dynorphin A (Dyn A (1-8)) and α -neoendorphin (α -Neo) (-2.04 mm from bregma, **Figure 6.2.5 a, c**, respectively) were 3 fold higher in the LH (**Figure 6.2.5 a, c**) and in the SNR (-5.64 mm from bregma, **Figure 6.2.5 b, d** respectively) (**Figure 6.2.5 p**) of HS coronal rat brain sections than in FF tissues. On the contrary, the related peptide fragments, Dyn A

(2-8) and α -Neo (2-10) (**Figure 6.2.5 e, h**) were 10 fold higher in the corresponding structures of the FF brains (**Figure 6.2.5 o, p**).

We further observed that Dyn B (1-13), Dyn B (1-6), Dyn B (15-28) and β -Neo were present in higher levels in HS brains than FF tissues (1.1 and 1.5 fold, respectively, Supporting Information Figure S6.2.2).

Regarding tachykinins, the levels of Neurokinin A were 3 times higher across HS tissues (**Figure 6.2.5 i, j – o, p**). Moreover, we found that Substance P (SP) (1-11) was detected at higher levels in the Hyp, the PIPAG, and the SNR of HS coronal brain section (2.3, 2.1 and 1.8 fold, respectively) at level -2.04 and -5.64 mm from bregma) (**Figure 6.2.5 k, l – o, p**). On the contrary, SP (1-9) was detected in FF tissues and not detected in HS tissues (**Figure 6.2.5 m, n – o, p**). Interestingly, in coronal rat brain sections at level -2.92 mm from bregma, C-terminal flanking peptide and neuropeptide gamma were mapped here for the first time and were exclusively detected in HS tissues (Supporting Information Figure S6.2.2).

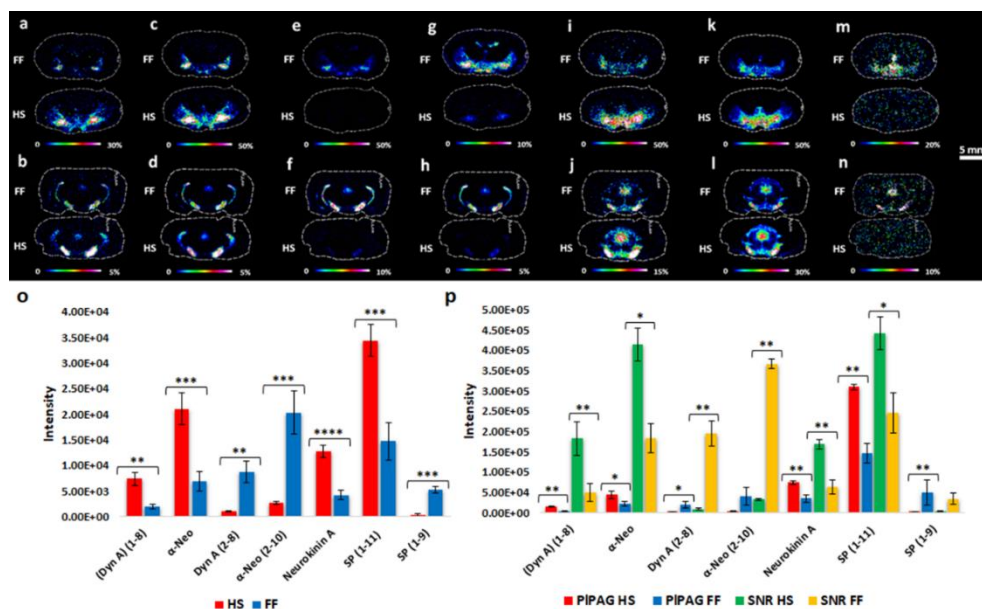


Figure 6.2.5. MALDI-MS images of dynorphins and tachykinins in coronal rat brain sections. Imaging experiments compared the distribution of full-length peptides (**a-d, i-l**) and related fragments (**e-h, m-n**) between FF and HS tissues at bregma -2.04 mm (**a, c, e, g, i, k, m**) and -5.64 mm (**b, d, f, h, j, l, n**) (Paxinos and Watson, 2014). **a, b**, Dyn A (1-8); **c, d**, α -Neo; **e, f**, Dyn A (2-8); **g, h**, α -Neo (2-10); **i, j**, Neurokinin A; **k, l**, SP (1-11); **m, n**, SP (1-9); **o, p**, Bar charts graphs reflecting normalized average intensity of full-length peptides and related fragments at bregma -2.04 mm (**o**) and -5.64 mm (**p**) between HS and FF protocols. Error bars represent standard deviation between technical replicates ($***p \leq 0.001$, $**p \leq 0.01$, $*p \leq 0.05$). Scale bar = 5 mm. Colour scale bars are shown as percentage of maximum intensity. Data were normalized against RMS. Lateral resolution, $150 \mu\text{m}$. Abbreviations: PIPAG, pleoiglia periaqueductal gray; SNR, reticular part of substantia nigra; FF, fresh frozen; HS, heat stabilized.

Other neuropeptides: SST-28, N-EI, PEP-19, PC1, and Cerebellin peptides.

Somatostatin 1-12 (SST-28(1-12)) is the bifunctional hormone released by the

monobasic and dibasic cleavages of the precursor prosomatostatin. Neuropeptide EI (N-EI) is derived from the melanin concentrating hormone (MCH) precursor. Interestingly, in this investigation, MALDI-MSI revealed that the biologically active peptides SST-28(1-12) (**Figure 6.2.6 a**) and N-EI (**Figure 6.2.6 b**) were respectively 13 and 2 fold increased in the Hyp of HS brains than FF tissues (**Figure 6.2.6 f**). Further evidence of the prevention of *post mortem* degradation was that PEP-19 (48-62) (**Figure 6.2.6 c**) and PEP 19 (51-62) (**Figure 6.2.6 d**), known fragments of the full-length PEP-19 (6.7 kDa neuronal calmodulin-binding polypeptide) [26], was exclusively detected in FF tissues. Moreover, nociceptin (**Figure 6.2.6 e**), was mapped for the first time in HS tissues.

Prohormone convertase 1 (PC1 (619-628)) were not detected in HS tissues, while there were no significant differences on the detection of Cerebellin neuropeptides between the two methods of stabilization (Supporting Information Figure S6.2.3).

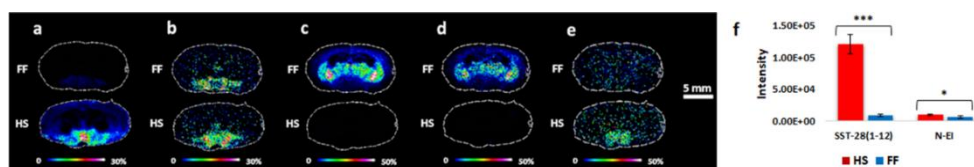


Figure 6.2.6. Molecular distributions determined by MALDI-MSI in coronal rat brain sections comparing FF with HS tissues (at bregma -2.04 mm, Paxinos and Watson, 2014) of **a**, SST-28(1-12); **b**, N-EI; **c**, PEP-19 (48-62); **d**, PEP-19 (51-62) and **e**, nociceptin; **f**, Bar charts graphs reflecting normalized average intensity of SST-28(1-12) and N-EI between HS and FF protocols. Scale bar = 5 mm. Colour scale bars are shown as percentage of maximum intensity. Data were normalized against RMS. Lateral resolution, 150 μ m. Abbreviations: FF, fresh frozen; HS, heat stabilized.

6.2.4. Discussion

In the present study, we evaluated the effectiveness of rapid and uniform heating of brain tissues, compared to conventional snap freezing, to inactivate *post mortem* enzymatic activity, thereby preventing the degradation of the neuronal chemical messengers. We used a MALDI-MSI approach to map the spatial distribution of both small molecule neurotransmitters and neuropeptides in heat stabilized rat brain sections. We monitored any possible variation in localization after heat treatment, as well as evaluated differences in relative intensity of the neurotransmitters and neuropeptides including their metabolites.

We assessed the usefulness of heat stabilization to prevent *post mortem* changes to better reflect the *in vivo* state of neurotransmitters. The developed MALDI-MSI approach allowed the visualization of neurotransmitters distribution across the brain regions. The neurotransmitter localizations were consistent with the distributions previously reported using MALDI-MSI methods [25, 27, 28].

The heat stabilization procedure did not destroy the integrity of the neurotransmitters, nor caused artificial diffusion of the molecules into other areas, and the tissue integrity alteration did not affect the MSI results at our experimental lateral resolution. However, the changes to the tissue morphology caused by heating had a negative effect on the data quality. In this regard, beyond the matrix effect, also the physical and structural properties of the sample can influence the ionization yield [29], leading to suppression or enhancement effects. For instance, heat stabilization can lead to increased salt levels, which can cause a global increase in ionization bias and thus lower MSI signal intensities [30]. A proper strategy is to use internal standards for the normalization of MSI data. This approach is extremely

useful to perform absolute quantitation ^[31] and to reduce various ion suppression effects caused by different chemical compositions and structural environments in a brain tissue section ^[32]. For efficient normalization, several parameters were taken into account when selecting the internal standard: i) the structural similarity between the labelled and unlabelled compounds, ii) the numbers of derivatized functional groups (phenolic and/or primary amines) of both internal standards and endogenous compounds, iii) the types of structural rearrangements (loss of the hydrogen ion or/and the methyl group) that occur in multi-derivatized molecules, resulting in single charged ions in MALDI ^[25]. In this way, we achieved for each neurotransmitters an optimized IS normalization that exhibited superior reduction ion suppression artifacts compared to RMS normalization in HS brain tissues.

A number of previous studies have found that sacrificing animals with FMW irradiation led to accurate regional measurements of brain labile neurotransmitters ^[10, 33]. In this regard, both FMW fixation and heat stabilization have been proposed in combination with MALDI-MSI to assess highly labile small molecules in tissues ^[34-37]. Our data extend the previous studies to an alternative heat stabilization approach in sample preparation for MALDI-MSI analyses, to capture a realistic visualization of labile neurotransmitters in brain tissues.

The effect of heat stabilization was pronounced also for GABA levels that increased *post mortem* in FF brains, most likely due to maintained activity of glutamate decarboxylase (GAD). Hence, the current study confirmed that the GAD enzyme was effectively inhibited by heat stabilization, as reported in brain regions thermally stabilized by FMW ^[14, 38].

Differently from recent investigation on the use of FMW when measuring biogenic monoamines ^[38, 39], the heat stabilization here developed prior to MALDI-

MSI analyses did not increase the DA and NE levels substantially. Interestingly, the treatment had a much more profound effect on the related metabolites (DOPAL, DOPAC, HVA, MOPAL and DOPEG) that, as expected, were all significantly lower in HS tissues.

More notable was the effect of heat transfer on tissue on the turnover of 5-HT. We observed a significant change between HS and FF tissues in both the metabolite 5-HIAA and the metabolite 5-HIAL. These results may indicate a reduction in the rapid serotonergic metabolism following heat stabilization, and are in contrast to previous findings from brain fixation by FWM technique studies which assumed a steady state level of 5-HT^[13,38]. Thus, combining the heat stabilization method with MALDI-MSI made it possible to prevent metabolic artefacts and conduct more accurate determination biogenic monoamines in brain tissues, and paved the way to possible relative quantitative analysis.

Investigating the distribution and the abundance of neuropeptides in brain tissues is important to highlight alterations in neurological diseases. However, it has been shown that following tissue sampling, active enzymes continue their proteolytic processes to generate peptide fragments that do not reflect the *in vivo* state of neuropeptides composition [38]. As stated before, rapid and controlled heating of intact tissue is an ideal tool to prevent brain peptidome degradation^[40]. MALDI-MSI is highly successful in identifying *in situ* markers for determination of peptide stabilization^[41].

In this work, we performed MALDI-MSI experiments to monitor if heat treatment, at the time of brain dissection, can reduce the rapid changes of bioactive neuropeptides integrity and their levels. Despite the alteration in tissue morphology caused by heating, as described above, we demonstrated that the heat treatment did

not affect the adhesion of the thaw-mounted tissues on the glass; in fact, was possible to perform tissue-washing procedure prior to application of matrix, without any problem of tissue detaching from the slide. The tissue-washing protocol has proven to be essential to reduce suppression effects from, e.g., lipids and improve S/N ratio even in heat stabilized tissues. The RMS approach was able to effectively normalize the spectra and reduce the ion suppression caused by physical and structural properties of HS samples. For this reason, it was not necessary to use labelled compounds for normalization, which otherwise would have been prohibitively expensive. Moreover, we asserted that, following the heat treatment, no delocalization or diffusion of the neuropeptides occurred; in fact, the neuropeptide distributions observed in our experiments were consistent with the distribution previously reported using both MALDI-MSI and other techniques [6, 9, 42-46].

Post mortem proteolytic activity of enzymes on PENK and PDYN neuropeptides was significantly inhibited. This is illustrated by a greatly reduction in the levels of most peptide degradation fragments in HS brain samples. Interestingly, the change in PENK peptide levels varied among peptides and brain structures, indicating that the enzymatic degradation directly reflects the abundance of the peptides in the brain structures and may depend on the *post mortem* time. In this regard, further investigation at various time points after dissection are required to fully understand a time-dependent relative changes in intensities of the peptide signals.

In addition to the well-known fragments of the full-length PEP-19 [26], the combination of the heat stabilization with MALDI-MSI allowed the detection of novel denaturation markers, as Dyn A (2-8) and SP (1-9) for the stabilization of dynorphins and tachykinins, respectively. Moreover, in the present study, we

detected the low-abundance neuropeptides C-terminal flanking peptide, neuropeptide gamma, and nociceptin, exclusively in HS tissues, highlighting their susceptibility to enzymatic degradation. It has been noted that cerebellin peptides levels were not affected by the fixation method. Also in this case, a time course experiment could support the hypothesis of the high stability of the cerebellin peptides to *post mortem* degradation.

6.2.5. Materials and methods

6.2.5.1. Chemicals

All chemicals were purchased from Sigma-Aldrich (Stockholm, Sweden) and were used without further purification unless otherwise stated. Isotope-labelled neurotransmitters were purchased from CDN Isotopes (Quebec, Canada). The matrix FMP-10 was synthesized and purified as previously reported [25].

6.2.5.2. Safety and precautions

Chloroform ACS reagent, $\geq 99.8\%$ has been handled according to all safety precautions indicated by the manufacturer.

6.2.5.3. Animal experiments

Female Sprague-Dawley rats (approximately 150 g; Scanbur, Sollentuna, Sweden) were housed in separate air-conditioned rooms (with 12 h dark/12 h light cycles) at 20 °C and 53% relative humidity. All animal procedures were carried out in agreement with the European Communities Council Directive of November 24, 1986 (86/609/EEC) on the ethical use of animals and were approved by the Uppsala Animal Ethical Committee.

Eight rats were sacrificed by decapitation and the brains were quickly removed. In the first experiments, four brains were immediately frozen by immersion in -45 °C dry-ice-cooled isopentane and stored at -80 °C. In the second experiment, the other four brains within 1 min following decapitation were heated at 95 °C with minimal compression and cavity vacuum, using the Stabilizer T1™ instrument (Denator AB, Sweden) at auto settings for fresh tissues.

6.2.5.4. Tissue sample preparation for MALDI-MSI

The rat brain samples were sectioned using a cryostat microtome (Leica CM1900, Leica Microsystems, Wetzlar, Germany) at thicknesses of 12 μm . Tissue sections were thaw-mounted onto indium tin oxide (ITO) coated glass slides (Bruker Daltonics, Bremen, Germany) and stored at -80 °C until analysis. MALDI-MSI for both neurotransmitters and neuropeptides were performed on coronal rat sections at six levels (distance from bregma): 2.28 mm, 0.00 mm, -2.04 mm, -2.92 mm, -5.04 mm, and -5.64 mm (Paxinos and Watson, 2014) (Supporting Information Figure S6.2.4).

6.2.5.5. Chemical derivatization of catecholaminergic and serotonergic neurotransmitters

We used a selective chemical derivatization method recently developed ^[25]. In detail, sections were desiccated at room temperature for 20 min before application of the reactive matrix. In the optimized protocol, a mixture of deuterated internal standards (IS) (dopamine-1,1,2,2- d_4 • HCl (DA- d_4), 4-hydroxy-3-methoxyphenyl- d_3 -acetic- d_2 acid (HVA- d_5), 4-aminobutyric acid-2, 2, 3, 3, 4, 4- d_6 (GABA- d_6) was applied prior to matrix coating. IS solution consisting of 0.666 $\mu\text{g}/\text{mL}$ DA- d_4 , 0.333 $\mu\text{g}/\text{mL}$ HVA- d_5 , 100 $\mu\text{g}/\text{mL}$ GABA- d_6 in 50% methanol, was homogeneously

sprayed over the tissues using an automated sprayer (TM-Sprayer, HTX Technologies, Chapel Hill, NC, USA) under the following conditions: nozzle temperature was set at 90 °C, with a nitrogen gas pressure of 6 psi, flow rate of 70 µL/min, nozzle velocity of 1100 mm/min with six passes, and 2 mm track spacing.

FMP-10 was dissolved in 70% ACN (4.4 mM, 5.5 mL). An automated pneumatic sprayer (TM-Sprayer, HTX Technologies) was used to spray the solution over the tissue sections in twenty passes at 80 °C, with a nitrogen gas pressure of 6 psi, flow rate of 80 µL/min, nozzle velocity of 1100 mm/min, and 2 mm track spacing.

6.2.5.6. Sample preparation for MALDI-MSI analysis of neuropeptides

To remove lipids that can cause ion suppression when measuring neuropeptides with low concentrations, a tissue-washing procedure prior to application of matrix was carried out as previously with slight modifications ^[6]. Briefly, prior to tissue washing, ITO slides with mounted rat brain sections were removed from -80 °C storage. The slides were dried with a stream of nitrogen and then they were immediately dried in a vacuum desiccator for 20 min. All tissue washes were performed by fully immersing the slide in a glass Petri dish containing 45 mL of chloroform for 35 s, with gentle swirling and continual movement of the slide in the chloroform throughout the wash. The chloroform was changed between washing each slide. After the washing, the slide was immediately placed in a vacuum desiccator and dried for 15 min before MALDI matrix application. 2,5-dihydroxybenzoic acid (DHB) was used as matrix at a concentration of 25 mg/mL in a solution of 0.2% TFA in 50% ACN (v/v). It was applied using an automated sprayer (TM-Sprayer, HTX Technologies). The nozzle temperature was set at 85

°C, with a nitrogen gas pressure of 6 psi, flow rate of 120 $\mu\text{L}/\text{min}$, nozzle velocity of 1200 mm/min with four passes, and 2 mm track spacing.

6.2.5.7. MALDI-MSI analysis

Optical images were acquired using a standard flatbed scanner (Seiko Epson, Japan). All MALDI-MSI experiments were performed on a solariX 7T-2 ω ESI/MALDI-Fourier-transform ion cyclotron resonance mass spectrometer (Bruker Daltonics) equipped with a Smartbeam II 2kHz laser. All analyses were performed in positive ionization, at a lateral resolution of 150 μm . The laser power was optimised at the start of each run and then held constant during the experiments. 100 laser shots were fired at each sampling position. The data for neurotransmitters were acquired across the m/z range of 100-1500 using 2 million data points, while MS spectra of neuropeptides were collected over the m/z range of 450-3000 using 514 thousand data points. Ion transmissions voltages parameters were set as follows: Funnel RF amplitude 120.0 Vpp, RF amplitude TOF 350.0 Vpp, TOF 0.8 ms, and RF frequency transfer optic 4 MHz for derivatized neurotransmitters analyses; TOF 0.450 ms and RF frequency transfer optic 6 MHz for acetylcholine analyses; TOF 1 ms and RF frequency transfer optic 4 MHz for neuropeptides analyses.

All of the methods were externally calibrated using red phosphorus and internal calibration was applied using different lock masses; the FMP-10 cluster ion (m/z 555.2231) for derivatized neurotransmitters analyses and the [PC (16:0/18:1) + K]⁺ molecular ion (m/z 798.54096) for neuropeptide experiments^[47]. Tissue sections were analysed in a random order to prevent any possible bias due to matrix degradation or variation in mass spectrometer sensitivity.

MSI data were visualized using flexImaging (Bruker Daltonics, version 4.1). A mixture of deuterated neurotransmitters was applied for internal calibration of related endogenous neurotransmitters (further explained in results). FT-ICR spectra of neuropeptides were normalized against the root-mean square (RMS) of all data points.

6.2.5.8. Neurotransmitter turnover ratio calculations in brain regions

Neurotransmitter turnover ratio was calculated using the average intensity ratio between the metabolite and the neurotransmitter for HS and FF brain tissues [48].

6.2.5.9. Statistical analysis

SCiLS Lab (version 2019b, Bruker Daltonics) was used to export maximum intensity values for each ion of interest (Table S1 and Table S2) from the average spectrum generated for each brain. Statistical analyses were performed using GraphPad prism 6.0 software for Windows (GraphPad Software, San Diego, CA, U.S). The differences of mean values of the metabolites between the two sample preparation techniques were analysed for statistical significance using the two-tailed Student's t-test, for independent groups. p values <0.05 have been considered significant.

6.2.6. Conclusions

In this work, a MALDI-MSI approach has been developed to highlight the effectiveness of rapid and uniform heating of brain tissues to inactivate native enzymatic activity and prevent the *post mortem* degradation of the neuronal chemical messengers. Through the *in situ* visualization of the molecules, MALDI-MSI mapped the spatial distribution of both small molecule neurotransmitters and neuropeptides in heat treated rat brain sections, identifying *in situ* markers for

determination of neuronal chemical messengers' stabilization. Despite changes to the tissue morphology and ion suppression artefacts, which was strategically overcome, the spatial information of the molecules was not altered. These results enforce the potential of the heat treatment for sample preparations in MALDI-MSI in order to provide a realistic snapshot of the levels of key signalling molecules in the brain, enhancing the information about their roles in both healthy and disease conditions, as well as their modulation following pharmacological treatment.

6.2.7. References

^[1] Bartus, R., Dean, R., Beer, B., Lippa, A. The cholinergic hypothesis of geriatric memory dysfunction. *Science* 1982, *80*, 408–414.

^[2] Lotharius, J., Brundin, P. Pathogenesis of Parkinson's disease: dopamine, vesicles and alpha-synuclein. *Nat. Rev. Neurosci.* 2003, *3*, 932–942.

^[3] Politis, M., Niccolini, F. Serotonin in Parkinson's disease. *Behav. Brain. Res.* 2015, *277*, 136–145.

^[4] Marin, C., Bonastre, M., Mengod, G., Cortés, R., Rodríguez-Oroz, M.C. From unilateral to bilateral Parkinsonism: Effects of lateralization on dyskinesia and associated molecular mechanisms. *Neuropharmacol.* 2015, *97*, 365–375.

^[5] Sgroi, S., Capper-Loup, C., Paganetti, P., Kaelin-Lang, A. Enkephalin and dynorphin neuropeptides are differently correlated with locomotor hypersensitivity and levodopa-induced dyskinesia in parkinsonian rats. *Exp. Neurol.* 2016, *280*, 80–88.

^[6] Hulme, H., Fridjonsdottir, E., Halla Gunnarsdottir, H., Vallianatou, T., Zhang, X., Wadensten, H., Shariatgorji, M., Nilsson, A., Bezard, E., Svenningsson, P.,

Andrén, P.E. Simultaneous mass spectrometry imaging of multiple neuropeptides in the brain and alterations induced by experimental parkinsonism and L-DOPA therapy. *Neurobiol. Dis.* 2020, *137*, 104738.

[7] Skold, K, Svensson, M., Nilsson, A., Zhang, X., Nydahl, K., Caprioli, R.M., Svenningsson, P., Andrén, P.E. Decreased Striatal Levels of PEP-19 Following MPTP Lesion in the Mouse. *J. Proteomics. J. Proteomics* 2006, *5*, 262–269.

[8] Shariatgorji, M., Svenningsson, P., Andrén, P.E. Mass spectrometry imaging, an emerging technology in neuropsychopharmacology. *Neuropsychopharmacol.* 2014, *39*, 34–49.

[9] Källback, P., Shariatgorji, M., Nilsson, A., Andrén, P.E. Novel mass spectrometry imaging software assisting labeled normalization and quantitation of drugs and neuropeptides directly in tissue sections. *J. Proteomics* 2012, *75*, 4941–4951

[10] Schmidt, D., Speth, R., Welsch, F., Schmidt, M. The use of microwave radiation in the determination of acetylcholine in the rat brain. *Brain Res.* 1972, *38*, 377–389.

[11] Jehl, B., Bauer, R., Dorge, A., Rick, R. The use of propane-isopentane mixtures for rapid freezing of biological specimens. *J. Microsc.* 1981, *123*, 307–309.

[12] Blank, C.L., Sasa, S., Isernhagen, R., Meyerson, L.R., Wassil, D., Wong, P., Modak, A.T., Stavinoha, W.B. Levels of norepinephrine and dopamine in mouse brain regions following degradation of striatal dopamine in decapitated animals. *J. Neurochem.* 1979, *33*, 213–219.

^[13] Ishikawa, K., Shibasaki, S., Saito, S., McGaugh, J. Effect of focused microwave irradiation on monoamine metabolism in dissected rat brain. *Brain Res.* 1982, *240*, 158–161.

^[14] Balcom, G., Lenox, R., Meyerhoff, J. Regional γ -aminobutyric acid levels in rat brain determined after microwave fixation. *J. Neurochem.* 1975, *24*, 609–613.

^[15] O’Callaghan, J.P., Sriram, K. Focused microwave irradiation of the brain preserves in vivo protein phosphorylation: comparison with other methods of sacrifice and analysis of multiple phosphoproteins. *J. Neurosci. Methods* 2004, *135*, 159–168.

^[16] Sugiura, Y., Zaima, N., Setou, M., Ito, S., Ikuko, Y. Visualization of acetylcholine distribution in central nervous system tissue sections by tandem imaging mass spectrometry. *Anal. Bioanal. Chem.* 2012, *403*, 1851–1861.

^[17] Hattori, K., Kajimura, M., Hishiki, T., Nakanishi, T., Kubo, A., Nagahata, Y., Ohmura, M., Yachie-Kinoshita, A., Matsuura, T., Morikawa, T., Nakamura, T., Setou, M., Suematsu, M. Paradoxical ATP Elevation in Ischemic Penumbra Revealed by Quantitative Imaging Mass Spectrometry. *Antiox. Redox Sign.* 2010, *13*, 1157–1167.

^[18] van der Heyden, J., Korf, J. Regional levels of GABA in the brain: Rapid semi-automated assay and prevention of post mortem increase by 3-mercaptopropionic acid. *J. Neurochem.* 1978, *31*, 197–203.

^[19] Belforte, N.A., Moreno, A.C., de Zavali, N., Sande, P.H., Chianelli, M.S., Keller Sarmiento, M.I., Rosenstein, R.E. Melatonin: a novel neuroprotectant for the treatment of glaucoma. *J. Pineal Res.* 2010, *48*, 353–364.

[20] Cai, R., Kalappa, B.I., Brozoski, T.J., Ling, L.L., Caspary, D.M. Is GABA neurotransmission enhanced in auditory thalamus relative to inferior colliculus? . *J. Neurophysiol.* 2014, *111*, 229–238.

[21] Che, F. Y., Lim, J., Pan, H., Biswas, R., Fricker, L. D. Quantitative neuropeptidomics of microwave-irradiated mouse brain and pituitary. *Mol. Cell. Proteomics* 2005, *4*, 1391–1405.

[22] Sköld, K., Svensson, M., Norrman, M., Sjögren, B., Svenningsson, P., Andrén, P.E. The significance of biochemical and molecular sample integrity in brain proteomics and peptidomics: stathmin 2-20 and peptides as sample quality indicators. *Proteomics* 2007, *7*, 4445–4456.

[23] Svensson, M., Boren, M., Skold, K., Falth, M., Sjogren, B., Andersson, M., Svenningsson, P., Andrén, P.E. Heat-stabilization of the tissue proteome: a new technology for improved proteomics. *J. Proteome Res.* 2009, *8*, 974–981.

[24] Colgrave, M.L, Xi, L., Lehnert, S.A., Flatscher-Bader, T., Wadensten, H., Nilsson, A., Andrén, P., Wijffels, G. Neuropeptide profiling of the bovine hypothalamus: Thermal stabilization is an effective tool in inhibiting post-mortem degradation. *Proteomics* 2011, *11*, 1264–1276.

[25] Shariatgorji, M., Nilsson, A., Fridjonsdottir, E., Vallianatou, T., Källback, P., Katan, L., Sävmarker, J., Mantas, I., Zhang, X., Bezard, E., Svenningsson, P., Odell, L.R., Andrén, P.E. Comprehensive mapping of neurotransmitters networks by MALDI-MS Imaging. *Nat. Methods* 2019, *16*, 1021–1028.

[26] Goodwin, R.J.A., Nilsson, A., Borg, D., Langridge-Smith, P.R.R., Harrison, D.J., Mackay, C.L., Iverson, S.L., Andrén, P.E. Conductive carbon tape used for

support and mounting of both whole animal and fragile heat-treated tissue sections for MALDI MS imaging and quantitation. *J. Proteomics* 2012, 75, 4912–4920.

[27] Shariatgorji, M., Strittmatter, N., Nilsson, A., Källback, P., Alvarsson, A., Zhang, X., Vallianatou, T., Svenningsson, P., Goodwin, J.A.R., Andrén, P.E. . Simultaneous imaging of multiple neurotransmitters and neuroactive substances in the brain by desorption electrospray ionization mass spectrometry. *Neuroimage* 2016, 136, 129–138.

[28] Shariatgorji, M., Nilsson, A., Goodwin, R.J.A., Källback, P., Schintu, N., Zhang, X., Crossman, A.R., Bezdard, E., Svenningsson, P., Andrén, P.E. Direct target quantitative molecular Imaging of neurotransmitters in brain tissues sections *Neuron* 2014, 84, 697–707.

[29] Taylor, A.J., Dexter, A., Bunch, J. Exploring ion suppression in Mass Spectrometry Imaging of a heterogeneous tissue. *Anal. Chem.* 2018, 90, 5637–5645.

[30] Mulder, I.A., Esteve, C., Wermer, M.J.H., Hoehn, M., Tolner, E.A., van den Maagdenberg, A.M.J.M., McDonnell, L.A. Funnel-freezing versus heat-stabilization for the visualization of metabolites by mass spectrometry imaging in a mouse stroke model. *Proteomics* 2016, 16, 1652–1659.

[31] Källback, P., Nilsson, A., Shariatgorji, M., Andrén, P. E. msIQuant – Quantitation software for Mass Spectrometry Imaging enabling fast access, visualization, and analysis of large data sets. *Anal. Chem.* 2016, 88, 4346–4353.

[32] Bergman, H.M., Lundin, E., Andersson, M., Lanekoff, I. Quantitative mass spectrometry imaging of small-molecule neurotransmitters in rat brain tissue

sections using nanospray desorption electrospray ionization. *Analyst* 2016, *141*, 3686–3695.

[33] Bertrand, N., Beley, P., Beley, A. Brain fixation for acetylcholine measurements. *J. Neurosci. Methods* 1994, *53*, 81–85.

[34] Sugiura, Y., Honda, K., Kajimura, M., Suematsu, M. Visualization and quantification of cerebral metabolic fluxes of glucose in awake mice. *Proteomics* 2014, *14*, 829–838.

[35] Sugiura, Y., Katsumata, Y., Sano, M., Honda, K., Kajimura, M., Kajimura, M., Fukuda, K., Suematsu, M., Visualization of in vivo metabolic flows reveals accelerated utilization of glucose and lactate in penumbra of ischemic heart. *Sci. Rep.* 2016, *6*, 32361.

[36] Barré, F.P.Y., Claes, B.S.R., Dewez, F., Peutz-Kootstra, C., Munch-Petersen, H. F., Grønbaek, K., Lund, A.H., Heeren, R.M.A., Christophe Côme, C., Cillero-Pastor, B. Specific lipid and metabolic profiles of R-CHOP-resistant diffuse large B-Cell lymphoma elucidated by Matrix-Assisted Laser Desorption Ionization Mass Spectrometry Imaging and in vivo Imaging. 2018, *90*, . *Anal. Chem.* 2018, *90*, 14198–14206. .

[37] Eveque-Mourroux, M. R., Emans, P. J., Zautsen, R. R. M., Boonen, A., Heeren, R.M.A., Cillero-Pastor, B. Spatially resolved endogenous improved metabolite detection in human osteoarthritis cartilage by matrix assisted laser desorption ionization mass spectrometry imaging. *Analyst* 209, *144*, 5953.

[38] Wasek, B.; Arning, E.; Bottiglieri, T. The use of focused microwave irradiation for quantitative analysis of neurotransmitters in the mouse brain. *J. Neurosci. Methods* 2018, *307*, 188–193.

[39] Groppetti, A., Algeri, S., Cattabeni, F., Di Giulio, A. Changes in specific activity of dopamine metabolites as evidence of a multiple compartmentation of dopamine in striatal neurons. *J. Neurochem.* 1977, *28*, 193–197.

[40] Goodwin, R. J. A., Lang, A.M., Allingham, H., Borén, M., Pitt, A.R. Stopping the clock on proteomic degradation by heat treatment at the point of tissue excision. *Proteomics* 2010, *10*, 1751–1761.

[41] Goodwin, R. J. A., Dungworth, J.C., Allingham, H., Cobb, S.R., Pitt, A.R. Time-dependent evolution of tissue markers by MALDI-MS imaging. *Proteomics* 2008, *8*, 3801–3808.

[42] Fallon, J.H., Leslie, F.M. Distribution of dynorphin and enkephalin peptides in the rat brain. *J. Comp. Neurol.* 1986, *249*, 293–336.

[43] Shults, C.W., Quirion, R., Chronwall, B., Chase, T.N., O'Donohue, T.L. A comparison of the anatomical distribution of substance P and substance P receptors in the rat central nervous system. *Peptides* 1984, *5*, 1097–1128.

[44] Hanrieder, J., Ljungdahl, A., Andersson, M. MALDI imaging mass spectrometry of neuropeptides in Parkinson's disease. *J. Vis. Exp.* 2012, *60*, e3445.

[45] Taban, I.M., Altelaar, A.F.M., van der Burgt, Y.E.M., McDonnell, L.A., Heeren, R.M.A. Imaging of peptides in the rat brain using MALDI-FTICR mass spectrometry. *J. Am. Soc. Mass Spectrom.* 2007, *18*, 145–151.

[46] Andersson, M., Andrén, P.E., Caprioli, R.M. , MALDI Imaging and profiling mass spectrometry in Neuroproteomics. In *Neuroproteomics*, Alzate, O., Ed. CRC Press/Taylor & Francis: Boca Raton (FL), 2010.

[47] Guenther, S., Römpp, A., Kummer, W., Spengler, B. AP-MALDI imaging of neuropeptides in mouse pituitary gland with 5 μm spatial resolution and high mass accuracy. *Int. J. Mass Spectrom.* 2011, *305*, 228–237.

[48] Barton, D.A., Lambert, E.A., Hastings, J., Bayles, R. Elevated brain serotonin turnover in patients with depression. *Arch. Gen. Psychiatry* 2008, *65*, 38–46.

6.3. Section II: Preliminary Mass-Spectrometry Imaging of hop bitter acids distribution in liver tissue

6.3.1. Abstract

Understanding the spatial distribution of bioactive natural compounds is a valid tool for elucidating their biological or pharmacological behaviour. In this study, we present a preliminary MALDI-MSI method to the simultaneously mapping of hop α - and β -acids and their metabolites in rat liver tissues after oral administration. Parents compounds of α -acids and phase I mono-oxidized metabolites were mapped across liver sections, revealing higher relative intensity of Humulinone derivative respect the related precursor compound after 2 h. Although, this approach has limitations of the detection sensitivity for β -acids and phase II metabolites, which will could overcome with the aim to improve the investigation of the *in vivo* biotransformation of the bioactive phytochemicals as well as the molecular changes following their distribution in target tissues.

6.3.2. Introduction

Natural products derived from natural matrices are an abundant source of biologically active phytochemicals, many of which have formed the basis for development of pharmaceuticals and nutraceuticals ^[1]. Imaging of primary and secondary metabolites is the most frequent applications of plant-targeted MSI ^[2, 3]. However, there is little information on the use of MSI to follow *in vivo* administration of bioactive dietary phytochemicals, in order to elucidate the precise mechanism underlying the bioactivity and/or to determine how a candidate compounds is distributed and metabolized within the body. Alpha and β -acids are a class of prenylated phloroglucinol derivatives present in *Humulus lupulus* L., known for their multiple healthy-beneficial properties ^[4, 5]. Despite this, pharmacokinetic properties of this compound are largely unknown. In Chapter V, an ultra high performance liquid chromatography-high resolution mass spectrometry (UHPLC-HRMS) method has been applied to assess the metabolic stability of hop α - and β -acids and the characterization of their metabolites *in vitro* and *in vivo*. Here, MALDI-MSI was used to map the lateral distribution of hop bitter acids and its metabolites in mouse liver tissues after oral administration.

6.3.3. Results and Discussion

To effectively ionize the analyte and ensure the highly sensitive imaging of the target compound in MALDI-MSI, the optimum matrix needs to be determined. Because little is known about what matrices can ionize phytochemicals, 3 potential matrices has been screened: 2,5-dihydroxybenzoic acid (DHB), α -cyano-4-hydroxycinnamic acid (CHCA) and 9-aminoacridine (9-AA). A solution of each matrix was mixed with an equal volume of ICE-4 solution, and the mixture was

spotted onto a stainless steel MALDI plate and analyzed by MALDI-FT-ICR-MS in both positive and negative mode. Although DHB and CHCA are the most widely used MALDI matrices, they are more effective for ionization and visualization of macromolecules such as lipids and proteins or peptides ^[6], and were not able to detect α - and β -acids peaks. Small molecules are not easily detected by MALDI-MSI, therefore 9-AA can achieve very low detection limits and a high linearity for synthetic metabolite standards or extracted metabolites in negative ion mode ^[7]. In this regard, 9-AA was the only matrix that allowed the detection of all target molecules in negative ionization mode; therefore, it was selected as matrix for MALDI-MSI application.

9-AA-based MALDI-MSI was applied to map the lateral distribution of hop bitter acids mixture and their metabolites simultaneously in mouse liver tissues 1 and 2 h after the oral administration. Two peaks corresponding to α -acids Cohumulone (m/z 347.1867, 0.28 ppm) and n+Adhumulone (m/z 361.2019, -0.10 ppm) were mapped across liver tissues. Clearly, FT-ICR analyzer was not able to distinguish the two isomers of Humulone. Moreover, the related oxidized phase I metabolites iso- α -acids Cohumulone (m/z 363.1813, -0.27 ppm) and n+adHumulone (m/z 377.1968, 0.28 ppm) [Chapter V] were detected (**Figure 6.3.1**). Interestingly, higher relative intensity of oxidized metabolites of humulone respect to parent compound was observed 2 h after oral administration. The characterization was based on the HRMS, high accuracy and the isotopic fine structure provided by FT-ICR-MS platform. Differently from α -acids, no peaks of β -acids or their metabolites were detected. Moreover, the developed MALDI-MSI method could not visualize phase II metabolites. The discrepancies may be related to their relatively low abundance and the difficult to analyze them in the target

tissues. In this regard, further improvement of the detection sensitivity, especially improvement of MALDI efficiency based on matrix development, is required. The heat stabilization during sample preparation could be considered, in order to have a more realistic snapshot of *in vivo* metabolization of hop bitter acids [Section I]. Moreover, other MALDI matrices performances could be evaluated, for instance 1,5-Diaminonaphthalene (1,5-DAN), which has been reported to enable the detection of orally administered polyphenols EGCG and its metabolites in tissue micro-regions by negative ionization mode [8]. Certainly, the temporal analysis, pathological models, and visualization of other metabolites will be required to unravel both the biological consequence of biotransformation of the hop bitter acids and its mechanisms of action in tissues districts.

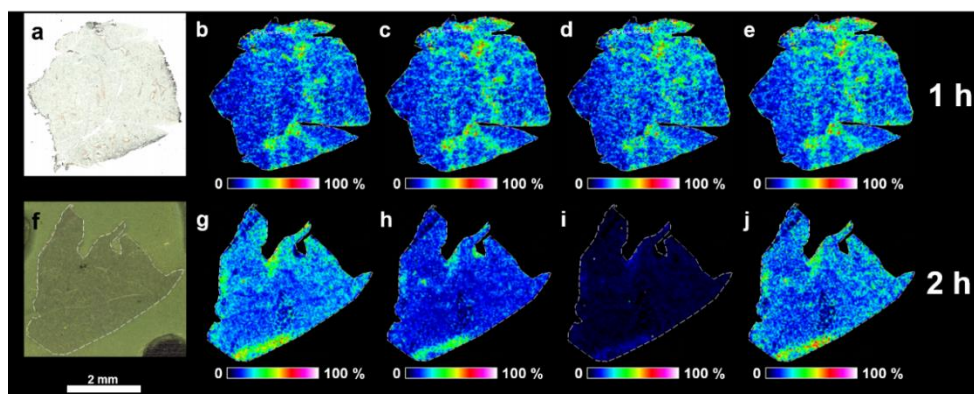


Figure 6.3.1. MALDI-MS images of ICE-4 α - and β -acids in mouse liver sections at 1 and 2 h after oral administration. Imaging experiments compared the distribution of parent compounds and mono-oxidized metabolites. **a, f**, optical images of mouse liver sections; **b, g**, Cohumulone (m/z 347.1867, -0.28 ppm) at 1 (**b**) and 2 h (**g**); **c, h**, Mono-oxidized cohumulone (m/z 363.1813, -0.27 ppm) at 1 (**c**) and 2 h (**h**); **d, i**, Humulone (m/z 361.2019, -0.10 ppm) at 1 (**d**) and 2 h (**i**); **e, j**, Mono-oxidized Humulone (m/z 377.1970, 0.28 ppm)

at 1 (e) and 2 h (j) ;Scale bar = 2 mm. Colour scale bars are shown as percentage of maximum intensity. Data were normalized against RMS. Lateral resolution, 100 μm .

6.3.4. Materials and methods

6.3.4.1. Chemicals

LC–MS-grade Water (H_2O) acetonitrile (ACN), methanol (CH_3OH), Ethanol (EtOH), additives formic acid (HCOOH), Trifluoroacetic acid (TFA) were all purchased from Sigma–Aldrich (St. Louis, MO, USA). International calibration standard ICE-4 bitter acids mixture was purchased by LaborVeritas (Zurich, Switzerland). Unless stated otherwise other reagent were all purchased by Merck.

6.3.4.2. Animal experiments

All experiments involving animals were conform to the guidelines for the Care and Use of Laboratory Animals published from Directive 2010/63/EU of the European Parliament.

Male C57BL/6 mice (25 ± 0.7 g body weight) were housed in groups (2-4 mice per cage) in a specific pathogen-free controlled environment (inverted 12 h light cycle; lights off at 10:00 hours). All mice had free access to standard mice chow and water.

ICE-4 sample was dissolved in 70% $\text{CH}_3\text{CH}_2\text{OH}$ and was administered by a single gavage (dosage 400 $\mu\text{g}/\text{Kg}$) in a total volume of 200 μL .

Two rats were sacrificed at 1 and 2 h from administration through cardiac puncture of isoflurane-anesthetized and the livers were quickly removed and immediately frozen by immersion in -45 °C dry-ice-cooled isopentane and stored at -80 °C.

6.3.4.3. Detection of ICE-4 spotted on a stainless steel MALDI sample plate

ICE-4 was prepared in methanol at 1 $\mu\text{g}/\text{mL}$ concentration. 2,5-dihydroxybenzoic acid (DHB), α -cyano-4-hydroxycinnamic acid (CHCA) and 9-aminoacridine (9-AA), were initially screened as matrices for the detection of α - and β -acids with solariX 7T ESI/MALDI-Fourier-transform ion cyclotron resonance mass spectrometer (Bruker Daltonics) equipped with a Smartbeam II 2kHz laser. 100 μL of 1 $\mu\text{g}/\text{mL}$ ICE-4 was added to an equal volume of one of the matrix solutions (DHB at 25 mg/mL in 50% MeOH, CHCA at 15 mg/mL in 50% ACN + 0.2% TFA *v/v*, 9-AA 10 mg/mL in 100% MeOH). Aliquots 0.5 μL of the matrix-sample mixtures were spotted onto a 384-well stainless steel MALDI sample plate and analyzed in both negative and positive ionization modes.

6.3.4.4. Tissue sample preparation for MALDI-MSI

The mouse liver sample were sectioned using a cryostat microtome (Leica CM1900, Leica Microsystems, Wetzlar, Germany) at thicknesses of 12 μm . Tissue sections were thaw-mounted onto indium tin oxide (ITO) coated glass slides (Bruker Daltonics, Bremen, Germany) and stored at $-80\text{ }^{\circ}\text{C}$ until analysis.

6.3.4.5. Sample preparation for MALDI-MSI analysis

The sections were dried in a vacuum desiccator for 20 min before MALDI matrix application. 9-aminoacridine (9-AA) was used as matrix at a concentration of 10 mg/mL in a solution of 80% EtOH. It was applied using an automated sprayer (TM-Sprayer, HTX Technologies). The nozzle temperature was set at $75\text{ }^{\circ}\text{C}$, with a nitrogen gas pressure of 6 psi, flow rate of 70 $\mu\text{L}/\text{min}$, nozzle velocity of 1100 mm/min with four passes, and 2 mm track spacing.

6.3.4.6. MALDI-MSI analysis

Optical images were acquired using a standard flatbed scanner (Seiko Epson, Japan). All MALDI-MSI experiments were performed on a solariX 7T ESI/MALDI-Fourier-transform ion cyclotron resonance mass spectrometer (Bruker Daltonics) equipped with a Smartbeam II 2kHz laser. All analyses were performed in positive ionization, at a lateral resolution of 100 μm . The laser power was optimised at the start of each run and then held constant during the experiments. 200 laser shots were fired at each sampling position. The data were acquired across the m/z range of 100-1000 using 2 million data points. Ion transmissions voltages parameters were set as follows: Funnel RF amplitude 120.0 Vpp, RF amplitude TOF 300.0 Vpp, TOF 0.6 ms, and RF frequency transfer optic 6 MHz.

All of the methods were externally calibrated using red phosphorus and internal calibration was applied using the 9-AA cluster ion (m/z 193.27712). Tissue sections were analysed in a random order to prevent any possible bias due to matrix degradation or variation in mass spectrometer sensitivity.

MSI data were visualized using flexImaging (Bruker Daltonics, version 4.1). FT-ICR spectra were normalized against the root-mean square (RMS) of all data points.

6.3.5. Conclusions

In present study, a MALDI-MSI platform was developed as an attractive label-free analytical tool to simultaneous detection and spatial visualization of an orally dosed phytochemicals mixture and oxidized metabolites. The preliminary data from this study indicate that 2 h after oral administration, hop α -acids and their oxidized isomer were accumulated in liver tissue. These results will open new possibility for investigating the spatial behaviour of bioactive phytochemicals, and could be

broadly applicable to understand in detail the absorption and metabolism of various bioactive small molecules, and evaluate the molecular alterations (proteins, lipids, polar metabolites) that occur after the exposure of a given bioactive compound.

6.3.6. References

^[1] Atanasov, A. G., Waltenberger, B., Pferschy–Wenzig, E. M., Linder, T., Wawrosch, C., Uhrin, P., Temml, V., Wang, L., Schwaiger, S., Heiss, E. H., Rollinger, J. M., Schuster, D., Breuss, J. M., Bochkov, V., Mihovilovic, M. D., Kopp, B., Bauer, R., Dirsch, V. M., & Stuppner, H. Discovery and resupply of pharmacologically active plant–derived natural products: A review. *Biotechnol. Adv.* 2015, 33, 1582–1614.

^[2] Sugahara, K., Kitao, K., Watanabe, T., Yamagaki, T., Imaging mass spectrometry analysis of flavonoids in blue viola petals and their Enclosure effects on violanin during color expression. *Anal. Chem.* 2019, 91, 896–902.

^[3] Beck, S., Stengel, J., Mass spectrometric imaging of flavonoid glycosides and biflavonoids in Ginkgo biloba L. *Phytochem.* 2016, 130, 201–206.

^[4] Van Cleemput, M., Cattoor, K., De Bosscher, K., Haegeman, G., De Keukeleire, D., Heyerick, A. Hop (*Humulus lupulus*)–Derived Bitter Acids as Multipotent Bioactive Compounds. *J. Nat. Prod.* 2009, 72, 1220–1230.

^[5] Salviati, E., Ciaglia, E., Sommella, E., Montella, F., Bertamino, A., Ostacolo, C., Parrino, B., Rubino, R., Vecchione, C., Puca, A., Novellino, E., Campiglia, P. Immunomodulatory activity of *Humulus lupulus* bitter acids fraction: Enhancement of natural killer cells function by NKp44 activating receptor stimulation. *J. Funct. Foods* 2019, 61, 103469.

^[6] Schwartz, S.A., Reyzer, M.L., Caprioli, R.M. Direct tissue analysis using matrix-assisted laser desorption/ionization mass spectrometry: practical aspects of sample preparation. *J. Mass. Spectrom.* 2003, 699–708.

^[7] Miura, D., Fujimura, Y., Tachibana, H. & Wariishi, H. Highly sensitive matrix-assisted laser desorption ionization–mass–spectrometry for high-throughput metabolic profiling. *Anal. Chem.* 2010, 82, 498–504 (2010).

^[8] Kim, Y.H., Fujimura, Y., Hagihara, T., Sasaki, M., Yukihiro, D., Nagao, T., Miura, D., Yamaguchi S., Saito, K., Tanaka, H., Wariishi, H., Yamada, K., Tachibana, H. In situ label-free imaging for visualizing the biotransformation of a bioactive polyphenol. *Sci. Rep.* 2013, 30, 2805.

CHAPTER VII: Supporting Informations

7.1. Supporting Informations for Chapter II “Chemical profiling of bioactive constituents in hop cones and pellets extracts by online comprehensive two-dimensional liquid chromatography with tandem mass spectrometry and direct infusion Fourier transform ion cyclotron resonance mass spectrometry”

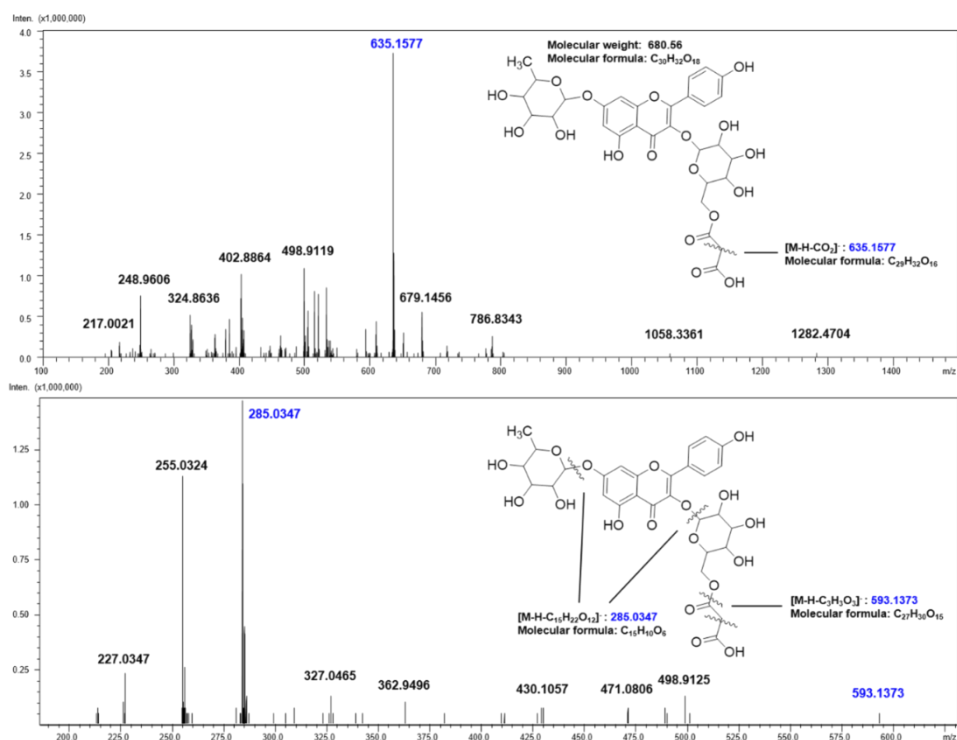


Figure S2.1. MS and MS/MS spectra showing structure elucidation and fragmentation pattern of peak 31.

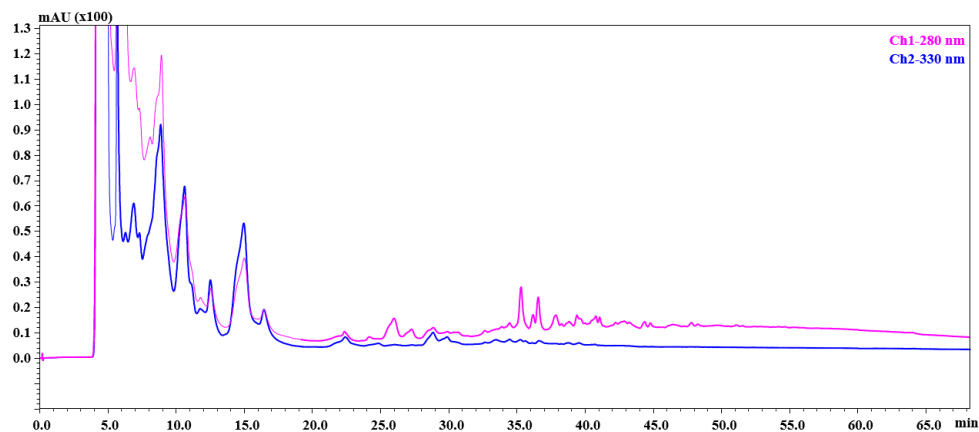


Figure S2.2. Separation of hop cones extract, column Luna[®] HILIC 150 × 2.1 mm, 3.0 μm, injection volume 2 μL, flow rate 0.1 mL/min, mobile phase: A) H₂O/ACN 80/20 + 0.1 % CH₃COOH; B) ACN.

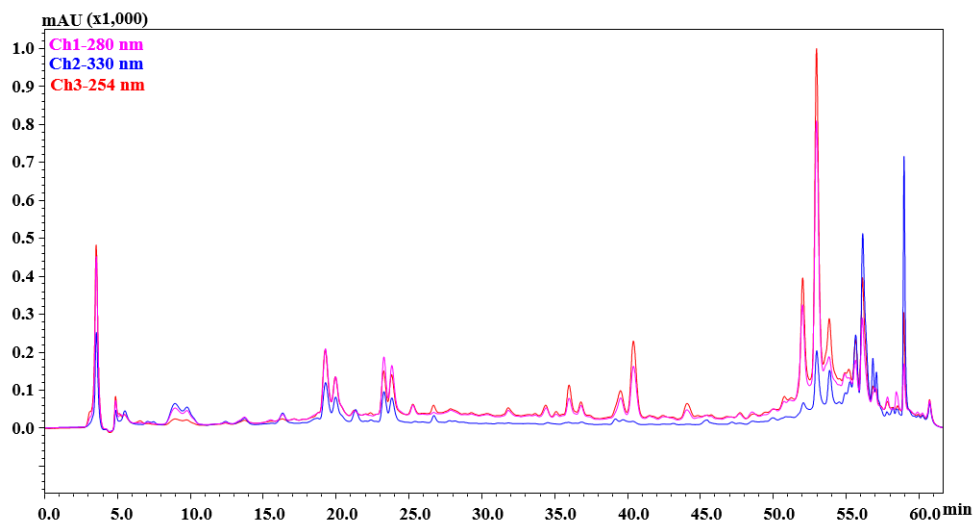


Figure S2.3. First dimension separation of hop cones extract, column Luna[®] C18 150 × 1.0 mm, 5.0 μm, injection volume 1 μL, flow rate 30 μL/min, mobile phase: A) 10 mM CH₃COONH₄ in H₂O, pH 9; B) ACN.

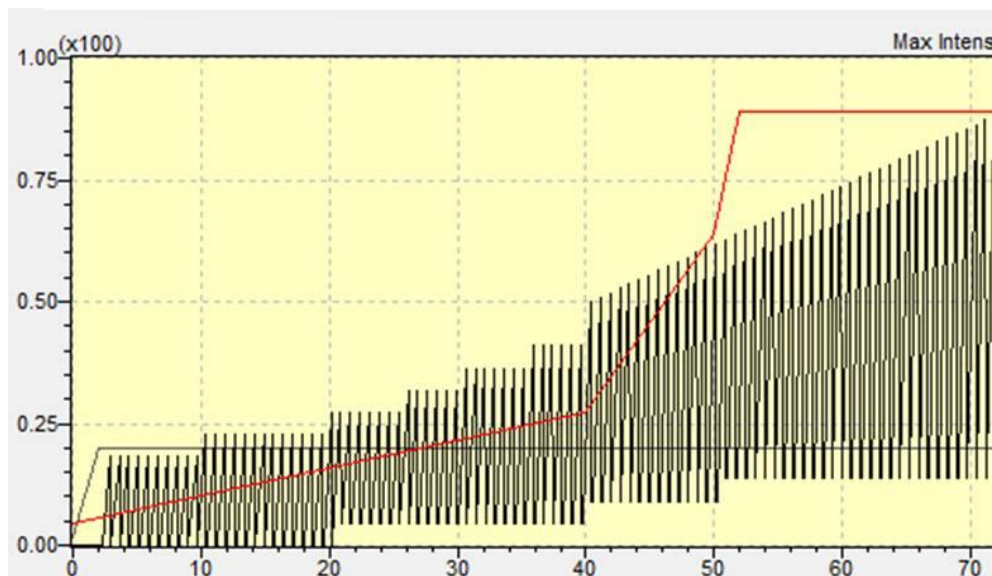


Figure S2.4. Shifted gradient approach employed in the ²D of LC × LC setup.

Table S2.1. DI-FT-ICR identification of hop cones and pellets extracts based on Accurate Formula and Compound Crawler Database searching.

Peak	Compound	[M-H] ⁻	Error (ppm)	Molecular Formula
1	Caffeoylquinic acid	353.08789	-0.01	C ₁₆ H ₁₈ O ₉
2	Coumaroylquinic acid	337.09287	0.07	C ₁₆ H ₁₈ O ₈
3	Feruloylquinic acid	367.10346	0.06	C ₁₇ H ₂₀ O ₉
4	Rutin / Quercetin 3-O-rhamnosyl-hexoside	609.14610	0.02	C ₂₇ H ₃₀ O ₁₆
5	Quercetin 3-O-hexoside	463.08820	-0.01	C ₂₁ H ₂₀ O ₁₂
6	Epicatechin dimer (EC-2)	577.13530	-0.26	C ₃₀ H ₂₆ O ₁₂
7	Epicatechin trimer (EC-3)	865.19679	2.02	C ₄₅ H ₃₈ O ₁₈
8	Kaempferol 3-O-β-(6-O-malonyl)-hexoside	533.18756	0.03	C ₂₃ H ₃₄ O ₁₄
9	Kaempferol 3-O-di-hexoside	593.15107	0.21	C ₂₇ H ₃₀ O ₁₅

Chapter VII: Supporting Informations

10	Kaempferol 3-O-hexoside / Astragalin	447.09329	0.00	C ₂₁ H ₂₀ O ₁₁
11	Catechin	289.07158	0.63	C ₁₅ H ₁₄ O ₆
12	Unknown	557.18161	0.17	C ₃₂ H ₂₉ O ₉
13	Unknown	489.10386	-0.03	C ₂₁ H ₃₀ O ₁₃
14	Cohumulone	363.18132	-0.02	C ₂₀ H ₂₈ O ₆
15	Unknown	237.11325	-0.07	C ₁₃ H ₁₈ O ₄
16	Ox-xanthohumol	369.13436	0.00	C ₂₁ H ₂₂ O ₆
17	Unknown	195.06629	-0.03	C ₁₀ H ₁₂ O ₄
18	Oxy-humulone	393.19188	-0.00	C ₂₁ H ₃₀ O ₇
19	Unknown	251.12887	0.03	C ₁₄ H ₂₀ O ₄
20	Unknown	333.17073	0.05	C ₁₉ H ₂₆ O ₅
21	Oxy-adhumulinone	409.18679	0.01	C ₂₁ H ₃₀ O ₈
22	Humulinone / Adhumulinone	377.19696	0.00	C ₂₁ H ₃₀ O ₆
23	Unknown	391.17623	-0.02	C ₂₁ H ₂₈ O ₇
24	Iso- α -ad/n-humulone	361.20206	-0.02	C ₂₁ H ₃₀ O ₅
25	Cohulupone	317.17583	0.02	C ₁₉ H ₂₆ O ₄
26	Deoxycohumulone	331.19148	0.00	C ₂₀ H ₂₈ O ₄
27	Lupulone E	415.24898	0.03	C ₂₅ H ₃₆ O ₅
28	Postlupulone	385.23835	0.22	C ₂₄ H ₃₄ O ₄
29	Unknown	349.12926	0.06	C ₁₈ H ₂₂ O ₇
30	Prehumulone	375.21768	0.06	C ₂₂ H ₃₂ O ₅
31	Cohumulone	347.18640	0.01	C ₂₀ H ₂₈ O ₅
32	Unknown	375.181321	0.02	C ₂₁ H ₂₈ O ₆
33	Colupulone	399.25407	0.04	C ₂₅ H ₃₆ O ₄
34	Adlupulone	413.26973	-0.00	C ₂₆ H ₃₈ O ₄
35	Prenyl-naringenin / Desmethylxanthohumol	339.12382	-0.08	C ₂₀ H ₂₀ O ₅
36	Unknown	305.13944	0.02	C ₁₇ H ₂₂ O ₅
37	Xanthohumol/Isoxanthohumol	353.13945	-0.01	C ₂₁ H ₂₂ O ₅
38	Diprenyl naringenin	407.18642	-0.07	C ₂₅ H ₂₈ O ₅
39	Unknown	351.12373	0.18	C ₂₁ H ₂₀ O ₅

40 Deoxyhumulone/deoxyadlupulone 345.20714 -0.01 C₂₁H₃₀O₄

Table S2.2. Peak capacity values corrected for undersampling (*) and orthogonality $A_0^{\#}$

Theoretical Peak capacity	2418.57
Practical Peak capacity*	1478.93
Practical Peak capacity**	756.67

[#] Excel equations used for orthogonality A_0 calculation according to Camenzuli et al. [24]

$$S_{z-} = \sigma \{1 \text{trnorm}(i) - 2 \text{trnorm}(i)\}$$

$$S_{z+} = \sigma \{2 \text{trnorm}(i) - (1 - 1 \text{trnorm}(i))\}$$

$$S_{z1} = \sigma \{1 \text{trnorm}(i) - 0,5\}$$

$$S_{z2} = \{2 \text{trnorm}(i) - 0,5\}$$

$$Z_{-} = |1 - 2,5|S_{z-} - 0,4||$$

$$Z_{+} = |1 - 2,5|S_{z+} - 0,4||$$

$$Z1 = 1 - |2,5 * S_{z1} * \sqrt{2-1}|$$

$$Z2 = 1 - |2,5 * S_{z2} * \sqrt{2-1}|$$

$$A_0 = \sqrt{(Z_{+}) * (Z_{-}) * (Z1) * (Z2)} = 0.51$$

$$N_{corr} = n_c * 0.51$$

Table S2.3. Repeatability data for 2D peak areas and 2D retention times.

CV% Area	CV% (¹ D+ ² D) <i>r</i> _t
10.2	0.1

7.2. Supporting Informations for Chapter III “Immunomodulatory activity of *Humulus lupulus* L. bitter acids fraction: enhancement of natural killer cells function by NKp44 activating receptor stimulation”

hop pellet fractions

1.1. UHPLC-PDA-MS/MS parameters

UHPLC analyses were performed on a Nexera Shimadzu UHPLC system consisting of a controller CBM-20A, two LC-30AD pumps, a DGU-20 A5 degasser, a SPD-M20A PDA detector, a column oven CTO-20A and a SIL-30AC autosampler. The system was coupled online to a LCMS-IT-TOF hybrid mass spectrometer by ESI source (Shimadzu, Milan, Italy). A Kinetex[®] EVO C18 150 × 2.1 mm, 2.6µm (Phenomenex[®]) column was employed at flow rate of 0.5 mL/min. The separation was carried out with the following parameters: mobile phase was: A) 0.1 % CH₃COOH in H₂O *v/v*, B) ACN plus 0.1 % CH₃COOH, gradient: 0-15 min, 5-30%B, 15-20 min, 30-70 %B, 20-22 min, 70-95 %B, 22-25 min, 98-98%B, 25-30 min, 5%B. Column oven was set at 45°C, 2 µL of sample was injected. PDA detection parameters were: sampling rate 12 Hz, time constant 0.160 s and chromatograms were extracted at 280 and 330 nm. ESI MS detection was performed as follows: detector, 1.60kV; CDL (curve desolvation line), 250 °C; heater block, 250 °C, nebulizer (N₂), 1.5 L/min, drying gas, 100 kPa. MS1 150-1500 *m/z*, ion accumulation time, 30 ms; IT, repeat =3. MS/MS data dependent

Chapter VII: Supporting Informations

acquisition precursor range: 150-900 m/z; peak width 3 Da, accumulation time 40 ms; CID energy, 50%; repeat =3.

Chapter VII: Supporting Informations

Table S3.1. List of all compounds detected in the hop pellets fractions.

Peak	t_r	Compound	[M-H] ⁻	[MS/MS]	Error (ppm)	PDA λ_{max} (nm)	Molecular Formula
Hop Fraction A (HFA)							
<i>Hydroxycinnamic acid</i>							
1	1.83	3'- caffeolquinic acid (Chlorogenic acid)*	353.0850	191.0625, 179.0385	0.85	320	C ₁₆ H ₁₈ O ₉
2	2.65	3'- coumaroylquinic acid	337.0922	163.0407, 119.0394	-2.67	304	C ₁₆ H ₁₈ O ₈
3	3.52	3' - feruloylquinic acid	367.1040	193.0516, 134.0216	1.36	322	C ₁₇ H ₂₀ O ₉
<i>Flavonols</i>							
4	6.50	Quercetin 3-O-(2-rhamnosyl) - hexoside	755.2036	301.0333, 255.0535 271.0211	-0.53	256, 299	C ₃₃ H ₄₀ O ₂₀
5	6.99	Quercetin 3-O-galactoside*	463.0855	301.0346, 271.0255 255.0290	-3.89	255	C ₂₁ H ₂₀ O ₁₂
6	7.48	Rutin*	609.1445	301.0362, 255.0306 271.0269	-4.43	353	C ₂₇ H ₃₀ O ₁₆
7	7.78	Quercetin 3-O-glucoside*	463.0855	301.0346, 271.0255 255.0290	-4.53	255	C ₂₁ H ₂₀ O ₁₂
8	8.33	Quercetin 3-O-(acetyl) -hexoside	505.0972	301.0381, 271.0204 255.0288	-3.17	311	C ₂₃ H ₂₂ O ₁₃
9	8.63	Kaempferol 3-O-hexoside	635.1601	285.0384, 593.1373 255.0300 227.0416	0.63	262, 345	C ₂₉ H ₃₂ O ₁₆
10	8.88	Kaempferol 3-O-di-hexoside	593.1413	285.0393, 255.0279 227.0656	-2.42	265, 344	C ₂₇ H ₃₀ O ₁₅

Chapter VII: Supporting Informations

11	8.94	Kaempferol 3-O--(malonyl-hexoside)-O-rhamnoside	447.0949	285.0433, 255.0302 227.0741	4.03	264, 345	C ₂₁ H ₂₀ O ₁₁
12	2.30	Epicatechin dimer	577.1247	407.0662, 289.0448	-4.97	279	C ₃₀ H ₂₆ O ₁₂
13	3.10	Epicatechin dimer isomer II	577.1288	407.0729, 289.0619	1.73	279	C ₃₀ H ₂₆ O ₁₂
Hop Fraction B (HFB)							
<i>α-acids and β-acids derivatives</i>							
14	13.50	Oxy-humulone	393.1912	349.2050, 263.1292 395.1898	-4.42	255, 323	C ₂₁ H ₃₀ O ₇
15	14.00	Humulinone isomer	377.1928	263.1259, 221.0969	-5.04	285, 323	C ₂₁ H ₃₀ O ₆
16	15.15	Oxidized humulinone derivative	409.1879	263.1285, 295.1130 333.1577	0.98	285, 323	C ₂₁ H ₃₀ O ₈
17	16.60	Oxidized humulinone derivative isomer	409.1879	263.1285, 295.1130 333.1577	0.98	285, 323	C ₂₁ H ₃₀ O ₈
18	17.69	Cohumulone	347.1862	235.0624, 278.1176 223.0747	-0.58	285, 323	C ₂₀ H ₂₈ O ₅
19	18.65	Cohumulone	363.1807	249.1125, 275.1418 233.1746	-1.38	275, 310	C ₂₀ H ₂₈ O ₆
20	19.15	Humulinone	377.1928	263.1259, 221.0969	-5.04	285, 323	C ₂₁ H ₃₀ O ₆
21	20.84	Cohumulone isomer	347.1862	235.0624, 278.1176 223.0747	-0.58	285, 323	C ₂₀ H ₂₈ O ₅
22	21.40	Iso- α -ad/n-humulone	361.2015	265.1428, 363.1836	2.21	285, 323	C ₂₁ H ₃₀ O ₅
23	21.70	Deoxycohumulone	331.1920	262.1292, 194.0621	1.51	290, 335	C ₂₀ H ₂₈ O ₄
24	24.30	Prehumulone	375.1818	306.1319	2.40	285, 325	C ₂₂ H ₃₂ O ₅
25	18.10	Cohulupone	317.1765	248.0959, 180.0271 152.2327	2.21	280, 335	C ₁₉ H ₂₆ O ₄
Hop Fraction C (HFC)							

Chapter VII: Supporting Informations

<i>β-acids and derivatives</i>							
26	21.70	Lupulone E	415.2489	259.1037, 303.1277	-0.24	235, 360	C ₂₅ H ₃₆ O ₅
27	22.56	Postlupulone	385.1228	273.0903, 248.9524	-3.63	280, 335	C ₂₄ H ₃₄ O ₄
28	24.10	Colupulone	399.2541	287.1253, 219.0712	-0.25	280, 335	C ₂₅ H ₃₆ O ₄
29	26.10	Deoxyhumulone/deoxyadlupulone	345.2064	346.2135, 301.2297 221.0866	-2.03	290, 335	C ₂₁ H ₃₀ O ₄
<i>Prenylflavonoids</i>							
30	18.25	Ox-Xanthohumol	369.1336	249.0772	-5.40	255, 307	C ₂₁ H ₂₂ O ₆
31	19.25	Xanthohumol*	353.1405	233.0921, 189.0277 175.0147	-0.85	370	C ₂₁ H ₂₂ O ₅
32	25.10	Prenyl-naringenin	339.1229	219.0672, 245.0805	-1.75	294, 337	C ₂₀ H ₂₀ O ₅

* Identified according to standard retention time

hop pellet phytocomplex and sub-fraction B3 (HFB3)

International Calibration Extract 4 (ICE-4) for α - and β -acids (Labor Veritas, Zurich, Switzerland) was reported to contain 10.88% cohumulone; 31.60% n+adhumulone; 13.02% colupulone; 13.52% n+adlupulone. ICE-4 was selected as external standards for the quantification of α and β acids isolated from hop phytocomplex and sub-fraction B3 (HFB3). Stock solution (10 mg/mL) of ICE-4 standard was prepared weighing 150 mg in a 15-mL volumetric flask. 8 mL of CH₃OH were added to the flask, which was sonicated for 10 min and filled to volume with CH₃OH. The ICE-4 stock solution was filtered through a 0.45 μ m nylon filter and was diluted with CH₃OH to concentration of working solutions. Calibration curve in the range of 5–250 μ g/mL (total ICE-4 concentration) with six concentration levels was constructed to generate calibration curve from regression analysis ($R^2 \geq 0.999$). Limits of detection (LODs) and quantification (LOQs) were calculated by the ratio between the standard deviation (SD) and analytical curve slope multiplied by 3 and 10, respectively. Note that each standard concentration level contained different amounts of the individual analytes, as following reported:

Concentration Level	5 μ g/mL	25 μ g/mL	50 μ g/mL	100 μ g/mL	250 μ g/mL
Compound (%)	Compound concentration in calibration curve level (μ g/mL)				
Cohumulone (10.88%)	0.794	3.971	7.943	15.885	39.714
n-Humulone (24%)	1.736	8.681	17.361	34.722	86.806
Adhumulone (7.6%)	0.550	2.749	5.498	10.995	27.488
Colupulone (13.02%)	0.942	4.709	9.418	18.837	47.092
n-Lupulone (10.30%)	0.745	3.725	7.451	14.902	37.251

Chapter VII: Supporting Informations

Adlupulone (3.22%)	0.233	1.164	2.329	4.659	11.646
---------------------------	-------	-------	-------	-------	--------

Table S3.2. Quantitative profile of bitter acids in hop target phytocomplex and sub-fraction B3.

Compound	Hop Phytocomplex (HP)	Hop Fraction B (HFB3)	LOD	LOQ
	µg/mg ± SD	µg/mg ± SD	µg/mL	µg/mL
Oxo-Humulone	0.541 ± 0.02	1.176 ± 0.01	0.022	0.073
Humulone	3.185 ± 0.12	6.71 ± 0.03	0.022	0.073
Cohumulone	0.485 ± 0.01	1.728 ± 0.01	0.016	0.054
Cohulupone	7.596 ± 0.16	35.63 ± 0.08	0.008	0.026
Deoxycohumulone	4.46 ± 0.02	12.79 ± 0.07	0.016	0.054

Compound	Hop Phytocomplex (HP)	Hop Fraction B (HFB3)	LOD	LOQ
	µg/mg ± SD	µg/mg ± SD	µg/mL	µg/mL
Oxo-Humulone	0.541 ± 0.02	1.176 ± 0.01	0.022	0.073
Humulone	3.185 ± 0.12	6.71 ± 0.03	0.022	0.073
Cohumulone	0.485 ± 0.01	1.728 ± 0.01	0.016	0.054
Cohulupone	7.596 ± 0.16	35.63 ± 0.08	0.008	0.026
Deoxycohumulone	4.46 ± 0.02	12.79 ± 0.07	0.016	0.054

7.3. Supporting Informations for Chapter IV “Indole-3-lactic acid, a metabolite of tryptophan, secreted by *Bifidobacterium longum* subspecies *infantis* is anti-inflammatory in the immature intestine”

Table S4.1. *B. infantis* culture media. The table shows the ingredients of the *B. infantis* culture media that is a modification of the combination of the intestinal epithelial cell culture media and the *B. infantis* culture media. Abbreviation: MEMNEAA- MEM non-essential amino acids, BPE-Bovine pituitary extract, BHI- Brain and heart infusion broth.

Ingredients	Amount	Final concentration
OptiMem media	1000 ml	-
Sodium Acetate	5 g	5 g/L= 60 mM
L-Cysteine	0.5 g	0.5 g/L
Album	1 g	1 g/L
Yest extract	5 g	5 g/L
Sodium Selenite	60 µl of 1mM	60 nM
Vitamine A	5 µl of 5 µg/µl stock	25 µg/L
Holo transferin	60 µl of 5 mg/ml stock	(0.3 µg/ml)
Inulin	100 mg	0.1 mg/ml
BPE	200 µl of 25 mg/ml stock	5 µg/ml
MEMNEAA	10 ml	1x
Glutamite	10 ml	2 mM
Hepes	10 ml	10 mM
BHI	8 ml of 0.5 g/ml Stock	4 g/L

7.4. Supporting Informations for Chapter V “Determination of phase I metabolites and glucuronide conjugates of hop bitter acids by a full scan/data dependent/targeted neutral loss UHPLC-HRMS strategy: In vitro metabolic stability and in vivo analysis after oral administration in mice”

Table S5.1. Concentrations of α - and β -acids in ICE-4 standard solutions at each concentration level of calibration curves.

Concentration Level	0.5 $\mu\text{g/mL}$	25 $\mu\text{g/mL}$	50 $\mu\text{g/mL}$	100 $\mu\text{g/mL}$	250 $\mu\text{g/mL}$
Compound (%)	Compound concentration in calibration curve level ($\mu\text{g/mL}$)				
Cohumulone (10.88%)	0.08	3.971	7.943	15.885	39.714
n-Humulone (24%)	0.174	8.681	17.361	34.722	86.806
Adhumulone (7.6%)	0.06	2.749	5.498	10.995	27.488
Colupulone (13.02%)	0.094	4.709	9.418	18.837	47.092
n-Lupulone (10.30%)	0.075	3.725	7.451	14.902	37.251
Adlupulone (3.22%)	0.023	1.164	2.329	4.659	11.646

Chapter VII: Supporting Informations

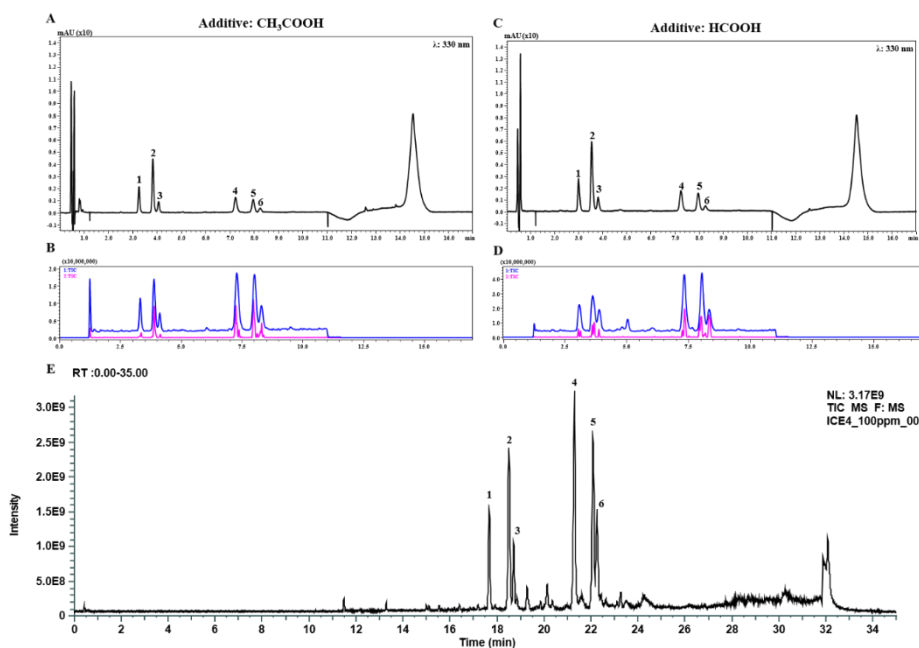


Figure S5.1. UHPLC-PDA chromatograms (λ : 330 nm) (a, c) with a gradient starting from high percentage of organic modifier (50% ACN) and ESI negative - MS/MS total ion chromatograms (TIC) (b, d) of ICE-4 sample using CH_3COOH (a, b) and HCOOH (c, d) as additives of the mobile phase. e, UHPLC-ESI Negative - MS TIC of ICE-4 sample with optimized conditions employed for the final UHPLC-HRMS setup. Peak: **1**, Cohumulone; **2**, n-Humulone; **3**, Adhumulone; **4**, Colupulone; **5**, n-Lupulone; **6**, Adlupulone.

Chapter VII: Supporting Informations

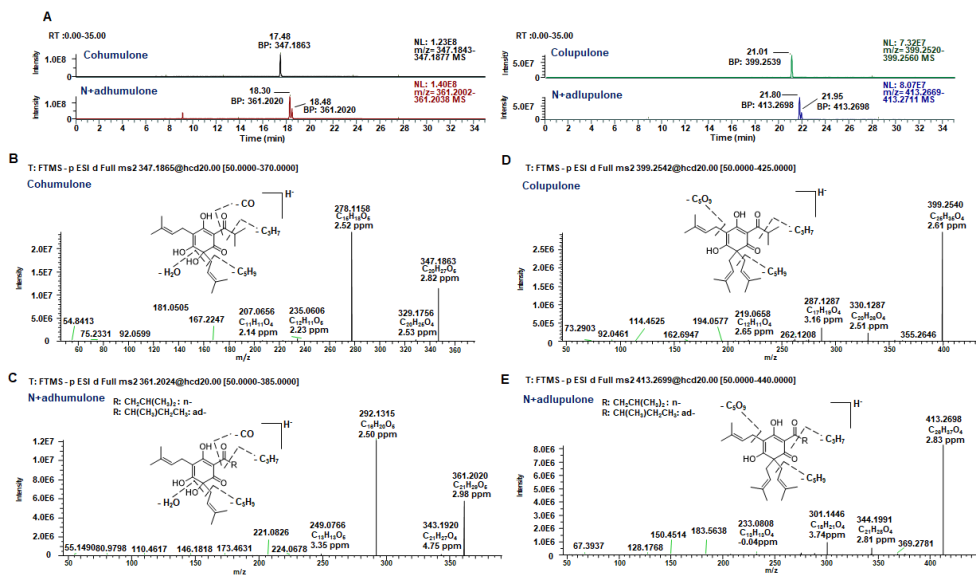


Figure S5.2. Extracted ion chromatograms (a) and MS² spectra with the fragmentation pathways (b-e) of ICE-4 α - (b,c) and β - (d,e) acids parent compounds.

Chapter VII: Supporting Informations

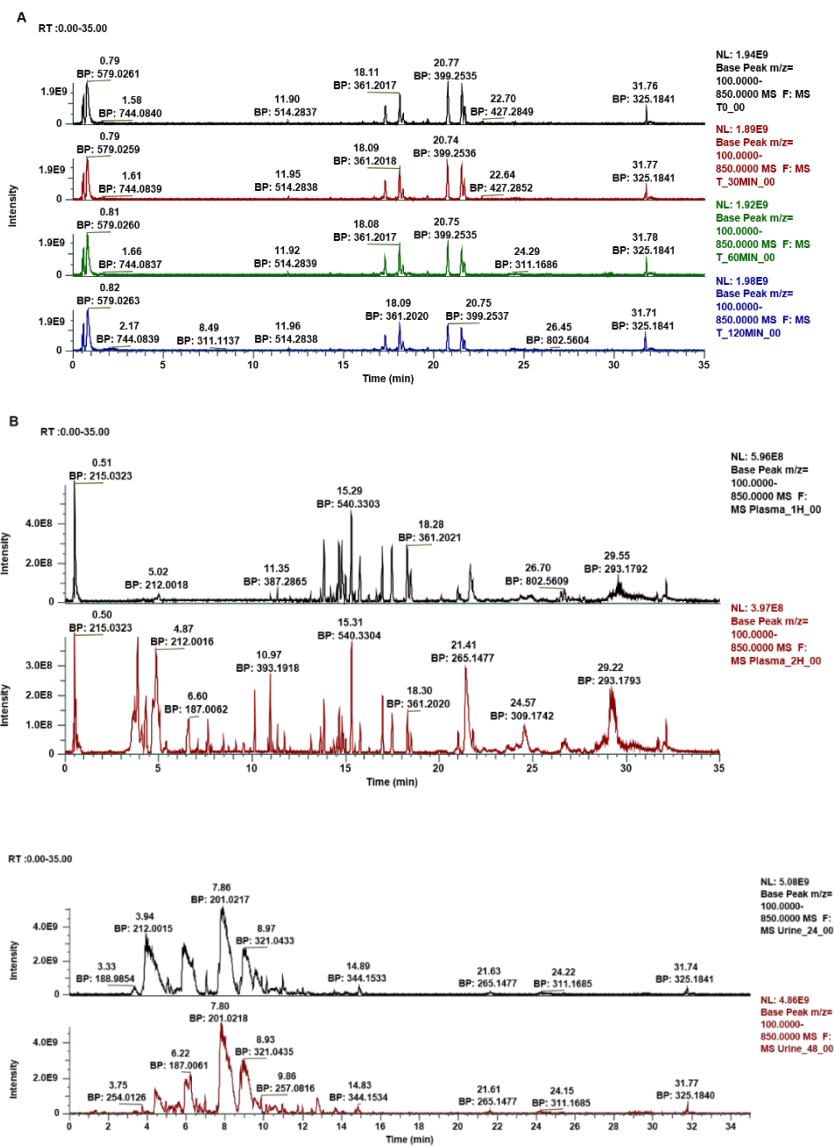


Figure S5.3. UHPLC-HRMS base peak chromatograms (BPC) of mouse liver microsomal digested at 0, 30, 60 and 120 min (a), mouse plasma at 1 and 2 h (b) and urine at 24 and 48 h (c) extracts.

Chapter VII: Supporting Informations

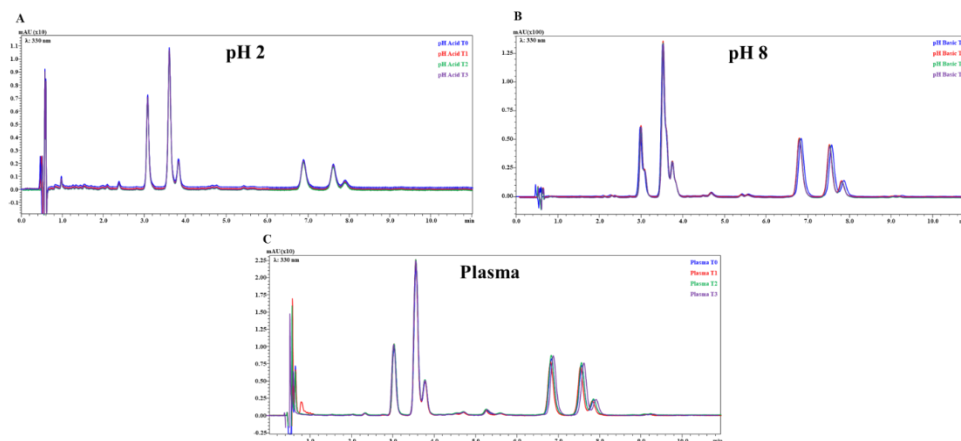
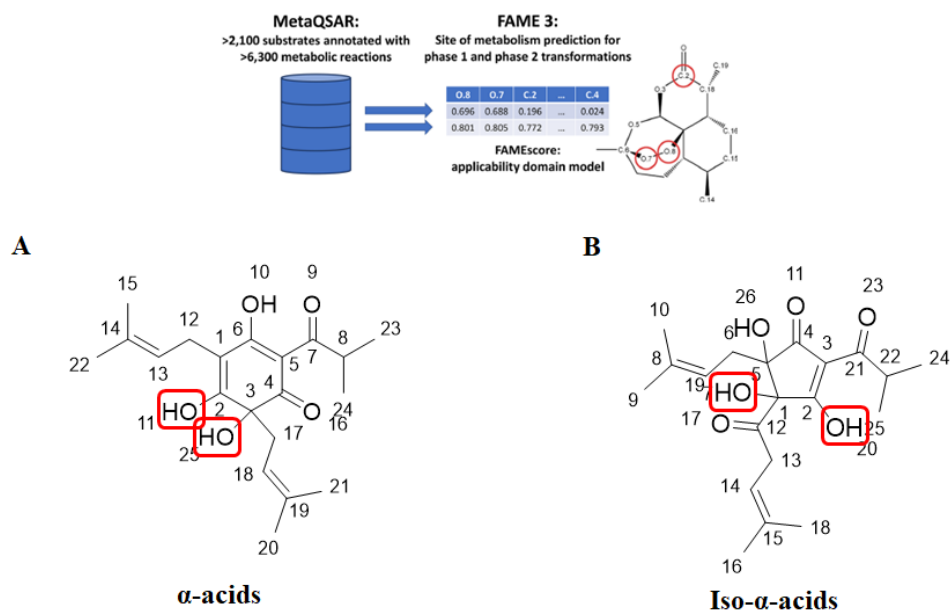


Figure S5.4. UHPLC-PDA chromatograms (λ : 330 nm) of ICE-4 sample subjected to gastric (0.1 M HCl, pH 2) (a), intestinal (HCOONH₄ 10 mM, adjusted to pH 8 with NaOH) (b) and mouse plasma (c) stability evaluation. **Time points:** T0, 0 min; T1, 30 min; T2, 60 min; T3, 120 min.



Substituent	FAME Probability	FAME3 score
OH linked to C2	0.156	0.405
OH linked to C3	0.148	0.517

Substituent	FAME Probability	FAME3 score
OH linked to C2	0.156	0.405
OH linked to C3	0.148	0.517

Figure S5.5. Potential prediction of glucuronide derivative of α - and iso- α -acids by FAME3 (<https://nerdd.zbh.uni-hamburg.de/fame3/>). As a result, the approach proposed as first hits the hydroxyl substituents in position C3 and C4 for α -acids and C1 and C2 for iso- α -acids as most probable SOM for UGTs catalyzed glucuronidation.

7.5. Supporting Informations for Chapter VI Section I “Evaluation and optimization of neurotransmitter and neuropeptide analysis in heat stabilized vs fresh frozen brains by MALDI-MSI”

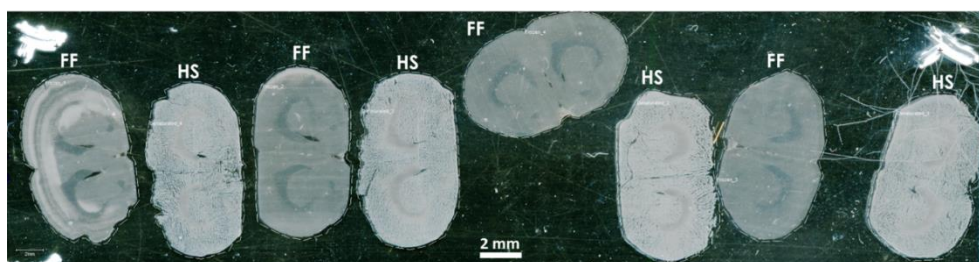


Figure S6.2.1. Optical images of coronal rat sections from four HS brains and four FF brains, which shows the changes to the tissue structure caused by heating. The HS tissues appear dryer, their edges are jagged and some holes can be observed (distance from bregma, 2.28 mm, Paxinos and Watson, 2014). Abbreviations: FF, fresh frozen; HS, heat stabilized.

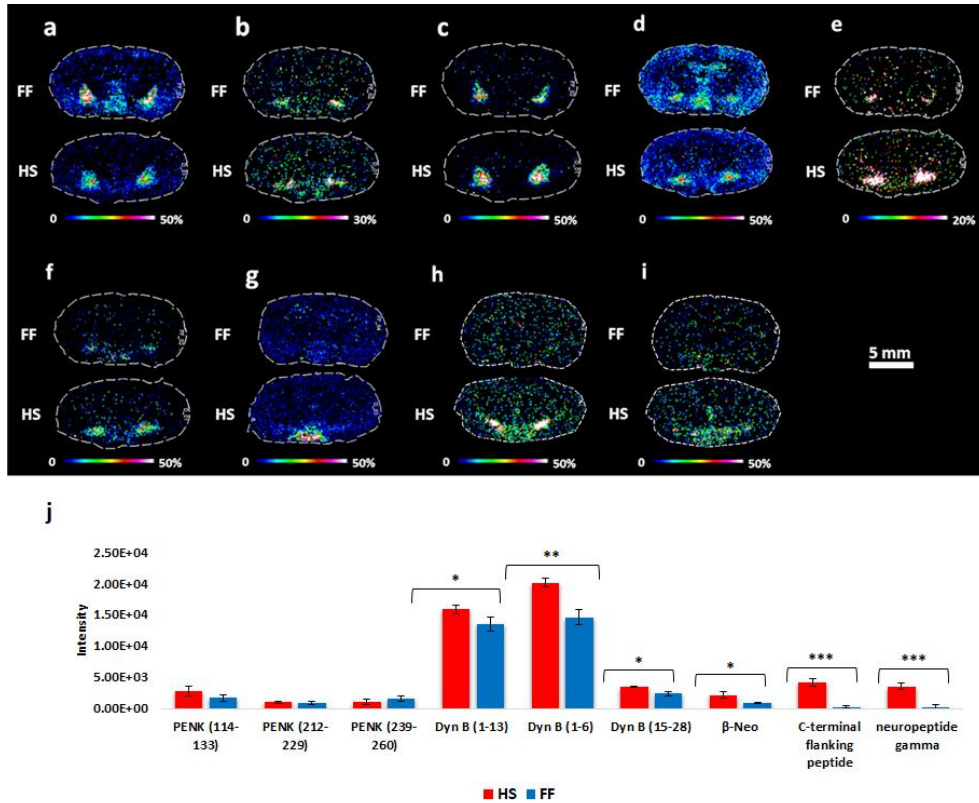


Figure S6.2.2. Molecular distributions determined by MALDI-MSI in coronal rat brain sections comparing FF with HS tissues. **a**, PENK (114-133); **b**, PENK (212-229); **c**, PENK A (239-260); **d**, Dyn B (1-13); **e**, Dyn B (1-6); **f**, Dyn B (15-28) (distance from bregma, -2.04 mm, Paxinos and Watson, 2014); **g**, β -Neo; **h**, C-terminal flanking peptide; **i**, neuropeptide gamma (distance from bregma, -2.92 mm, Paxinos and Watson, 2014); **j**, Bar charts graphs reflecting normalized average intensity of full-length peptides and related fragments between HS and FF protocols. Error bars represent standard deviation between technical replicates ($***p \leq 0.001$, $**p \leq 0.01$, $*p \leq 0.05$). Scale bar = 5 mm. Colour scale bars are shown as percentage of maximum intensity. Data were normalized against RMS. Lateral resolution, $150 \mu\text{m}$. Abbreviations: FF, fresh frozen; HS, heat stabilized.

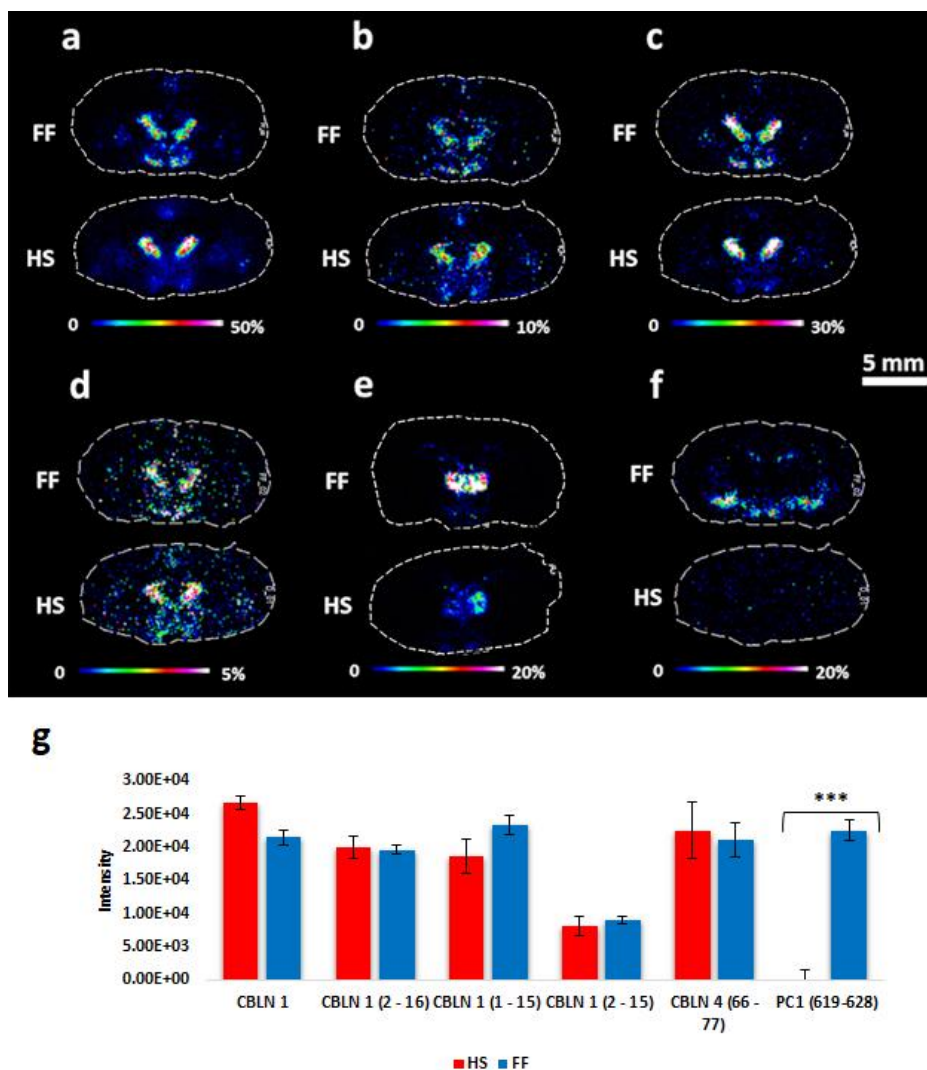


Figure S6.2.3. Molecular distributions determined by MALDI-MSI in coronal rat brain sections comparing FF with HS tissues. **a**, cerebellin 1; **b**, cerebellin 1 (2-16); **c**, cerebellin 1 (1-15); **d**, cerebellin 1 (2-15); **e**, cerebellin 4 (66-77); **f**, PC1 (619-628); **g**, Bar charts graphs reflecting normalized average intensity of peptides between HS and FF protocols. Error bars represent standard deviation between technical replicates (***) $p \leq 0.001$). Scale

Chapter VII: Supporting Informations

bar = 5 mm. Colour scale bars are shown as percentage of maximum intensity. Data were normalized against RMS. Lateral resolution, 150 μm . Abbreviations: FF, fresh frozen; HS, heat stabilized.

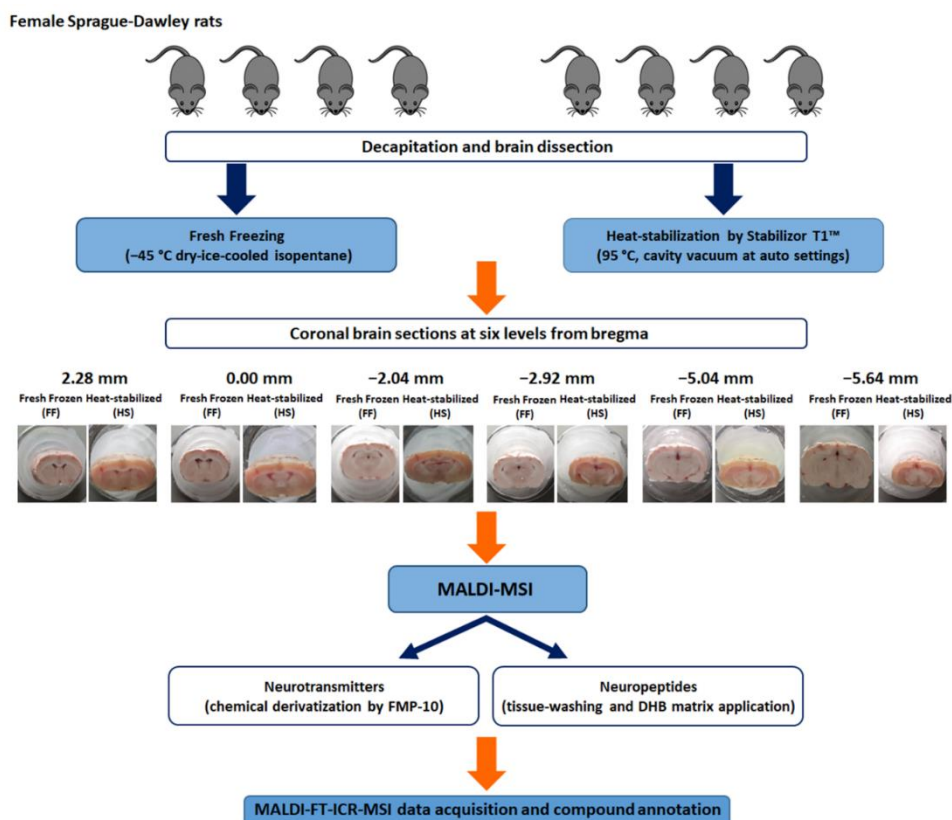


Figure S6.2.4. Schematic of the experiments performed in rat brains to monitor preservation of neurotransmitters and neuropeptides from *post mortem* degradation, comparing fresh freezing and heat-stabilization as tissue fixation approaches. Eight rats were sacrificed by decapitation and the brains were quickly removed. Four brains were immediately frozen by immersion in $-45\text{ }^{\circ}\text{C}$ dry-ice-cooled isopentane and stored at $-80\text{ }^{\circ}\text{C}$, the other four brains were heated at $95\text{ }^{\circ}\text{C}$ within 1 min following decapitation with minimal compression and cavity vacuum, using the Stabilizer T1™ instrument. MALDI-MSI for both neurotransmitters and neuropeptide were performed on coronal rat sections at six levels, distance from bregma: 2.28 mm, 0.00 mm, -2.04 mm , -2.92 mm , -5.04 mm ,

Chapter VII: Supporting Informations

–5.64 mm (Paxinos and Watson, 2014). Abbreviations: FF, fresh frozen; HS, heat stabilized.

Table S6.2.1. Complete list of the neurotransmitters detected in heat-stabilized (HS) and fresh frozen (FF) brain tissues by MALDI MSI.

Compound	Theoretical <i>m/z</i>	Observed <i>m/z</i>	Mass accuracy (ppm)	IS for spectrum normalization
DA-double derivatized	674.2802	674.2801	-0.44	DA- <i>d</i> ₄
DOPAL-double derivatized	673.2485	673.2481	-0.43	DA- <i>d</i> ₄
DOPAC-double derivatized	689.2435	689.2434	-1.16	DA- <i>d</i> ₄
3-MT-single derivatized	435.2067	435.2071	0.91	DA- <i>d</i> ₄
MOPAL-single derivatized	434.1745	434.1756	1.38	DA- <i>d</i> ₄
HVA-single derivatized	450.1699	450.1702	0.66	HVA- <i>d</i> ₅
NE-double derivatized	690.2751	690.2755	-0.58	DA- <i>d</i> ₄
DOPEG-double derivatized	691.2591	691.2589	-0.28	DA- <i>d</i> ₄
5-HT-single derivatized	444.2070	444.2074	0.90	DA- <i>d</i> ₄
5-HIAL-single derivatized	443.1754	443.1758	0.91	DA- <i>d</i> ₄
5-HIAA single derivatized	459.1703	459.1708	1.08	DA- <i>d</i> ₄
GABA-single derivatized	371.1754	371.1760	1.61	GABA- <i>d</i> ₆

The maximum intensity value of the ion was exported from the average spectrum generated for each brain by SCiLS Lab and mean values were used for statistical analysis.

Table S6.2.2. Average intensity ratio between metabolite and neurotransmitter for heat stabilized (HS) and fresh frozen (FF) brain tissues.

Brain tissue	DOPAL/DA	MOPAL/DA	3-MT/DA	HVA/DA	DOPEG/NE	5-HIAA/5-HT	5-HIAL/5-HT
HS	0.130 ± 0.01	0.008 ± 0.15	0.015 ± 0.05	0.038 ± 0.01	0.011 ± 0.05	0.223 ± 0.70	0.002 ± 0.01
FF	0.197 ± 0.21	0.018 ± 0.03	0.016 ± 0.12	0.087 ± 0.30	0.534 ± 0.03	0.494 ± 0.45	0.084 ± 0.02

Table S6.2.3. Complete list of the neuropeptides detected in heat stabilized (HS) and fresh frozen (FF) brain tissues by MALDI MSI.

Peptide precursor	Peptide name	Peptide sequence	Theoretical <i>m/z</i>	Observed <i>m/z</i>	Mass accuracy (ppm)
Cerebellin 1 (CBLN 1) Precursor protein	Cerebellin 1 (2-15) #	GSAKVAFSAIRSTN	1408.7543	1408.7570	1.92
	Cerebellin 1 (1-15) #	SGSAKVAFSAIRSTN	1495.7863	1495.7853	-0.66
	Cerebellin 1 (2-16) * #	GSAKVAFSAIRSTNH	1545.8132	1545.8129	-0.54
	Cerebellin 1 * #	SGSAKVAFSAIRSTNH	1632.8452	1632.8460	0.48

Chapter VII: Supporting Informations

Cerebellin 4 (CBLN 4)	66-77 [#]	SKVAFSAVRSTN	1266.6800	1266.6828	2.21
Proenkephalin (PENK)	Leu-enk *	YGGFL	556.2765	556.2781	1.97
	Met-enk *	YGGFM	574.2329	574.2330	0.01
	Des-Tyr- Met-enk-Arg-Phe * #	GGFMRF	714.3391	714.3401	1.53
	Met-enk-Arg *	YGGFMR	730.3341	730.3357	2.32
	Met-enk-Arg-Phe * (heptapeptide)	YGGFMRF	877.4025	877.4038	1.48
	Met-enk-Arg-Gly-Leu * (octapeptide)	YGGFMRGL	900.4396	900.4405	0.55
	PENK 212-219 * # (metorphamide)	YGGFMRRV-NH ₂	984.5196	984.5217	2.03
	PENK 201-209	LEDEAKELQ	1074.5313	1074.5321	1.02

Chapter VII: Supporting Informations

	PENK 198-207	SPQLEDEAKE	1145.5320	1145.5340	1.02
	PENK 221-229	RPEWWMDYQ	1310.5622	1310.5623	0.22
	PENK 220-229 *	GRPEWWMDYQ	1367.5837	1367.5830	-0.65
	PENK 198-209	SPQLEDEAKELQ	1386.6747	1386.6780	2.38
	PENK 219-229 *	VGRPEWWMDYQ	1466.6521	1466.6549	1.30
	PENK 114-133 #	MDELYPVEPEEEANGGEILA	2204.9903	2204.9992	4.08
	PENK 212-229 #	YGGFMRRVGRPEWWMDYQ	2334.0695	2334.0765	2.99
	PENK 239-260 #	FAESLPSDEEGESYSKEVPEME	2489.0548	2489.0538	-0.41
	Dynorphin A (1-8) *	YGGFLRRI	981.5628	981.5635	0.50
	Dynorphin A (2-8) *	GGFLRRI	818.4995	818.4999	-0.12
	Dynorphin A (10-17)	PKLKWDNQ	1028.5523	1028.5540	1.94
Prodynorphin (PDYN)	β -neoendorphin #	YGGFLRKYP	1100.5887	1100.5910	1.81
	Dynorphin B (1-13)	YGGFLRRQFKVVT	1570.8852	1570.8822	-1.90
	Dynorphin B (1-6) #	YGGFLR	712.3776	712.3787	1.96
	Dynorphin B (15-28) #	SQENPNTYSEDLDV	1610.6816	1610.6836	1.24

Chapter VII: Supporting Informations

	α -neoendorphin *	YGGFLRKYPK	1228.6837	1228.6862	1.55
	α -neoendorphin (3-10)	GFLRKYPK	1008.5989	1008.5979	-0.99
	α -neoendorphin (2-10) *	GGFLRKYPK	1065.6203	1065.6230	0.94
Protachykinin-A	Neurokinin A *	HKTDSFVGLM-NH ₂	1133.5771	1133.5778	0.70
	Substance P (1-11) *	RPKPQQFFGLM-NH ₂	1347.7354	1347.7380	2.25
	Substance P (1-7)	RPKPQQF	900.5050	900.5062	2.22
	Substance P (1-9) *	RPKPQQFFG-NH ₂	1104.5948	1104.5960	2.22
	C-terminal flanking peptide #	ALNSVAYERSAMQNYE	1845.8435	1845.8410	-1.62
	Neuropeptide gamma #	DAGHGQISHKRHKTDSFVGLM-NH ₂	2320.1727	2320.1757	1.29
Prohormone convertase 1 (PC1)	619-628	GVEKMVNVVE	1103.5765	1103.5770	0.45

Chapter VII: Supporting Informations

Promelanin concentrating hormone	Neuropeptide EI * #	EIGDEENSAKFPI-NH ₂	1447.7063	1447.7062	-0.06
Proneurotensin	Neurotensin	QLYENKPRRPYIL	1672.917	1672.9160	-0.59
Pronociceptin/ orphanin	Nociceptin #	FGGFTGARKSARKLANQ	1808.9878	1808.990	1.65
Prosomatostatin	Somatostatin (1-12) *	SANSNPAMAPRE	1244.5688	1244.5707	1.60
Calmodulin regulator protein (PEP-19)	PEP-19 (48-62)	SQFRKFQKKKAGSQS	1754.9660	1754.9620	-2.27
	PEP-19 (51-62)	RKFQKKKAGSQS	1392.8070	1392.8060	-0.71

The maximum intensity value of the ion was exported from the average spectrum generated for each brain by SCiLS Lab and mean values were used for statistical analysis; # neuropeptides detected here for the first time in HS brain tissues.

Chapter VIII

Conclusions

The PhD research project aims to the study of novel *onconutraceuticals* obtained from natural matrices for their potential use in the prevention and as valid support to the pharmacological therapies for the treatment of cancer pathologies and chronic disease. This PhD thesis is mainly focused on the development and application of analytical techniques suitable for the characterization in detail of the chemical diversity of target compounds, to evaluate their biological properties and to elucidate the fate of key molecules after assumption.

A combined approach consisting of two high resolution analytical techniques, namely Online comprehensive two dimensional liquid chromatography-tandem mass spectrometry (LC \times LC) and direct infusion Fourier transform ion cyclotron mass spectrometry (DI-FT-ICR MS) has been developed and applied for the accurate profiling of *Humulus lupulus* L. phytocomplex. A reversed phase \times reversed phase approach with a shifted gradient in the second dimension provided increased peak capacity and was able to resolve with satisfactory selectivity multiple compound classes, as well isomeric compounds. Hyphenation with an Ion Trap-Time of Flight analyzer led to the identification of 101 compounds in 70 minutes. On the other hand, the ultra-high mass accuracy, resolution and the isotopic fine structure provided by FT-ICR-MS was very useful and complementary to LC \times LC-MS/MS for the assignment of molecular formula, leading to more confident identification results (**Chapter II**). Subsequently, the possible use of hop secondary metabolites as natural immunomodulators and adjuvants in chemotherapy protocols has been evaluated. After fractionation by semi-preparative Liquid Chromatography, three different fractions were obtained. The

phytochemicals and the fractions were tested to verify the ability to modulate the Lymphocytes CD3+ and Natural Killer compartment. Cytofluorimetric analysis revealed that a fraction containing bitter acids was able to up-regulate of NKG2D and Nkp44 activating receptors. A further simplification yield a fraction mainly composed by Humulinones and Cohulupone derivatives, that at the concentration of 0.1 µg/mL induced selective activation of Nkp44 receptor and enhanced the cytolytic activity of NK cells against leukemia cell line K562 (**Chapter III**). In addition to immunomodulant potential of hop bioactive compounds, the mechanism for ingested breastmilk and probiotic to act in a complementary manner for the prevention of necrotizing enterocolitis (NEC) in very premature infants has been investigated. In detail, molecular cutoff fractionation and ultra-high-performance liquid chromatography-tandem mass spectrometry were used to identify indole-3-lactic acid (ILA), a metabolite of breastmilk tryptophan, as the anti-inflammatory molecule of *Bifidobacterium longum* subsp *infantis* (*B. infantis*) secretions. ILA was tested on human fetal small intestinal cell line, necrotizing colitis enterocytes and also fetal human organoids, providing to be able to reduce the inflammatory cytokine IL-8 response after IL-1β stimulus through the interaction with the factor aryl hydrocarbon receptor (AHR) and TLR-4 of premature enterocytes surface, preventing the transcription of IL-8 (**Chapter IV**).

Moreover, an ultra high performance liquid chromatography-high resolution mass spectrometry (UHPLC-HRMS) method has been developed and validated to assess the metabolic stability of hop α- and β-acids and the detection of their metabolites *in vitro* and *in vivo*. Mice liver microsomes were used to assess metabolic stability, *in vitro* $t_{1/2}$ and clearance values calculated, showing a slow and moderate metabolism for α-acids (avg $t_{1/2}$: 120.01 min, avg CL_{int} 11.96 µL/min/mg),

while β -acids were metabolized faster (avg $t_{1/2}$: 103.01min, avg CL_{int} 13.83 $\mu\text{L}/\text{min}/\text{mg}$). Furthermore, phase I metabolites and phase II glucuronide were characterized both *in vitro*, and *in vivo*, in mouse plasma and urine after oral administration, by a combined full scan/data dependent/targeted neutral loss (FS/DDA/tNL) strategy. As a result, 12 phase I metabolites, including 2 novel potential di-oxygenated metabolites (M6, M7) of humulones were detected. In addition, the tNL was able to detect for the first time 10 glucuronide conjugates of α -acids, comprising 7 glucuronide derivatives of oxidized phase I metabolites (M16-M22) (**Chapter V**).

Since UHPLC-HRMS methods are unable to report the spatial distribution of biomolecules of interest, the final part of the project has been focused on the application of matrix-assisted laser desorption/ionization-mass spectrometry imaging (MALDI-MSI). A comparison of tissue stabilization protocols to highlight the *post mortem* degradation differences has been performed to image key neurotransmitters, metabolites and neuropeptides in rat brain. Although the heat stabilization did not showed differences in the levels of precursors dopamine, norepinephrine, and serotonin, their related metabolites (DOPAL, DOPAC, HVA, MOPAL, DOPEG and 5-HIAA) were all significantly lower, revealing a reduced neurotransmitter turnover ratios in heat stabilized brains compared to fresh frozen. *In situ* markers associated with the stabilization of enkephalin, dynorphin, and tachykinin derived neuropeptides were also imaged. Moreover, heat stabilization enabled the detection of very low-abundant neuropeptides such as the C-terminal flanking peptide, neuropeptide gamma, and nociception, providing evidence for the potential use of the heat stabilization prior to MALDI-MSI analyses to improve the

examination of the *in vivo* state of neuronal chemical messengers in brain tissues
(Chapter VI Section I)

Finally, MALDI-MSI technique has been applied to the simultaneously mapping of hop α - and β -acids and their metabolites in rat liver sections after oral administration. Parents compounds of α -acids and phase I mono-oxidized metabolites were distributed across liver sections, revealing higher relative intensity of Humulinone derivative respect the related precursor compound (**Chapter VI Section II**).

Future prospective foresees the application of advanced analytical techniques in both pharmaceutical and biomedical field, with the aim to understand the mechanism of action of key molecules by the analysis of metabolic changes occurring in biological systems following their employment in pathology states, to highlight the potential positive modulation of key molecular pathways.

List of Papers

This thesis is based on the following papers:

- Sommella, E., Pagano, F., **Salviati, E.**, Chieppa, M., Bertamino, A., Manfra, M., Sala, M., Novellino, E., Campiglia, P. Chemical profiling of bioactive constituents in hop cones and pellets extracts by online comprehensive two-dimensional liquid chromatography with tandem mass spectrometry and direct infusion Fourier transform ion cyclotron resonance mass spectrometry. *J. Sep. Sci.* 2018, *41*, 1548–1557.
- **Salviati, E.**, Ciaglia, E., Sommella, E., Montella, F., Bertamino, A., Ostacolo, C., Parrino, B., Rubino, R., Vecchione, C., Puca, A., Novellino, E., Campiglia, P. Immunomodulatory activity of Humulus lupulus bitter acids fraction: enhancement of natural killer cells function by NKp44 activating receptor stimulation. *J. Func. Foods.* 2019, *61*, 103469.
- Meng, D., Sommella, E., **Salviati, E.**, Campiglia, P., Ganguli, K., Djebali, K., Zhu, W., Walker, A.W. Indole-3-lactic acid, a metabolite of tryptophan, secreted by Bifidobacterium longum subspecies infantis is anti-inflammatory in the immature intestine. *Ped. Res.* 2020, *88*, 209–217.
- **Salviati, E.**, Sommella, E. Carrizzo, A., Vecchione C., Campiglia, P. Determination of phase I metabolites and glucuronide conjugates of hop bitter acids by a full scan/data dependent/targeted neutral loss UHPLC–HRMS strategy: *In vitro* metabolic stability and *in vivo* analysis after oral administration in mice. *Manuscript in preparation*
- **Salviati, E.**, Nilsson, A., Shariatgorji, R., Campiglia, P., Tjernström, N., Roman, Andrés, P.E. Evaluation and optimization of neurotransmitter and

List of Papers

neuropeptide analysis in heat stabilized vs fresh frozen brains by MALDI-MSI. *Manuscript in preparation.*

List of Additional Papers

- Sommella, E., Conte, G.M., **Salviati, E.**, Pepe, G., Bertamino, A., Ostacolo, C., Sansone, F., Del Prete, F., Aquino, R.P., Campiglia, P. Fast profiling of natural pigments in different spirulina (*arthrospira platensis*) dietary supplements by DI–FT–ICR and evaluation of their antioxidant potential by pre–column DPPH–UHPLC assay. *Molecules* 2018, *23*, 1132.
- Badolati, N., Sommella, E., Riccio, G., **Salviati, E.**, Heintz, D., Bottone, S., Di Cicco, E., Dentice, M., Tenore, G.C., Campiglia, P., Stornaiuolo, M., Novellino, E. Annurca apple polyphenols ignite keratin production in hair follicles by inhibiting the pentose phosphate pathway and amino acid oxidation. *Nutrients* 2018, *10*, 1406.
- Riccio, G., Sommella, E., Badolati, N., **Salviati, E.**, Bottone, S., Campiglia, P., Dentice, M., Tenore, G.C., Stornaiuolo, M., Novellino, E. Annurca apple polyphenols protect murine hair follicles from taxane induced dystrophy and hijacks polyunsaturated fatty acid metabolism toward beta–oxidation. *Nutrients* 2018, *10*, 1808.
- Sommella, E., Badolati, N., Riccio, G., **Salviati, E.**, Bottone, S., Dentice, M., Campiglia, P., Tenore, G.C., Stornaiuolo, M., Novellino, E. A boost in mitochondrial activity underpins the cholesterol–lowering effect of annurca apple polyphenols on hepatic cells. *Nutrients* 2019, *11*, 163.
- Sommella, E., **Salviati, E.**, Merciai, F., Manfra, M., Bertamino, A., Gasparri, F., Novellino, E., Campiglia, P. Online comprehensive hydrophilic interaction chromatography × reversed phase liquid chromatography coupled to mass spectrometry for in depth peptidomic

List of Additional Papers

- profile of microalgae gastro-intestinal digests. *J. Pharm. Biomed. Anal.* 2019, *175*, 112783.
- Sommella, E., **Salviati, E.**, Musella, S., Di Sarno, V., Gasparri, F., Campiglia, P. Comparison of online comprehensive HILIC × RP and RP × RP with trapping modulation coupled to mass spectrometry for microalgae peptidomics. *Separations* 2020, *7*, 25.
 - Pepe, G., **Salviati, E.**, Rapa, S.F., Ostacolo, C., Cascioferro, S., Manfra, M., Autore, G., Marzocco, S., Campiglia, P. Citrus sinensis and Vitis vinifera protect cardiomyocytes from doxorubicin-induced oxidative stress: Evaluation of onconutritional potential of vegetable smoothies. *Antioxidants* 2020, *9*, 378.
 - Pepe, G., Rapa, S.F., **Salviati, E.**, Bertamino, A., Cascioferro, S., Autore, G., Quaroni, A., Marzocco, S., Campiglia, P. Bioactive polyphenols from pomegranate juice reduce 5-fluorouracil-induced intestinal mucositis in intestinal epithelial cells. *Antioxidants* 2020, *9*, 699.
 - Badolati, N., Masselli, R., Sommella, E., Saggiocchi, S., Di Minno, A., **Salviati, E.**, Campiglia, P., Dentice, M., Tenore, G.C., Stornaiuolo, M., Novellino, E. The hepatoprotective effect of taurisolo, a nutraceutical enriched in resveratrol and polyphenols, involves activation of mitochondrial metabolism in mice liver. *Antioxidants* 2020, *9*, 410.
 - Grimaldi, M., Marino, C., Buonocore, M., Santoro, A., Sommella, E., Merciai, F., **Salviati, E.**, De Rosa, A., Nuzzo, T., Errico, F., Campiglia, P., Usiello, A., D'Ursi, A.M. Prenatal and early postnatal cerebral D-Aspartate depletion influences L-Amino acid Pathways, bioenergetic processes, and developmental brain metabolism. *J. Proteome Res.* 2021, *20*, 727–739.

Participation in conferences

- Sommella, E, **Salviati, E.**, Pepe, G., Novellino, E., Campiglia, P. Unraveling the composition of bioactive compounds in hop (*Humulus lupulus* L.) by comprehensive LC × LC-IT-TOF assisted by DI-FT-ICR. **Poster communication** at the “42nd International Symposium on Capillary Chromatography and 15th GC × GC Symposium”. May 13-18, 2018, Riva del Garda (TN), Italy.
- **Salviati, E.**, Sommella, E., Pepe, G., Novellino, E., Campiglia, P. Unraveling the composition of bioactive compounds in hop (*Humulus Lupulus*) by comprehensive LC × LC-IT-TOF. **Poster communication** at Chimali 2018-XII Italian Food Chemistry Congress. September 24-27, 2018, Camerino (MC), Italy.
- Sommella, E., Conte, G.M., **Salviati, E.**, Pepe, G., Sansone, F., Aquino, R.P., Novellino, E., Campiglia, P. Elucidation of Antioxidant Pigments in Spirulina based formulations by DPPH-UHPLC and FT-ICR-MS. **Poster communication** at Chimali 2018- XII Italian Food Chemistry Congress. September 24-27, 2018, Camerino (MC), Italy.
- **Salviati, E.**, Sommella, E., Stornaiuolo, M., Novellino, E., Campiglia, P. Direct Infusion FT-ICR based metabolomics of Hair Follicles treated with Annurca apple extract reveals increased Keratine production through inhibition of Pentose Phosphate Pathway and Amino Acid Oxidation. **Oral communication** at 10° MS Pharmaday. October 24-26, 2018. Bioindustry park, Colleretto Giacosa (TO), Italy.
- **Salviati, E.**, Sommella, E., Pepe, G., Novellino, E., Campiglia, P. Comparison of online comprehensive RP × RP vs HILIC × RP with enhanced trapping modulation coupled to High Resolution Mass Spectrometry for microalgae peptidomics: a critical evaluation. **Poster communication** at “HPLC 2019 48th International Symposium on High-Performance Liquid Phase Separations and Related Techniques”. June 16-20, 2019, Milan (MI), Italy.

Participation in conferences

- Sommella, E., **Salviati, E.**, Witt, M.; Thompson, C.J., Campiglia, P. Metabolic changes in murine hair follicles treated with procyanidin-B2 rich nutraceuticals by magnetic resonance mass spectrometry (MRMS). **Poster communication** at “Metabolomics 2019”. June 23-27, 2019, The Hague, Netherlands.
- **Salviati, E.**, Pepe, G., Sommella, E., Ostacolo, C., Manfra, M., Coppola, D., Coppola, L., Novellino, E., Campiglia, P. Development of online comprehensive reversed-phase × reversed-phase ultra-high pressure liquid chromatography approach for the analysis of onconutraceutical smoothies. **Poster communication** at “XXVI National Meeting in Medicinal Chemistry”. July 16-19, 2019, Milan (MI), Italy.
- **Salviati, E.**, Pepe, G., Sommella, E., Ostacolo, C., Manfra, M.; Marzocco, S., Campiglia, P. Development of comprehensive hydrophilic interaction chromatography × reversed-phase ultra-high pressure liquid chromatography platform for the analysis of Punica granatum fruit juice. **Poster communication** at “XXVI National Meeting in Medicinal Chemistry”. July 16-19, 2019, Milan (MI), Italy.
- Sommella, E., **Salviati, E.**, Witt, M., Thompson, C.J. Metabolic changes in murine hair follicles treated with procyanidin-B2 rich nutraceuticals by magnetic resonance mass spectrometry (MRMS). Presented at ASMS 2020 Reboot, June, 1-12, 2020.
- Sommella, E., **Salviati, E.**, Conte, G., Witt, M., Campiglia, P. Elucidation of carotenoids in microalgae formulations by ultra-high resolution mass spectrometry combined with APCI. Presented at ASMS 2020 Reboot, June, 1-12, 2020.

Ringraziamenti

Ringrazio il mio tutor il Prof. Pietro Campiglia per avermi dato questa opportunità e per la sua continua disponibilità.

Grande ringraziamento va ai miei supervisori, il Dott. Eduardo Sommella ed il Dott. Giacomo Pepe, per i preziosi insegnamenti ed il costante supporto.

Inoltre, la mia gratitudine va al Prof. Per E. Andrén e a tutto il gruppo di ricerca del Medical Mass Spectrometry Imaging (BMC, Uppsala University), per avermi fatta sentire parte integrante ed attiva del gruppo.

Desidero ringraziare i miei colleghi del laboratorio “La baita” e tutto il gruppo di ricerca del Lab. 15.

Il mio più grande ringraziamento va alla mia famiglia e ad Eduardo, punti di riferimento della mia vita.